Examining the regional physiology of the transplant kidney during normothermic machine perfusion

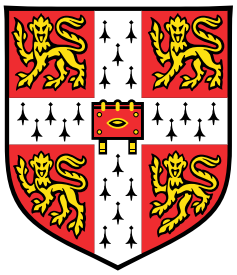

Thomas David Adams

Supervisor: Prof. M.L. Nicholson

Department of Surgery

University of Cambridge

This dissertation is submitted for the degree of

Doctor of Philosophy

Darwin College

September 2020

To my family - my parents Dave and Judy, my sister Beki and my wife Victoria.

Declaration

I hereby declare that except where specific reference is made to the work of others, the contents of this dissertation are original and have not been submitted in whole or in part for consideration for any other degree or qualification in this, or any other university. This dissertation is my own work and contains nothing which is the outcome of work done in collaboration with others, except as specified in the text and Acknowledgements. This dissertation contains fewer than 60,000 words excluding figures, photographs, tables, appendices and bibliography.

Thomas David Adams

September 2020

Abstract

Ischaemia-reperfusion injury (IRI) is an unavoidable consequence of deceased-donor kidney transplantation that has a profound effect upon both immediate and long-term graft function. Disruption to microvascular perfusion (MVP) and tissue oxygenation (P_tO_2) are central to the development of IRI, but detailed regional pathophysiology remains unresolved in the context of renal transplantation.

Normothermic machine perfusion (NMP) is a novel preservation technology that aims to improve pre-implantation kidney quality, but may also be used experimentally to investigate transplant reperfusion. My PhD set out to determine the optimal perfusion conditions to improve kidney quality, and to investigate the underlying heterogeneity in pathophysiology within regions of the kidney which may impact kidney quality.

Firstly, we used a porcine model of donor kidney retrieval, NMP, and simulated reperfusion to test the hypothesis that reducing current NMP perfusate oxygenation (P_PO_2) from supraoxic levels would improve renal function and reduce reperfusion injury. In kidneys exposed to either short or long cold ischaemic times, reducing P_PO_2 from the clinical standard to normoxic or hypoxic P_PO_2 altered oxygen kinetics during NMP but did not influence tubular function, clearance, urine output, or biomarkers of renal injury during simulated reperfusion.

Secondly, we used porcine and human models of transplant reperfusion to test the hypothesis that the renal medulla would be disproportionately affected by tissue hypoperfusion,

hypoxia and acute inflammation. In a porcine reperfusion series, P_tO_2 and MVP were significantly altered following IRI when compared to pre-ischaemic baselines, with greater variation and heterogeneity seen in the medulla than in the cortex. In a human reperfusion series, there was widespread initial microcirculatory disruption, persistent lower medullary P_tO_2 and a distinct medullary inflammatory environment.

In summary we have described novel porcine and human renal medullary physiology and inflammation during transplant reperfusion that highlight the need for medulla-specific strategies to ameliorate IRI. We have further determined changes to renal physiology and injury in response to perfusate oxygenation in a novel preservation technology that may guide clinical implementation.

Acknowledgements

I am profoundly thankful to all the Donors and their families, who gave so much to others at a time of such personal loss. Their selfless actions made this research possible, and their generosity embodies the amazing spirit of the transplantation family.

To my supervisor, Prof. Mike Nicholson, thank you so much for your tireless support, wit and wisdom; for the opportunity to pursue this work, the encouragement to follow my interests, and the tools to bring an idea to fruition. To Dr. Sarah Hosgood, thank you for leading me through the world of transplantation; be it a late-night experiment or an international conference. You were always on hand to help and offer advice and I couldn't have done any of this without your incredible expertise and knowledge.

I am immensely grateful to Mr. Kourosh Saeb-Parsy, who first encouraged me to work in the Department of Surgery and continued to offer help and inspiration throughout. I am also most grateful for the constructive feedback I received from my first year examiners, Mr. Neil Russell and Mr. Simon Harper.

I am indebted to the Rosetrees Trust, the Geoffrey Fisk Scholarship, Darwin College and the NIHR Blood and Transplant Research Unit in Organ Donation and Transplantation for their support. My special thanks go to Dr. Duncan Needham.

Thank you to all those at the Department of Surgery who contributed to this work: Tom Moore and Keziah Crick for countless hours assisting with perfusions, bench work and

presentations; Dr. Jenna DiRito for help with perfusions, staining and MATLAB code; Dr. Timothy Elliot Beach, Mr. Mazin Hamed and Mr. Jack Martin for assistance with porcine experiments; Dr. Anja Gruszczyk for help with RNA extraction; Dr. Arnaldo Silva for help with MATLAB analysis; and Dr. Krishnaa Mahbubani for help with registry data and frequent problem-solving. My thanks also to Addenbrooke's histopathology and biochemistry laboratories, and all the support from Rachel Brown, Dr. Rachel Seear, Sylvia Rehokova, Faye Hill, Lila Tran, Alison Warrington and Linda Butler.

Thank you to all of my colleagues at the Department of Surgery; cherished memories of the times we spent working, laughing and despairing together are woven between the lines of this thesis. I am also so grateful for my Emergency Department and Intensive Care colleagues at Addenbrooke's hospital, whose understanding and camaraderie helped me get over the finish line during the first wave of the Covid-19 pandemic.

My deepest gratitude to my inspirational mentors Prof. David Howard and Prof. Valerie Lund; your support and advice gave me the confidence to continue during challenging moments. To my friends, especially Luke, Adam, Pete, Charlotte, Ina, Aleks and James; I'll be forever grateful for your support throughout this journey. This is a finish!

To my family I owe so much. To Beki, thank you for your love, laughter, for keeping me grounded and for so much inspiration from your own amazing journey. To my parents, thank you for a lifetime of unconditional love, happiness and unfailing support during so many (often harebrained) adventures.

To Victoria - ma sosie, ma mariée. Our story and that of this project have been entwined from the beginning; I could not have done any of it without your unswerving love, support, drive, empathy and intellect. Whilst this story is now ending, ours together is only just beginning and I could not be more excited. Thank you, so much, for everything.

Table of contents

List of figures

List of tables

Abbreviations

AKI	acute kidney injury
ANOVA	analysis of variance
ATN	acute tubular necrosis
ATP	adenoside triphosphate
ATP	adenosine triphosphate
AUC	area under the curve
C_aO_2	arterial oxygen content
C_VO_2	venous oxygen content
CIT	cold ischaemic time
CrCl	creatinine clearance
CS	cold storage
DBD	donation after brainstem death
DCD	donation after cardiac death
DD	deceased donor

DGF delayed graft function

DO_2 oxygen delivery

ECD expanded criteria donors

ELISA enzyme linked immunosorbent assay

ESRF End-stage renal failure

ETC Electron Transport Chain

FENa fractional excretion of sodium

H&E hematoxylin and eosin

Hb haemoglobin

HCT haematocrit

HMGB-1 high-mobility group box 1

HMP hypothermic machine perfusion

ICAM intercellular adhesion molecule

IL interleukin

IRI ischaemia-reperfusion injury

IRR intra-renal resistance

kPa Kilopascal

KT kidney transplantation

LD living donor

LDF laser-Doppler flow

LED light-emitting diode

MAP mean arterial pressure

MBF medullary blood flow

MI myocardial infarction

mPTP mitochondrial permeability transition pore

MSB Martius scarlet blue

MVP microvascular perfusion

NFκB nuclear factor kappa B

NGAL neutrophil gelatinase-associated lipocalin

NHS National Health Service

NHSBT NHS Blood and Transplant

NMP normothermic machine perfusion

OER oxygen extraction ratio

P_PO_2 perfusate oxygen tension

P_tO_2 tissue oxygen tension

PCA principle component analysis

PCR polymerase chain reaction

PCr plasma creatinine

PNF primary non-function

PO_2 partial pressure of oxygenation

RBC red blood cell

RBF renal blood flow

RC renal cortex

RM renal medulla

RNS reactive nitrogen species

RO_2 oxygen return

ROS reactive oxygen species

SCS static cold storage

SD standard deviation

SEM standard error of the mean

SO_2 haemoglobin saturation

TIRI transplant ischaemia-reperfusion injury

TNF tumour necrosis factor

UCr urine creatinine

UO_2 urine oxygen tension

VO_2 oxygen consumption

WIT warm ischaemic time

Chapter 1

Introduction

1.1 Introduction and project rationale

In the space of half a century, kidney transplantation has advanced from being experimental science to a mainstay of modern clinical practice. Transplantation is now well-established as the definitive treatment of end-stage renal failure (ESRF), and practice continues to grow year-on-year worldwide.

Despite advances in dialysis and strategies to avert ESRF, demands for kidney transplantation continue to rise as a growing global burden of diabetes and hypertension precipitates a rising tide of nephropathy [128]. To counter the rise in kidney transplantation (KT) demand a number of strategies have been trialled, including transplanting organs from older donors, donation after circulatory death, and utilising organs that may have sustained greater injury during prolonged transit to the recipient's centre. Together this has been called 'expansion of the donor pool'.

A central focus for transplantation science is the unavoidable ischaemia-reperfusion injury (IRI) sustained during KT, particularly by deceased donor organs. Ischaemia-reperfusion

injury has a profound impact upon the immediate and long-term function of transplant kidneys; any approach to increase successful donation must address IRI, as most of the kidneys in the expanded pool have either increased susceptibility or exposure to ischaemia.

One area of practice that has changed little since the advent of transplantation is the preservation of deceased donor organs during transit from donor to recipient. Static cold storage (SCS) has long been the preferred method as it is quick, cheap and reliable. However, it permits only limited organ assessment and it is known that organs deteriorate during this period of hypothermic ischaemia [136].

Normothermic machine perfusion (NMP) is a novel preservation technology that aims to improve the quality and success of KT through improving pre-transplant reconditioning, assessment, and direct delivery of therapeutics. Whilst it has been demonstrated in a clinical series that NMP may reduce rates of delayed graft function [124], questions remain over the optimal conditions for kidney perfusion, and how best to assess kidneys during perfusion [87]. Alongside bringing potential benefits to clinical practice, the NMP model may be run as an ex-vivo model of reperfusion injury, and thus may be a valuable tool in interrogating mechanisms during transplantation IRI (TIRI).

Intricately linked to the problem of TIRI is renal oxygenation. Normothermic machine perfusion is postulated to ameliorate TIRI through restoration of cellular metabolism and replenishment of adenosine triphosphate (ATP). For historical reasons, most NMP circuits deliver a supra-physiological oxygen tension to the kidney. However, there is an increasing focus upon the negative effects of over-oxygenation in disease states involving IRI, amid fears that excess oxygen during ischaemia and subsequent reperfusion may worsen injury through production of harmful reactive oxygen species (ROS). Thus, optimising oxygen delivery to the allograft during NMP may prevent further injury.

During IRI, damage to the highly specialised renal circulation plays a central role in initial tissue injury; experiencing a breakdown of integrity and autoregulation that causes acute kidney dysfunction, promotes further acute damage and hampers organ recovery. Whilst the cortex receives a quarter of cardiac output the renal medulla remains on the edge of hypoxia as a necessity for solute concentration [31], a situation that leaves the outer medulla exceptionally vulnerable to ischaemic damage. Whilst this has been demonstrated experimentally, studying the renal medulla in-vivo is challenging, and little is known about the human renal medulla, and even less about the allograft medulla. It is not known, for example, the relative extents to which cortical and medullary perfusion and oxygenation are affected by TIRI; nor whether regions exhibit specific inflammatory patterns that may reveal underlying pathophysiology and thus offer therapeutic targets. One promising tool in assessing medullary function may be the urine oxygen tension, as this is thought to equilibrate with the inner medullary parenchyma [54].

The overall aims of this project are to use the normothermic machine perfusion of porcine and human kidneys to address gaps in our knowledge surrounding optimal allograft oxygenation during NMP and patterns of regional oxygenation, perfusion and inflammation during transplant reperfusion.

1.2 Methods of organ donation in the United Kingdom

1.2.1 Living donation

Uniquely for a solid organ, whole kidneys may be procured for transplantation from living donors. Living donor (LD) kidney transplantation is considered by many to be the gold standard for patients with end-stage renal failure. It offers a number of advantages over deceased organ donation, predominantly prolonged recipient and graft survival [16].

Elective organ retrieval and implantation permit recipient desensitisation (and thus immunologically incompatible transplant), pre-emptive surgery prior to starting dialysis (and all the associated risks and costs) and consideration of recipients who wouldn't be suitable for emergency surgery [141]. Living donor organs further avoid the complex multi-organ failure that occurs after brainstem death in DBD organs, and the ischaemic insults that affect DD organs, especially donation after cardiac death (DCD) [58]. However, living donors are at a higher risk of end-stage renal disease, and as the donor pool expands to include donors previously considered too high-risk, the validity of long-term data becomes less clear and less is known about the long-term risks for this current cohort [61].

Furthermore, stringent tests must be passed to ensure that the risks to the donor in terms of ill health, loss of earning and psychological harm are balanced with the potential benefits of the recipient in an ethical manner [141].

1.2.2 Donation after death

Whilst the initial successful cases relied upon living-related transplant between identical twins, in effect an auto-transplant, the seminal work of Medawar, Starzl and others in the mid-20th century paved the way for the allotransplantation of organs from non-related donors [57]. Following this breakthrough, deceased donors rapidly became an invaluable source of transplant kidneys. Today, the majority of kidney transplantation operations in the UK use organs from deceased donors [6]. Deceased donors are often geographically distant from potential recipients, and organs from one donor may go to multiple recipients. A form of organ preservation is therefore required to maintain kidney integrity during transport and allocation. Current methods of static cold storage (see below) mean that DBD organs sustain an additional period of cold ischaemic injury when compared to LD kidneys.

Donation after brainstem death

Donation after brainstem death (DBD) is the mainstay of transplant organ supply in the UK. DBD donors are more likely to donate multiple transplantable organs and until relatively recently have been the primary source for donor hearts [114].

Brainstem-dead donors have sustained severe, non-reversible neurological injury that has caused a cessation of brainstem function, and are therefore deeply unconscious, apnoeic, and require mechanical ventilation. Two qualified clinicians are needed to separately conclude that a potential donor has brainstem death by ruling out reversible causes, confirming apnoea and the absence of brainstem reflexes [129]. Continued organ support during donor work-up and retrieval allows optimisation of the donor organs and a reduction of the critical warm ischaemic retrieval period. Such optimisation is necessary because physiological changes following brainstem death including cardiorespiratory instability, hypothalamic failure and the autonomic storm can adversely influence donor organ function and likelihood of rejection.

Whilst DBD organs remain the majority, deceased donor demographics are changing. With progress in road safety legislation and management of conditions that may lead to brain death, potential donors are now more elderly and may harbour more medical co-morbidities, meaning both that the number of DBD donors and the gap in outcomes compared to DCD organs may be in decline [121].

Expanded criteria donors

As average donor age and chronic disease burden increases, there has been the creation of so-called expanded criteria for the consideration of higher risk donors. Expanded criteria donors (ECD) are defined as any deceased donor aged over 60, or aged over 50 with at least two of the following three criteria: serum creatinine greater than 133μmol/L, a history of hypertension or death from ischaemic stroke [117]. To compound higher donor risk factors, ECD kidneys may be subject to longer CIT than standard criteria donor (SCD) kidney

counterparts, possibly due to difficulties in recipient matching. Despite a rapid increase in use of ECD kidneys throughout the UK and Europe, and the fact that an ECD kidney transplant affords survival benefit versus dialysis, rates of graft loss are higher compared to standard criteria donor organs, and cautious allocation is required to maximise graft survival [14].

Donation after circulatory death

Donation after circulatory death (DCD) describes organ donation following withdrawal of life-supporting measures and circulatory arrest. There has been a rapid expansion in the number of DCD kidneys transplanted in the UK over the past 15 years, which looks set to increase further [88].

Whilst protocols exist for the rapid retrieval of organs from donors who arrest out-of-hospital or in the emergency department (so-called uncontrolled donors, Maastricht categories I and II), in the United Kingdom only donors for whom treatment withdrawal and progression to arrest can be controlled (Maastricht category III-V) are considered [96]. In practice, this equates predominantly to patients who sustain severe, non-survivable brain injury but do not meet brainstem death criteria [6].

Because life-supporting measures must be withdrawn and cardiac death confirmed prior to commencement of retrieval, there are differences with DBD organs in terms of retrieval technique. There follows an unavoidable period of warm ischaemia during a five-minute standoff period between confirmation of death and the start of the retrieval, which continues once the rapid retrieval has begun until the abdominal compartment is cooled with ice and organs flushed with cold preservation solution. The time between treatment withdrawal and circulatory arrest is variable, posing logistical challenges for retrieval teams and potentially adding to organ ischaemia as end-organ perfusion may be compromised by fluctuating blood pressure [112].

Whilst DCD kidneys have higher rates of delayed graft function, defined as a need for dialysis in the first 7 days post-transplant, analysis in the UK suggests that 5-year outcomes for DCD kidneys are comparable to those from DBD kidneys [160].

1.3 Ischaemia-reperfusion injury in transplantation

The process of transplantation represents a significant, multiform and complex insult to kidney integrity. Retrieval, storage and implantation of a kidney may each cause potential harm to a graft that may have longstanding effects.

1.3.1 Ischaemia-reperfusion injury

Ischaemia-Reperfusion injury (IRI) is an unavoidable consequence of transplantation, and has a pivotal role in affecting the outcome of deceased donor organs.

The phenomenon of IRI describes the pattern of cellular and vascular injury sustained following a period of minimal blood flow and the subsequent restoration of blood flow. Paradoxically, much of the injury, sustained on a sub-cellular, cellular and vascular level, manifests after the return of blood flow [71]. The injuries sustained can be divided into that sustained during ischaemia and during reperfusion.

The hypoxia that follows ischaemia has an immediate effect on cellular metabolism, as without oxygen as the final acceptor in the electron transport chain, oxidative phosphorylation is unable to occur. Metabolism is shunted largely to the anaerobic glycolytic pathway, markedly reducing the net production of adenosine triphosphate (ATP) and adenosine diphosphate (ADP) [145]. Reductions in ATP and ADP limit the functioning of the transmembrane Na-K ATPase pump responsible for maintaining the high-sodium, low-potassium composition of extracellular fluid. Cells become hypernatraemic and hypercalcaemic, further damaging mitochondria and other organelles and promoting the formation of reactive oxygen

species (ROS). As the extracellular osmolality falls, fluid is drawn intracellularly by the higher oncotic pressure, causing cellular oedema and rupture. Anaerobic glycolysis further causes intracellular acidosis through the production of lactate and hydrogen ions [23]. The cessation of oxidative phosphorylation causes a build-up of the citric acid cycle intermediate succinate due to reversal of complex II (succinate dehydrogenase) [38].

Upon reperfusion, cellular deoxygenation prompts a rapid complex II reversal, driving mitochondrial ROS production [38]. A burst of ROS and reactive nitrogen species production causes mitochondrial dysfunction and permeability transition pore (mPTP) opening, leading to further cytoplasmic calcium influx and cellular apoptosis and necrosis [155].

Endothelial cells (critical mediators of vascular tone, leukocyte function, and smooth muscle responsiveness) are damaged early in IRI, losing complete integrity within hours in rodent models [26]. Cellular hypoxia and oxidative stress break down cadherin-mediated intercellular adhesion and tight junction integrity, causing increased capillary leakage and interstitial oedema. Endothelial nitric oxide synthase (NOS3) activity is reduced (as evidenced by reduced post-ischaemic reactivity to bradykinin and acetylcholine), especially in the renal medulla [21], and small arterioles become hyperresponsive to increased tissue levels of endothelin-1, angiotensin II, thromboxane A2, prostaglandin H2, leukotrienes C4 and D4, and adenosine as well as sympathetic nerve stimulation, all of which promote vasoconstriction [26]. The damaged vascular and tubular epithelial cells release proinflammatory damage-associated molecular patterns (DAMPs), cytokines such as IL-4, IL-6, interferon-γ and tumor necrosis factor-α [145]. There is upregulated expression of adhesion molecules such as ICAM-1, Toll-Like Receptors (TLRs) and hypoxia-inducible factors (HIF) that enhance leukocyte-endothlial attraction and interaction. Activated macrophages foment a vicious pro-inflammatory environment that promote further cellular recruitment and vasoconstriction through the release of vasoactive cytokines such as interleukin (IL) -1β, IL-6, IL-12, IL-15, IL-18, IL-32, tumour necrosis factor alpha (TNF-α) and endothelin [26].

The cellular inflammatory response is augmented by activation of complement, resident tissue macrophages and dendritic cells, and there is subsequent infiltration of a wide range of systemic leucocytes including T and B cells, Natural Killer (NK) cells, macrophages and neutrophils [84]. This post-ischaemic population of immune cells inflict much of the downstream damage upon renal tissue, causing acute tubular necrosis, and promoting harmful fibrosis. Neutrophils produce ROS, proteases and myeloperoxidases that further increase vascular permeability and reduce epithelial cellular integrity. Systemic circulating monocytes infiltrate the renal intersititium, and differentiate into M1-type macrophages and dendritic cells that respectively produce ROS and inflammatory cytokines, and activate naïve T cells [26]. Enhanced vasoconstriction together with small vessel occlusion due to capillary collapse, red cell trapping and activation of the coagulation system, results in persistent or secondary localised ischaemia, especially in the outer medulla (discussed in greater detail in section 1.4).

Acute damage caused by cellular dysfunction and the subsequent inflammatory response can overwhelm repair mechanisms, and cause persistent inflammation, incomplete tubular repair, fibroblast proliferation and excess extracellular matrix deposition. Localised areas of tissue hypoxia can persist, especially in the outer medulla, where irreversible loss of up to 50% of proximal convoluted tubules has been demonstrated experimentally [20]. Thus IRI can cause chronic renal failure and fibrosis [145]. In the renal allograft, the degree of ischaemia suffered may have serious implications for both initial function and long-term survival. The incidence of acute rejection correlates with degree of ischaemic injury in animal models of solid organ transplantation, possibly through promoting antibody production by B-lymphocytes [59]. Ischaemic times during transplantation correlate with delayed graft function (DGF), whereby there is poor initial graft function, which may shorten the lifespan of a renal graft. Furthermore, the amount and type of ischaemic injury suffered by an organ is an independent factor for its function [160].

1.3.2 The renal transcriptome during ischaemia-reperfusion injury

At all levels from the cellular to the anatomical, the kidney is arguably more complex than most other solid organs. The functional unit, the nephron, is composed of at least 13 distinct epithelial cell types, with each segment supported by specialised immune cells, stroma and vasculature [134]. This manifold complexity has hampered efforts to understand both renal physiology and the pathophysiology of renal disease, including transplant ischaemia-reperfusion injury. The heterogeneity of the kidney has made it challenging to identify cell- or even tissue-specific associations with known pathophysiological events such as ROS production, especially in a dynamically-evolving environment such as IRI.

However, current and emerging high-throughput nucleic acid sequencing techniques allow the analysis of multiplexed or total gene expression – transcriptomics – with far greater granularity than that permitted by older methods.

Transcriptomic profiling along the nephron, by co-localisation of highly expressed transcripts in kidney tissue with antibody expression and histology, is helping to provide comprehensive information on gene expression in poorly studied tubular segments – such as the medullary tubules and the collecting duct – and revealing unforeseen regional gene enrichments [103, 65].

Within renal transplantation, all the evidence suggests that a single biomarker is highly unlikely to accurately reflect either the health state of an allograft, nor predict its performance after transplantation [119]. Examining the renal transcriptome during IRI may highlight broad, coordinated disruption and dysregulation of cellular and physiological processes that may not be recognised by more focused assays.

Perhaps the most complete description of transcriptional changes in renal TIRI have come from Cippa and colleagues, who analysed the transcriptomes of renal allograft cortex biopsies taken from 42 recipients at four timepoints both pre- and post-implantation. To overcome the large amount of heterogeneity and individual variation associated with such datasets, they

employed machine learning techniques to create a composite pseudotime axis upon which to plot transcriptional changes between pre- reperfusion and later biopsies. In human kidney and liver and a murine IRI model, Cippa et. al describe dynamic gene expression changes during early ischaemia reperfusion, with a primary wave of stress response gene (such as FOS and EGR1) expression peaking at 2 hours followed by transcriptional and inflammatory regulators (e.g. SOCS3, CCL2) rising at 4 hours and beyond. They further characterised a key role for mitochondrial dysregulation in promoting progression to fibrosis and chronic disease [40].

However, whilst aforementioned studies have characterised global or cortical transcriptional changes during IRI, the next-generation sequencing era is yet to impact significantly on our understanding of ischaemic damage and repair in the renal medulla.

1.4 Perfusion and oxygenation of the human kidney

The renal vasculature is highly specialised and highly unusual. Indeed, it has been said that there '...are few vascular beds with such unique anatomical and physiological characteristics as the renal circulation'[156].

The circulation of most visceral organs is arranged to support organ metabolism, with anatomy and physiology tightly coupled to oxygen demand. However, the primary functions of the kidney, haematic filtration and urine formation, necessitate renal blood flow to be far greater than would be sufficient to just meet metabolic demand. Consequently, whilst the kidneys represent less than 1% of total body metabolic demand, they receive up to a quarter of cardiac output [102]. This section will describe the renal circulation oxygenation in light of this functional paradigm, and explain how this arrangement leads to vastly disparate renal micro-environments with their own unique challenges in both health and disease.

1.4.1 The renal macrocirculation

Upon entering the renal sinus, the renal artery divides into interlobar arteries that ascend between the medullary pyramids to gain the corticomedullary junction (CMJ). Although proximal, these interlobar arteries are functionally terminal as there are no intersegmental anastomoses. Arcuate arteries describe the curved bow of the CMJ, giving rise to numerous cortical radial arteries that penetrate cortical tissue. In contrast, no arteries directly supply the medulla. Renal veins drain peritubular capillaries at all levels of the cortex and medulla, and remain closely related to arterial counterparts (as radial, arcuate and interlobar veins) until the interlobar veins coalesce to form the renal vein at the renal hilum. The cortical radial arteries and afferent arterioles are the major preglomerular resistance vessels, through which most of renal pressure-induced autoregulation of GFR and RBF is mediated [33]. Afferent arterioles arise from smaller cortical radial arteries and supply the glomerular apparatus which, uniquely amongst vascular beds [97], is then drained by a second serial arrangement of arteriole and vascular bed, namely the efferent arterioles and peritubular capillaries. Whilst more superficial efferent arterioles supply cortical peritubular capillaries, juxtamedullary efferent arterioles descend to the medulla (see Fig.1.1).

Cortical microcirculation and oxygenation

Renal cortical blood flow is the highest recorded, per gram of tissue, in the human body [93]. In the cortex, the afferent arterioles divide into tufts of specialised capillaries that form the nexus of the glomerulus, the filtration unit of the kidney. Capillary tufts are held together by mesangium and enclosed by a glomerular basement membrane. The ultrafiltrate collects in Bowman's capsule, which opens up into the proximal tubule lumen. To accommodate the enormous reabsorption of the glomerular filtrate back into the circulation, a dense capillary network arising from the efferent arteriole enmeshes the proximal and distal convoluted tubules [131].

To maintain a constant renal blood flow (RBF) and thus glomerular filtration rate (GFR), the kidney autoregulates RBF through modulating pre-glomerular renovascular resistance (RVR). Renal autoregulation ensures that the delicate glomerular structure is protected from barotrauma arising from systemic arterial hypertension, and protects the tubular apparatus from fluctuations in GFR that would affect transport processes dependent upon balanced microenvironments [33]. Fluctuations in systemic arterial pressure are accommodated through a fast-acting 'myogenic' response whereby intramural VSMC tone, and thus RVR, increases proportionally to transluminal pressure gradient. A slower response couples renal autoregulation to renal metabolism through macula-densa tubuloglomerular feedback (MD-TGF). Through MD-TGF, the composition of distal tubular fluid regulates blood flow to the individual glomerulus whence the ultrafiltrate arose. Rising distal tubular Na+ concentration activates macula densa cells in the juxtaglomerular apparatus (situated between the thick ascending limb and both afferent and efferent arterioles) to mediate afferent arteriolar contraction through purinergic transmission [98]. Through these paired mechanisms the kidney exhibits exquisite, localised, bi-directional control over renal blood flow based on both systemic and local conditions.

As renal filtration is driven by RBF and GFR, renal metabolism increases linearly with these factors; because of tubuloglomerular feedback it also increases with solute load. Tubular reabsorption and secretion are highly active processes (comprising 80% of total renal oxygen consumption [62]) and renal VO_2 is second only to myocardium (10 vs 15 ml/min/g), but because of the hyperperfusion of the renal cortex, renal oxygen extraction is only around 10% (compared to 50% in the heart) [93].

With a low metabolic demand relative to perfusion, cortical tissue PO_2 ought to be high, rendering the cortex hyperoxic and thus susceptible to oxidative stress through the production of free radicals. However, experimental values for cortical tissue PO_2 in mammals range only from 4-10kPa [93], whilst renal PvO_2 remains high. Such a marked drop in PO_2 from

renal artery to cortical tissue, in a highly perfused and vascularised tissue prompted many to suggest that excess oxygen was functionally shunted through the kidney [50]. Directly measuring A-V diffusion is extremely technically challenging [123], but several lines of evidence support the theory of cortical arteriovenous (AV) shunting. Anatomically, the renal cortical arteries and veins are closely apposed along almost their entire length, and smaller renal veins exhibit a capillary-like structure consisting only of a flattened, fenestrated epithelial layer on a basement membrane [97]. Experimentally, Welch and colleagues [169] demonstrated that murine efferent arteriolar PO_2 (average of 6 kPa) was lower than that in the renal vein (average of 6.2 kPa), suggesting that some of the oxygen in renal arterial blood diffuses directly to adjacent veins, bypassing the peritubular capillaries; observations that have been supported by subsequent mathematical modelling [123]. It has further been hypothesised that gaseous A-V shunting in the renal cortex acts as an 'anatomical antioxidant' that protects against hyperoxic damage [126].

Medullary microcirculation and oxygenation

The primary function of the renal medulla is to concentrate urine and thereby conserve body water [122]. The kidney employs a countercurrent mechanism, whereby active sodium transport from the thick ascending limb of the loop of Henle creates an osmolar gradient, allowing tubular fluid osmolality to rise fourfold against plasma [30]. Thus, the medulla maintains an axial osmotic gradient from the corticomedullary boundary to the inner medullary tip; whilst cortical tissue remains isotonic against plasma, the inner medullary tissue is hypertonic [98].

In order to maintain these osmolar gradients, medullary blood flow (MBF) is necessarily restricted compared to the cortex. The entire medullary circulation is supplied exclusively by the juxtamedullary efferent arterioles, which divide into descending vasa recta (DVR) as they enter the medulla. Juxtamedullary glomeruli comprise roughly a tenth of all glomeruli; thus

whilst a quarter of cardiac output flows into the kidney, only 10% of that even reaches the renal medulla, and then only after first passing through the cortex [53].

The unique placement of efferent arterioles after a (glomerular) capillary bed continues as the DVR descend into the medulla. The DVR are functionally similar to arterioles, with mural VSMC and contractile pericytes that can together change local vascular resistance and thus flow to the medulla [130]. As DVR approach the papillary tip they become more capillary-like, with less smooth muscle, and increased pericytes and fenestration before terminating in a medullary capillary plexus [131]. Arising from terminal plexi are the ascending vasa recta (AVR). In the same way that cortical venules appropriate capillary features, ascending vasa recta (AVR) also have a flat, densely fenestrated endothelium [97]. In contrast to the cortex, the isolated medulla exhibits poor autoregulation to changes in solute load and renal perfusion pressure, and is reliant upon pre-glomerular autoregulation [33].

The DVR and AVR are clustered into vascular bundles that become encircled by the collecting ducts and loops of Henle, which are themselves perfused by dense medullary capillary plexus [97]. Functionally, this counterflow arrangement traps NaCl and urea deposited by collecting ducts and the loop of Henle, thus maintaining the corticomedullary osmotic gradient. Metabolically however it reduces oxygen and nutrient delivery to deeper tissues as both can theoretically diffuse from the DVR to capillary-like AVR, thus being shunted back to the cortex [131, 54, 123]. Most studies of human medullary PO_2, using fine-bore Clark electrodes, suggest that tissue PO_2 is between 1-4 kPa, with values inversely related to depth and homogenous at a given depth (compared to the isohypsic heterogeneity seen in the cortex) [93]. In the outer medulla (OM), cellular processes are driven by oxidative metabolism, but in the inner medulla (IM) a significant proportion of metabolism occurs anaerobically through glycolysis and may contribute to maintaining a hyperosmolar interstitium through lactate trapping [18]. Despite lower perfusion and oxygenation, solute loading can lead to high oxygen consumption in the medullary thick ascending limbs (TAL) [31].

Measuring medullary perfusion and oxygenation

The renal medulla is challenging to study. As a deep, segmented tissue surrounded by highly vascular cortex, it is difficult to biopsy safely and more challenging to resolve using imaging techniques [135, 53]. No robust biomarkers for medullary health exist [151].

However, Evans and colleagues have postulated that the urinary oxygen tension (UO_2) may provide a 'clinical window' into the health of the renal medulla [54]. It has been demonstrated that UO_2 correlates closely with medullary PO_2, likely due to the aforementioned close anatomical association of the medullary vasa recta and the collecting ducts, and that UO_2 increases during loop diuresis, suggesting that it may accurately reflect reductions in medullary active transport and therefore oxygen consumption [107, 49].

As medullary hypoxia is a hallmark of injury, it would be expected that urine in the collecting ducts and thus renal pelvis would equilibrate with the tissue PO_2 of the inner medulla. The renal pelvis is relatively easy to instrument with probes to measure oxygenation. In experimental models of ovine septic acute kidney injury with simultaneous instrumentation of both renal medulla and renal pelvis, Evans and colleagues demonstrated that oxygenation in the renal pelvis changed rapidly with that of the medulla and was responsive to vasoactive stimuli such as norepinephrine and angiotensin II, that would alter oxygenation of the renal medulla [101, 100]. Furthermore, continuous bladder UO_2 measurement, via an indwelling catheter with fiberoptic oxygen probe, has been demonstrated during cardiopulmonary bypass surgery [89] and associated with a rapid prediction of post-operative AKI [174].

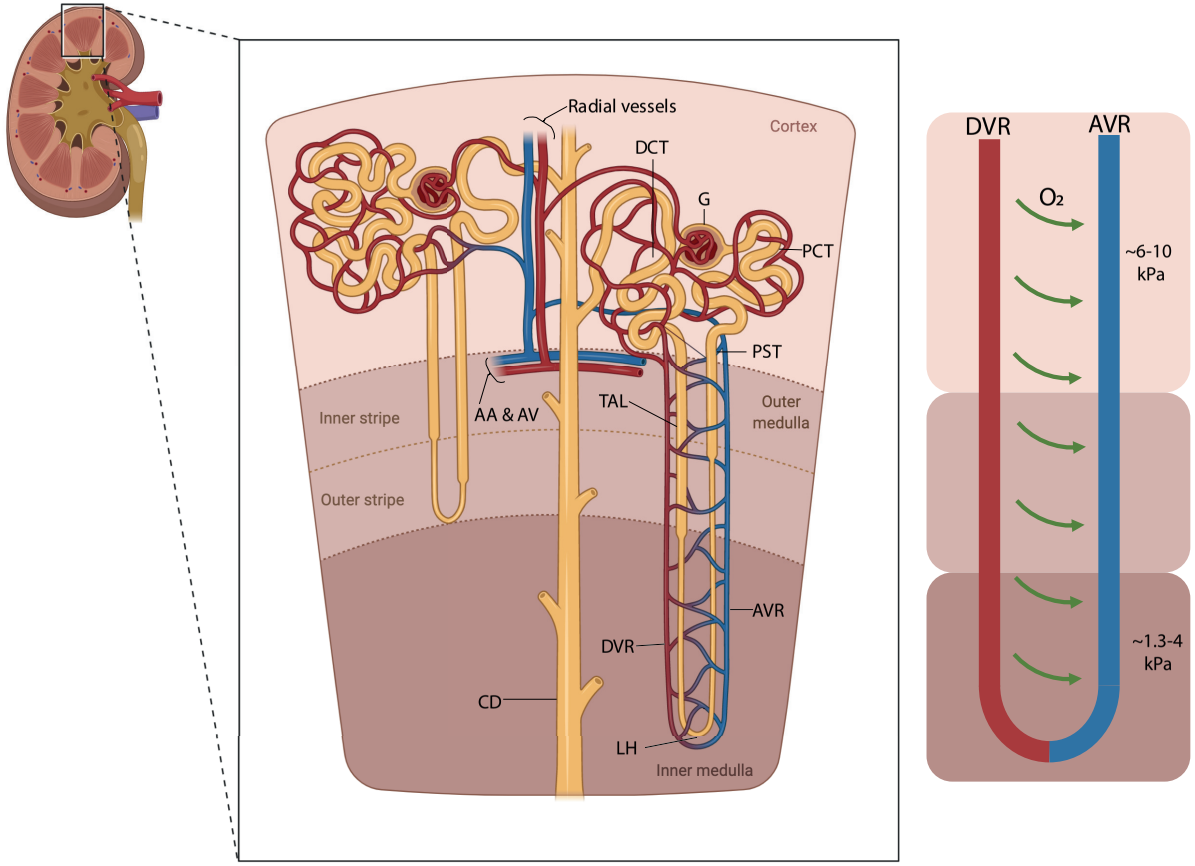

Fig. 1.1 **The renal macrocirculation.**
The renal artery divides into interlobar arteries (not shown) then arcuate arteries (AA) at the corticomedullary junction, from whence radial arteries penetrate cortical tissue. There are no anastomoses between segments (expanded feature). All blood supply to the medulla arises indirectly through efferent arterioles (coalescing as descending vasa recta (DVR)) that derive from radial arteries supplying juxtamedullary nephrons. Renal arteries and veins remain in close anatomical approximation, resulting in diffusional oxygen shunting and an overall corticomedullary oxygen gradient. AVR, ascending vasa recta; CD, collecting duct; DCT, distal convoluted tubule; G, glomerulus; kPa, kilopascal; LH, loop of henle; PCT, proximal convoluted tubule; PST, proximal straight tubule; TAL, thick ascending limb.

1.4.2 The renal circulation during ischaemia-reperfusion injury

Pertubation of the renal circulation is central to the onset, development and recovery from ischaemia-reperfusion injury as discussed in section 1.3. An overall decrease in renal blood flow (RBF) of approximately 40%–50% has been observed in poorly functioning kidney transplant allografts [11].

Cortical circulation during ischaemia-reperfusion

Endothelial damage and circulating inflammatory mediators cause heterogenous vasoconstriction in the cortex, meaning that both global RBF, cortical perfusion and GFR fall following reperfusion [138, 19, 153]. Inadequate sodium reabsorption in the injured proximal parts of the tubule leads to the macula densa sensing more solute delivery to the distal nephron, further reducing glomerular filtration through MD-TG feedback [26].

The cortical circulation and function fall dramatically during early reperfusion, with reduced vascular integrity a central cause of reduced glomerular filtration [21]. Schmitz and colleagues used intraoperative orthogonal polarization (OPS) imaging to show a heterogeneous peritubular capillary perfusion and microvascular thrombosis, resembling the classic cardiac 'no reflow' phenomenon ([70]), during the early reperfusion of human kidneys following static cold storage [147]. In a porcine model of septic AKI, a similar hypoperfused state to IRI [32], Lima and colleagues [108] used contrast-enhanced ultrasound (CUES) to demonstrate dynamic changes to cortical microcirculation during haemodynamic compromise. They reported prolonged contrast enhancement, suggestive of increased transit time across the microvascular beds and thus reduced flow; and increased baseline enhancement following a fluid bolus, suggestive of fluid 'trapping' in the microcirculation.

During IRI cortical PO_2 varies little, as cortical oxygenation remains stable despite wide variations in renal perfusion [30] and in response to both extrarenal changes in perfusion and intrarenal vasoconstriction and vasodilatation [48, 153]. During mild reductions in

renal perfusion, cortical tissue can avoid hypoxia because basal oxygen extraction is so low compared to delivery [48]. Even when changes in DO_2 and O_2 demand are mismatched in ischaemia alterations to the cortex may have the capacity to alter gaseous A-V shunting to further extract delivered oxygen [51] though there is no experimental evidence for this.

Medullary circulation during ischaemia-reperfusion

Blood flow to the outer medulla is reduced disproportionately to the reduction in total kidney perfusion in animal models of AKI [44]. As all MBF arises from post-glomerular efferent arterioles, the pathological pre-glomerular vasoconstriction that reduces GFR and cortical blood flow will also directly reduce MBF. Furthermore, it is likely that vasoconstriction of DVR (whose diameter is only just greater than erythrocytes [131]) in response to the altered endothelial microenviroment is central to promoting medullary hypoperfusion and hypoxia [102]. Moreover, localised vascular plugging due to altered rheology [72], oedema and the intrinsic lack of local autoregulation [33] compound the low-flow and low-oxygen state.

Furthermore, unlike the inner medulla, the S3 proximal tubule (pars recta) and medullary thick ascending limb (TAL) of the outer medulla are exquisitely sensitive to further reductions in PO_2 as cells cannot convert from oxidative to glycolytic metabolism [31, 122]. Thus, the greatest tissue hypoxia and cellular damage appears to occur in the outer medullary tissue [8, 20].

Circulatory recovery following ischaemia-reperfusion

After the reversal of renal artery occlusion, global renal blood flow recovers quickly within minutes [21]. However, recovery of GFR and pre-ischaemic patterns of regional RBF following IRI can be drawn out. In one series of 38 cadaveric renal allografts with postischaemic acute kidney injury, GFR one week post-implantation was up to 90% lower than that of a cohort of long-standing optimally functioning allografts [139]. Animal models suggest that

kidney autoregulation remains impaired at least 7-days after reperfusion (despite resistution of global blood flow), as evidenced by reduced reactivity to hypovolaemic and vasodilatatory challeges, likely due to persistent endothelial dysfunction [21].

As in ischaemia however, regional disparity in reperfusion may be more important that global perfusion [26]. In a rat model of renal IRI, Regner et. al describe a rapid return of cortical perfusion to baseline following 30 minutes ischaemia but a persistent, secondary decline in MBF to less than half the pre-ischaemic baseline 2 hours post-insult [144], findings that have been replicated in several other small-animal models [143] but as yet remain unexplored in either large-animal models or humans. Prolonged periods of reduced MBF post-reperfusion permanently reduces capillary density in the OM [20] promotes endothelial senesence (thus reducing repair) and promotes both early tubular necrosis and progression to tubulointerstitial fibrosis [142, 19, 176].

1.5 Methods of transplant organ preservation

The primary objective of transplant organ preservation is to permit transportation between centres, which in turn allows better histocompatibility matching and less urgent implantation [125]. The ideal kidney preservation method would have to satisfy many challenging criteria: First, it would need to avoid preservation-related injury, for long enough to allow for organ matching, transportation, and assessment, and for recipient immune-induction and surgical preparation. In practice this is a median 13.3 hours in the UK [6], and may be much longer in larger countries such as the United States. Second, an ideal method would permit investigation of the organ condition. Analysis might include physical or radiological examination, functional parameters, such as urine production, fractional excretion of sodium, renal blood flow; or tissue biomarkers that may predict graft function, such as serological markers of acute kidney injury or chronic fibrosis. In addition to providing an up-to-date assessment of the terminal organ state, ideal analysis would also inform on aspects of the retrieval and preservation process that are known to independently influence outcome, such as ischaemic damage [58]. Third, should it become clear that the organ was unlikely to function well upon engraftment, an ideal method would permit either surgical or pharmaceutical organ repair. Finally, any preservation method needs to be financially, logistically and technically feasible to permit widespread implementation, as optimal matching and organ utilisation rely upon national and international cooperation between transplant centres. Three broad methods of preservation exist: Static cold storage (SCS), hypothermic machine perfusion (HMP) and normothermic machine perfusion (NMP).

1.5.1 Static cold storage

The potential of hypothermia to promote organ storage and preservation was first mooted by Carrel and Guthrie in 1908 [34]. A century later, storage in cold (4°C) specialist solutions remains the most prevalent method of organ preservation. The aim is to reduce metabolic

demand and thus the cellular degradation that occurs during prolonged anaerobic respiration [149]. It has been demonstrated that cooling cells to near-zero degrees Celsius reduces cellular metabolism tenfold or more [23]. However, hypothermia alone is not sufficient for kidney preservation due to the deleterious effects of cold ischaemia as previously discussed. To counteract these deleterious effects, specialist solutions were developed in order to prevent cell oedema and intracellular acidosis, and promote metabolic restoration upon implantation. Many commercial solutions have been produced, with most using starches or mannitol to create a hyperosmolar solution, intracellular electrolytes, and complex anionic carbohydrates such as raffinose and lactobionate that act as lactate buffers and as substrate for ATP regeneration. The commonest kidney preservation solutions in clinical use currently are Belzer UW®, formerly known as University of Wisconsin solution (UW, Preservation Solutions Inc, USA) and Viaflex® (Soltran, Baxter, UK). At retrieval, the isolated organ is first flushed and then immersed in a cold preservation solution, sealed inside sterile bags and placed inside an insulated boxed filled with crushed ice. This method is quick, easy and affordable. However, despite the many-fold reduction in cellular metabolism, ATP and ADP depletion still continues, as the residual energy demand of the cell outstrips the ability of the cell to respire anaerobically. Over time, organ viability is lost, and a further limitation is that SCS permits only limited organ assessment prior to implantation.

1.5.2 Cold machine perfusion

The potential for a perfusion system to maintain organ vitality was postulated and investigated long before its relatively recent entrance into clinical practice. The first serious efforts to define a continuous perfusion system were made by Carrel and Lindbergh in the early 20th century [35, 41]. Following the advent of clinical transplantation, it was demonstrated experimentally that continuous cold perfusion of an organ could triple its viable storage time [22]. Hypothermic machine perfusion (HMP) describes a sterile circuit attached to

the renal vasculature, through which a preservation solution is pumped, with or without oxygen. Most devices, such as the LifePort® (Organ Recovery Systems, USA) are designed to be used in place of SCS for the duration of the preservation time. Hypothermic machine perfusion without oxygen reduces rates of DGF in DBD kidneys when compared to SCS [68], and may be similarly beneficial in DCD kidneys, although the most recent meta-analyses have produced conflicting results, with the European multicentre trial [86] demonstrating reduced rates of DGF that were not reproduced in the contemporaneous UK multicentre trial [167]. The improved preservation benefits of HMP over SCS may be due to introducing a degree of vascular shear stress, which promotes microcirculatory autoregulation [36]. Experimentally, oxygenating kidneys during HMP appears to improve preservation further, replenishing ATP and reducing oxidative stress. However, clinical data are awaited [85]. Whilst HMP offers conditioning advantages over SCS, organ assessment remains challenging. In a prospective analysis, perfusion parameters such as perfusate flow, vascular resistance and levels of perfusate injury markers such as neutrophil gelatinase-associated lipocalin (NGAL) and liver-type fatty-acid binding protein (L-FABP) offered limited correlation with 6-monthly rates of DGF; but many recipients with acceptable graft function had kidneys that had demonstrated isolated high levels of one or more marker.[133] It is further unclear to what extent such markers simply reflect pre-perfusion condition, rather than offering a contemporaneous indication of perfusion effect. The potential for targeted therapeutics to be delivered during HMP exists and has been demonstrated experimentally [87]. However, in a hypothermic system without concomitant accurate organ assessment, titrating doses to individual kidneys and monitoring renal response and toxicity may be challenging.

1.5.3 Normothermic machine perfusion

Normothermic machine perfusion (NMP) represents a logical scientific progression from HMP. The rationale is to harness the beneficial effects of perfusion and oxygen delivery

upon organ preservation whilst warming organs to near-normothermia in order to avoid the detrimental effects of hypothermia upon metabolism, organ assessment and therapeutics. The theoretical benefits of NMP over HMP and SCS are numerous, and many have been demonstrated experimentally:

Preservation

In canine and porcine experimental models of kidney transplantation, kidneys undergoing NMP have consistently demonstrated lower levels of DGF when compared to SCS or HMP [115, 80, 28]. Resuscitating the kidney to near-normothermia increases mitochondrial enzyme activity, and thus restores oxidative metabolism. A subsequent replenishment of depleted ATP and ADP [15] permits the re-establishment of intracellular homeostasis dependent upon active transmembrane transporters such as the Na-K ATPase pump. Vascular integrity is maintained through constitutive and inducible nitric oxide synthase (iNOS) flux [29], due to physiological vessel wall shear stress. Alongside restoration of physiological environment and oxidative metabolism, it appears that NMP promotes the expression of cytoprotective genes including heme-oxygenase 1 (HO-1) [165] and heat-shock protein 70 (HSP-70) [29, 80].

Assessment

The restitution of near-physiological conditions greatly aids the analysis of kidney condition during the NMP period. Perfused kidneys demonstrate renal blood flow comparable to those in vivo [74], and many organs produce appreciable volumes of urine. Such functional parameters, combined with an assessment of organ macroscopic appearance, have been combined to form a composite score that correlates well with initial graft function in a clinical series [76]. Urine and serum samples offer the potential to analyse biomarkers such

as NGAL alongside biochemistry, and appear to faithfully reflect organ damage [78], but it is unclear to what extent prognostic significance can be apportioned.

Treatment

An isolated organ perfusion circuit offers the potential to deliver targeted therapeutics direct to the intended organ, negating issues of whole-body pharmacodynamics and toxicities. Normothermia and normotension are further likely to provide more stable and predictable pharmacokinetics and monitoring over HMP. However, whilst NMP therapy has long been considered [28], and delivery of agents such as noble gases [78] demonstrate proof of principle, it remains in its infancy. More promising in the interim period are modifications to the NMP circuit to promote a beneficial immunomodulatory environment. Ferdinand and colleagues recently demonstrated transcriptional upregulation of oxidative metabolism and attenuation of inflammatory pathways in paired human kidneys following the addition of a haemoadsorption filter to the NMP circuit [55].

Normothermic machine perfusion as a research tool

Transplant IRI differs from other forms of IRI in that cessation of blood flow is complete, instantaneous and affects the entire organ (c.f. the heterogeneous occlusion of thromboemboli) and due to intervention rather than the insidious evolution of an intraluminal atherosclerotic plaque. There are therefore limited conclusions that can be drawn from models of other forms of IRI, and the use of TIRI-specific models is necessary and preferable. Whilst the NMP circuit has been designed as a therapeutic aid to clinical transplantation, the perfusion of kidneys under relatively physiological conditions permits a rare insight into whole-organ physiology during TIRI. The parameters of NMP may be altered, by removing all protective perfusate supplements, to closer mimic in-vivo reperfusion conditions. In this manner, kidney

NMP has been used to elucidate the isolated effect of WIT and relative effects of CIT and WIT upon TIRI [75, 81].

Clinical experience

The clinical use of NMP was first demonstrated in 2011 with the successful transplant of an ECD kidney following 11 hours of SCS and 1 hour of NMP [77]. A clinical series of 18 ECD kidneys followed, with significantly lower rates of DGF compared to a historical ECD control group [124]. A multi-centre UK-based randomised trial to compare NMP to SCS in DCD kidneys is ongoing (IRSCTN15821205) [79].

Perfusion circuitry and conditions

The archetypal NMP circuit is similar in principle to the HMP circuit, with the addition of a water heat-exchanger in order to warm the perfusate fluid to achieve normothermia. The current interest in kidney NMP has been driven largely by the work of Lauren Brasile (Breonics Inc, USA), and Hosgood and Nicholson (University of Cambridge, UK) who have described much of the initial large-animal experimental and human clinical data. Whilst optimal circuit conditions have been determined for certain parameters such as haematocrit [15], perfusion pressure [74] and temperature [10], others remain to be optimised. Opinions remains divided over the ideal perfusate solution, with advocates for both acellular [29] and blood-based solutions. Most clinical experience with NMP has been with the technology used as an adjunct to SCS immediately prior to transplantation. However, other modalities may be equally or more beneficial to graft function; continuous normothermic perfusion of transplant livers has shown promising early clinical results [140] and porcine models of kidney NMP suggest that similarly lengthy periods may be feasible [90, 92].

Oxygenation during kidney NMP

Most proponents of this technology have perfused kidneys with a 95% O_2 / 5% CO_2 mixture. Oxygen delivery is highly likely to be supra-physiological, as the membrane oxygenator is highly efficient and oxygen is delivered directly into the renal artery, as opposed to diffusing down the oxygen cascade. As previously described, tissue hypoxia is central to the pathophysiology of TIRI and indeed is a hallmark of many types of AKI [26]. Whilst the essential role of adequate oxygenation in normal cellular metabolism is universally appreciated, there is an increasing focus upon the negative effects of over-oxygenation in disease states involving ischaemia-reperfusion injury (IRI). Whilst the detrimental effects of hyperbaric hyperoxia were described by Paul Bert in the late 19th century [25], normobaric hyperoxia was routinely prescribed, in the form of high-flow oxygen, to patients suffering from clinical syndromes involving IRI such as myocardial infarction (MI) and stroke, until recently [113].

Growing evidence that an oxidative burst underlines reperfusion injury [120], and concerns that excess oxygen during ischaemia and subsequent reperfusion may worsen injury through ROS production [175] have prompted changes to clinical guidelines whereby oxygen delivery to patients, both in the ischaemic and reperfusion stages of MI and stroke, is now titrated to maintain arterial saturation (S_aO_2) greater than 95%.

Hypoxaemic reperfusion, whereby blood or perfusate oxygenation during reperfusion is slowly titrated upwards from a hypoxic to normoxic range, is hypothesised to reduce surplus cellular oxygen liable to contribute to ROS during reperfusion [162]. This method has demonstrated favourable reductions in circulating inflammatory markers and oxidative stress and improved oxygenation experimentally in a variety of organs in both small and large-animal models [7]. However, this method remains untested in the field of transplant kidney NMP and renal IRI.

Other organ NMP systems have successfully used much lower, physiological gas mixtures [140, 166], and concerns have been raised over whether supraphysiological oxygenation during kidney NMP may promote oxidative free radical production and thus worsen reperfusion injury [87].

1.6 Hypothesis and aims

The following hypotheses will be tested:

1. Delivering supraphysiological oxygen tensions to the kidney during NMP limits the conditioning effect of NMP upon renal function during subsequent reperfusion, due to exacerbation of oxidative damage.

2. Compared to a pre-ischaemic baseline, regional perfusion and oxygenation in a large animal model of transplant reperfusion will be dysfunctional, specifically with temporary reductions in global renal blood flow and cortical blood flow and oxygenation, and with more persistent reductions in medullary perfusion and oxygenation.

3. During a period of clinically-relevant normothermic machine perfusion, regional perfusion and oxygenation of human kidneys will be dysfunctional, specifically with temporary reductions in cortical blood flow and oxygenation and with more persistent reductions in medullary perfusion and oxygenation.

4. A period of normothermic machine perfusion following static cold storage will elicit specific and different regional inflammatory responses beyond the difference exhibited between regions during static cold storage.

Chapter 2

Methodology

2.1 Introduction

Whilst different chapters of this thesis examine varying aspects of porcine and human renal allograft physiology, all experimental models employ normothermic machine perfusion (NMP) either as a therapeutic tool or a model by which to simulate allograft reperfusion. In this chapter, methods of perfusion, measurement and analysis common to all studies are described. Specific study aims, hypotheses and study design will be described in the appropriate chapters.

2.2 Porcine kidney perfusion

2.2.1 Uncontrolled donation-after-circulatory-death retrieval

Adult female Landrace pigs weighing approximately 50kg were terminated under Schedule 1 of the Home Office Scientific Act (1986) regulations at a commercial research facility (Envigo, Huntingdon, UK). Animals were sacrificed by electrocution and rapid carotid exsanguination, from which blood was collected into a sterile receiver containing 25,000

units of heparin. Death was confirmed by absence of heart sounds upon auscultation. Kidneys were retrieved *en bloc* after a period of 10 minutes *in situ* warm ischaemia to simulate that experienced by kidneys during clinical DCD retrieval. Once retrieved, kidneys were placed on wet ice in a kidney dish and flushed with 500mL cold (4°C) Soltran® solution through the renal artery via a Tibbs cannula (Bolton Surgical, Sheffield, UK). One litre of blood was collected and stored on wet ice at 4°C in CPDA-1 blood bags for use during NMP and reperfusion experiments.

2.2.2 Controlled donation-after-circulatory-death retrieval

Controlled DCD retrieval experimental procedures were approved by the University of Cambridge Animal Welfare and Ethical Review Body. All relevant experimental procedures were carried out by personnel holding the appropriate personal animal license (Dr. T. Beach, Mr. K. Saeb-Parsy or Mr. J Martin) at an approved commercial research facility (Envigo, Huntingdon, UK). Experiments were conducted upon adult female Landrace pigs weighing approximately 50kg. Animals were pre-medicated with intramuscular ketamine (10 $mgkg^{-1}$), medetomidine (0.02 $mgkg^{-1}$) and midazolam (0.1 $mgkg^{-1}$). A peripheral intravenous catheter was placed in the marginal ear vein and anaesthesia was induced with propofol to effect. Pigs were intubated and 100% oxygen supplied with intermittent positive pressure ventilation provided to maintain normocapnia. Anaesthesia was maintained with continuous infusions of propofol (starting at 10 $mgkg^{-1}hr^{-1}$ and titrating down to effect) and either remifentanil (starting at 2.4 $\mu gkg^{-1}hr^{-1}$ and titrating up to effect) or alfentanil (starting at 30 $\mu gkg^{-1}hr^{-1}$ and titrating up to effect). If required, isoflurane was provided at approximately 2% to maintain anaesthesia. Saline was administered intravenously at approximately 10 $mlkg^{-1}hr^{-1}$. During anaesthesia a Datex Ohmeda Cardiocap (Wisconsin, USA) patient monitoring system was used to monitor ECG waveform, pulse oximetry, temperature and capnography parameters.

A midline laparotomy was performed to expose both renal pedicles, the inferior vena cava and distal abdominal aorta. The arteries and veins of both kidneys were slung with ties. Two fibre-optic probes (MNP100NX and NX-LAS-8/OT/E, Oxford Optronics, Oxford, UK) were inserted into the kidney as described in section 2.4.4 sequentially into upper pole cortical and medullary tissue to measure microvascular perfusion and tissue oxygenation at baseline and during the subsequent period of warm ischaemia. At an interval of 30 minutes, the left and right renal pedicles were ligated and kidneys were left in the abdomen to simulate 30 minutes of warm ischaemia. Once retrieved, kidneys were placed on wet ice in a kidney dish and flushed with 500mL cold (4°C) Soltran® solution through the renal artery via a Tibbs cannula (Bolton Surgical, Sheffield, UK). An intravenous bolus of heparin (500IUkg^{-1}) was administered, and after 5 minutes systemic heparinisation the distal abdominal aorta was cannulated and the pig exsanguinated. One litre of blood was collected and stored on wet ice at 4°C in CPDA-1 blood bags for use during NMP and reperfusion experiments. Pigs were euthanased by an overdose of pentobarbitone at approximately 200 mgkg^{-1}.

2.2.3 Porcine normothermic machine perfusion

The NMP circuit is designed around a paediatric cardio-pulmonary by-pass circuit (Biocon-sole 550, Medtronic, Watford, UK) consisting of venous reservoir (medtronic), non-pulsatile centrifugal pump, a heat exchanger (Chalice Medical, Worksop, UK) and an affinity mem-brane oxygenator (Medtronic) (Fig.2.1). Components were connected by ¼-inch PVC tubing. The circuit was primed with a perfusate solution (table 2.1) followed by autologous whole blood depleted of leukocytes using a white cell filter (LeukoGuard® RS; Pall Medical, Portsmouth, UK) to give a total circulating volume of approximately 1 litre. The perfusate was oxygenated with pre-mixed gases (BOC, Guildford, UK) at 0.2L/min. The standard gas mixture was 95% O_2 and 5% CO_2. The renal artery, vein and ureter were cannulated with soft silastic catheters (Pennine, UK) and kidneys were flushed with 100mL of Ringer's

Lactate solution at 4ºC immediately before perfusion to remove the high-potassium Soltran® solution. Kidneys were placed in the kidney chamber and perfused at a renal perfusion pressure (RPP) of 75mmHg for 1 hour. As a period of NMP is designed to recondition the *ex-vivo* organ, protective supplements (table 2.1) were infused into the venous reservoir and arterial arm of the circuit. Perfusion occurred at a temperature of 38.0°C, just below the normal porcine core temperature of 39.0°C.

Kidneys undergoing a subsequent period of simulated ex-vivo reperfusion (section 2.2.4) were removed from the NMP circuit and flushed with 100mL of Ringer's Lactate solution at 4°C to remove the blood and cool the organ prior to reperfusion.

Infusion fluid	Volume (mL)	Additives	Protocol	Infusion rate (mL/h)
Ringer's Lactate	1000	Creatinine 0.116g Mannitol 5g Sodium bicarbonate 8.4% 12mL Dexamethasone 3.3mg/1mL	NMP & Reperfusion NMP only	titrated to urine output
Sodium Chloride 0.9%	100	Epoprostenol 0.5mg / 16mL	NMP only	20
Synthamin 10%	500	Insulin 100 IU Sodium bicarbonate 15mL 8.4%	NMP & Reperfusion	20
Glucose 5%	1000	-	NMP & Reperfusion	5

Table 2.1 Priming solution and infusions for normothermic machine perfusion and reperfusion.

2.2.4 Porcine *ex-vivo* reperfusion

The isolated organ perfusion system described above was also used to simulate transplant organ reperfusion, either alone or after a period of NMP, to assess renal function and injury. The reperfusion model differs from NMP in that autologous whole blood is used (containing all blood components) and certain protective additives are omitted (table 2.1. The system has no ability to produce creatinine metabolically; therefore, 1000μmol creatinine (Sigma-Aldrich, Steinheim, Germany) was added to the circuit to permit creatinine clearance measurement. Kidneys were then placed on the circuit and reperfused at an RPP of 85mmHg for 3 hours at 38ºC. All kidneys were reperfused with a 95% O_2 and 5% CO_2 gas mixture.

2.3 Human kidney perfusion

2.3.1 Human organ procurement

From November 2017 until April 2019, 25 human kidneys offered for research by the national organ allocation system (after being deemed unsuitable for transplantation [125]) were recruited into studies in this thesis. Consent for organ use in research was obtained from the donor's family by a specialist nurse in organ donation prior to retrieval. Donor organs exhibiting any absolute contraindication to transplantation, such as malignancy, were excluded from recruitment. All organs were retrieved by one of the National Organ Retrieval teams; after an *in-situ* flush of abdominal organs with either University of Wisconsin solution or hyperosmolar citrate, kidneys were retrieved and stored on ice at 4°C. After recruitment into studies, organs were transported during SCS to Addenbrooke's Hospital, Cambridge, UK. Ethical approval was granted for studies by the National Research Ethics Committee in the UK (number 5/NE/0408). Where possible, donor demographic information was recorded including age, sex, cause of death and terminal creatinine.

2.3.2 Human kidney normothermic machine perfusion

The methodology for human kidney NMP is broadly similar to that described above for porcine kidneys (see above) aside from three key differences. Firstly, the human kidney was placed into a custom sterilisable metal chamber as opposed to a custom glass chamber; all other circuit components were identical. Secondly, one unit of O-positive blood group packed red cells from the local blood bank was added to the priming solution, as opposed to autologous donor blood. Finally, different infusions were added to the perfusate: manntiol 10% 15 mL (Baxter Healthcare), dexamethasone 6 mg (Organon Laboratories, Cambridge, UK) and 3mL of heparin 1000 IU/mL (CP Pharmaceuticals, Wrexham, UK). Amino acids (Synthamin, Baxter Healthcare UK) with sodium bicarbonate 15 mL 8.4% and insulin 100

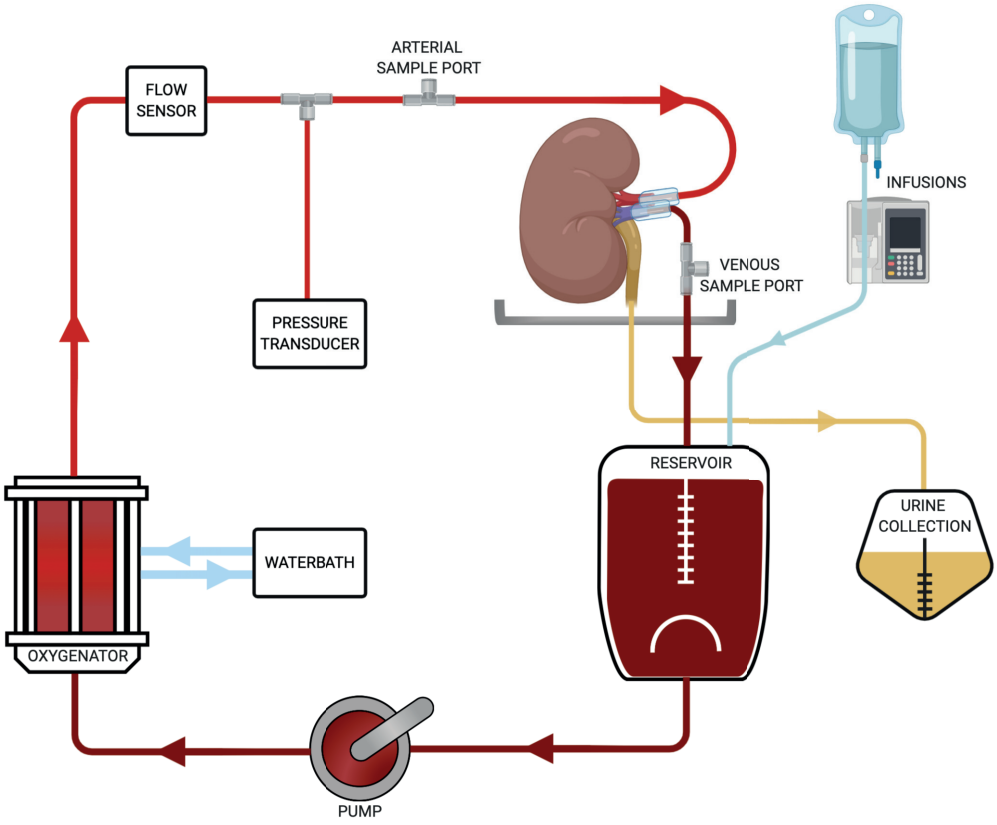

Fig. 2.1 **Human and porcine kidney normothermic machine perfusion.**
Schema of porcine and human kidney normothermic machine perfusion. The organ is placed in an organ chamber and the renal artery, vein and ureter cannulated. The blood-based perfusion solution drains from the kidney with gravity into the venous reservoir, whereby continuous infusions (detailed in table 2.1) are added. A non-pulsatile centrifugal pump drives the solution through a heater-oxygenator, past flow and pressure sensors back to the renal artery.

IU (Novo Nordisk, Denmark)was infused into the circuit at a rate of 20 mL/h. Prostacyclin 0.5 mg (Flolan, Glaxo-Wellcome, Middlesex, UK) was infused into the arterial arm of the circuit at a rate of 4 mL/h and glucose 5% (Baxter Healthcare) at 5 mL/h. Ringer's solution was used to replace urine output at a 1:1 ratio. As per the porcine reperfusion model, 1000 μmol creatinine was added to the circuit to permit creatinine clearance measurement.

2.4 Analytical techniques

2.4.1 Renal function and oxygen kinetics

Renal function

Renal blood flow (RBF) and Renal Perfusion Pressure (RPP) were recorded continuously and intra-renal resistance (IRR) calculated (RPP/RBF). Urine output was also measured during reperfusion and hourly serum, urine and tissue collected. Percentage fall in creatinine clearance was calculated, and fractional excretion of sodium also calculated as:

$$((Na_{urine} \cdot Vol_{urine}/(GFR \cdot Na_{plasma}) \cdot 100))$$

Oxygen kinetics

Blood gas analysis (Blood Gas Analyser; OPTI CCA-TS, Optimedical, Roswell, GA, USA) was used to record arterial, venous and urinary partial pressures of oxygen (P_aO_2, P_vO_2 and UO_2 respectively), arterial partial pressure of carbon dioxide (P_aCO_2) and acid–base homeostasis. In porcine experiments oxygen saturation values were corrected using a porcine-specific hemoglobin dissociation equation [150], where:

$$S_aO_2 = (0.13534 \cdot PO_2)^{3.02}/(0.13534 \cdot PO_2)^{3.02} + 91.2$$

to which a factor of $0.022(-0.3 \cdot \Delta pH)$ was applied to correct for Bohr effects upon HbO binding.

Arterial and venous oxygen content (C_aO_2 and C_vO_2 respectively) were calculated:

$$C_aO_2 = (1.34(Hb) \cdot S_aO_2 \cdot 0.01) + (0.023 \cdot P_aO_2)$$

Oxygen consumption (VO2) was calculated by comparing oxygen delivery ($DO_2 = C_aO_2 \cdot RBF$) and return ($RO_2 = C_vO_2 \cdot RBF$). The oxygen extraction ratio ($OER = VO_2/DO_2$) was also calculated.

2.4.2 Perfusate and urine biochemistry

Samples of circulating perfusate solution and urine were collected hourly. Samples were processed by the Addenbrooke's Hospital Biochemistry Laboratory under a research protocol to yield clinical markers of haematology, renal function and osmolality.

2.4.3 Histology

During NMP experiments, tissue biopsies were taken for later histological analysis. It was possible to take cortical wedge biopsies during perfusion; however it was not possible to take deeper medullary samples during perfusion without causing considerable haemorrhage from the heparinised kidney. Therefore, after the cessation of perfusion the kidney was immediately bivalved and medullary biopsies taken. Biopsies were immediately divided and samples for molecular analysis snap-frozen in liquid nitrogen before storage at -80°C. Tissue for histology was fixed overnight in 10% formalin before storage in 100% ethanol. Haematoxilin and Eosin (H&E) stained slides and formalin-fixed paraffin blocks (FFPE) were obtained from the Addenbrookes Hospital Histopathology service. For assessment of tubular injury, a blinded observer (TDA) scored 10 fields per sample under light microscopy

at 40x magnification for evidence of tubular damage, according to criteria outlined in table 2.2.

Category	Percentage of field affected and associated score			
	0-24%	25-49%	50-74%	>75%
Epithelial Flattening Tubular Dilatation Vacuolation Tubular Debris Interstitial Oedema	0	1	2	3
Cumulative Score	0 – 15			

Table 2.2 Histological score for cortical tubular injury

Martius, scarlet and blue staining for fibrin deposition

Four micrometre tissue sections were cut from FFPE blocks using a microtome, mounted upon standard glass slides and dried overnight. Mounted sections were de-waxed through two changes of xylene, two changes of 100% ethanol and sequential changes of 95%, 70% and 50% ethanol, each for 5 minutes. Slides were stained with Haemalum Mayer (3m) and rinsed in 95% EtOH; then with Martius Yellow Alcoholic for 2m, Brilliant Crystal Scarlet for 10m, Phosphtungstic Acid for 7m and Soluble (Aniline) Blue for 10m; with brief water washes between stains. Slides were then dehydrated through four 5m changes of EtOH (95%, 95%, 100%, 100%) and cleared in three 5m changes of xylene. Slides were mounted with DPX and a coverslip and left to dry overnight.

Twenty bright-field images of each slide (each corresponding to a single kidney region) were taken in a blinded fashion at 2448 x 1920 pixel resolution. Fibrin deposition for each section was quantified objectively using a MATLAB (v. R2017b, Mathworks, UK) script (see appendix B) by filtering image pixels according to user-defined RGB pixel-profiles of fibrin-

positive and -negative regions in representative images. Binary images of positive/negative pixels were thus created, from which percentage fibrin deposition was derived. The MATLAB code was developed by Dr. J. DiRito and samples from this project were analysed by Dr. A. Silva.

2.4.4 Measurement of microvascular oxygenation and perfusion

To measure intrarenal microvascular perfusion and tissue oxygenation, fibre-optic probes were inserted into the cortex or medulla of kidneys.

The tissue oxygenation probe used (NX-LAS-8/OT/E, Oxford Optronix, Oxford, UK) is a fluorescence lifetime oximeter (FLO) that quantitatively measures the tissue partial pressure of oxygen (tPO_2) across an area of $8mm^3$. The probe tip optode contains a platinum-complex photolumiphore excited by light (475nm) pulsed along a fibre-optic cable. Upon excitation the lumiphore emits 600nm light back to a detection unit (Oxylite Pro, Oxford Optronix, Oxford UK). Dissolved tissue oxygen in the probe vicinity quenches the fluorescent light, increasing the decay time of light returned in inverse proportion to the local tPO_2. This inverse relationship means that it is possible to accurately quantify tPO_2 even at values close to zero.

The microvascular perfusion flow probe (MNP100NX, as above) utilises Laser-Doppler Flowmetry (LDF) to provide a continuous measure of tissue blood flow. A low-power laser light illuminates and is scattered within the tissue region of interest. Scattered laser light incident upon moving red blood cells becomes Doppler-frequency shifted as a result and is returned by a second optical fibre to the monitor (Oxyflo Pro, as above). The photo-detected signal comprises a broad spectrum of Doppler frequency shifted signals generated as a result of the movement of red blood cells within the tissue. Microvascular blood flow is electronically calculated as the product of mean red blood cell velocity and mean red blood cell concentration in the volume of tissue under illumination from the sensor.

In order to site probes, a small incision in the kidney capsule was made. Cortical probes were sited <3mm from the surface; medullary probes were advanced until a depth of 10mm and a change in resistance was felt, denoting entry into medullary tissue. Probes were sited in the kidney prior to the commencement of perfusion. Probes then remained in-situ throughout perfusion unless otherwise stated. Probes were sited in both medulla and cortex concomitantly (unless otherwise stated). In experiments where probes were not continuously situated, care was taken to ensure that probes were reintroduced to the same incision as before. Probe depths were confirmed *post-hoc* by sectioning the kidney.

Oxygen and Perfusion probes were connected to dual-channel monitors (Oxylite Pro and Oxyflo Pro respectively, both Oxford Optronix). Data were recorded using Labchart Pro v7.3.8 (AD instruments, Dunedin, NZ).

2.4.5 Molecular biology techniques

Enzyme-linked immunosorbent assay

Cortical tissue and pelvicalyceal urine samples from certain porcine NMP experiments were analysed after 3 hours reperfusion for levels of high-mobility group box 1 protein (HMGB-1) and neutrophil gelatinase-associated lipocalin (NGAL) using porcine NGAL and HMGB-1 sandwich ELISA kits (Elabscience and Cusabio respectively, both Wuhan, P.R. China). Cortical tissue and fresh urine samples were snap frozen in liquid nitrogen, and tissue was cryogenically homogenized. Samples and standards were added in duplicate to pre-coated plates and the assays were carried out as per the manufacturer's instructions. Cortical tissue was diluted to 1:100 for the HMGB-1 assay, and urine to 1:40 for the NGAL assay.

RNA extraction from tissue samples

All tissue samples were snap frozen at -70°C. Tissue was homogenized in 1 μL lysis buffer using a Precellys 24 homogenizer (Bertin Instruments, France) for 2x15s at 6000rpm and

centrifuged at 13000g for 1min until tissue appeared homogenized. Samples were then spun in a tabletop microcentrifuge for 5min at 2600g. Supernatants were added to EtOH and RNA was extracted using the Purelink RNA Mini Kit (Thermo Fisher Scientific, USA) according to manufacturer's instructions. Sample DNA was digested using the Turbo DNA-Free kit (Thermo Fisher Scientific, USA) according to manufacturers instructions and samples eluted in 50μL RNAase- and DNAse-free water. The RNA yield was assessed using a NanoDrop ND-100 Spectrophotometer (Thermo Fisher Scientific, USA) and RNA integrity quantified using an Agilent 2100 bioanalyzer (Agilent Technologies, USA) according to the manufacturer's specifications. Samples with an RNA integrity number (RIN) >8 and A260/280 ratio of 1.8 were considered acceptable for further analysis.

Nanostring nCounter multiplex analysis

The expression of 255 pre-selected genes was quantified in RNA samples without amplification using nCounter analysis (Nanostring Technologies, USA) according to manufacturer instructions. The nCounter codeset consists of biotinylated 'capture' probes for 249 pre-selected human inflammation-related genes (see appendix D.1) and 6 internal reference genes, and corresponding 'reporter' probes encoding a molecular barcode specific to the gene of interest. Hybrids of the sample RNA and codeset probes were formed. The target-probe complexes were then purified, aligned and immobilised before digital imaging and quantification. Purified RNA samples were diluted to give a final assay concentration of 100ng. Five microliter aliquots of sample RNA were hybridized for 20 hours at 65°C with 10 μL nCounter XT Human V2 Reporter codeset, 5 μL capture probeset snd 10 μL hybridization buffer. Target-probe complexes were then loaded into the nCounter prep station for digital counting.

2.5 Statistical analysis

Data passing the Shapiro-Wilk normality test (alpha=0.05) are presented as mean ± SD and data failing this test are presented as median (range). Levels of continuous variables such as RBF were plotted against time using GraphPad Prism version 7.00 for Mac (GraphPad Software; San Diego, CA, USA, www.graphpad.com). Mean values of parametric data passing the normality test were compared using one-way ANOVA and Tukey's multiple comparisons test , and data failing this test by non-parametric tests of null hypotheses and variance (Mann-Whitney and Kruskall-Wallis respectively).

Ncounter Advanced Analysis software v.2.0.115 (Nanostring Technologies, USA) was employed to normalise Ncounter data against selected housekeeper genes present on the codeset by the geNorm algorithm [163]. Differential gene expression expression was calculated using nCounter Advanced Analysis optimal method with the Benjamini-Yekutieli *P*-value adjustment [82]. Volcano plots of differentially-expressed genes were plotted using GraphPad Prism version 7.00 for Mac (GraphPad Software; San Diego, CA, USA). To visualise mRNA expression data, principle component analysis and heatmaps were created using the ClustVis web tool [116]. Principle component analysis was calculated by Singular Value Decomposition (SVD) method with unit variance scaling. Heatmaps were clustered by Euclidean distance and average linkage methods. The expression of genes of interest during these experiments was qualitatively compared with in-vivo expression in healthy tissues by interrogation of the Genotype-Tissue Expression (GTEx) project database of kidney-specific gene expression. The GTEx database contains gene expression data of 54 non-diseased tissue sites across 980 individuals [63]. The data used for the analyses described in this manuscript were obtained from the GTEx Portal (gtexportal.org) on 11/06/20.

Chapter 3

Reducing perfusate oxygenation during porcine kidney normothermic machine perfusion

3.1 Introduction

Normothermic machine perfusion is a promising technology that may increase utilization of marginal deceased-donor kidneys [87]. However, ideal perfusion conditions for a donor kidney - including duration [91], temperature [10], perfusate composition and oxygenation - remain unclear. Most experimental and clinical NMP systems, including the Hosgood-Nicholson circuit, perfuse kidneys with a gaseous mixture of 95% O_2 and 5% CO_2. There is no clear evidence base for providing supraphysiologically oxygenated perfusate, but it likely arises from a desire to avoid the the tissue hypoxia universally associated with IRI [26] by perfusing the injured kidney with excess oxygen to overcome IRI-related hypoperfusion.

However, oxygen surplus to metabolic requirements may cause *de novo* tissue injury through the production of reactive oxygen species (ROS) [121, 175] which experimentally have been reduced through rendering reperfusion perfusates hypoxaemic, and other organ

perfusion systems have successfully employed more physiological gas mixtures (section 1.5.3).

The aim of this study was to investigate the physiological effects of reducing NMP perfusate oxygenation upon renal function and oxygen kinetics during NMP and subsequent reperfusion. Related to our aim, we hypothesised that:

1. Reducing perfusate oxygenation (P_PPO_2) to normoxaemia or hypoxaemia would reduce renal oxygen delivery and consumption during NMP.

2. Reducing P_PO_2 to normoxaemia or hypoxaemia would reduce renal function during NMP.

3. Reducing P_PO_2 to normoxaemia or hypoxaemia would reduce tissue injury following reperfusion.

The finding of this chapter have been published in the *American Journal of Physiology-Renal Physiology* [9].

3.2 Methodology

Using a porcine model of donor kidney retrieval and perfusion, two experiments were designed to interrogate the effects of lowering reducing perfusate oxygen tension (P_PO_2) upon kidney performance during NMP and upon subsequent reperfusion. Both studies were designed to simulate current clinical trial protocols for donor organ perfusion in the immediate pre-implantation phase.

In a 'minimal injury' experiment (MI), designed to investigate the effect of P_PO_2 upon renal function during NMP, groups of kidneys were subjected to 10 minutes of warm ischaemia (WI) and 2 hours of static cold storage (SCS) before 1 hour of NMP with different gas concentrations. Pilot data suggested that a 12% O_2 mixture would result in a P_PO_2

similar to in-vivo P_aO_2(12kPa) and a 6% mixture would result in a hypoxic P_PO_2 of half that *in-vivo* (6kPa). Hence these, and an intermediate hyperoxic gas mixture (25%), were chosen to compare against standard (95%). A further group was perfused with medical air (20.9% O_2, 0.04% CO_2, 78.09% N_2, 0.93% Argon and other trace gases).

In a 'clinical injury' experiment (CI), groups of kidneys underwent similar retrieval and WI before a longer and more clinically relevant SCS time of 17 hours prior to NMP with either 95%, 25% or 12% O_2. These kidneys, plus a control group that had not undergone NMP, then underwent 3 hours of simulated reperfusion. This second experiment was designed to investigate the effects of varying P_PO_2 upon renal function and injury during reperfusion following a period of NMP designed to simulate the restoration of perfusion in a kidney transplant.

Kidneys from adult female landrace pigs underwent uncontrolled DCD retrieval (section 2.2.1) prior to storage in Soltran solution at 4°C for 2 hours (MI study) or 17–18 hours (CI study). Normothermic machine perfusion was performed for one hour (see section 2.2.3) during which renal function (section 2.4.1) and oxygen kinetics (section 2.4.1) were measured. In the CI experiment, kidneys then underwent a further 3 hours of simulated reperfusion (section 2.2.4) after which cortical biopsies were taken for analysis of tissue injury markers high-mobility group box 1 protein (HMGB-1) and neutrophil gelatinase-associated lipocalin (NGAL) using porcine ELISA kits (section 2.4.5).

3.3 Results

3.3.1 Minimal injury model

Baseline Perfusion Characteristics (Table 3.1)

Initial perfusion conditions were well matched, with no significant differences in starting pH (mean 7.41±0.04), haematocrit (0.18±0.07) or haemoglobin concentrations (49.1±2.0g/L)

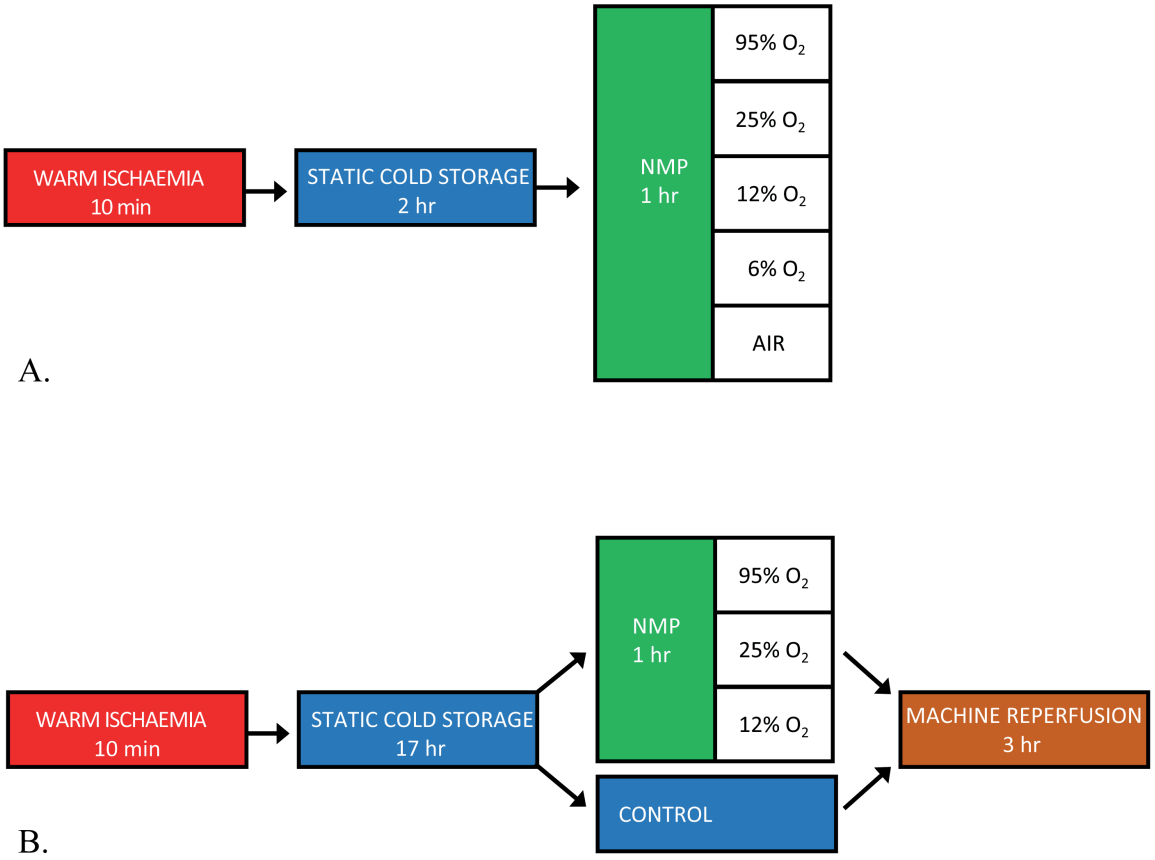

Fig. 3.1 **Experimental design for porcine normothermic machine perfusion and reperfusion with variable perfusate oxygenation.**
In a 'minimal injury' experiment (MI, diagram A), designed to investigate the effect of P_PO_2 upon renal function during normothermic machine perfusion (NMP), groups of kidneys were subjected to 10 minutes of warm ischaemia (WI) and 2 hours of static cold storage (SCS) before 1 hour of NMP with different gas concentrations. In a 'clinical injury' experiment (CI, diagram B), groups of kidneys underwent similar retrieval and WI before a longer and more clinically relevant SCS time of 17 hours prior to NMP with either 95%, 25% or 12% O_2. These kidneys, plus a control group that had not undergone NMP, then underwent 3 hours of simulated (machine) reperfusion.

between groups (Table 3.1). Perfusate oxygenation was significantly greater in the 95% group (81.7±7.1) than all other groups (adjusted P>0.0001 for all comparisons). Delivering 25% O_2 and air returned led to a similar P_PO_2 (21.7±3.4 and 19.1±2.4 kPa respectively, P=0.8). The air group P_PO_2 was significantly lower than the 95% and 6% groups but not 25% or 12% groups. Values in the two groups given the lowest P_PO_2, 12% and 6%, were also similar (11.9±0.7 and 7.2±0.7 kPa respectively, P=0.4) but significantly lower than the 25% and 95% groups.

Renal function and haemodynamics (Fig. 3.1)

After 1 hour of NMP, mean RBF in the 6% group (82.4±6.9 ml/min/100g) was the highest, significantly so compared to all other groups (Fig.3.2A). The lowest mean RBF was in the 25% group (21.5±5.2 ml/min/100g), also signicantly so versus all other groups. Urine output at the end of NMP (Fig.3.2B) was highest in the 6% group (6.1±4.0 ml/min/100g); significantly higher than in the 95% and 25% groups (2.0±1.6ml/min/100g P=0.01 and 1.8±0.7ml/min/100g P=0.03 respectively). Creatinine clearance (Fig.3.2C) and fractional excretion of sodium (Fig.3.2D) were comparable across groups, with no significant intergroup variation.

Oxygen kinetics (Table 3.2)

Arterial oxygen content (C_aO_2) was similar across groups, as was end-NMP pH; save for in the air group, which had a significantly higher pH (7.55±0.11) compared to all other groups (table 3.2). Oxygen delivery (DO_2) in the 95% group was significantly greater than in the 25% O_2 group (4.2±2.0 vs. 1.7±1.1 mL/min/100g, Tukey's multiple comparisons test P=0.017) but not the 12% group (2.9±1.1). Oxygen consumption in the 95% O_2 group (1.1±0.4ml/min/100g) was significantly greater than both 25% and air groups (0.4±0.2, P=0.035, and 0.4±0.2, P=0.032 respectively, both Tukey's multiple comparisons test). Oxy-

gen extraction (OER) was greatest in the 95% and 6% groups (both 0.3±0.1) and smallest in the 12% group.

Correlations between circuit parameters, renal function and oxygen kinetics (Fig. 3.3)

A correlation matrix was performed on the pooled terminal (1-hour) values for NMP circuit parameters, renal function and oxygen kinetics, revealing a number of significant relationships (Fig. 3.2).

Linear regression demonstrated a significant positive relationship between renal blood flow and urine output (Fig. 3.3A), creatinine clearance (Fig. 3.3B), oxygen delivery (Fig. 3.3C) and consumption (Fig. 3.3D). There was a significant negative relationship between fractional sodium excretion and both renal blood flow (Fig. 3.3E) and VO_2 (Fig. 3.3F).

Urine Oxygenation

Pelvicalyceal urine oxygen tension, measured at the end of NMP, was significantly higher in the 95% group (19.16±2.5 kPa) compared to all other groups (Fig.3.6A). No other significant inter-group variation was demonstrated. Linear regression of the relationships between markers of renal function and oxygen kinetics revealed that both renal blood flow (Fig.3.6B) and oxygen consumption (Fig.3.6 C) had significant positive associations with UO_2 and that there was a significant negative relationship between sodium excretion and UO_2 (Fig.3.6D).

3.3.2 Clinical injury model

Baseline Perfusion Characteristics (Table 2)

As with the minimal injury experiment, perfusate oxygenation differed significantly between groups. The starting pH and haematocrit of groups was similar. However, the starting Hb of the 25% group, 39.2±4.9 g/L, was significantly decreased compared to the other two groups (47.6±1.7 in 95%, *P*=0.034; 47.8±7.6 in 12% group, *P*=0.021).

Normothermic perfusion renal function and haemodynamics

Percentage sodium excretion was significantly decreased in the 25% group (70.5±19.3%) compared to the 12% group (86.7±4.9%, *P*=0.048). No statistical differences were seen in perfusate pH, urine output or creatinine clearance (*P*=0.726, 0.375 and 0.562 respectively, all one-way ANOVA). Renal blood flow in the 25% group was significantly increased compared to the 95% group (42.8±4.1 vs. 35.2±6.6 ml/min/100g, *P*=0.035). Oxygen content in the 95% group, 7.9±0.9 ml/100mL, was significantly greater than the other groups (*P*=0.0005 vs. 25%, *P*=0.006 vs. 12%) but this did not result in greater oxygen delivery (*P*=0.97). Oxygen consumption was similar across groups, but extraction was significantly greater in the 95% group compared to the 12% group (0.3±0.1 vs 0.2±0.1, *P*=0.037).

Reperfusion

Urine output, sodium excretion and creatinine clearance were not significantly different between groups (Fig. 3). Mean RBF was significantly elevated in the 25% group when compared to all other groups, (42.8±12.0 ml/min/100g vs. 23.3±7.1 in 95% group *P*= 0.001, vs. 27.7±6.7 in 12% group *P*=0.012, vs. 28.4±6.0. in control group *P*=0.017). The control group pH (7.18±0.04) was lowest of all groups, significantly versus the 25% group (7.41±0.12, *P*=0.0007). There were no significant differences observed in oxygen content, delivery, consumption or extraction during the reperfusion phase (table 3.4).

Injury Biomarkers

After 3 hours of reperfusion, NGAL was present in urine samples from all kidneys, although no differences were noted between groups (95% 152.5±150.7, 25% 232.1±46.6, 12% 237.3±51.5, control 238.4±127.0 ng/m; P=0.54). Similarly, end-perfusion tissue levels of HMGB-1 were not significantly disparate (1.0±0.1, 0.9±0.2, 0.8±0.1 and 0.8±0.1µg/mL for 95%, 25%, 12% and control groups respectively, P=0.11) (Fig.3.8).

3.4 Discussion

We used a porcine model of donor kidney retrieval, NMP and reperfusion to test the hypothesis that reducing perfusate oxygenation (P_PO_2) to normoxic levels would have detrimental effects upon renal function and cause injury. In kidneys exposed to either short or long cold ischaemic times, we measured renal function and biomarkers of kidney injury after NMP with hyperoxic or normoxic P_PO_2. The main finding of our study was that reducing P_PO_2 altered oxygen kinetics during NMP, but did not convincingly influence tubular function, clearance, urine output or biomarkers of renal injury during reperfusion.

These results are significant primarily because we are not aware of previous reported studies comparing various P_PO_2 during renal NMP; furthermore, our model uses the same NMP protocol as the first randomised clinical trial comparing NMP with SCS in DCD kidneys (IRSCTN15821205) and so may inform nascent clinical practice.

In studies demonstrating NMP in canine and bovine renal autotransplant models, Brasile and Stubenitsky utilised a proprietary acellular perfusate solution complemented with either pyridoxylated bovine haemoglobin or a perfluorocarbon emulsion as an oxygen carrier [157]. Their perfusion circuit included controllers to maintain a P_PO_2 of 200mmHg (26.6kPa) though it is not clear what gas mixture was used or the rationale behind choosing this value [158]. With a reported P_PO_2 similar to that seen in our 25% O_2 groups, the authors demonstrate cytoprotective gene induction [27] and delivery of therapies [28] during NMP. However, comparisons with our circuit are limited, as perfusion was carried out at 32°C rather that 37°C, with an acellular solution rather than a blood-based solution, and P_PO_2 was analysed using a blood gas analyser calibrated for human rather than bovine haemoglobin measurement. Comparisons with our own circuits are therefore limited.

3.4.1 The effects of perfusate oxygenation on renal function and oxygen kinetics during NMP

Changing perfusate oxygenation did not appear to have any consistent effect upon renal function or oxygen kinetics. In the MI study, the greatest differences (in terms of RBF, UO and pH) were seen between the 25% and 6% groups rather than the more oxygenated 95% group; no significant differences were demonstrated in terms of oxygen delivery, consumption or extraction. Different trends were seen in the CI study, with the 25% group here having significantly greater RBF and lower FE_{Na} than the 95% or 12% groups.

As differences between groups were not consistently proportional to perfusate oxygenation we would instead suggest that differences between groups may represent limitations of our model in terms of varying hemodilution, or ischaemia-induced vasoconstriction.

As pump speed and perfusate PCO_2 were constant, perfusion pressure and RBF are a direct function of vascular resistance. We suggest that heterogenous vascular resistance may reflect variation in IRI-induced endothelial damage [26]. Furthermore, whilst the kidney maintains tight vascular autoregulation in vivo, IRI-induced endothelial damage, vascular congestion and oedema, compounded by an absence of neuro-humoral input, may limit renovascular responses to hyperoxia during ex-vivo NMP. It has further been suggested that the renal vasculature is more sensitive to changes in CO_2, which was controlled in our experiments. In the CI study, CaO_2 during NMP was significantly raised in the 95% group compared to other groups. This may reflect haemodilution of the other groups, and also a significantly reduced starting Hb in the 25% group (table 3.6). Differences in haemodilution may occur due to varying rates of circulating fluid replacement in response to urine output.

We suggest that our results correspond with current understanding on renal responses to arterial oxygenation, and the unique regulation of renal metabolism by systemic fluid status rather than local conditions. Unlike other tissues, renal oxygen consumption normally increases linearly with RBF because the rate of glomerular filtration and tubular resorption,

the primary renal active processes, normally increase with RBF [53]. Positive relationships between RBF, urine output and oxygen consumption were also seen on our *ex-vivo* circuits (Fig.3.3 and 3.4). Regulation of extracellular fluid and electrolyte predominates over local metabolic requirements, and neither hypoxemia nor hyperoxemia alter vasomotor tone in the presence of isocapnia. [51, 152] Reducing arterial, or perfusate, oxygen tensions to normoxia from hyperoxia would therefore not be expected to influence RBF or renal function [52]. In the unique hyperoxic NMP setting, diffusional arterio-venous oxygen shunting - thought to exist to prevent tissue oxidation that might otherwise arise due to the mismatch between metabolic needs and the disproportionately high blood flow needed for filtration [49] - may limit superfluous oxygen delivery to the renal microvasculature.

3.4.2 The effect of altering NMP P_PO_2 upon renal function, injury and oxygen kinetics during subsequent reperfusion.

Importantly, none of the differences in renal function or oxygen kinetics during NMP translated into differences during subsequent reperfusion. Kidneys receiving 25% P_PO_2 during NMP did have significant greater RBF during reperfusion, but this did not lead to higher UO or lower FE_{Na}. After 3 h of reperfusion, NGAL was present in urine samples from all kidneys, although no differences were noted between groups. Similarly, end-perfusion tissue levels of HMGB-1 were not significantly disparate.

During reperfusion, oxygen extraction values were much greater than those reported in-vivo (0.10-0.15)[Hansell et al.], and fractional sodium excretion was greater than in-vivo across experiments. These supra-physiological results may represent further limitations to our model. The high FE_{Na} may represent the considerable tubular damage sustained due to ischaemic injury in this model, but also the fact that perfusate sodium levels tend to be hypernatremic (150-160mmol/L), leading to a high solute load. The increased oxygen extraction during reperfusion, compared to NMP, may represent the absence of vasodilators

and dexamethasone that are added to the NMP perfusate. Without prostacyclin there could be localised reductions in DO_2 (despite no differences in global delivery), and without dexamethasone there could be increased VO_2 following greater IRI-related inflammation.

3.4.3 Limitations

The pigs used were young, healthy females, a healthier and more homogenous population than transplant kidneys that are older and frequently come from donors with systemic or renal pathologies. The electrical stunning used in termination causes massive catecholamine release [12] which may cause renal vasospasm, thereby affecting perfusion during back-bench flushing and subsequent machine perfusion. A porcine model of DCD retrieval using an asphyxia technique suggests that catecholamine rises after withdrawal of life support may occur more slowly [83]. Our model may therefore have caused greater vasospasm than might be expected in the clinical setting. The use of a 'controlled' model of porcine DCD kidney retrieval, whereby the animal is subjected to terminal anaesthesia prior to a rapid en bloc retrieval, may reduce stress-related vasospasm, however it is more costly and inhaled anaesthetic agents have a protective effect against IRI [37]. During the clinical-injury study, all organs undergoing NMP were subsequently reperfused with a 95% O_2 gas mixture. This was performed in order to be able to compare these data with historical groups. However, it is possible that oxidative damage suffered by all groups during the reperfusion period may negate any differences that might have been seen directly after NMP with different P_PO_2. The calculation of renal blood flow and mean arterial pressure are derived from the circuit flow transducer. It therefore describes global changes in perfusion. Similarly, global VO_2 was calculated using arterial and venous blood. The kidney is an organ with a markedly heterogeneous blood flow, in which localised microcirculatory changes are thought critical to the renal response to IRI [44]. It is likely therefore that measurements of global RBF and MAP are insensitive to differential changes between cortex and medulla. As renal DO_2 and

VO_2 have a linear relationship with RBF, it is likely that regional differences in oxygenation are similarly critical [49]. The use of invasive needle probes could elucidate localised changes in perfusion and oxygenation. There are limitations to the conclusions that can be drawn from plasma samples taken from the NMP circuit, as they represent a circulating perfusate operating without physiological buffering or hepatic clearance. Creatinine was added to the circuit as a bolus, rather than the continuous 'loading' seen in vivo as a by-product of muscle turnover. Creatinine clearance therefore is not comparable to clinical parameters, and clearance measurement is limited to assessing the percentage clearance of the initial bolus.

Our porcine model provided ample tissue for measurement of tissue injury. However, HMGB-1 is a global marker rather than a specific marker of oxidative stress or IRI. It is possible therefore that the differences seen were due to pre-existing injury rather than P_PO_2. Our results could be complimented by histologically scoring for tissue injury, and examining samples for more specific markers of oxidative stress such as lipid peroxidation or mitochondrial DNA damage. The NMP period was set at 1 hour as this is comparable to current clinical practice. However, is it possible that this period is too short to elucidate protective transcriptional changes. Other groups have demonstrated that longer periods of NMP may be safe and indeed beneficial to transplant kidneys [90, 92]; it may be that longer perfusion in the experimental setting may throw differences due to perfusion conditions into sharper relief.

Our measurements of UO_2 correlate well with data from the limited existing literature. The ability to take pelvicalyceal urine from the NMP kidney obviates clinical concerns over obtaining 'fresh' urine samples. However, without a direct measure of medullary oxygenation, we could only compare our data with historical literature on the medullary PO_2. Direct measurement with fine-bore oxygen probes would provide more compelling evidence for medullary health in the face of lowering P_PO_2.

Future work may consider examining markers of cellular and mitochondrial oxidative damage in order to accurately assess the reperfusion injury status of kidneys perfused with reduced oxygen concentrations. Comparing shorter (i.e. 1–2 hour) with longer (i.e. 6–8 hour) periods of NMP with reduced oxygenation could throw potential benefits, versus greater oxygenation, into sharper relief. Porcine auto- and allotransplantation models would provide more definitive evidence of benefits post-implantation.

3.5 Conclusion

Perfusing porcine kidneys with reduced oxygen concentrations compared to those currently used is not detrimental to renal function and does not raise biomarkers of kidney injury. However, further work is required to characterise any underlying change in oxidative stress and to determine the duration of NMP with reduced oxygenation required to exert any beneficial effects.

3.6 Tables and figures

Study	CI (h)	Oxygen (%)	CO_2 (%)	N_2 (%)	Number	P_PO_2 (kPa)	Hb (g/L)	HCT	pH
Minimal Injury	2h	95	5		8	81.7 (7.1)^{A,B,C,D}	50.4 (18.8)	0.19 (0.01)	7.41 (0.03)
		25	5	70	6	21.7 (3.4)^{A,E,F}	47.8 (5.1)	0.16 (0.02)	7.31 (0.03)
		12	5	83	6	11.9 (0.7)^{B,E}	52.0 (9.1)	0.20 (0.03)	7.39 (0.05)
		6	5	86	6	7.2 (0.7)^{C,F,G}	47.3 (20.2)	0.17 (0.07)	7.43 (0.01)
		Air (20.9%)	0.04	78.9	5	19.1 (2.4)^{D,G}	47.8 (18.9)	0.16 (0.07)	7.46 (0.06)
Clinical Injury	17h	95	5	5	8	80.4 (2.5)^{H,I}	47.6 (1.7)^{G}	0.14 (0.03)	7.51 (0.05)
		25	5	70	6	22.8 (0.7)^{H,J}	39.2 (4.9)^{G,H}	0.13 (0.02)	7.47 (0.03)
		12	5	83	9	11.2 (1.1)^{I,J}	47.8 (7.6)^{H}	0.17 (0.01)	7.46 (0.10)

Table 3.1 **Experimental Groups and Baseline Biochemical Characteristics.** Kidneys were subjected to either a short (2 hours, minimal injury model) or long (17 hours, clinical injury model) cold ischaemic time (CIT). Kidneys were then perfused for 1 hour with a gas mixture containing 95%, 25%, 12% or 6% O_2 with 5% CO_2 and N_2 balance; or air. Values shown are mean (SD) with superscript values denoting adjusted *P*-values from Tukey's multiple comparisons test following one-way ANOVA. *A,B,C,D,F*, $P<0.0001$; *E*, $P=0.005$; *G*, not significant, *H,I,J*, $P<0.0001$.

Parameter	Experimental Groups				
	95%	25%	12%	6%	Air
pH	7.37(0.1)	7.54 (0.3)[a]	7.37 (0.1)	7.25 (0.1)[a,b]	7.59 (0.1)[b]
C_aO_2	9.30 (0.7)	8.08 (2.4)	7.52 (1.4)	6.95 (2.8)	7.01 (2.7)
DO_2	4.19 (2.0)	2.00 (0.8)	2.90 (1.1)	2.16 (1.6)	2.05 (1.1)
VO_2	1.06 (0.4)[c,d]	0.37 (0.2)[c]	0.43 (0.2)	0.85 (0.7)	0.36 (0.2)[d]
OER	0.26 (0.04)[e]	0.18 (0.05)[f]	0.14 (0.03)[e,g]	0.35 (0.10)[f,g,h]	0.19 (0.05)[h]

Table 3.2 **The effect of perfusate oxygenation upon oxygen kinetics and pH during normothermic machine perfusion following brief ischaemic injury.**
Porcine kidneys underwent normothermic machine perfusion (NMP) with varying perfusate oxygenation (see text) after 2 hours cold ischaemia. Values of pH, oxygen content (C_aO_2), delivery (DO_2), consumption (VO_2) and extraction ratio (OER) were obtained after 1 hour of NMP. Data presented as mean (SD) and compared by Tukey's multiple comparisons test following one-way analysis of variance. Superscript letters denote *P* values. a, 0.026; b, 0.01; c, 0.035; d, 0.032; e, 0.009; f, 0.0003; g, <0.0001; h, 0.0006

Parameter	Experimental Groups		
	95%	25%	12%
pH	7.39 (0.06)	7.39 (0.04)	7.37 (0.07)
C_aO_2	7.90 (0.9)[a,b]	5.74 (0.6)[a]	6.29 (1.0)[b]
DO_2	2.82 (0.8)	2.48 (1.1)	2.53 (1.4)
VO_2	0.77 (0.4)	0.60 (0.3)	0.47 (0.2)
OER	0.27 (0.1)	0.23 (0.1)	0.20 (0.1)

Table 3.3 **The effect of perfusate oxygenation upon oxygen kinetics and pH during normothermic machine perfusion following long ischaemic injury.**
Porcine kidneys underwent normothermic machine perfusion (NMP) with varying perfusate oxygenation after 17 hours of cold ischaemia (see text). Values of pH, oxygen content (C_aO_2), delivery (DO_2), consumption (VO_2) and extraction ratio (OER) were obtained after 1 hour of NMP. Data presented as mean (SD) and compared by Tukey's multiple comparisons test following one-way analysis of variance. Superscript letters denote *P* values. a, 0.0007; b, 0.0045

Parameter	Experimental Groups			
	95%	25%	12%	Control
pH	7.33 (0.06)	7.44 (0.12)[a]	7.33 (0.08)	7.22 (0.04)[a]
C_aO_2	6.64 (0.2)	8.18 (1.3)	8.21 (1.2)	8.38 (2.4)
DO_2	2.30 (0.7)	4.35 (2.4)	3.07 (1.6)	2.90 (1.3)
VO_2	1.35 (0.3)	2.01 (0.8)	1.46 (0.6)	1.47 (0.7)
OER	0.62 (0.2)	0.49 (0.1)	0.50 (0.1)	0.51 (0.02)

Table 3.4 **The effect of perfusate oxygenation upon oxygen kinetics and pH during machine reperfusion following long ischaemic injury.**
Porcine kidneys underwent normothermic machine perfusion (NMP) with varying perfusate oxygenation (see text) after 17 hours cold ischaemia, before machine reperfusion for 3 hours. Values of pH, oxygen content (C_aO_2), delivery (DO_2), consumption (VO_2) and extraction ratio (OER) were obtained after 3 hours. Data presented as mean (SD) and compared by Tukey's multiple comparisons test following one-way analysis of variance. Superscript letters denote *P* values. a, 0.0007

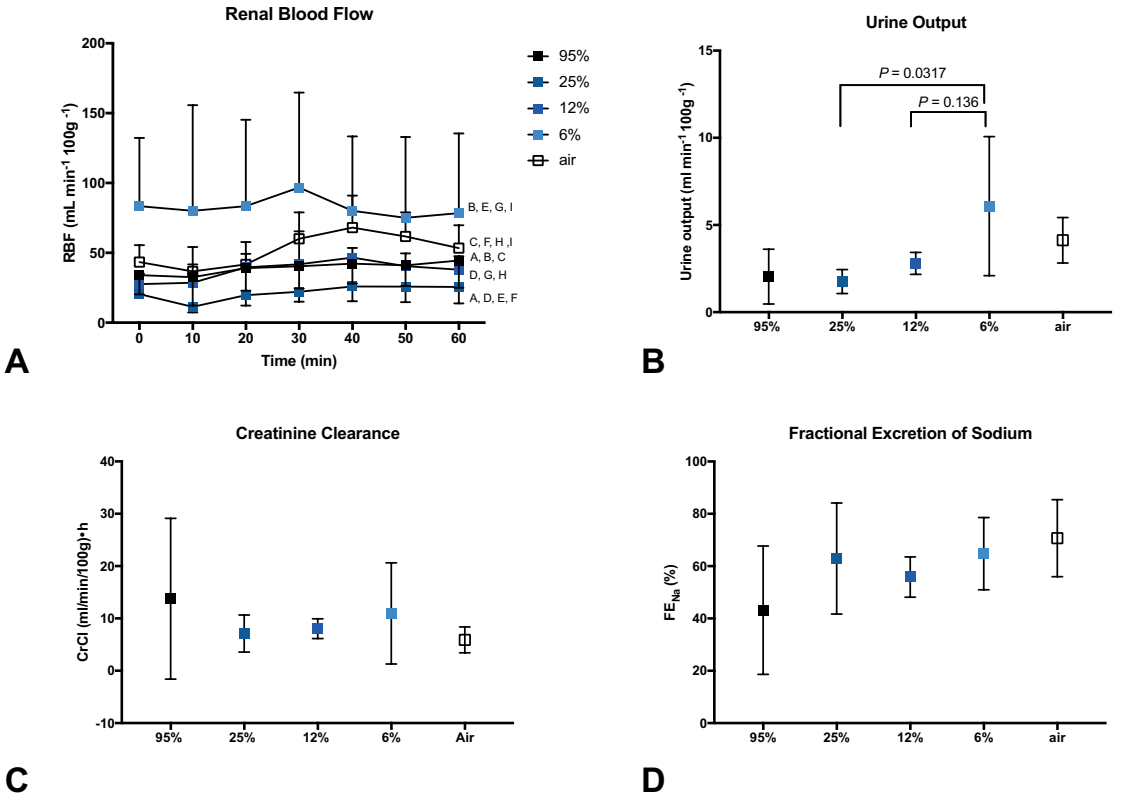

Fig. 3.2 **The effect of reducing oxygenation on renal function during normothermic machine perfusion after a short cold ischaemic injury.**
Porcine kidneys were subjected to 10 minutes of warm ischaemia and 2 hours of cold ischaemia, before 1 hour of normothermic machine perfusion (NMP). During NMP, groups were perfused with either 95% (n=8), 25% (n=6) 12% O_2 (n=6), 6% (n=6) or with air (n=5). At the end of the period of NMP, mean RBF (A), urine output (B), creatinine clearance (C) and fractional excretion of sodium (FE_{Na}) (D) were measured. Data shown as mean (SD). Letters denote adjusted *P*-values by Tukey's multiple comparisons test following one-way analysis of variance. A, 0.001; B, <0.0001; C, 0.02; D, 0.004; E, F, and G, <0.0001; H, 0.08; I, <0.0001.

	RBF	UO	CrCl	FE_{Na}	pH_{art}	C_aO_2	DO_2	VO_2	OER	pH_{ur}	P_UCO_2	P_UO_2
RBF		0.55	0.66	-0.70	0.08	0.18	0.81	0.70	0.25	-0.06	-0.17	0.49
UO	0.55		0.91	-0.52	0.12	-0.21	0.23	0.10	-0.15	-0.35	0.04	-4.93×10^{-3}
CrCl	0.66	0.91		-0.67	-0.01	0.02	0.37	0.28	-0.02	-0.60	0.17	0.03
FE_{Na}	-0.70	-0.52	-0.67		0.01	-0.36	-0.62	-0.66	-0.33	0.31	0.18	-0.45
pH_{art}	0.08	0.12	-0.01	0.01		0.09	0.20	0.24	0.26	0.36	-0.28	-0.08
C_aO_2	0.18	-0.21	0.02	-0.36	0.09		0.64	0.56	0.28	0.23	0.03	0.26
DO_2	0.81	0.23	0.37	-0.62	0.20	0.64		0.87	0.40	0.25	-0.19	0.54
VO_2	0.70	0.10	0.28	-0.66	0.24	0.56	0.87		0.75	0.28	-0.35	0.70
OER	0.25	-0.15	-0.02	-0.33	0.26	0.28	0.40	0.75		0.32	-0.52	0.62
pH_{ur}	-0.06	-0.35	-0.60	0.31	0.36	0.23	0.25	0.28	0.32		-0.54	0.31
P_UCO_2	-0.17	0.04	0.17	0.18	-0.28	0.03	-0.19	-0.35	-0.52	-0.54		-0.63
P_UO_2	0.49	-4.93×10^{-3}	0.03	-0.45	-0.08	0.26	0.54	0.70	0.62	0.31	-0.63	1.00

Fig. 3.3 **Correlation matrix of perfusion parameters, renal function and oxygen kinetics during normothermic machine perfusion.**
A correlation matrix was performed on the pooled terminal (1-hour) values for NMP circuit parameters, renal function and oxygen kinetics, revealing a number of significant relationships. Values depicted are Spearman's rank coefficient (r-value). Green shading denote a significant positive relationship; red shading denotes a significant negative relationship with *P*-value significance <0.05. RBF, renal blood flow; UO, urine output; CrCl, creatinine clearance; FE_{Na}, fractional excretion of sodium; pH_{art}, arterial pH; C_aO_2, perfusate oxygen content; DO_2, oxygen delivery; VO_2, oxygen consumption; OER, oxygen extraction ratio; pH_{ur}, urine pH; P_UCO_2, urine CO_2; P_UO_2, urine oxygen content.

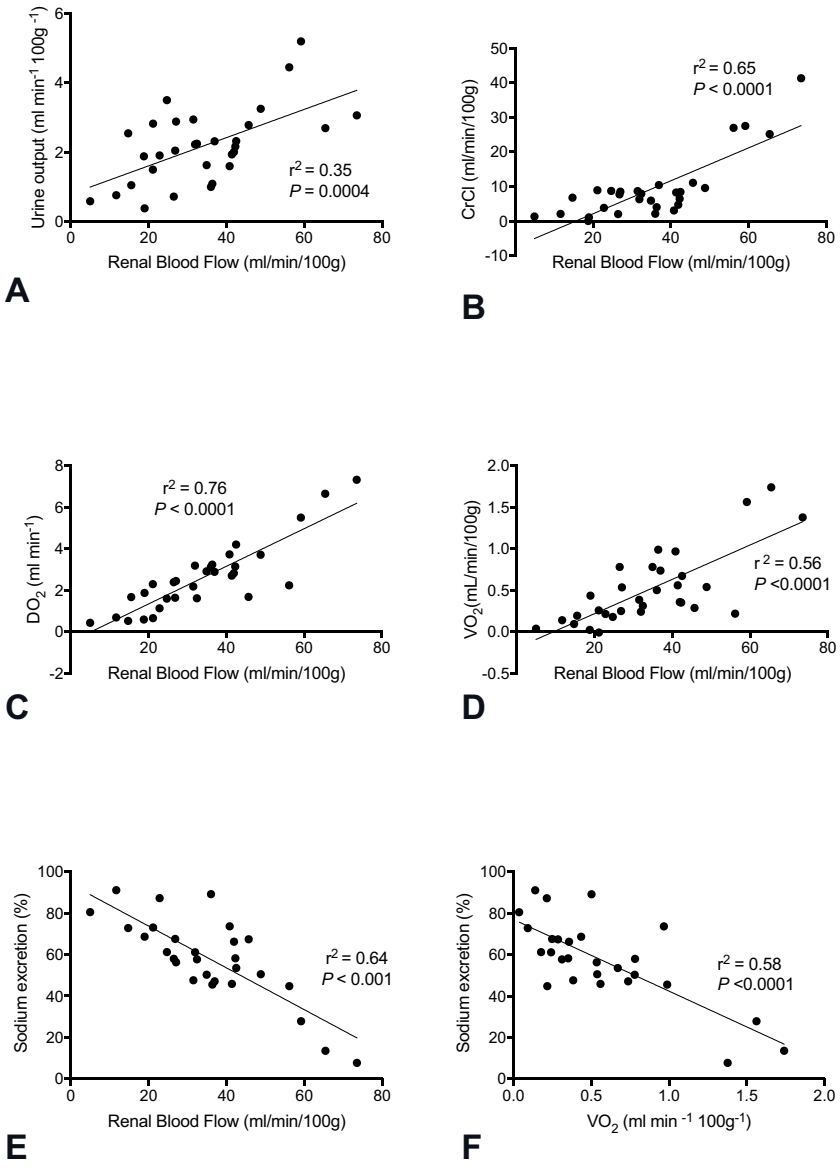

Fig. 3.4 **The association between circuit-defined renal blood flow, renal function and oxygen kinetics during normothermic machine perfusion.**
To examine whether renal blood flow remained the primary determinant of renal function and oxygen use during normothermic machine perfusion, the relationships between pooled values for renal blood flow (RBF) – determined by normothermic machine perfusion circuit pump speed – and renal functional parameters were assessed by linear regression. *P*-values denote significance of slope deviation from zero. R-values denote goodness of fit. CrCl, Creatinine Clearance; DO_2, oxygen delivery; VO_2, oxygen consumption.

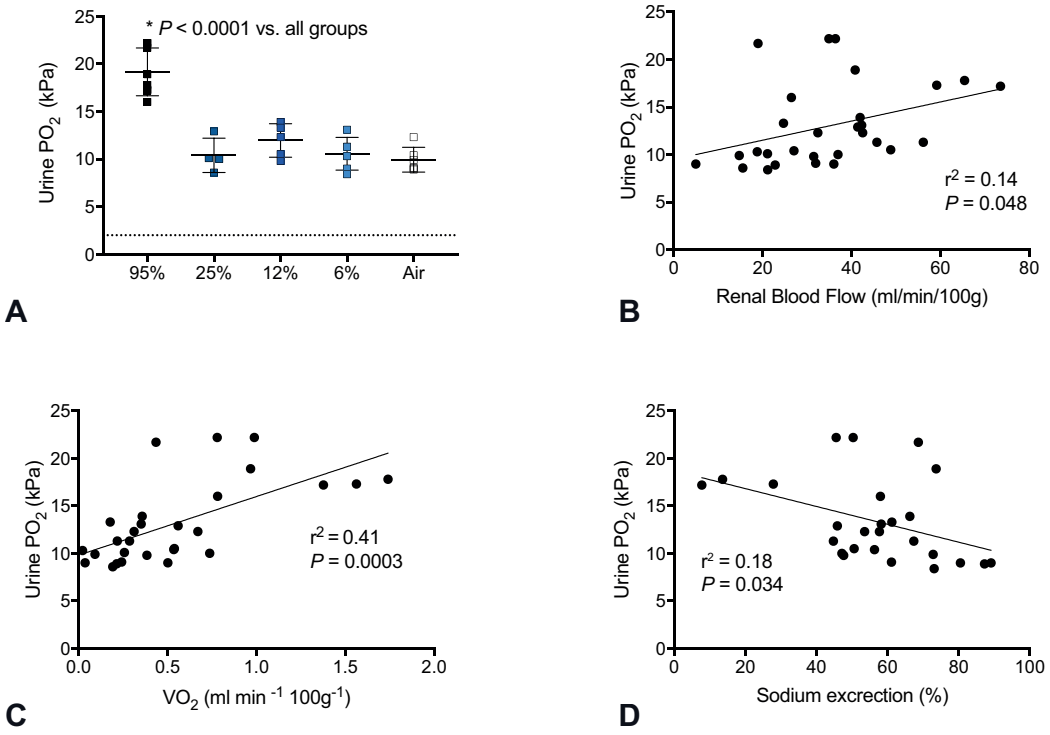

Fig. 3.5 **The relationships between urine and perfusate oxygen tensions during normothermic machine perfusion, and relationships to other perfusion parameters.**
To examine the effect of perfusate oxygen concentration upon urine oxygen tension, pelvicalyceal urine oxygen tension was measured in porcine kidneys following 1 hour of normothermic machine perfusion with different perfusate oxygen concentrations (A). Groups were perfused with either 95% (n=8), 25% (n=6) 12% (n=6) or 6% O_2 (n=6) or with air (n=5). The relationships between UO_2 and renal blood flow (B), oxygen consumption (VO_2, C) and fractional sodium excretion (D) was assessed by linear regression of pooled values from all kidneys.

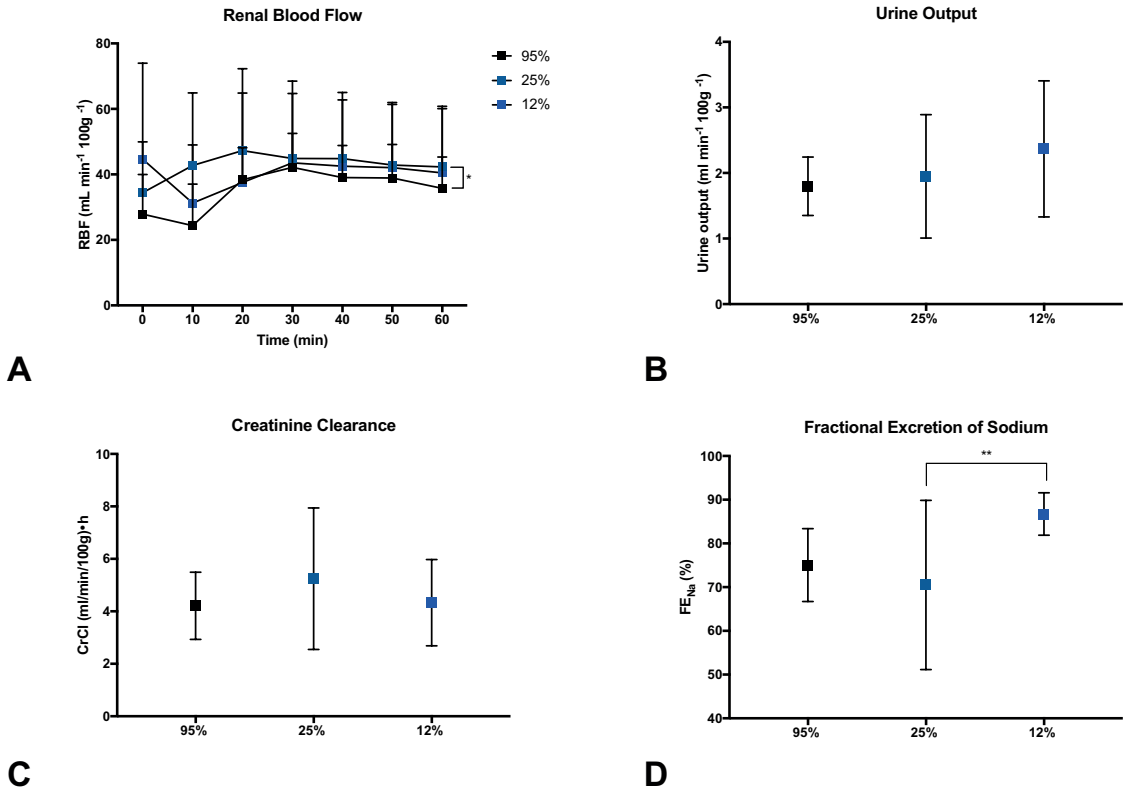

Fig. 3.6 **The effect of reducing oxygenation on renal function during normothermic machine perfusion after a long cold ischaemic injury.**
Porcine kidneys were subjected to 10 minutes of warm ischaemia and 17 hours of cold ischaemia before 1 hour of NMP. During NMP, groups were perfused with either 95% (n=8), 25% (n=6) or 12% O_2 (n=9), all with 5% CO_2 and N2 balance. At the end of NMP, mean renal blood flow (A) urine output (B), creatinine clearance (C) and fractional sodium excretion (D) were measured. Data presented as mean (SD) all compared using one-way ANOVA with Tukey's multiple comparisons test. * 25% group vs. 95% group P=0.035; ** 25% group vs. 12% group P=0.048

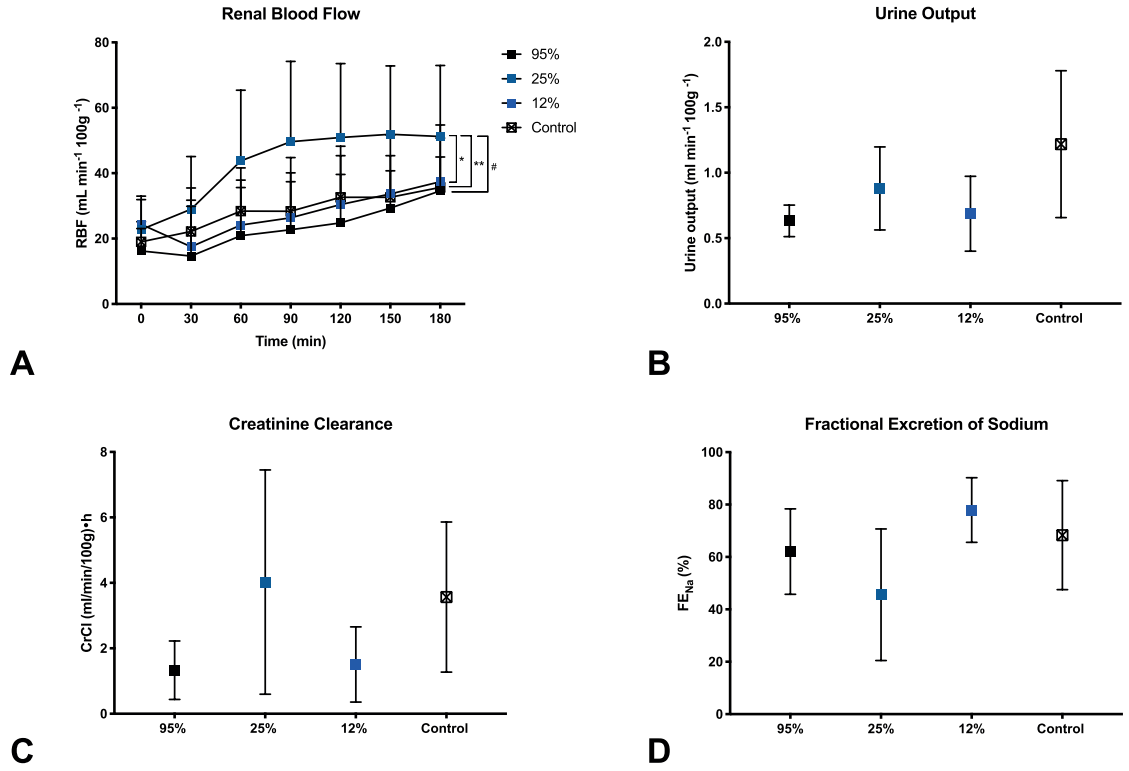

Fig. 3.7 **The effects of reducing perfusate oxygenation during normothermic machine perfusion (NMP) upon renal function during subsequent reperfusion.**
Kidneys receiving either 95%, 25% or 12% O_2 during NMP then underwent reperfusion for 3 hours, whilst a control group was reperfused after a further hour of cold storage. At the end of reperfusion, mean renal blood flow (A) urine output (B), creatinine clearance (C) and fractional sodium excretion (D) were measured. Data presented as mean (SD) all compared using one-way ANOVA with Tukey's multiple comparisons test. * 25% vs. 95% P= 0.001, ** 25% vs. 12% P=0.012, # 25% vs. control P=0.017.

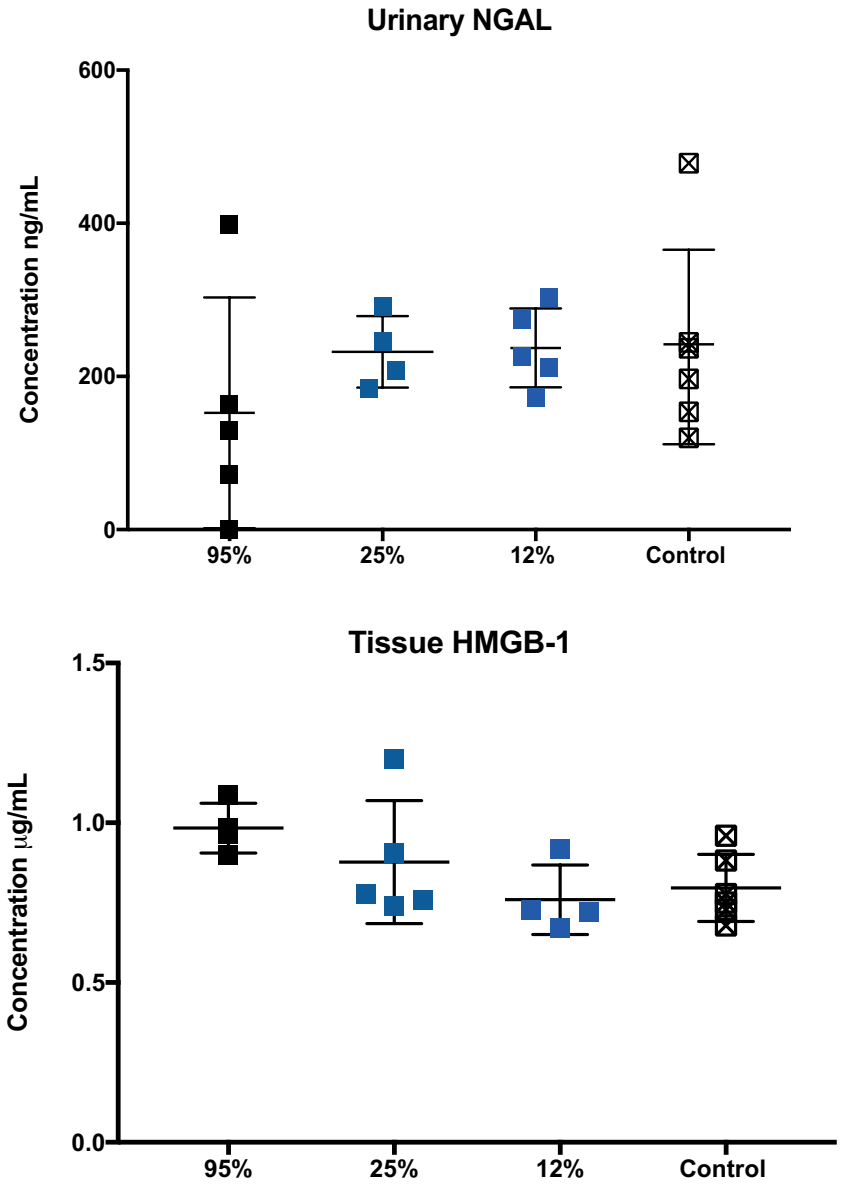

Fig. 3.8 **Lowering perfusate oxygenation during NMP does not do not effect urinary concentration of NGAL or tissue HMGB1 levels.**
After 3 hours of reperfusion, pelvicalyceal urine samples were analysed for levels of tubular injury marker Neutrophil Gelatinase-Associated Lipocalin (NGAL) and cortical tissue samples were analysed for levels of High Motility Group Box-1 (HMGB1).

Chapter 4

Regional oxygenation and perfusion during porcine kidney reperfusion

4.1 Introduction

The circulation of the mammalian kidney is well described, as are the differences between renal cortical and medullary circulation - namely a ten-fold discrepancy in flow, absence of collateral vessels, and a medullary circulation that relies entirely on blood that has already passed through the renal cortex. However, less is known about the regional oxygenation arising from this unique circulatory arrangement, especially during reperfusion following ischaemia. The medullary circulation is disproportionally affected by ischaemic hypoperfusion, meaning that inherent differences between regions are likely to be greatly amplified in the reperfusion period. This in turn may lead to greater medullary damage from IRI, compounding injury in an already-vulnerable tissue.

Detailed measurements of large-animal and human renal circulation and oxygenation before and after ischaemia have been limited by physical and imaging access to the deeper medullary tissues. However, an experimental NMP circuit affords measurement of renal function, oxygen kinetics and microvascular perfusion for kidneys undergoing ischaemia-

reperfusion, in an *ex-vivo* environment designed to closely model *in vivo* conditions (section 1.5.3). Until now, an NMP circuit has not been used to answer experimental questions about regional oxygenation and perfusion of the renal transplant allograft.

The aim of this study was threefold; firstly to ascertain baseline values for regional renal P_tO_2 and MVP in a large animal model. Secondly, to investigate the effect of clinically relevant periods of cold ischaemia and machine reperfusion upon the aforementioned baseline values. Finally, it was anticipated that this study would supplement subsequent investigations into human regional reperfusion by providing baseline values that would be challenging to obtain.

Related to our aims, we hypothesised that:

1. Baseline in-vivo MVP and P_tO_2 would be greater in the cortex than the medulla
2. Ischaemia-Reperfusion would cause a global reduction in both MVP and P_tO_2, but greater reductions in the medulla

4.2 Methodology

To provide baseline measurements of regional oxygenation and perfusion in the porcine kidney, three adult female landrace pigs underwent controlled DCD kidney retrieval (section 2.2.2). The renal pedicles were exposed and slung with ties, and two fibre-optic probes were inserted into the kidney sequentially into upper pole cortical and medullary tissue to measure microvascular perfusion and tissue oxygenation (section 2.4.4). After 5-minute serial recordings, in both cortex and medulla, probes were withdrawn and their position noted. The retrieval then proceeded as previously described with *in-situ* renal artery ligation and 30 minutes warm ischaemia followed by a cold flush and 6 hours of SCS.

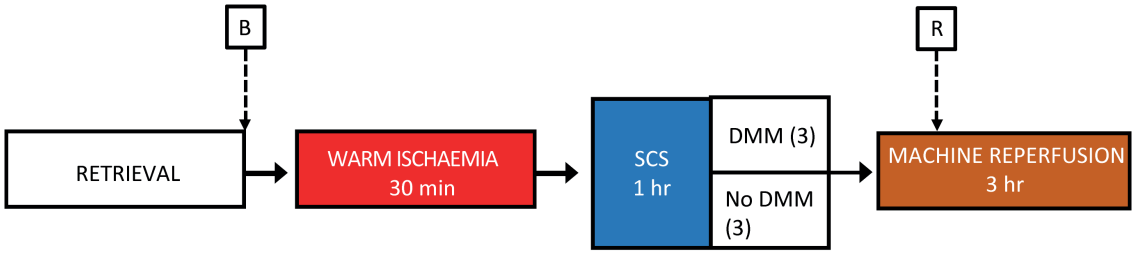

Fig. 4.1 **Experimental design for determining baseline and reperfusion values for regional renal microvascular perfusion and tissue oxygenation.**
Three adult female landrace pigs underwent controlled DCD kidney retrieval. During retrieval and prior to occlusion of renal blood flow, 5-minute serial recordings of baseline laser doppler flowmetry and fluorescence optode phosphorimetry were taken in both cortex and medulla (point B). Kidneys were subjected to 30 minutes warm ischaemia followed by 6 hours of static cold storage (SCS), either with or without dimethymalonate (DMM) for an unrelated concomitant experiment. Kidney pairs were then subjected to 3 hours of normothermic machine reperfusion After 1 hour of reperfusion, probes were re-sited in cortical and medullary tissue to assess the effect of reperfusion (R) upon regional perfusion and oxygenation.

To provide measurements of regional oxygenation and reperfusion during normothermic machine reperfusion, kidney pairs were subjected to 3 hours of normothermic machine reperfusion (as described in section 2.2.4). After 1 hour of reperfusion, fibre-optic probes were re-sited and sequential measurements recorded as previously described.

4.3 Results

4.3.1 Intraoperative baseline characteristics

Intraoperative measurements of peripheral oxygen saturation, respiratory and heart rate and E_tCO_2 were similar between all animals (table 4.1).

4.3.2 Intraoperative regional perfusion and oxygenation

Paired regional comparisons were made during the pre-ischaemic phase. Intraoperative microvascular perfusion (Fig.4.2A) was similar in the medulla and cortex (5.46±0.6 vs. 3.95±1.2 kPa, *P*=0.563). Similarly, median tissue oxygenation (Fig.4.2B) in the medulla was comparable to that in the cortex (489.7±181.7 vs. 308.4±126.8 BPU, *P*=0.313)

Whilst there were no significant differences between groups' regional baseline MVP and P_tO_2, within regions there was notable inter-kidney variation. For example, mean cortical P_tO_2 in kidney '49' was 0.84±0.1 kPa, whereas in kidney '50' it was 17.34±0.2 kPa (Fig.4.2B). Whilst mean medullary MVP in kidney '51' was 873.7±74.4 BPU, in kidney '49' it was 83.5±2.7 BPU (Fig.4.2A). There was a greater inter-kidney variation of P_tO_2 in the cortex at baseline than in the medulla (Fig.4.2B). There was a greater inter-kidney variation of MVP in the medulla at baseline than in cortex (Fig.4.2A).

4.3.3 Regional perfusion and oxygenation during machine reperfusion

All six kidneys underwent machine reperfusion after 6 hours of cold ischaemia. The mean renal blood flow across all kidneys was 68.3±5.9 ml/min/100g. Measurement of starting haemoglobin and pH was inaccurate for some kidneys, indicating that values were outside of measurable range. However, readings were within acceptable range upon re-measurement at 1h reperfusion.

A sub-group analysis suggested that the compound delivered during the cold flushing phase may have significantly affected renal blood flow and regional blood flow (supplemental Fig.C.1A in appendix C); therefore the non-control kidneys were removed from analysis of the machine reperfusion phase of the experiment.

Paired regional comparisons were made during this reperfusion phase. At the end of machine reperfusion, whilst overall median tissue oxygenation (Fig.4.3A) in the medulla (10.28±4.63 kPa) was different to that in the cortex (2.72±1.01 kPa), there were no differences

on paired comparison (Wilcoxon's matched-pairs signed rank test P=0.25). Similarly, no significant differences in regional microvascular perfusion (Fig.4.3B) between areas (median values cortex 372.1±84.5 vs. medulla 287.1±38.7 BPU).

As with the intraoperative readings, there was a marked inter-kidney variety, especially in medullary P_tO_2 (Fig.4.3A) and equally across regions in MVP (Fig.4.3B)

4.3.4 The effect of ischaemia-reperfusion upon regional perfusion and oxygenation

The perfusion and oxygenation of the cortex and medulla during reperfusion were compared against their respective pre-ischaemic baselines.

Unpaired analysis with Mann-Whitney tests (due to samples lost from DMM kidneys) did no suggest significantly different cortical tissue oxygenation during reperfusion (Fig.4.4A, overall median 2.72±1.01 vs. a baseline of 3.95±1.2 kPa, P=0.76). Whilst numerically the overall medullary median oxygenation was higher during reperfusion (Fig.4.4B, overall median 10.28±4.63 vs. a baseline 5.481±0.6 kPa) this apparent difference did not reach significance (P=0.61).

Unpaired analysis of cortical microvascular perfusion suggested no post-reperfusion change from baseline (Fig.4.5A, overall median values 372.1±84.5 vs. 308.4±126.8 BPU respectively, P=0.91), neither was this demonstrated in medullary tissue (Fig.4.5B, overall median reperfusion value 287.1±38.7 vs. a baseline of 489.7±181.7 BPU, P=0.48).

4.4 Discussion

Using a porcine model of DCD kidney retrieval and NMP reperfusion, we examined the effect of transplant ischaemia-reperfusion injury upon regional microvascular perfusion and tissue oxygenation.

The major findings of this study were that baseline values for both MVP and P_tO_2 were widely variable ; and that transplant IRI did not appear to consistently disrupt these values in either overall or in a regionally distinct manner. These preliminary findings important because they are the first to describe regional MVP and P_tO_2 in a commonly-used transplantation animal model and during NMP. They further add to the limited observations describing medullary physiology during transplant ischaemia-reperfusion.

4.4.1 Baseline measurements of regional perfusion and oxygenation

In the pre-ischaemic anaesthetised pig, overall laser Doppler flux in individual kidneys varied greatly, with no clear regional differences. Tissue oxygenation at baseline mirrored MVP, with overall greater values in the medulla but inter-kidney variability in the magnitude of regional differences.

Our results may initially seem to contradict the large body of anatomical and physiological evidence suggesting that mammalian medullary renal blood flow is lesser than that of the cortex. We suggest however that our findings relate to probe placement, and the unusual renal vascular anatomy. The LDF and FLO probes measure an area of approximately $1cm^3$; thus they sample only a small volume of total regional tissue. Probes were sited by depth only, with position confirmed post-hoc. The renal pyramids containing the medulla are surrounded by ascending interlobar arteries. As LDF does not delineate flow direction, interlobar arterial blood flow at the level of the medulla may have been sampled though it was not supplying medullary tissue. Near the cortical surface however large vessels have long since divided,

thus the cortical probes may have sample only the localised microvasculature. Furthermore, as the LDF probes calculate a relative value of blood transit (Blood Perfusion Units) it is difficult to ascertain what physiological significance the baseline differences represent.

Our comparatively low cortical P_tO_2 values also appear to differ from the literature, with most reports in small mammals suggesting lower medullary P_tO_2 [93]. However, studies of the renal microcirculation rarely 'scale up' from mouse to large mammal [94] and only one study has previously compared both cortical and medullary P_tO_2 in the pig, using Clark-type electrodes to describe mean P_tO_2 of around 6kPa in the cortex [173]. Fluorescence optodes give less variable and proportionally lower P_tO_2 values than Clark microelectrodes [106], which may partly explain the differences between our findings.

Furthermore, lower cortical values may represent arteriovenous oxygen shunting arising from close anatomical relationship between cortical preglomerular arterioles and venules [123]. It is thought that this relationship may act as an anatomical antioxidant to mitigate the effects of cortical tissue receiving far higher renal blood flow (for filtration) that it requires for metabolism [127].

The heterogeneity of cortical P_tO_2 measurements may represent sampling points upon a radial arterio-glomerular gradient. Upon passing a Clark microelectrode sequentially through the cortex and medulla of rat and dog kidneys Lubbers and Baumgartl demonstrated values ranging from near-arterial (11kPa) down to 5.5kPa [109]. Similarly, ultramicroelectrode measurements of single-nephron oxygen tension suggest a wide range of values (10.7–6.0 kPa) from artery to afferent arteriole [169]. Hence, tissue along an isobathic line may have differing oxygen tension depending upon its distance from an artery.

The proportionally high medullary P_tO_2 we found again differs from many murine data suggesting lower oxygenation in the medulla [93]. Zhang et. al found lower porcine medullary P_tO_2 (of around 3.5kPa compared to 6kPa in the cortex) using Clark microelectrodes [172]. However, Evans and colleagues found proportionally higher medullary P_tO_2, in

a rabbit model using FLO.[48] suggesting that our values may relate to the FLO technique. Given that the greater P_tO_2 follows the higher values in MVP; this may thus represent a similar sampling effect. The heterogeneity of medullary P_tO_2 differ from reports in the literature, with Lubbers and Baumgartl having found medullary P_tO_2 to be much less variable than cortical P_tO_2 [109].

Finally, we cannot exclude the possibility that some probes were placed outside of medullary tissue, close to an ascending interlobar artery.

4.4.2 Reperfusion measurements of oxygenation and perfusion

Following 6 hours of cold ischaemia and 1 hour of NMP reperfusion, no significant shifts in either microvascular perfusion and tissue oxygenation were seen when compared to their respective regional baselines, or inter-regionally during reperfusion itself. The marked inter-individual heterogeneity noted in the baseline measurements was also present during reperfusion.

These data provide the first description of regional MVP and P_tO_2 during porcine kidney NMP, and suggest distinct regional responses to transplant IRI.

In a porcine autotransplantation model, Maiga and colleagues demonstrated a 50% reduction in cortical perfusion after 1 hour reperfusion.[111] Similarly, Siegemund et. al describe a steady decline in cortical blood flow during the first 4 hours following pig aortic cross-clamp removal [153]. Comparable post-reperfusion reductions in cortical blood flow have been demonstrated in human [13] rabbit [48] and rat [72] models using a variety of techniques.

There was more apparent numerical fall in medullary MVP during reperfusion (though not one reaching significance), with the net effect that cortical perfusion became greater than medullary during reperfusion. In contrast to studies of porcine (and other mammalian) cortical perfusion following IRI, no available studies have examined porcine medullary

MVP. Our results would appear consistent with murine and rabbit studies that describe proportionally greater reduction in medullary perfusion post-ischaemia [48, 72, 142, 171].

In contrast to perfusion, reperfusion regional oxygenation was greater than baseline in the medulla and lesser than baseline in the cortex, with absolute values also greater in the medulla.

Cortical P_tO_2 readings were heterogenous, with two kidneys recording P_tO_2 close to zero, and another reading closer to 10kPa. As in the cortex tissue oxygenation appears to have followed perfusion, this pattern may represent patchy cortical perfusion. Other groups have described such a relationship between cortical perfusion and oxygenation in a reperfusion state, however most have observed significant paired decrements to both factors.

Reperfusion P_tO_2 in medullary tissue was similarly heterogenous. Interestingly, in certain kidneys a post-reperfusion increase in oxygenation occurred whilst perfusion decreased. This seemingly paradoxical picture has also been described during studies of medullary oxygenation by phase-contrast MRI imaging [66] and a model of rabbit renal hypoperfusion [48]. As tissue oxygenation is a factor of oxygen delivery and consumption [170] it has been suggested that a rise in medullary P_tO_2 during reperfusion may represent decreased oxygen consumption secondary to reduced resorptive workload [66].

4.4.3 Limitations

The conclusions drawn from this study are qualified by a number of important limitations.

Our porcine model, whilst well-described, is likely to have underestimated the ischaemic damage sustained during SCS, as young porcine kidneys lack the pre-existing kidney injury found in the older, comorbid human donors. Age and comorbidity are independent factors for graft failure [160] and are likely to heterogeneously affect kidney regions. In our model we cannot comment upon the effects of age or comorbidities upon clinical donor kidney regional reperfusion. Because only single readings of MVP and P_tO_2 were taken

after 1 hour of reperfusion, we are not able to determine whether values in this model are dynamic or stable. Similarly, as we did not measure creatinine clearance, sodium excretion or oxygen consumption from the NMP perfusate, we are not able to correlate differences in regional perfusion and oxygenation with either function (glomerular filtration and urine concentration respectively) or with oxygen kinetics. The inhaled anaesthetic agent and high FiO_2 / P_PO_2 during baseline readings and both experimental phases respectively are likely to have influenced renal oxygenation and blood flow, but are factors we cannot account for as we did not measure baseline cardiac output or arterial oxygen content.

In an effort to reduce animal numbers, kidneys in this pilot study formed the control arm for another study investigating the use of a pharmaceutical addition to the NMP perfusate. Consequently, reperfusion measurements for 2 of the 6 kidneys from which we took baseline readings were not available. Furthermore, only one area of cortex and medulla was sampled per kidney at each timepoint, with considerable inter-kidney regional variation. These low sample numbers increase the chance of standard error in our results and prevented us from performing more powerful paired analyses to compare reperfusion and baseline values. Whilst numerical trends in our data appear to follow previous findings in other animal models, statistical non-significance clearly precludes our ability to draw any firm conclusions from our data.

Whilst measurement of microvascular perfusion by LDF is well-validated, it provides only a limited assessment of flow, given that it can only demonstrate flux in arbitrary units relative to a normalized baseline [47] and cannot determine the direction of flow. In the kidney and especially the medulla, opposing vessels (such as AVR and DVR) may lie in close approximation and this technique is not sensitive enough to differentiate between such vessels. Fluorescence optometry compares favorably with gold standard Clark microelectrode measurement [93, 118, 106] the presence of tissue oxygenation does not preclude cellular

hypoxia. In a rabbit model of renal ischaemia, Abdelkader and colleagues demonstrated outer medullary cellular hypoxia – as evidenced by pimonidazole immunohistochemistry - despite stable P_tO_2 when measured by fluorescence optode [8]. Therefore we cannot comment upon the effect of TIRI on regional cellular oxygenation.

4.4.4 Conclusions and future work

In conclusion, these data provide a snapshot of regional oxygenation and perfusion in the porcine kidney under general anaesthesia and following recent ischaemia-reperfusion, including the first description of both during clinically-relevant normothermic machine perfusion. Microvascular perfusion and tissue oxygenation differ markedly within areas of both cortex and medulla, but do not appear to exhibit binary inter-regional differences. Transplant IRI disrupted MVP and P_tO_2 in both regions but it is not clear if it did so in a consistent fashion. Future work should look to collect multiple samples of regional oxygenation and perfusion across different reperfusion timepoints, and correlate these data with markers of renal function, oxygen kinetics and tissue injury to better understand their significance.

4.5 Tables and figures

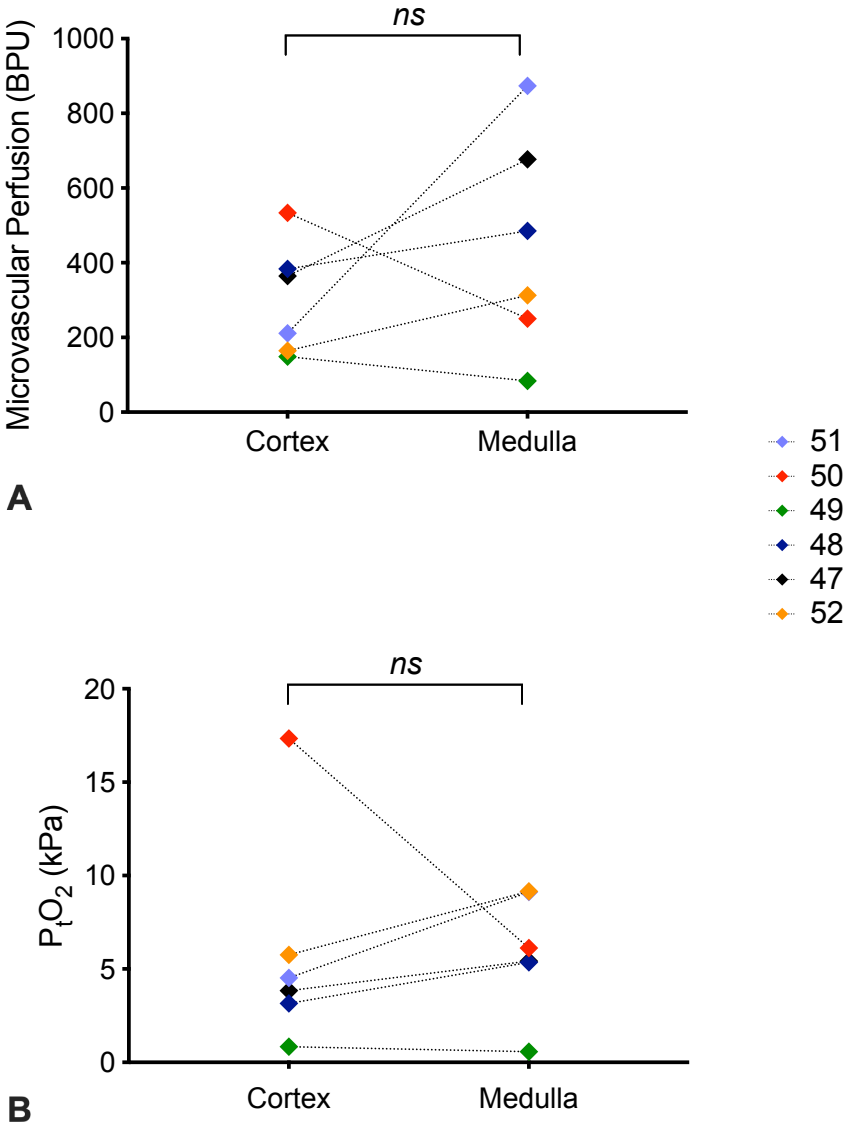

Fig. 4.2 **Pre-ischaemic renal regional oxygenation and perfusion.**
To determine in-vivo regional patterns of intrarenal tissue oxygenation (P_tO_2) and microvascular perfusion, porcine kidneys (n=6) were instrumented under general anaesthesia with laser Doppler (A) or fluorescence lifetime oximetry (B), placed for 5 minutes sequentially into cortex and medulla. To compare cortex and medulla and inter-kidney variation, median values from all kidneys were paired. *ns*, non-significant value for Wilcoxon's matched-pair signed rank test; kPa, kilopascal; BPU, blood perfusion units.

Kidney	Date	Weight (g)	Sats (%)	$ETCO_2$ (kPa)	HR
TBP47	11/15/18	143	99.1 (0.5)	3.7 (1.3)	74 (19)
TBP48		153			
TBP49	11/28/18	153	99.2 (1.1)	5.0 (0.8)	76 (14)
TBP50		167			
TBP51	12/6/18	144	99.3 (0.7)	5.1 (0.8)	62 (11)
TBP52		161			

Table 4.1 **Baseline intraoperative physiological characteristics of female landrace pigs.** Three adult female landrace pigs (coded TBP47-52) underwent controlled DCD kidney retrieval, prior to which kidneys were instumented with fibre-optic probes into upper pole cortical and medullary tissue to measure microvascular perfusion and tissue oxygenation. Values are mean (SD). There were no significant differences between animals in terms of intraoperative peripheral oxygen saturations (Sats), end-tidal CO_2 ($ETCO_2$,) or heart rate (HR).

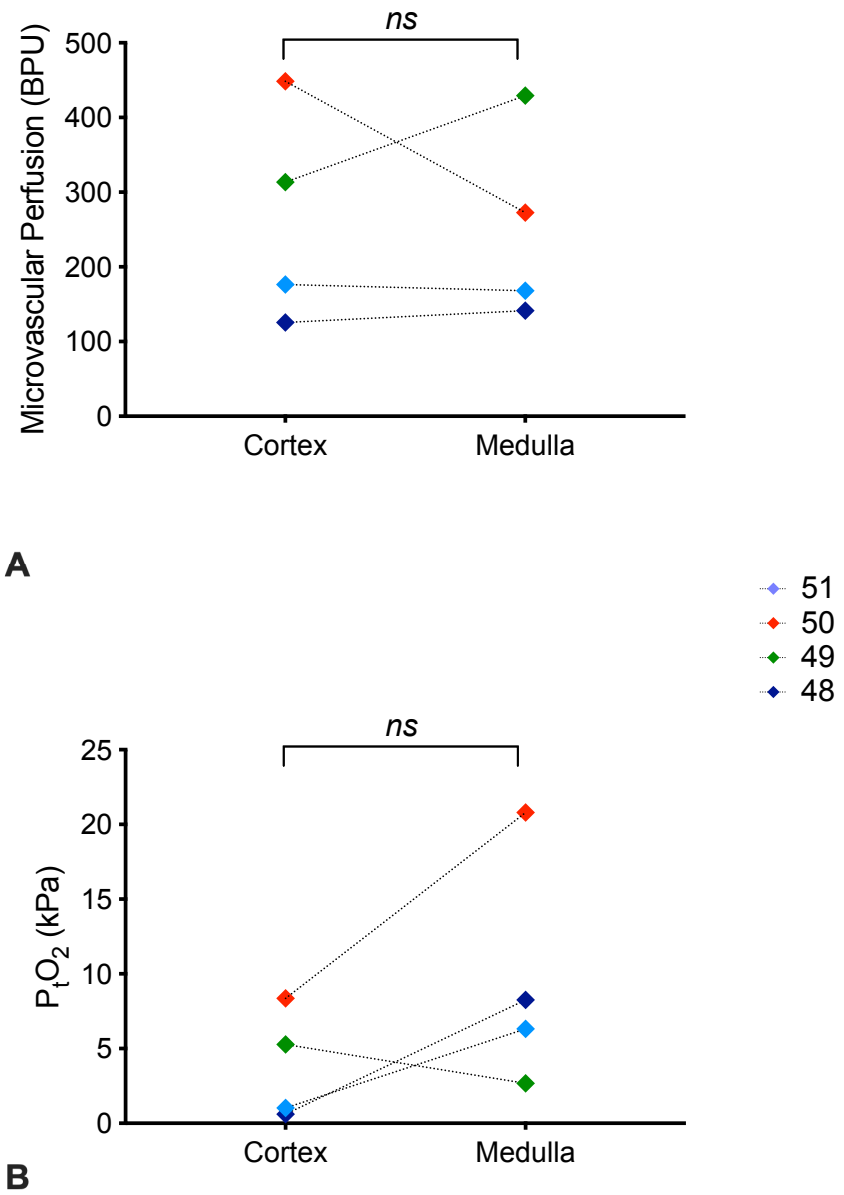

Fig. 4.3 **Post-reperfusion renal regional oxygenation and perfusion.**
To examine regional patterns of intrarenal microvascular perfusion (MVP) and tissue oxygenation (P_tO_2) during machine reperfusion, porcine kidneys (n=4) underwent 3 hours of machine reperfusion following 30 minutes of warm ischaemia and 6 hours of cold ischaemia. Laser Doppler perfusion (A) and fluorescence lifetime oximetry (B) probes were placed in the same area as baseline (4.2) for 5 minutes sequentially into cortex and medulla. To compare cortex and medulla and inter-kidney variation, median values from all kidneys were paired. *ns*, non-significant value for Wilcoxon's matched-pair signed rank test. kPa, kilopascals; BPU, blood perfusion units.

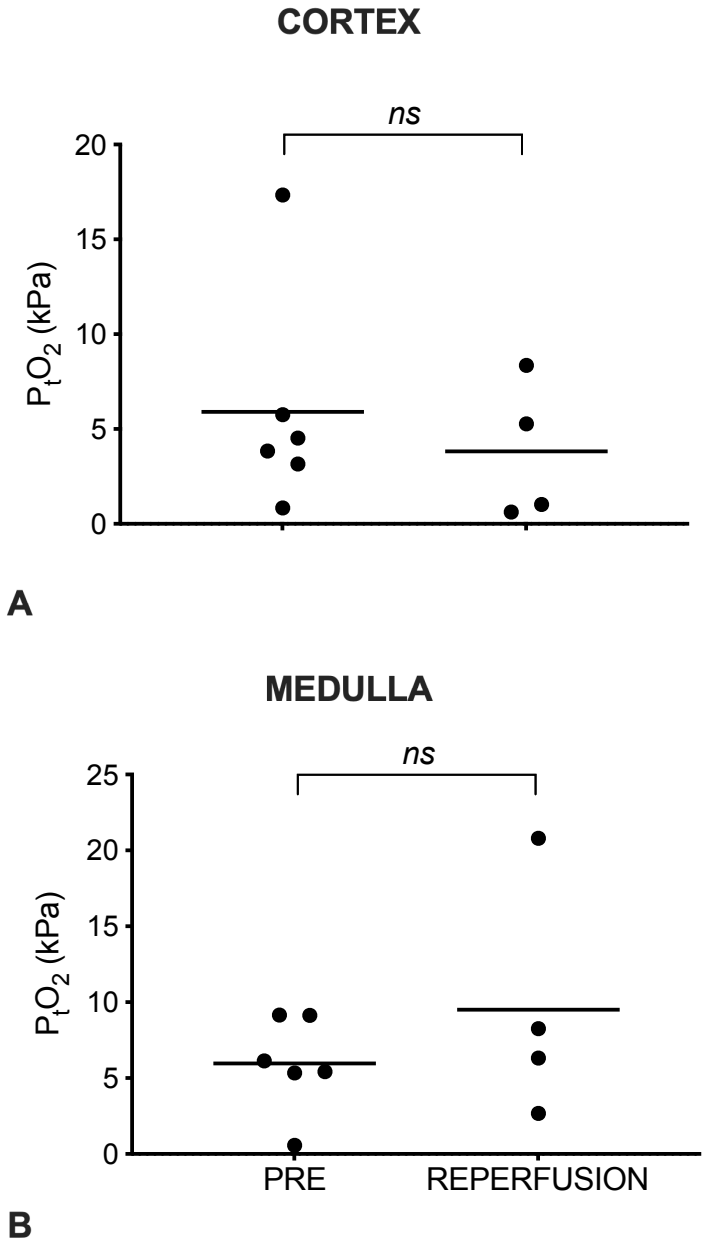

Fig. 4.4 **The effect of ischaemia-reperfusion injury upon cortical and medullary tissue oxygenation.**
To investigate the effect of ischaemia-reperfusion injury upon regional oxygenation in transplant kidneys, cortical and medullary tissue oxygenation (P_tO_2) was measured in the cortex and medulla of pig kidneys pre-ischaemia (n=6) and during machine reperfusion (n=4) after 30 minutes of warm ischaemia and 6 hours of static cold storage. Represented are unpaired median values from each kidney. *ns*, non-significance for Mann-Whitney U value; kPa, kilopascal.

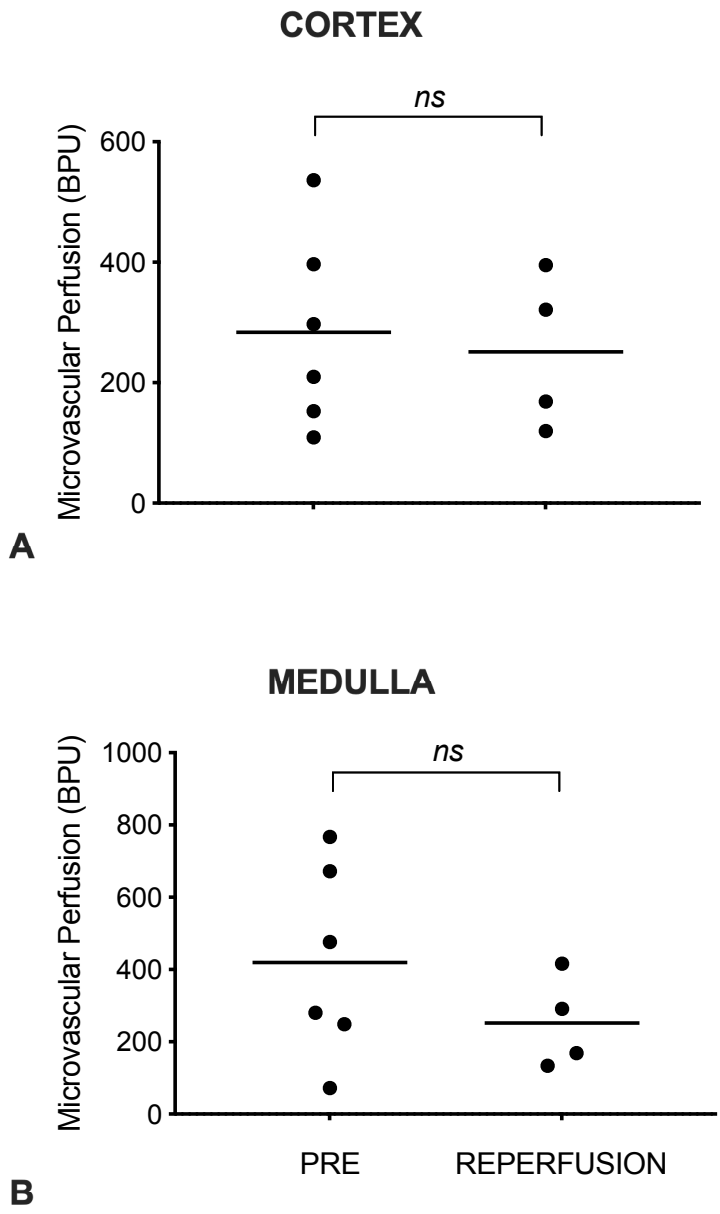

Fig. 4.5 **The effect of ischaemia-reperfusion injury upon cortical and medullary tissue perfusion.**
To investigate the effect of ischaemia-reperfusion injury upon regional microvascular perfusion (MVP) in transplant kidneys, cortical and medullary MVP was measured in the cortex and medulla of pig kidneys pre-ischaemia (n=6) and during machine reperfusion (n=4) after 30 minutes of warm ischaemia and 6 hours of static cold storage. Represented are unpaired median values from each kidney. *ns*, non-significance for Mann-Whitney U value; BPU, blood perfusion units.

Chapter 5

Regional microcirculation and oxygenation during human kidney normothermic machine perfusion

5.1 Introduction

In the previous chapter (4) we measured regional renal microvascular perfusion and tissue oxygenation in a porcine NMP model of transplant reperfusion, demonstrating heterogeneous regional microvascular perfusion and tissue oxygenation following transplant ischaemia-reperfusion. These data provided compelling evidence that the circulatory disruption during reperfusion demonstrated previously in myriad small-animal models was also present in larger mammalian kidneys, and further that these regional changes could be measured accurately during normothermic machine perfusion.

From this pre-clinical work arose several important questions. Firstly, to what extent findings from young healthy porcine kidneys could be applied to the typical adult human deceased-donor allograft, with their added multifactorial ischaemic injuries, comorbidities and heterogeneity (section1.2). Secondly, the time-scale over which regional disturbances

occur, given that reperfusion injury describes a rapidly evolving condition of cellular, tissue-level and systemic responses (section1.3).

Finally, whether existing hypotheses regarding vascular injury during kidney reperfusion could explain the observed disruptions to renal physiology. Heterogeneous capillary perfusion, oedema and microvascular thrombosis have been observed in the cortex of human kidneys during early reperfusion [147, 108] and postulated to be responsible for reductions in blood flow and oxygenation, but these have not been examined in the human medulla.

The aim of this chapter was therefore to expand upon the previous chapter's findings, investigating the compartmental oxygenation and microvascular perfusion during normothermic machine perfusion reperfusion in human kidneys declined for transplantation. Microvascular fibrin deposition is a common and ubiquitous feature of tissue injury, is associated with thrombosis and tissue oedema [110] and readily asssayed in histological samples. We therefore further aimed to examine regional fibrin deposition following reperfusion, as a surrogate marker of tissue injury.

In relation to our aims, we hypothesised that:

1. There would be little correlation between circuit parameters and microvascular perfusion and oxygenation. This is similar to findings in other studies that have struggled to find easily measurable corroloraries to MVP and P_tO_2.

2. Histological evidence of fibrin deposition, secondary to vascular injury, would be greater in the medulla than in the cortex and would correlate with tissue perfusion.

5.2 Methodology

In an initial 'pilot' series, twelve kidneys underwent normothermic machine perfusion (section 2.3.2) with the primary aim of collecting preliminary human data on the feasibility of probe use. No selection was made of the kidneys based upon condition, donor characteristics

or ischaemic times. These kidneys were also being utilised in other studies (in a similar manner to the '3R' principles applied to animal studies); some received pharmacological compounds and underwent a variety of lengths of perfusion under different sampling schedules. To assess regional fluctuations in tissue oxygenation and microvascular perfusion, fiber-optic probes were placed simultaneously into upper pole cortical and medullary tissue (section 2.4.4). To capture the initial reperfusion, probes were sited prior to the start of NMP, and recordings made continuously for 90 minutes.

In a subsequent 'Platform' series (so named because tissue from this series would be used to run highly-multiplexed expression analysis, (see Chapter 6) a more select group of 7 human kidneys underwent 90 minutes of machine reperfusion (identical in methodology to the pilot series). The inclusion criteria for kidney recruitment into this group were: an estimated CIT <24 hours before onset of NMP (accounting for travel time to Addenbrookes hospital), absence of any absolute contraindications to transplantation and absence of AKI prior to retrieval. Perfusion and fiber-optic probe placements followed the same protocol as the pilot group. Additionally, perfusate and urine samples were taken hourly and cortical and medullary tissue samples (section 2.4.1).

To assess for post-perfusion deposition of fibrin, end-perfusion cortical and medullary samples from the Platform series were stained by the Martius Scarlet Blue (MSB) method and analysed for percentage fibrin composition according to methods described in section 2.4.3.

5.3 Results

5.3.1 Baseline donor characteristics and initial normothermic machine perfusion parameters

Because some of the pilot group kidneys received pharmacological compounds and underwent a variety of lengths of perfusion under different sampling schedules, we decided therefore to do a sub-analysis of the pilot control kidneys only. Data were graphed sequentially as the pilot, pilot control and platform (table 5.1 onwards). The mean donor age was 62 years in the pilot group and 57 years in the platform groups, with no difference reported between the groups. Kidneys were perfused following both DBD and DCD retrieval and donors of both sexes. The mean cold ischaemic time (CIT) was 1475 mins (24.5 hours) in the pilot group kidneys, and significantly shorter in the platform group at 995 mins (16.5 hours, unpaired t-test P=0.03). There was no significant difference between groups in terms of warm ischaemic times.

There were no significant differences between groups' starting haemoglobin concentration, haematocrit, kidney weight, pH, P_PO_2 or perfusate temperature (table 5.2).

5.3.2 Renal function and oxygen kinetics during machine reperfusion

Oxygen kinetics were calculated for the platform series at 60 and 90 minutes, and for some (n=7) of the pilot series at 60 minutes (table 5.3). After one hour of reperfusion, renal blood flow was significantly higher in the platform series (P=0.026) as was oxygen delivery (P=0.035) However, oxygen content and extraction ratio were higher in the pilot series (P=0.0012 and 0.0047 respectively). There were no differences between groups in terms of urine output, perfusate pH or oxygen consumption (table 5.3).

5.3.3 Regional microvascular perfusion during machine reperfusion

In the pilot series, mean MVP was greater in the cortex than in the medulla (718.9±363.7 vs. 438.7±254.8 BPU, P<0.0001). However, medullary MVP was greater than cortical MVP during the initial 15 minutes of perfusion (appendix C, Fig.C.2A).

When only the pilot control kidneys were analysed, MVP was significantly greater in the medullary region (452.5±374.6 vs. 305.7±280.4, P=0.025). There was a decline in MVP across both regions with time (appendix C Fig.C.2B).

In the platform series, overall MVP was higher in the cortex (791.3±494.1 vs. 459.6±144.1 BPU P<0.0001) however, towards the end of reperfusion regional values were similar (appendix Fig.C.2C)

When the pilot controls and platform kidney perfusions were pooled for analysis (Fig.5.1A) median microvascular perfusion was greater in the cortex (582.9 BPU) than the medulla (372.3 BPU, Mann-Whitney test P<0.0001). However during the initial 15 minutes of reperfusion, there was no clear region receiving greater blood flow (Fig.5.2).

When regional MVP was compared against global RBF (Fig.5.1B), an initial fall in RBF appears to be mirrored by both cortical and medullary MVP. A subsequent increase in RBF does not appear to be apparent in either region. However, overall there was a significant weak-positive correlation between cortical MVP and global RBF (Fig.5.5, Spearman's rank coefficient r = 0.341, P=0.041).

5.3.4 Regional tissue oxygenation during machine reperfusion

In the pilot series, mean P_tO_2 was higher in the cortex than the medulla (13.3±4.1 vs. 4.4±1.5 kPa P<0.0001) Against time, cortical oxygen remained higher than medulla values throughout the reperfusion (appendix Fig.C.3A).

In the controls-only pilot analysis, mean cortical and medullary P_tO_2 was 6.07±3.1 and 2.26±2.0 respectively (P<0.0001). Whilst mean values were higher, cortical oxygenation fell

from the peak in the first 10 minutes to similar levels as the medulla by 30 minutes, before rising again towards the end of 90 minutes (appendix Fig.C.3B).

The platform series mean P_tO_2 was greater in the cortex than the medulla (13.23±±4.0 vs. 3.93±2.2 kPa, P<0.0001). Medullary oxygenation fell precipitously during the initial 10 minutes of reperfusion, and remained low for the rest of the experiment. Cortical P_tO_2 continued to rise throughout the reperfusion (appendix Fig.C.3C).

When the pilot controls and platform kidney perfusions were pooled for analysis (Fig. 5.3A) mean tissue oxygenation was higher in the cortex than the medulla (10.24±2.03 vs. 3.20±1.2 kPa respectively, Mann-Whitney test P<0.0001). Medullary P_tO_2 fell over the initial 30 minutes of reperfusion, whilst cortical P_tO_2 increased with time. When regional P_tO_2 was plotted against global RBF (Fig.5.3B), cortical P_tO_2 appeared to be more closed related to RBF than medullary P_tO_2. However, neither demonstrated significant correlation with RBF (Fig. 5.5, see section below for greater detail).

5.3.5 Correlations between donor characteristics, performance during machine reperfusion and regional oxygenation and perfusion

For the combined pilot-control and platform series, a correlation matrix was performed on pooled values for donor characteristics, circuit parameters, renal function, oxygen kinetics, regional MVP and regional P_tO_2 (Fig. 5.5).

There was a strongly positive correlation between medullary P_tO_2 and urine output (r=0.8 P=0.0003 and by linear regression in Fig. 5.6).

There was no significant relationship between the perfusion and oxygenation in the cortex (P=0.29). However, there was a significant positive relationship between the two in the medulla (Spearman's rank coefficient r=0.45, P=0.01, Fig.5.5). There were weakly-positive correlations between cortical MVP and medullary MVP (r=0.45 P=0.01), global RBF (r=0.34 P=0.04) and medullary P_tO_2 (r=0.45 P=0.01). There was further a weakly-positive

correlation between medullary MVP and medullary P_tO_2 (r=0.45 *P*=0.01). There were no significant relationships between cortical P_tO_2 and any other parameters.

5.3.6 Regional fibrin deposition following reperfusion

In total, 560 images from each region were analysed, pooled from all platform kidneys. Representative images from each region are shown in figure 5.7A and B. The median percentage positive staining for fibrin was 0.0046 in the cortex and 0.0063 in the medulla (*P*=0.003, unpaired Mann-Whitney test). The majority of cortical deposition occurred in Bowman's spaces, and medullary fibrin deposition was concentrated in tubular lumina, rather than peritubular capillaries (Fig. 5.7C).

5.4 Discussion

Using an NMP model of transplant reperfusion, we examined regional patterns of microvascular reperfusion and tissue oxygenation in human kidneys. Our major findings were that NMP reperfusion led to widespread changes in microvascular perfusion, with relative medullary hyperperfusion especially prominent immediately following restoration of blood flow. Fluctuations in perfusion continued throughout the first 90 minutes of reperfusion and appeared to be unrelated to global renal blood flow, function or oxygen kinetics or have a reliable relationship to tissue oxygenation. In contrast, regional tissue oxygenation rapidly diverged, reaching pre-ischaemic values in cortex and medulla after an hour of reperfusion. Medullary tissue oxygenation correlated with urine output, providing the only strong association between either phosphorimetric parameter and global kidney condition.

These results are important because they provide the first description of regional microcirculation and oxygenation of human transplant kidneys during normothermic machine perfusion. They provide a novel insight into regional discrepancies within the kidney dur-

ing early (simulated) transplant reperfusion, and emphasise the difficulties of predicting medullary (and indeed cortical) condition using global markers of renal function alone.

5.4.1 Regional microvascular perfusion during reperfusion

Overall, microvascular perfusion was greater in the cortical compartments. However, there was little disparity between compartments at the beginning and end of perfusions (fig.5.1); indeed the greatest inter-compartmental flux was observed during the initial 15 minutes of perfusion (Fig. 5.2) Under normal conditions close to 80 percent of total RBF is delivered to the cortex, so this represents a significant medullary hyper-perfusion during early reperfusion. There is no clear resolution of these disruptions after 90 minutes of reperfusion, suggesting they may persist beyond our experimental time-frame.

Very few studies have examined human renal microvascular perfusion following IRI; and none have described medullary perfusion, used phosphorimetry, nor described findings during NMP. Using a thermodiffusion technique inserted into the cortex of 30 donor kidneys during engraftment and for up to 7 days post implantation, Angelscu and colleagues described low initial cortical blood flow of 69.9 mL/100g/min that rose to 85.7 mL/100g/min around a hour later but do not report more detailed initial changes [13]. Our findings of relatively reduced cortical perfusion are consistent with findings in porcine autotransplant ([111]) and cross-clamp ([153]) studies and others in small mammals [48, 72].

The fluctuating perfusion we describe in the medulla mirrors conflicting data from the small number of existing small-animal studies. Evans et al. ([48]) recorded a reduction in rabbit medullary flow during reperfusion, whereas other murine studies have variously reported a gradual return to baseline ([171]), hyperperfusion prominently in the inner medulla ([72, 170]) or sustained reductions in flow ([142]). Overall, this would support the notion that early medullary reperfusion is heterogenous, labile and liable to sampling and temporal

discrepancies. In our model, which necessitates a large volume of 'bypass'-style tubing, erythrocyte deformity may also increase microvascular shunting [72].

5.4.2 Regional tissue oxygenation during reperfusion

Unlike microvascular perfusion, P_tO_2 diverged early between regions. Cortical P_tO_2 fell initially, before increasing after 30 minutes reperfusion; in contrast medullary P_tO_2 fell across reperfusion, with brief interspersed periods of higher oxygenation (Fig.5.3).

Experimental studies of regional renal tissue oxygenation following ischaemic injury are sparse, with no reports to our knowledge in human kidneys. Most studies in rat [105], rabbit [48] and pig [153] report a post-reperfusion fall in cortical oxygenation; a finding repeated by our own porcine study (chapter 4). Our finding of rising cortical P_tO_2 following an initial fall may represent sampling at a later timepoint, and more importantly a recovery in tissue oxygen. Two lines of reasoning support this theory. Firstly, values in both regions stabilise after around 70 minutes of perfusion (Fig.5.3), and the initial disturbances seen in values (which has previously been described in the rat cortex in a model of sepsis [44]) are no longer seen. Secondly, the cortico-medullary oxygen differential after 70 minutes is similar to that seen *in-vivo*, with the important caveat that the NMP circuit delivers supra-physiological P_PO_2. At the end of 90 minutes reperfusion, cortical P_tO_2 was 13kPa and medullary P_tO_2 3kPa. Thus, at the end of 90 minutes NMP perfusion, cortical oxygenation approximates closely to that found in the highly-oxygenated perfusate ($\approx$12kPa, see chapter 3.3.1). The 90-minute perfusion medullary values of 3kPa broadly corresponds to that found *in-vivo* (whereas cortical values are usually reported 6-7kPa across mammals [93]).

The surprising absence of a clear relationship between regional MVP and P_tO_2, described in the previous chapter, was also seen in this study (Fig.5.4A and B). The apparent decoupling of these inseparable axioms of aerobic respiration may be explained by a number of phenomena. Firstly, it may be that anatomical shunts remain relatively intact following

IRI, as whilst severe endothelial and tubular damage may occur, the overarching proximity of opposing vasculature will not change. Thus, regional P_tO_2 values can return to those similar *in-vivo* despite ongoing circulatory dysregulation. Secondly, heterogeneous local reductions to filtrative (cortical) and resorptive (medullary) demand, secondary to patchy reperfusion, may given have been measured globally as a disruption to the normally linear relationship between perfusion and oxygen consumption [93]. Finally, this may represent technical limitations, as the LDF probe is not able to determine directional flow or give perfusion in absolute terms, and nor is tissue oxygenation necessarily a surrogate for cellular respiration in the complex and evolving reperfusion micro-environment.

5.4.3 The relationship between phosphorimetry and global renal function

An important clinical question arising from these phosphorimetric data is whether we can infer regional perfusion and oxygenation from existing measurements taken during NMP.

There was a convincing positive relationship between urine output and medullary oxygenation (Fig. 5.6) The absence of a relationship between UO and urine osmolality suggests intact concentrating mechanisms (i.e. medullary function) in higher-output kidneys. Based on a series of human kidneys declined for transplantation, Hosgood et al. derived a grading system for organ assessment during NMP. Alongside patchy physical appearance, poor renal blood flow (<50mL/h) and urine output (<43mL total) were associated with higher rates of DGF and lower 12-month eGFR in a subsequent series of transplanted kidneys [81]. Whilst we might infer therefore that higher medullary oxygenation might be associated with better graft outcomes, all of the kidneys analysed for this correlation exceeded threshold values for RBF and UO (table 5.4) and thus fall outside the negative-predictive scope of the scoring system.

Whilst pooled values for regional MVP, taken at either 60 or 90 minutes perfusion correlated weakly with global RBF, medullary MVP and medullary oxygenation, sequential temporal comparisons (Fig. 5.4) suggest against these being reliable relationships. This uncoupling of global blood flow from microvascular perfusion and other functional parameters is well-documented across organs and disease states [137]. However, whilst MVP does not easily correlate with more established markers, a large body of work examining microvascular changes in septic shock suggests that MVP (and equivalent microvascular parameters) may offer earlier signs of compromise and recover and thus merit independent monitoring [64].

5.4.4 Regional fibrin deposition following reperfusion injury

There was significantly greater fibrin deposition in the medulla than in the cortex. This is consistent with earlier work, where greater deposition has been demonstrated in the OM of rat kidneys and was consistent with higher tubular injury scores [161]. However, whilst percentage deposition was similar across cortical samples, medullary fibrin deposition was less uniform (Fig.5.7C). This may represent heterogeneous injury, or more consistent sampling of superficial cortical tissues.

Such extravascular fibrin deposition post-IRI has previously been demonstrated in rat kidney Bowman's spaces [45] and medullary tubular lumina [161].

Our group has recently described time-dependent cold-storage induced fibrin deposition in the cortex of human kidneys that prompts intravascular release of fibrinogen, and correlates with red cell aggregation and microvascular plugging [42]. Furthermore, DiRito and colleagues then describe successful fibrinolysis following delivery of plasminogen and tissue plasminogen activator during NMP, with improved function and reduced injury markers.

Several reports exist of medullary red cell trapping [72], vascular clogging and tissue oedema [108] during reperfusion. Combined with the results of DiRito et. al's study,

our evidence strongly suggests the presence of medullary vascular plugging, secondary to increased fibrin deposition that in turn explains the heterogeneous alterations in perfusion seen.

Anticoagulants are routinely used intra-operatively to prevent anastomotic thromboses, so our results on a heparinised NMP circuit are likely consistent with the clinical early-reperfusion environment. Given that anticoagulation has been demonstrated to reduce post-ischaemic inflammation (through reduced fibrin deposition [56]) this may represent a mechanism through which NMP exerts a beneficial effect on early graft outcomes. However, whilst the persistent presence of some fibrin deposition suggests that further anticoagulation may be beneficial, fibrin exerts pleimorphic effects in acute inflammation, and total knockout uniformly results in harm in murine models [110].

5.4.5 Limitations

This study employed a clinically-relevant NMP model to examine a heterogeneous group of human kidneys from both DCD and DBD donors. Because we did not perfuse any kidneys that with absolute contraindications discovered at retrieval, those we did perfuse very closely represent the 'marginal donor' organs that are increasingly considered for transplantation. We did not attempt to delineate the influence of retrieval methods on regional physiology. Whilst the regional changes in perfusion and oxygenation described will be similar to the trajectory of implanted kidneys post-reperfusion, certain factors necessary for the NMP circuit are likely to have influenced our findings. Firstly, the absence of infiltrating immune cells (from whole blood) and addition of prostacyclin and steroid to the perfusate are likely to have modulated (and reduced) endothelial injury. Secondly, circuit heparinisation may have reduced the observed fibrin deposition and the associated tissue oedema and inflammation. Finally, whilst regional differences in P_tO_2 at end-perfusion appear stable, we cannot draw firm conclusions from the absolute regional P_tO_2 described because the NMP circuit uses

a clinical standard of 95% (i.e. hyperoxic) perfusate. Future work to delineate specific reperfusion phenomena could utilise NMP with a normoxic, whole blood perfusate, without protective additives.

Using paired phosphorimetric and Doppler probes we were able to make novel dynamic and simultaneous recordings of cortical and medullary MVP and P_tO_2 in human kidneys. A major benefit of this technique is that it causes minimal trauma to the surrounding tissue, which is essential when sampling the renal medulla deep to the highly vascular CMJ region. Due to high probe sensitivity and a desire to collect continuous data, we elected only to instrument one paired-probe site per kidney region. This may represent a major study limitation, as the heterogeneous nature of reperfusion injury means that it is possible that the data collected may not have been representative of the whole regional micro-environment. Furthermore, as previously discussed we cannot determine directional flow from laser-Doppler flowmetry, nor examine cellular hypoxia with a fluorescence optode with a large sampling field (see chapter 4.4). Future work could consider multiple probe sites, or the concomitant use of imaging techniques such as contrast-enhanced ultrasound to gauge regional heterogeneity and confirm probe placement.

Martius Scarlet Blue (MSB) staining is a well-established technique for assessing fibrin deposition. However, without concomitant histological or biochemical evidence of tissue injury, we cannot determine whether the significant regional difference in deposition described has any functional importance. Regional inflammatory gene expression analysis was subsequently analysed on samples from the platform kidney series and discussed in the next chapter (6).

5.4.6 Conclusions

Transplant reperfusion exerts differential regional effects on the renal microcirculation, likely due in part to microvascular plugging, that are not easily identified by global measurements

of kidney function. Compartmental oxygenation appears to return to baselines relatively quickly, with the uncoupling of these two parameters possibly explained by diffusional anatomical shunting. Urine output may be a useful marker of medullary oxygenation during normothermic machine perfusion.

5.5 Tables and figures

Group	Age		Sex		Donation		Chirality		CIT (h)	
	x	sd	M	F	DCD	DBD	L	R	x	sd
Pilot	61.0	12.8	3	2	5	7	4	8	19.7	12.8
Pilot Control	71.7	7.6	1	2	2	3	2	3	24.0	8.7
Platform	57.2	11.9	4	2	4	3	3	4	15.9	5.6
Platform Control	58.6	16.5	3	1	5	0	4	1	17.5	11.1

Table 5.1 **Kidney donor characteristics.**
DCD, donation after circulatory death; *DBD*, donation after brainstem death; *CIT*, cold ischaemic time

Study	N	Hb(g/L)		HCT		pH		P_PO_2 (kPa)		Weight(g)		T(°C)	
		x	sd	x	sd	x	sd	x	sd	x	sd	x	sd
Pilot	12	104.40	18.84	0.31	0.06	7.24	0.11	75.46	5.41	275.48	106.57	35.73	0.72
P.controls	5	108.00	27.64	0.33	0.08	7.21	0.09	73.98	3.31	290.48	126.21	35.30	0.82
Platform	7	93.67	7.97	0.29	0.02	7.23	0.11	77.42	4.97	203.29	61.95	35.81	0.71

Table 5.2 **Initial kidney parameters prior at the start of normothermic machine perfusion.**
Hb, haemoglobin; HCT,haematocrit;PPO2, perfusate oxygen tension

Group	Time(m)	RBF/100g		UO/100g		pH		C_aO_2		DO_2		VO_2		OER	
		x	sd	x	sd	x	sd	x	sd	x	sd	x	sd	x	sd
Pilot	60	60.18[A]	43.72	0.83	0.79	7.31	0.07	13.61[B]	2.70	8.43[C]	5.43	1.64	0.55	0.23[D]	0.08
	90	82.36	50.08	0.32	0.52	7.33	0.10								
P.controls	60	43.30	45.51	0.77	0.82	7.31	0.09	13.87	0.66	8.37	8.43	1.39	0.66	0.23	0.10
	90	63.89	53.89	0.15	0.13	7.30	0.14								
Platform	60	132.91[A]	45.69	1.18	0.77	7.32	0.07	13.25[B]	1.10	17.32[C]	6.16	1.36	0.62	0.09[D]	0.06
	90	142.87	53.56	2.48	2.21	7.35	0.09	12.40	2.56	16.57	5.83	0.95	0.75	0.07	0.07

Table 5.3 **Grouped perfusion characteristics and oxygen kinetics during NMP.**
Functional parameters and oxygen kinetics were taken at 60 and 90 minutes perfusion A, *P*=0.026; B, *P*=0.035; C, *P*=0.0012 and D, *P*=0.0047

Time	CrCl		FeNa		UrOsm		C_aO_2		DO_2		VO_2		OER	
	x	sd	x	sd	x	sd	x	sd	x	sd	x	sd	x	sd
60	6.33	3.52	17.02	13.80	352.67	47.13	13.25	5.03	17.32	8.54	1.36	0.62	0.09	0.06
90	10.34	5.82	28.52	25.30	353.67	36.11	1.10	2.56	6.16	5.83	0.62	0.75	0.06	0.07

Table 5.4 **Platform group renal function and oxygen kinetics after 90 minutes normothermic machine perfusion.** CrCl, creatinine clearance; FeNa, fractional sodium excretion; UrOsm, urine osmolality (mOsmol /kg), C_aO_2, perfusate oxygen context (mL/kg); DO_2, oxygen delivery (mL/kg/min); VO_2, oxygen consumption (mL/kg/min); OER, oxygen extraction ratio.

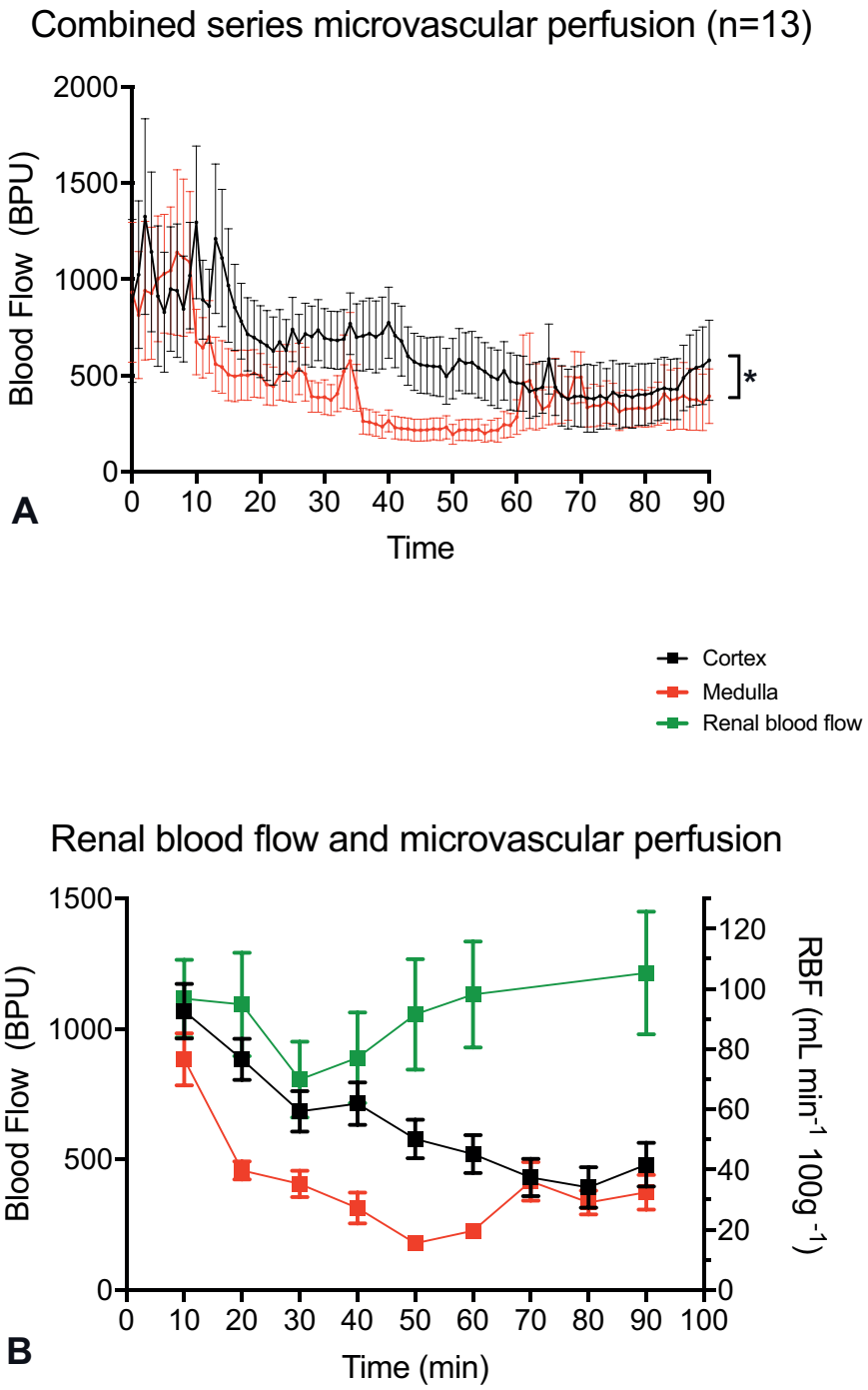

Fig. 5.1 **Regional microvascular and global perfusion during human kidney machine reperfusion.**
To investigate regional variations in microvascular perfusion (MVP) during transplant reperfusion and compare against current measurements during machine perfusion, human kidneys declined for transplantation from two series (n=12)) underwent 90 minutes of normothermic machine reperfusion. Simultaneously, MVP was measured in the cortex and medulla (A) and compared against global kidney perfusion (B). * P>0.0001, two-tailed Mann-Whitney test. Values are mean and SEM.

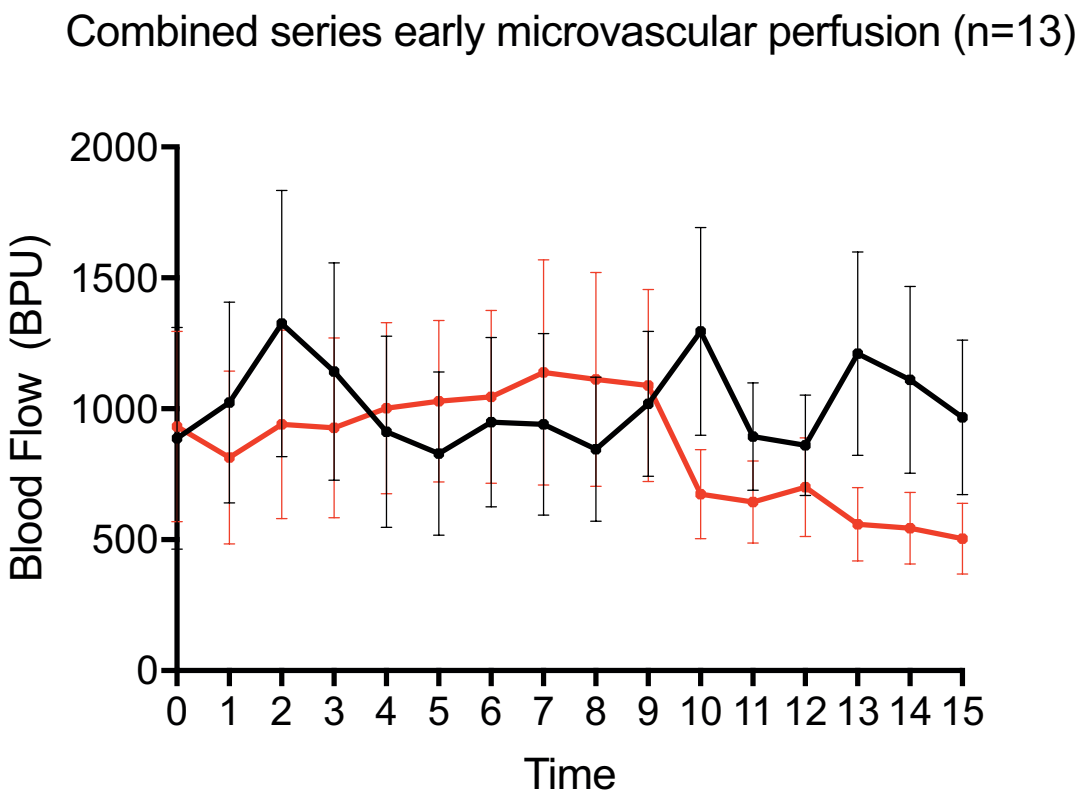

Fig. 5.2 **Regional microvascular perfusion during early machine reperfusion.**
To examine early variation in regional blood flow during transplant reperfusion, microvascular perfusion (MVP) was measured in two series of human kidneys declined for transplantation (n=12) during the first 15 minutes of normothermic machine reperfusion. BPU, Blood perfusion units. P=0.105, two-tailed Mann-Whitney test. Values are mean and SEM.

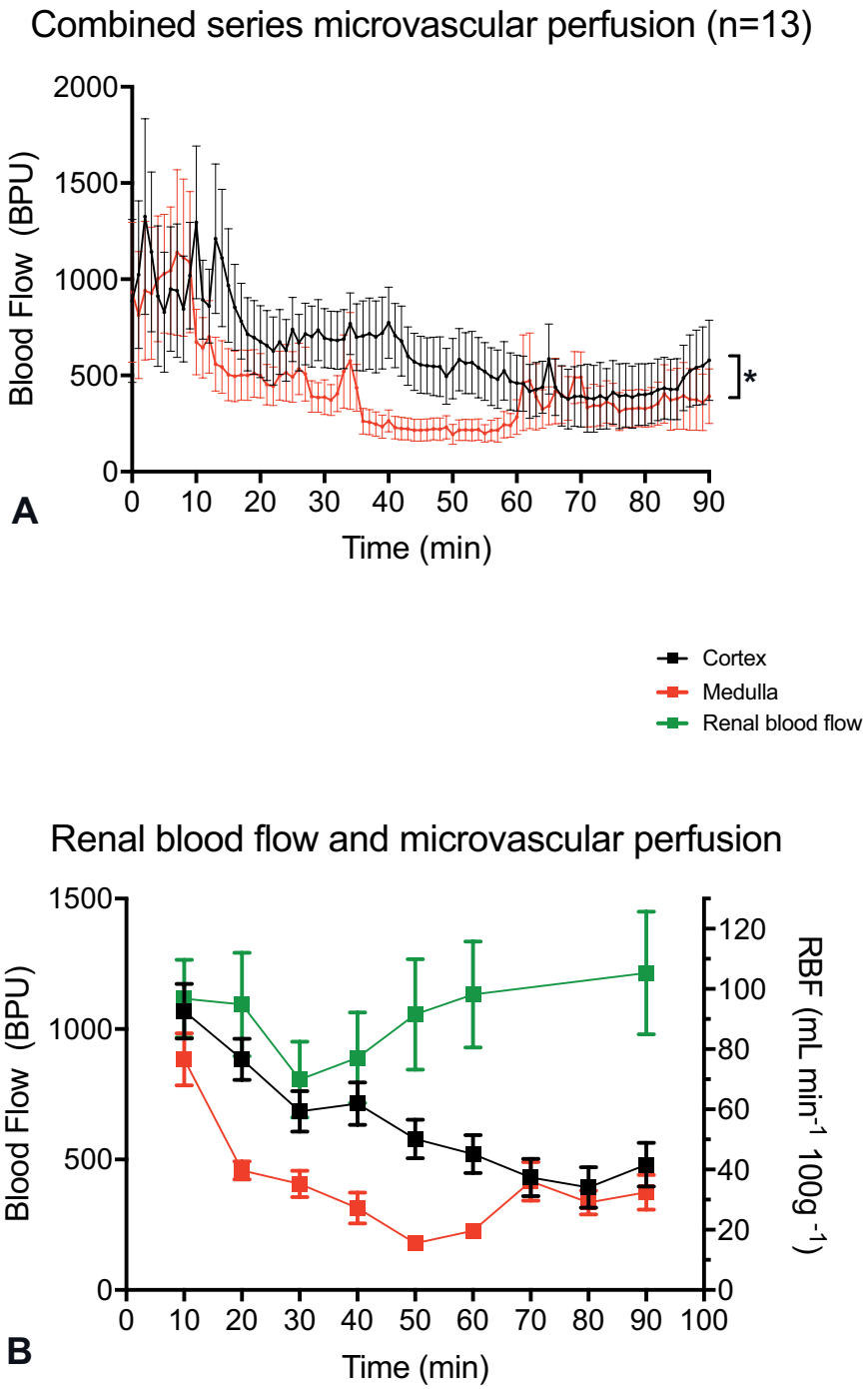

Fig. 5.3 **Regional tissue oxygenation and global perfusion during human kidney machine reperfusion.**
To investigate regional variations in tissue oxygenation (P_tO_2) during transplant reperfusion and compare against current machine perfusion measurements , human kidneys declined for transplantation from two series (n=12)) underwent 90 minutes of normothermic machine reperfusion. Regional P_tO_2 was measured simultaneously in cortex and medulla (A) and compared against global kidney perfusion (B). * P>0.0001, two-tailed Mann-Whitney test. Values are mean (SEM).

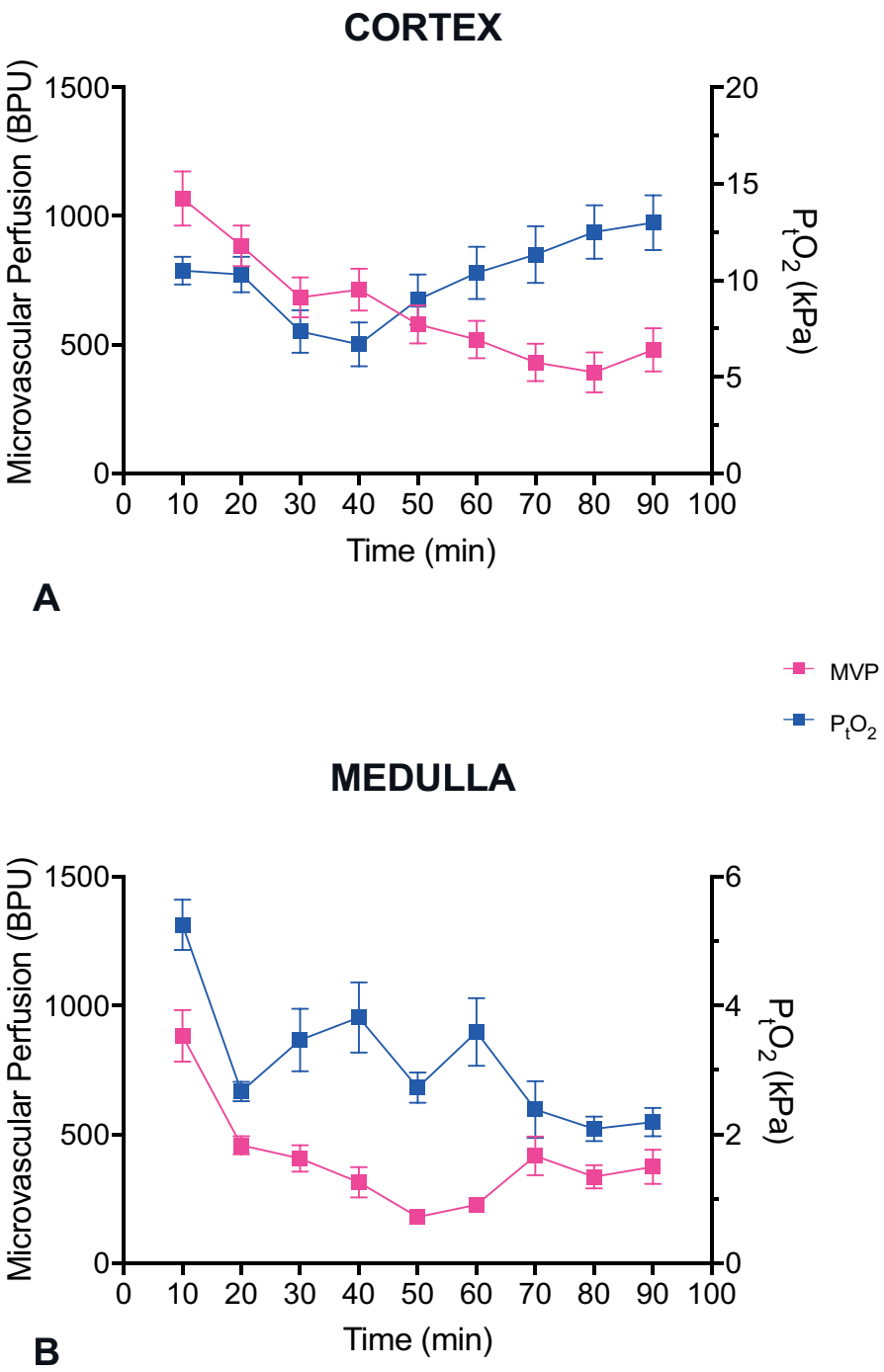

Fig. 5.4 **Regional variations in oxygenation and perfusion during machine reperfusion.** The simultaneous variations in tissue oxygenation (PtO2) and microvascular perfusion (MVP) during 90 minutes of machine reperfusion of human kidneys (n=12) were measured in the cortex (A) and medulla (B). Values are 10-minute mean (SEM).

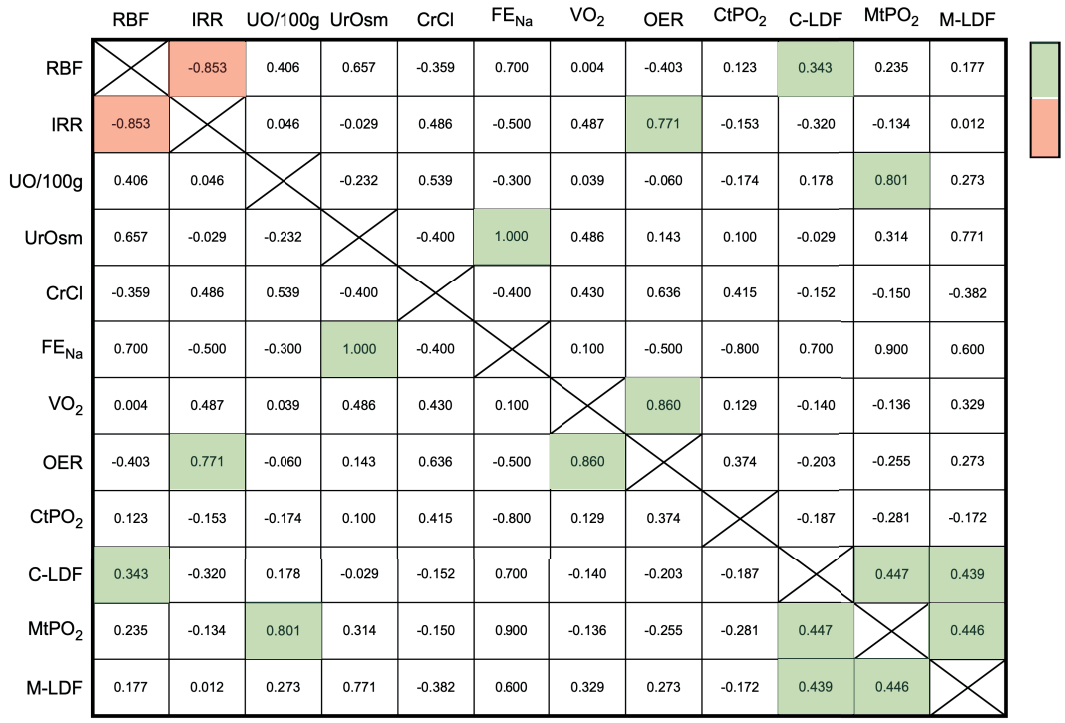

Fig. 5.5 **Correlation matrix of renal function, oxygen kinetics and regional perfusion during machine reperfusion.**
Twelve human kidneys declined for transplantation underwent machine reperfusion for 90 minutes. Renal function and regional oxygenation/perfusion measurements were assessed for correlation. Values depicted are Spearman's rank coefficient (r-value). Green shading denote a significant positive relationship; red shading denotes a significant negative relationship. There was a strongly positive correlation between medullary tissue oxygenation (P_tO_2) and urine output (UO, P=0.0003). There was a significant positive relationship between medullary microvascular perfusion (MVP) and P_tO_2 (P=0.01). There were weakly-positive correlations between cortical MVP and medullary MVP (P=0.01), global renal blood flow (RBF, P=0.04) and medullary P_tO_2 (P=0.01). There was further a weakly-positive correlation between medullary MVP and medullary P_tO_2 (P=0.01). CrCl, creatinine clearance; FE_{Na}, fractional excretion of sodium; C_aO_2, perfusate oxygen content; DO_2, oxygen delivery; VO_2, oxygen consumption; OER, oxygen extraction ratio.

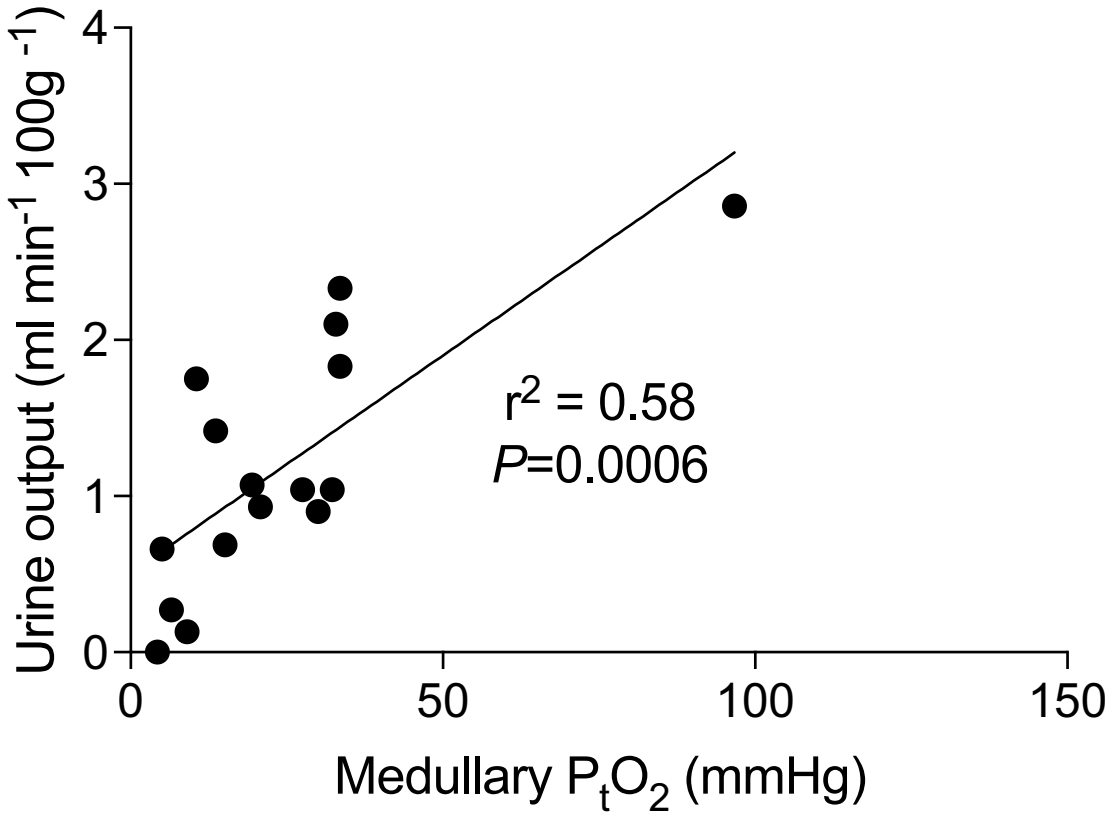

Fig. 5.6 **The relationship between medullary oxygenation and urine output during machine reperfusion.**
The relationship between medullary tissue oxygenation (PtO2) and urine output (UO) during machine reperfusion of human kidneys declined for transplantation (n=12) was assessed by linear regression. Each point represents a reading from one kidney at either 60 or 90 minutes reperfusion. R-square goodness of fit (r^2), significance of slope deviation from zero *P*.

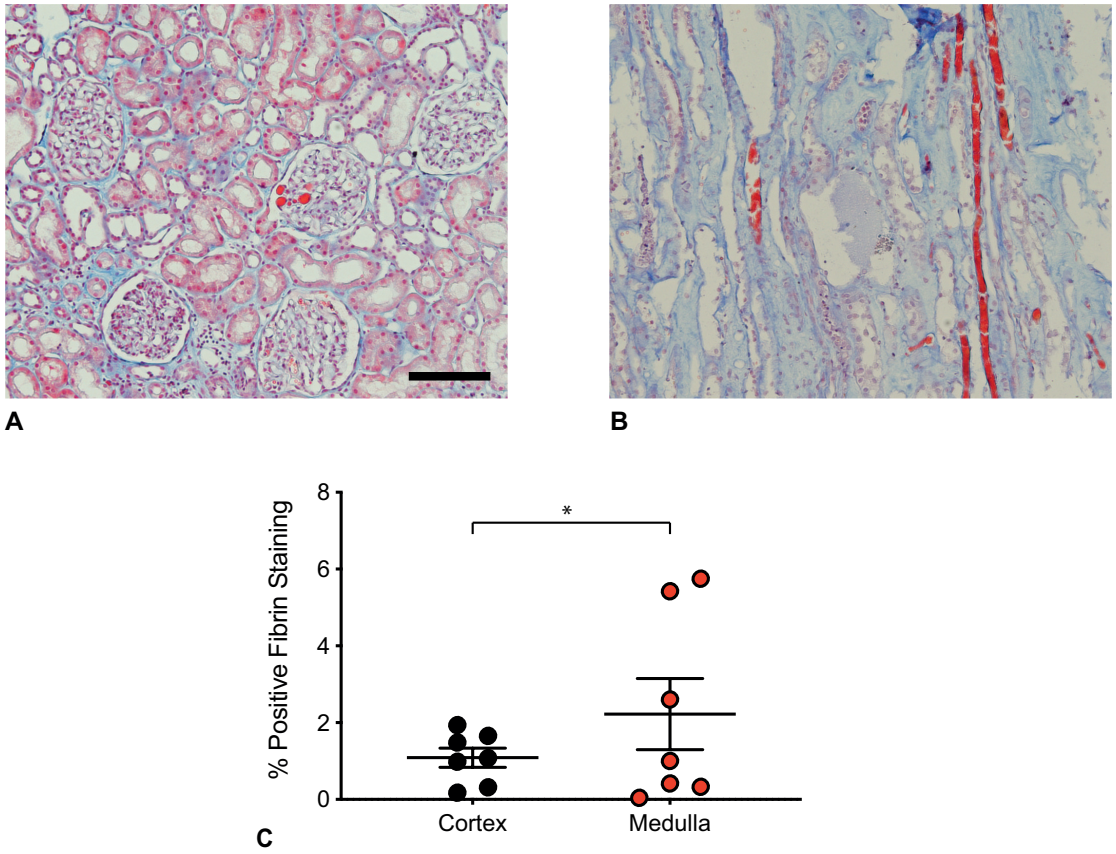

Fig. 5.7 **Regional fibrin deposition in human kidney following normothermic machine perfusion.**
Seven human kidneys declined for transplantation underwent machine reperfusion for 90 minutes, after which cortical and medullary tissue was stained for martius scarlet blue for fibrin deposition. Representative images of cortex (A) and medulla (B) are shown. Percentage fibrin deposition was analysed in each region (C). Scale bar represents 100μm. * P=0.003, unpaired Mann-Whitney test.

Chapter 6

Regional inflammatory gene expression during human transplant kidney normothermic machine perfusion

6.1 Introduction

The kidney is a complex solid organ comprised of as many as 26 differentiated cell types spread across multiple specialised segments of its functional unit, the nephron [119]. The circulation, oxygenation and cellular biology of each segment are optimised for renal function, with the greatest differences being seen between the cortex and medulla. The critical influence of ischaemia-reperfusion injury upon the trajectory of the renal allograft has long been appreciated, with well-described cellular mechanisms and effects upon graft function and survival (see section 1.3).

However, the manifold complexity of the kidney and dynamically-evolving nature of IRI have hampered attempts to delineate the pathophysiology underpinning tissue- and organ-level dysfunction in IRI and thus ameliorate its sizeable impact upon clinical transplantation.

Longitudinal analyses of early inflammatory biomarkers have been correlated to later graft function [148, 127] but no single biomarker of IRI is accepted as a reflection of current organ state nor a prediction of its future performance [119]. Emerging next-generation sequencing (NGS) techniques are being employed to overcome these challenges, and are permitting more detailed transcriptional analysis of the evolution of the renal IRI phenotype, both in the context of AKI and in TIRI [40].

Whilst NGS studies have characterised global or cortical transcriptional changes during IRI, this new era is yet to impact significantly on our understanding of ischaemic damage and repair in the renal medulla. Histological studies suggest disproportionate injury to the renal medulla during IRI. In the previous chapter (5), we demonstrated widespread disruption to renal medullary perfusion during early transplant perfusion, further supporting the existence of a unique environment during this critical phase of transplantation. Examining the renal medullary transcriptome during IRI may highlight broad, coordinated disruption and dysregulation of cellular and physiological processes that may not be recognised by more focused assays. Describing inflammatory pathways within the highly specialised kidney regions may help guide target therapeutic strategies to ameliorate damage.

The aim of this study was therefore to investigate the effect of normothermic machine perfusion upon human renal regional inflammatory gene expression, as compared to static cold storage.

Related to our aim, we hypothesised that:

1. Normothermic machine perfusion would alter the expression of inflammatory genes in both human renal cortex and medulla, when compared to a baseline of static cold storage.

2. Inflammatory gene expression in human renal medulla would demonstrate a different pattern to that shown in human renal cortex during normothermic machine perfusion.

3. Because of the greater propensity of medullary tissue for ischaemic and reperfusion damage, inflammatory gene expression would be greater in medulla when compared to cortex.

6.2 Methodology

To investigate regional inflammatory gene expression in human transplant kidneys following machine perfusion, cortical and medullary samples were taken from 7 unpaired kidneys at the end of 90 minutes normothermic machine perfusion (as detailed in section 2.3.2). Hourly perfusate and urine samples were taken as described in section 2.4.1. To act as a control for the kidneys undergoing NMP, cortical and medullary samples were also taken from 4 unpaired kidneys during SCS. The same inclusion criteria were applied to these as to the NMP kidneys (described in Chapter 5.2). RNA was extracted and assessed for concentration and quality (section 2.4.5). The mRNA expression of a panel of 251 inflammatory genes was quantified using the Nanostring nCounter (section 2.4.5). Because the priority of this study was to investigate regional inflammatory gene expression differences, and due to limited access to Nanostring processing, SCS and NMP samples were processed in different batches. Regional gene expression during SCS and NMP and the effect of NMP, versus a control of SCS, was analysed using Nanostring nCounter advanced analysis software (section 2.5). The normal in-vivo expression of selected genes over-expressed regionally during our experiments was sought from the GTEx project portal (section 2.4.5) for comparison against our own data.

6.3 Results

6.3.1 Donor characteristics

Donor characteristics can be found in the results section of the previous chapter (5) in table 5.1. There were no significant differences between the platform and platform control kidneys in terms of donor age or CIT. Of note, whilst all control kidneys were from DCD donors, 3 of the 7 platform kidneys were from DBD donors.

6.3.2 The effect of normothermic machine perfusion upon inflammatory gene expression.

Paired cortical and medullary samples were taken from five kidneys following SCS, and six kidneys following the period of NMP and normalized mRNA expression obtained (appendix D). No quality control flags were raised during analysis. Principle component analysis revealed distinct clustering of cortical inflammatory gene expression by treatment (Fig.6.1A); unsupervised clustering of all cortical gene expression by Euclidean distance and average linkage also grouped total geneset expression by treatment (Fig.6.1B). Twenty four genes were significantly differentially expressed by the cortex during NMP compared to SCS, with 10 upregulated and 14 downregulated (Fig.6.2). In the medullary tissue, the total inflammatory geneset similarly grouped by treatment upon principle component analysis (Fig.6.3A) and unsupervised heirarchical clustering (Fig.6.3B). Fifty-two genes were differentially expressed in the medulla following NMP, with 22 upregulated and 30 downregulated when compared to SCS (Fig.6.4).

6.3.3 Regional inflammatory gene expression during static cold storage (SCS)

Five paired samples of SCS kidney cortex and medulla were analysed. Principle component analysis revealed overlapping prediction ellipses suggesting that there was no distinct clustering by kidney region (Fig.6.5A). Unsupervised clustering of all data by Euclidean distance and average linkage similarly did not reveal sample clustering by region Fig6.5B).

Differential gene expression

In total, 26 genes were significantly differentially expressed in the medulla during SCS when compared to the cortex (Fig.6.6A). Three genes were significantly underexpressed in medullary tissue by $\log_2$ fold changes of -1.5 or greater; Interleukin-6 Receptor (*IL6R*), Complement component 4A (*C4A*) and Complement component 2 (*C2*). Two genes were significantly upregulated in medullary tissue; Complement Factor D (*CFD*) and Phospholipase A2 group 4A (*PLA2G4A*)(Fig.6.6B). When gene expression data were fitted to selected GO pathway scores (using nCounter advanced analysis) there was no clustering of samples by their region (Fig.6.7).

6.3.4 Regional inflammatory gene expression during normothermic machine perfusion

Six paired samples of kidney cortex and medulla from the end of normothermic machine perfusion were analysed. Samples from one kidney were not analysed due to low RNA yield and quality. Initial PCA suggested that one medulla sample, lying within the cortex prediction ellipse, may have been cortical tissue. This sample was therefore removed from further analysis. Subsequent PCA revealed distinct clustering of inflammatory gene expression based on kidney region (Fig.6.8A); unsupervised clustering of all reperfusion gene expression by

Euclidean distance and average linkage was also suggestive of clustering by kidney region (Fig.6.8B).

Differential gene expression

Nineteen genes were significantly differentially expressed in the medullary samples at the end of perfusion when compared to cortical samples (Fig.6.9A). Complement C-4A was significantly underexpressed in medullary tissue by $\log_2$ fold change of greater than -1.5. Three genes were significantly over-expressed in medullary tissue by a $\log_2$ fold change >1.5; *IL6*, *CCL2* and *CXCL1*. When gene expression data were fitted to selected GO pathway scores, medullary tissue demonstrated greater activation of a broad range of biological process pathways including inflammatory response, programmed cell death, signal transduction and biopolymer metabolic process (Fig.6.10).

6.4 Discussion

Using an NMP model of transplant reperfusion and a novel highly-sensitive digital barcoding technology we described compartmental inflammatory gene expression during static cold storage and early reperfusion of human transplant kidneys. Our main findings were that simulated transplant reperfusion leads to distinct regional expression of inflammatory genes that had been similarly expressed during prior static cold storage. This suggests the presence of a unique medullary inflammatory environment during early reperfusion that may prove mechanistically important in understanding why the human renal medulla fairs poorer following transplantation. This study represents the first description of regional differences in inflammatory gene expression in the human transplant kidney during simulated reperfusion, and the most comprehensive examination of inflammation during normothermic machine perfusion to date. Our findings are important because few descriptions of medullary inflammation during IRI exist; and they may illuminate mechanisms of a pathological state

common to several forms of acute kidney injury. They further complement physiological data from previous chapters, building up a more complete picture of reperfusion pathophysiology.

6.4.1 The effect of normothermic machine perfusion upon inflammatory gene expression

Somewhat unsuprisingly, NMP prompted a striking difference in inflammatory gene expression when compared to SCS, both in cortical and medullary tissue. This is consistent with earlier work demonstrating changes to inflammatory gene expression during NMP, and importantly, these data agree with existing transcriptomic analysis of renal cortical tissue after NMP and clinical reperfusion.

In a pre-clinical series of human kidneys subjected to NMP, SCS or whole-blood machine reperfusion Hameed et al. demonstrated upregulation of pro-inflammatory cytokines, chemokines and heat shock proteins [67]. One of the genes most upregulated following NMP in that study, C-C Motif Chemokine Ligand 2 (*CCL2*), was also significantly differentially expressed after NMP in our study here. Cippà and colleagues performed transcriptome analysis of 163 protocol biopsy samples from 42 kidney transplant recipients at the end of SCS and immediately following clinical reperfusion [40]. Their analyses showed a rapid upregulation of immediate-early genes involved in stress and inflammatory responses following reperfusion in all patients. Seven of the ten genes over-expressed in the cortex after NMP in our study (*CCL2, CEBPD, CXCL2, IRF1, JUN, MYC* and *TNFAIP3*) were also differentially expressed in Cippa et al's early clinical reperfusion transcriptome (supplementary data from [40]), suggesting that the inflammatory signatures seen in our study may have considerable applicability to early clinical post-reperfusion phase. Furthermore, the broad concordance of these datasets provide some validation of the Nanostring molecular-barcoding technique

against other next-generation sequencing techniques, and also reassure against a gross batch effect, as the SCS samples and NMP samples were analysed in separate batches.

6.4.2 Regional inflammatory gene expression during static cold storage

Principal component analysis and k-means clustering did not reveal any clear grouping of SCS samples by region (Fig.6.5). This would suggest that, during cold storage following retrieval ischaemia, there were no differences between renal compartments in terms of inflammatory gene expression.

Despite broadly similar inflammatory profiles, there was some differential transcription, with reduced medullary transcription of complement components C2 and C4 and interleukin-6 receptor (IL6R), and greater expression of complement factor D (CFD) and cytosolic phospholipase A2 (PLA2G4A).

Kidneys in the SCS control group had already undergone a significant and heterogeneous period of warm ischaemia followed by cold ischaemia. In a porcine model of DCD kidney retrieval, Giraud et al. described alterations to cortical and CMJ gene expression, both immediately after a period of warm ischaemia and later changes following a period of cold storage. However, only one gene differentially expressed during our SCS experiment, complement factor D (CFD), was affected by cold ischaemia and only then in the cortical tissue [60]. Song and colleagues described greater relative expression of C2, C3 and C4 in tubular fractions than medullary fractions of normal human kidney post-nephrectomy [154], consistent with our finding of greater baseline cortical expression of C2 and C4A (an isoform of C4). In the kidney, phospholipase A2 activity broadly affects many processes including modulating vascular tone, glomerular filtration rate, solute, and water transport and inflammation, through eicosanoid synthesis [17]. Whilst PLA2G4A knockout mice

exhibit long-term urine-concentrating defects [43], the conclusions we can draw from basal overexpression in the human renal medulla are limited since it has such broad functions. Furthermore, the five most regionally-enriched genes in Fig. 6.6B were clustered by compartment when selected from the GTEx dataset of normal human tissue expression (Fig.6.6C). Finally, when expression data were fitted to biological pathways, samples did not cluster by region (Fig.6.7). Thus, the regionally-enriched transcripts present during SCS are likely to represent baseline differences in tissue expression, rather than regional differences in inflammation during static cold storage.

6.4.3 Regional inflammatory gene expression during machine reperfusion

In contrast to SCS, there was significantly altered regional inflammatory gene expression during NMP reperfusion. The inflammatory panel of 256 genes clustered by region (as demonstrated by hierarchical clustering, Fig.6.4 and principle component analysis). Overall, medullary reperfusion led to greater metabolic activity, inflammation and cell death, as evidenced by regional pathway scores (Fig.6.6), suggesting that kidney compartments orchestrate a distinct inflammatory response to simulated transplant reperfusion injury.

Nineteen genes were significantly differentially expressed by the cortex and medulla during reperfusion (Fig.6.9A). Notably, only 2 genes (C4A and Mitogen-Activated Protein Kinase 1, MAPK1) were significantly regionally enriched during both SCS and NMP reperfusion, suggesting the majority of altered transcription occurred in response to reperfusion, rather than basal expression.

The most significantly over-expressed medullary genes were IL6, CCL2 and CXCL1 (Fig.6.9B). Interleukin-6 is an immunomodulatory cytokine with numerous renal roles executed through a number different signalling cascades. In IRI, IL-6 is widely produced by

kidney cells and resident macrophages and has a maladaptive and largely pro-inflammatory effect, promoting neutrophil activation alongside microvascular dysfunction, tubular atrophy and promotion of tubulointerstitial fibrosis [159]. Kielar and colleagues demonstrated reperfusion-dependent macrophage-derived IL-6 production in the outer medulla of murine kidneys after ischaemia-reperfusion [95]. This reperfusion expression of IL-6 has also been shown in the murine cortex [46], but there has been no direct comparison of compartmental expression during reperfusion. Clinically, urine IL-6 levels have been shown to correlate with acute graft rejection [164].

Medullary expression of CCL2 and CXCL1 were significantly higher than the cortex during reperfusion, and such differences were not seen during SCS baseline. CCL2 and CXCL2 are chemokines constitutively expressed for homeostatic functions (such as regulating lymphocyte trafficking from blood to lymph nodes) and are induced during inflammatory responses to promote tissue infiltration of monocytes, basophils, T lymphocytes and NK cells for tissue defence and repair [99, 146]. Tubular epithelial expression of a number of monocyte chemotactic molecules, including CCL2 and CXCL1, increases in proportion to renal interstitial hypersalinity, and greater basal expression of CXCL1 and CCL2 has been demonstrated in the medulla putatively as part of a zonal response to combat ascending infections [24]. That we did not replicate this basal enrichment could theoretically represent disruption to medullary salinity during cold storage, due to the infusion of hyponatraemic preservation solution [23].

In a similar manner to IL-6, elevated urinary levels of CCL2 in the early phase post-transplantation have been demonstrated to be an independent predictor of 24-month interstitial fibrosis and tubular atrophy, histological surrogates of graft loss and indeed an early predictor for graft loss, independent of early acute rejection and donor-specific antibody (DSA) [73]. Whilst there is less evidence of the influence of the CXCL1 chemokine on renal

transplantation, it has a well-defined pro-inflammatory role in experimental AKI mediating neutrophil recruitment and activation during renal IRI [39].

Thus, during simulated reperfusion there is significant medullary over-expression of a number of detrimental pro-inflammatory cytokines associated with prolonged acute tissue injury and later fibrosis.

6.4.4 Limitations

This study examined a heterogeneous group of kidneys with varying sex, pre-terminal injury mechanism, WIT and CIT. It therefore describes regional inflammation in kidneys similar to those that would be considered clinically for a trial NMP. However, whilst kidneys for this study came from both DCD and DBD donors, it is likely that only DCD kidneys would initially be considered for NMP.

We used a clinically relevant model of human kidney normothermic machine perfusion, with an identical protocol to that used in a current clinical trial. There is however evidence that periods of NMP longer than 90 minutes may be beneficial for graft outcomes [90, 92, 91], although transcriptomic data from these protocols are not yet forthcoming. As other physiological markers of overall graft health appear to benefit from longer periods of perfusion, the striking relative medullary inflammation shown in this study may also benefit from longer perfusions.

Normothermic machine perfusion appears to prompt an inflammatory response that is broadly similar to that seen in early clinical reperfusion. However, the absence of infiltrating immune cells (from whole blood) and addition of prostacyclin and steroid are likely to have influenced gene expression. Hameed et al. demonstrated 65 differentially expressed cortical genes in a period of whole-blood machine reperfusion, when compared to a prior period of

NMP with a similar protocol to the one employed here [67]. There are limits therefore to the conclusions about medullary inflammation in early reperfusion that we can draw from this experiment.

The low number of kidneys sampled (5 and 6 in the SCS and NMP groups respectively) and single-data-points collected represent the high value but relative paucity of human kidneys available for perfusion experimentation. There are also inherent difficulties in obtaining medullary tissue, which is impossible during NMP due to subsequent haemorrhage. Unfortunately, these low numbers and single data-points precluded meaningful correlation of transcriptomic expression data with physiological parameters or biomarkers during NMP, although there are no widely-accepted urinary or serum biomarkers of medullary health.

Tissue samples were taken immediately post-perfusion from the bivalved kidney, where corticomedullary and medullary-papillary borders were not always well delineated. One 'medullary' sample (M1) clustered consistently with cortical samples, suggesting that this was either a cortical or CMJ sample, and thus was lost to analysis. However, the repeated and distinct medullary clustering and grouping based on principle component analyses supports the notion that, broadly, samples came from the same tissue areas.

The Nanostring molecular barcoding technique is validated method of gene expression quantification, and a viable alternative to high throughput RNA sequencing methods (RNA-seq), that avoids the associated issues of amplification bias and detailed computational analysis [132]. It permits focused analysis of gene subsets and thus requires a degree of a-priori panel selection and hypothesis-driven experimental design. The panel used for this experiment, designed for 'focused screening of the inflammation response'; has a relatively small pre-selected geneset of 251 genes that precludes the detailed initial study of underlying pathway activation. Given that there are at least 26 differentiated cell types in the

adult renal parenchyma [119] our division of samples into only two anatomical areas likely limits the mechanistic conclusions we can draw. Furthermore, we have not undertaken any confirmatory experiments by alternate methods such as histology or immunohistochemistry that may help to localise or delineate cellular roles in the regional inflammation that we have demonstrated. Because the priority of this study was to investigate regional inflammatory gene expression differences, and due to limited access to Nanostring processing, SCS and NMP samples were processed in different batches. The concordance of cortical inflammatory gene upregulation between this study and previous studies, on broad terms and including specific gene expression, adds weight to the plausibility of these findings. However, we cannot exclude the possibility that the differences demonstrated in inflammatory gene expression between treatments (i.e. the comparisons of cortical expression across SCS and NMP) were due to a batch effect rather than biological effect and no effort to account for this computationally (e.g. [104]) was undertaken.

6.4.5 Conclusions and future work

Normothermic machine perfusion of human kidneys prompts a marked early inflammatory response in both renal cortex and medulla, when compared to static cold storage, with distinctive regional patterns. The renal medulla in particular over-expresses cytokines associated with a vigorous pro-inflammatory response in transplant reperfusion injury, that have been correlated with poor initial and later graft function, suggesting that medullary reperfusion injury is under-recognised and may critically influence transplantation outcome.

To better understand the evolving pathophysiology of early regional reperfusion injury, future work should look to examine human transplant kidneys during longer periods of perfusion, ideally utilising a whole-genome-sequencing technique such as RNA-seq, and correlate transcription with regional oxygenation, perfusion and renal function.

6.5 Tables and figures

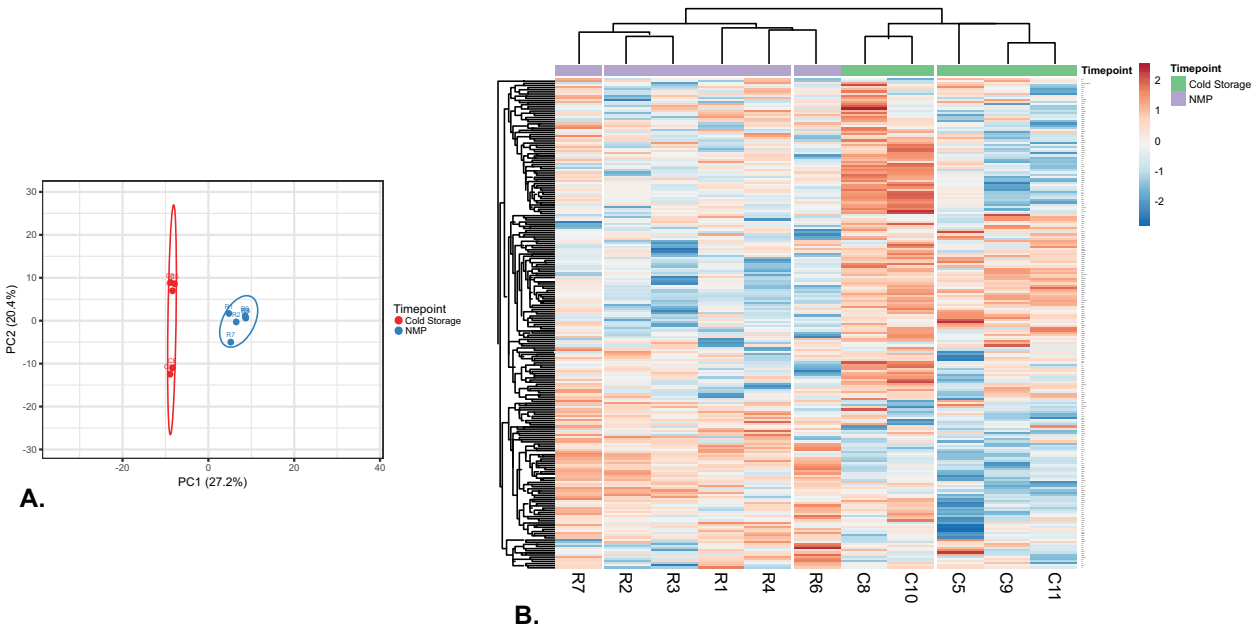

Fig. 6.1 **The effect of normothermic machine perfusion upon human renal cortex inflammatory gene expression.**
To compare renal cortex inflammatory gene expression during SCS and NMP, ribonucleic acid (RNA) was extracted during cold storage (n=5) and after 90 minutes of normothermic machine reperfusion (n=6) and analysed for messenger RNA (mRNA) expression of a multiplex of 251 inflammatory genes using the Nanostring nCounter digital counter. (A and B) Principle component analysis (PCA) of global mRNA expression. Each point represents the global mRNA expression in one sample. The X and Y axis represent the percentage of total variance explained by the first and second principle component (PC1 and PC2). Prediction ellipses represent areas into which new observations from the same group will fall with 95% probability. (B) Heatmap of all normalized data, scaled to give all genes equal variance. Each coloured box represents a cumulative z-score for normalised gene expression, with red indicating greater expression and blue indicating lower expression. Rows and columns are clustered by Euclidean distance and average linkage. R, Reperfusion sample; C, Control (SCS) sample.

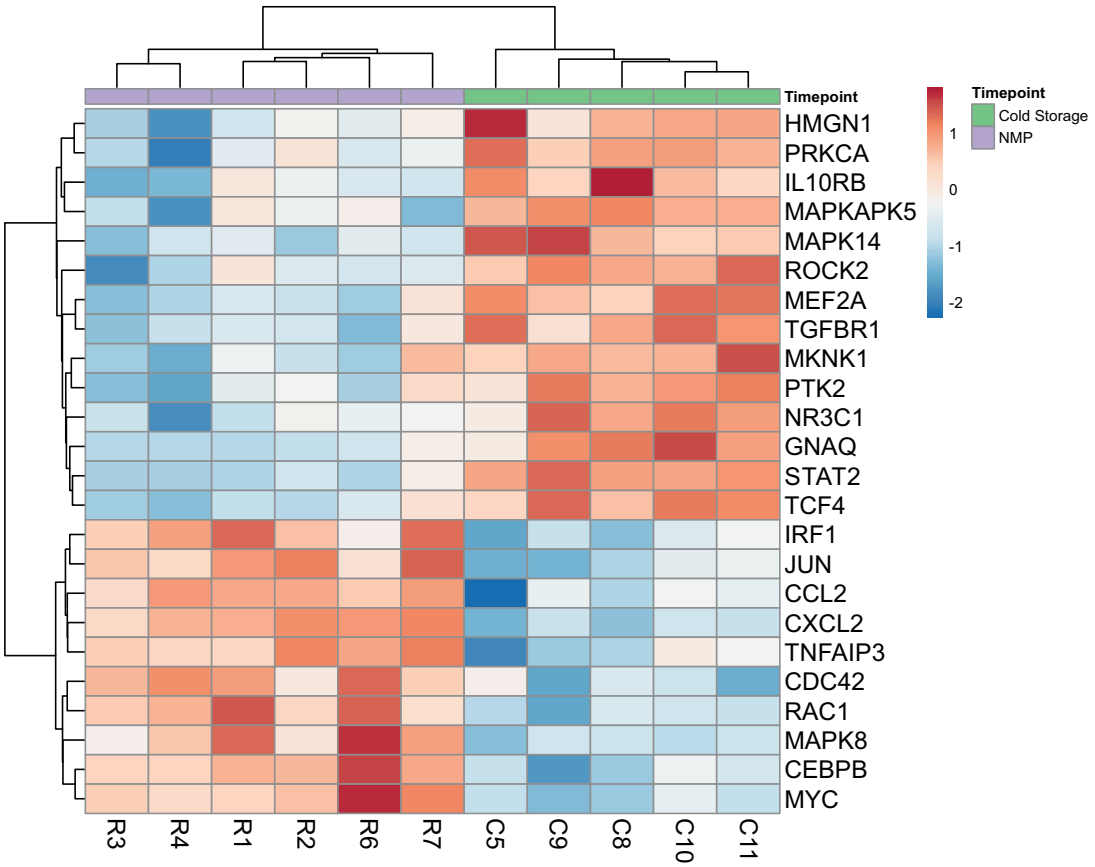

Fig. 6.2 **Differential cortical inflammatory gene expression during cold storage and normothermic machine perfusion.**
To investigate cortical inflammatory responses to normothermic machine perfusion, ribonucleic acid (RNA) was extracted during cold storage (n=5) and after 90 minutes of normothermic machine reperfusion (n=6) and analysed for messenger RNA (mRNA) expression of a multiplex of 251 inflammatory genes using the Nanostring nCounter digital counter. All 24 genes significantly (P=0.05) differentially expressed during NMP vs. SCS were clustered by Euclidean distance and average linkage. Each coloured box represents a cumulative z-score for $\log_2$ differential expression, scaled to give genes equal variance, with red indicating greater expression and blue indicating lower expression. Rn, NMP sample ID; Cn, SCS sample ID.

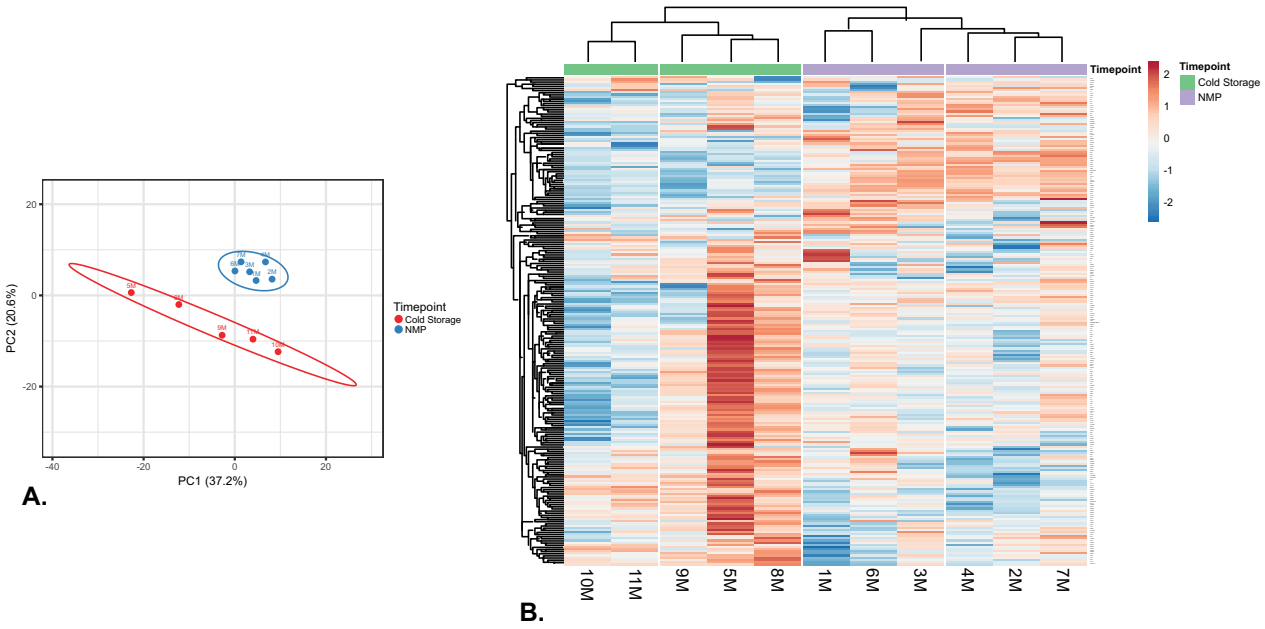

Fig. 6.3 **The effect of normothermic machine perfusion upon human renal medullary inflammatory gene expression.**
To compare renal medulla inflammatory gene expression during SCS and NMP, ribonucleic acid (RNA) was extracted during cold storage (n=5) and after 90 minutes of normothermic machine reperfusion (n=6) and analysed for messenger RNA (mRNA) expression of a multiplex of 251 inflammatory genes using the Nanostring nCounter digital counter. (A and B) Principle component analysis (PCA) of global mRNA expression. Each point represents the global mRNA expression in one sample. The X and Y axis represent the percentage of total variance explained by the first and second principle component (PC1 and PC2). Prediction ellipses represent areas into which new observations from the same group will fall with 95% probability. (B) Heatmap of all normalized data, scaled to give all genes equal variance. Each coloured box represents a cumulative z-score for normalised gene expression, with red indicating greater expression and blue indicating lower expression. Rows and columns are clustered by Euclidean distance and average linkage. nM, sample number.

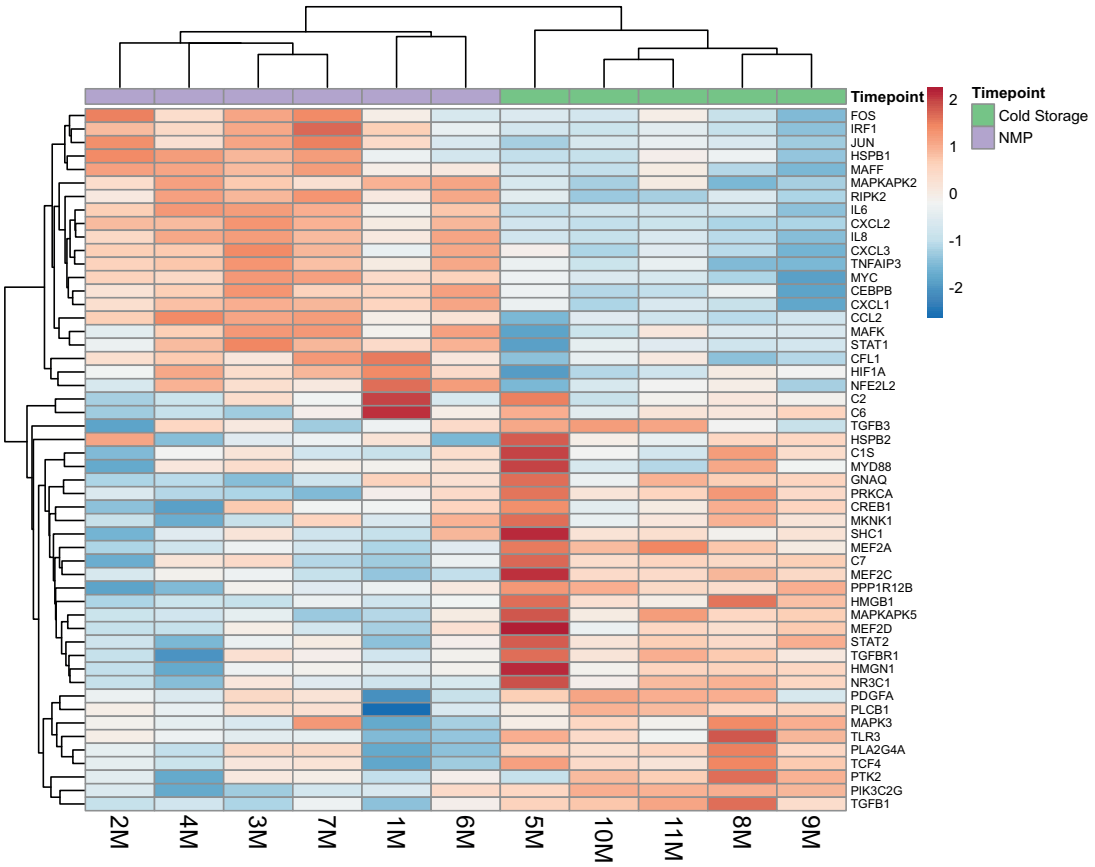

Fig. 6.4 **Differential medullary inflammatory gene expression during cold storage and normothermic machine perfusion.**
To investigate medullary inflammatory responses to normothermic machine perfusion, ribonucleic acid (RNA) was extracted during cold storage (n=5) and after 90 minutes of normothermic machine reperfusion (n=6) and analysed for messenger RNA (mRNA) expression of a multiplex of 251 inflammatory genes using the Nanostring nCounter digital counter. All 52 genes significantly (P=0.05) differentially expressed during NMP vs. SCS were clustered by Euclidean distance and average linkage. Each coloured box represents a cumulative z-score for $\log_2$ differential expression, scaled to give genes equal variance, with red indicating greater expression and blue indicating lower expression. Rows and columns are clustered by Euclidean distance and average linkage. nM, sample ID.

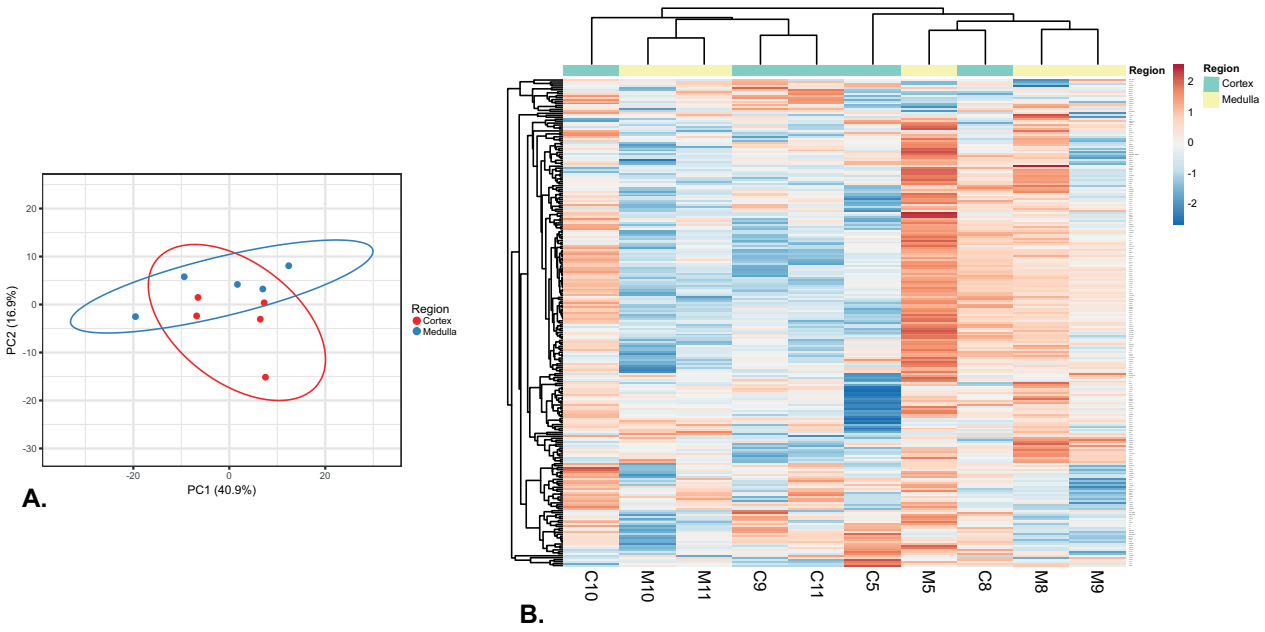

Fig. 6.5 **Inflammatory gene expression in human renal cortex and medulla during static cold storage (SCS).**
To investigate intrarenal regional differences due to transplant ischaemia and storage, ribonucleic acid (RNA) was extracted from human renal cortex and medulla (n=5 paired samples) during cold static cold storage (SCS, mean time X hrs mins) and analysed for messenger RNA (mRNA) expression of a multiplex of 251 inflammatory genes using the Nanostring nCounter digital counter. (A) Principle component analysis (PCA) of global mRNA expression. Each point represents the global mRNA expression in one sample. The X and Y axis represent the first and second principle component (PC1 and PC2) that explain 40.9% and 16.9% of the total variance respectively. Prediction ellipses represent areas into which new observations from the same group will fall with 95% probability. N=11 data points. (B) Heatmap of all normalized data, scaled to give all genes equal variance. Each coloured box represents a cumulative z-score for normalised gene expression, with red indicating greater expression and blue indicating lower expression. Rows and columns are clustered by Euclidean distance and average linkage.

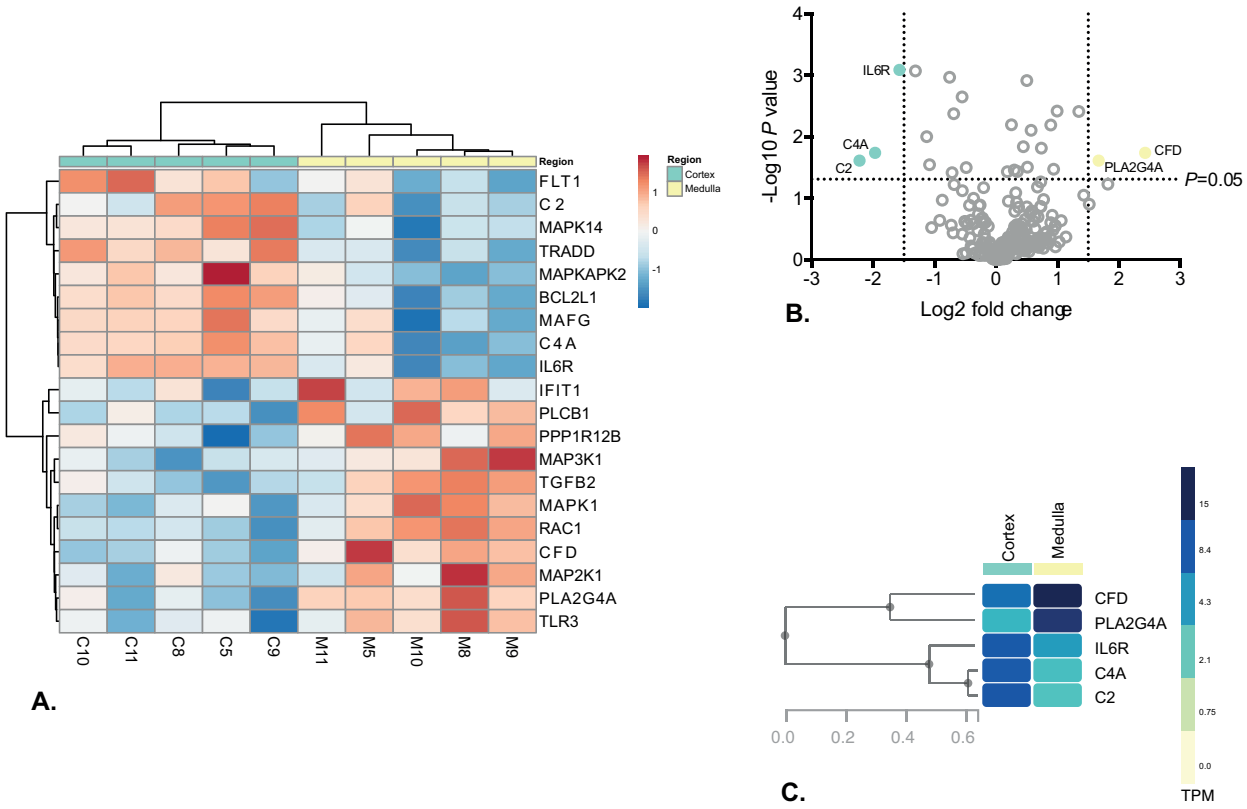

Fig. 6.6 **Differential inflammatory gene expression in human renal medulla and cortex during static cold storage.**
To investigate intrarenal regional differences to transplant ischaemia and storage, ribonucleic acid (RNA) was extracted from human renal cortex and medulla (n=5 paired samples) during cold static cold storage (SCS, mean time X hrs mins) and analysed for messenger RNA (mRNA) expression of a multiplex of 251 inflammatory genes using the Nanostring nCounter digital counter. (A) Heatmap of all genes significantly(P=0.05) differentially expressed in renal medulla vs. cortex. Each coloured box represents a cumulative z-score for $\log_2$ differential expression, scaled to give genes equal variance, with red indicating greater expression and blue indicating lower expression. Rows and columns are clustered by Euclidean distance and average linkage. (B) Volcano plot describing the magnitude and significance of differential gene expression in medullary samples as compared to cortical samples. Each point represents the combined fold-change of a gene in medullary samples compared to cortical samples. Vertical lines represent a fold change of $\log_2$ 1.5 and -1.5 respectively. The Y-axis line at 1.31 represents a significance of 0.05. Genes that have a statistically significant fold-change >1.5 are coloured and labelled. IL6R, Interleukin 6 Receptor; C4A, complement factor 4; C2, complement factor 2; CFD, complement factor D; PLA2G4A, phospholipase A2 group 4A. (C) Five genes with significant regional enrichment in Fig. 6.6A were interrogated in the GTEx database and clustered hierarchically. TPM, transcripts-per-million. Heatmap scale denotes linkage distance.

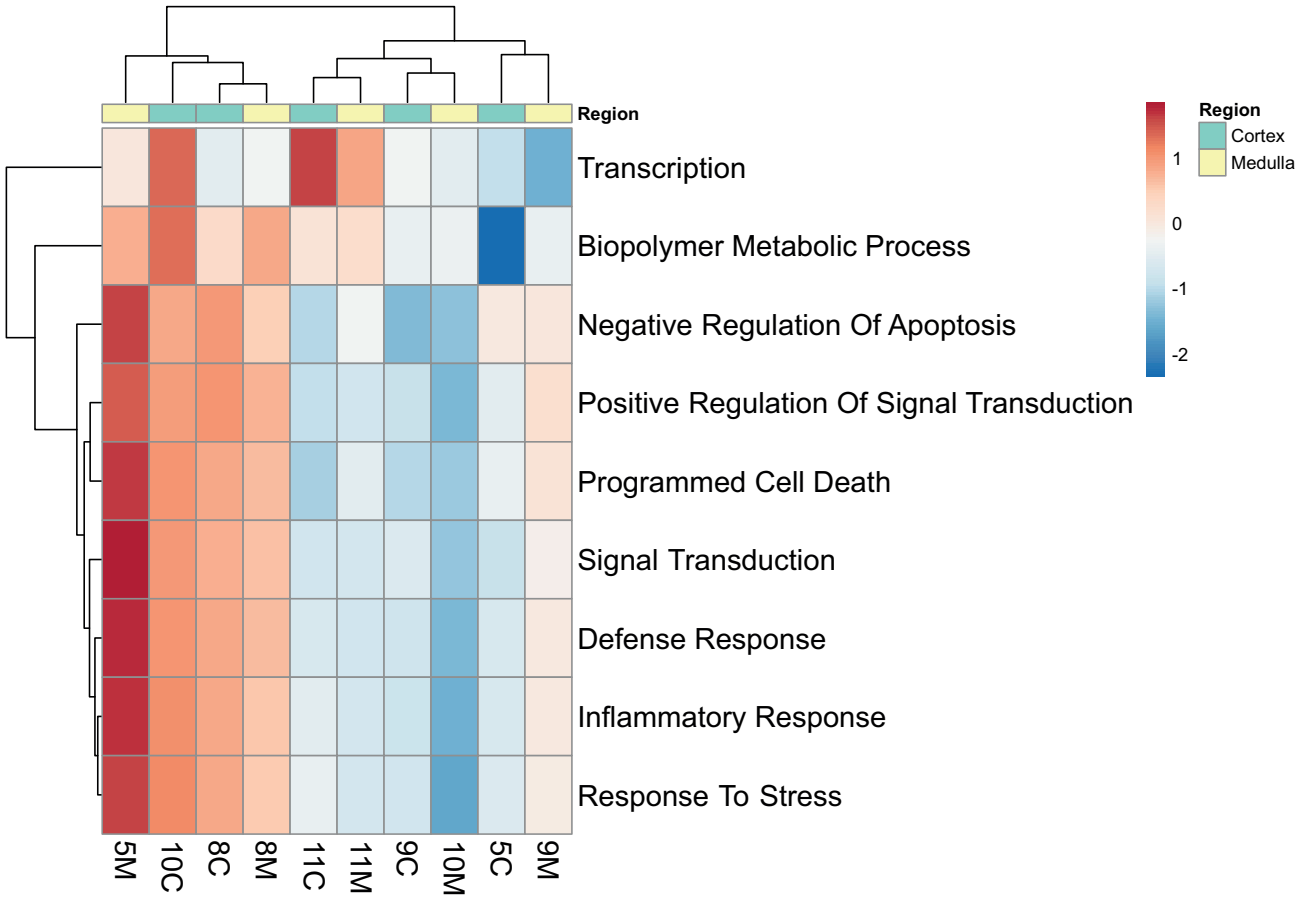

Fig. 6.7 **Pathway scores of human renal cortex and medulla during static cold storage.** To review the effect of transplant reperfusion upon inflammatory pathways in different kidney regions, inflammatory gene expression data from paired cortical and medullary samples (n=5) during static cold storage (SCS) were fit to selected pathway scores using Nanostring advanced analysis software. Pathway scores were fitted using a linear combination of pathway gene expression, weighted to capture the greatest variability in the data using principle component analysis. Increasing scores correspond to a positive weight for at least half of a pathway's genes. Pathways and samples were then clustered by Euclidean distance and average linkage. nC, cortical sample; nM, medullary sample.

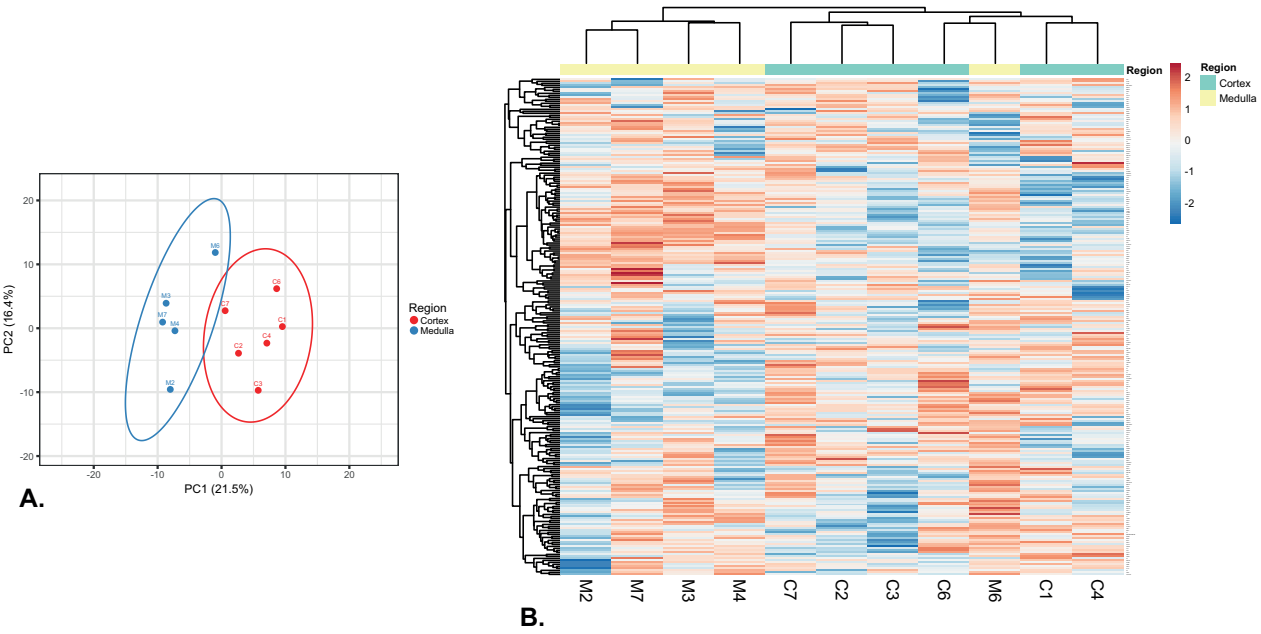

Fig. 6.8 **Inflammatory gene expression in human renal cortex and medulla during normothermic machine perfusion.**
To investigate intrarenal regional responses to transplant reperfusion, ribonucleic acid (RNA) was extracted from human renal cortex and medulla (n=5 paired samples) after 90 minutes of normothermic machine reperfusion and analysed for messenger RNA (mRNA) expression of a multiplex of 251 inflammatory genes using the Nanostring nCounter digital counter. (A and B) Principle component analysis (PCA) of global mRNA expression. Each point represents the global mRNA expression in one sample. The X and Y axis represent the percentage of total variance explained by the first and second principle component (PC1 and PC2). Prediction ellipses represent areas into which new observations from the same group will fall with 95% probability. In (B) the medullary sample outlying in the cortical prediction ellipse (M1) was removed. (C) Heatmap of all normalized data, scaled to give all genes equal variance. Each coloured box represents a cumulative z-score for normalised gene expression, with red indicating greater expression and blue indicating lower expression. Rows and columns are clustered by Euclidean distance and average linkage. nC, cortical sample; nM, medullary sample.

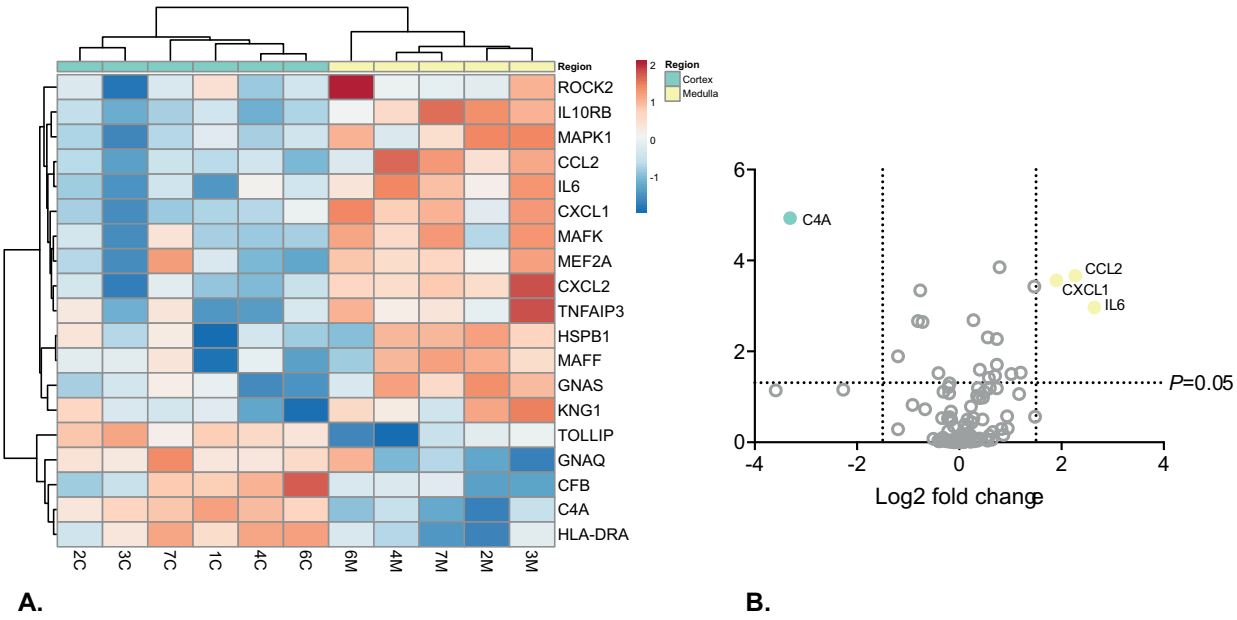

Fig. 6.9 **Differential inflammatory gene expression in human renal cortex and medulla during normothermic machine perfusion.**
To investigate intrarenal regional responses to transplant reperfusion, ribonucleic acid (RNA) was extracted from human renal cortex and medulla (n=5 paired samples) after 90 minutes of normothermic machine reperfusion and analysed for messenger RNA (mRNA) expression of a multiplex of 251 inflammatory genes using the Nanostring nCounter digital counter. (A) Heatmap of all genes significantly(P=0.05) differentially expressed in renal medulla vs. cortex. Each coloured box represents a cumulative z-score for $\log_2$ differential expression, scaled to give genes equal variance, with red indicating greater expression and blue indicating lower expression. Rows and columns are clustered by Euclidean distance and average linkage. nC, cortical sample; nM, medullary sample (B) Volcano plot describing the magnitude and significance of differential gene expression in medullary samples as compared to cortical samples. Each point represents the combined fold-change of a gene in medullary samples compared to cortical samples. Vertical lines represent a fold change of $\log_2$ 1.5 and -1.5 respectively. The Y-axis line at 1.31 represents a significance of 0.05. Genes that have a statistically significant fold-change >1.5 are coloured and labelled. C4A, complement C4A ; IL6, interleukin-6; CCL2, C-C motif chemokine ligand 2 ; CXCL1, C-X-C motif chemokine ligand 1.

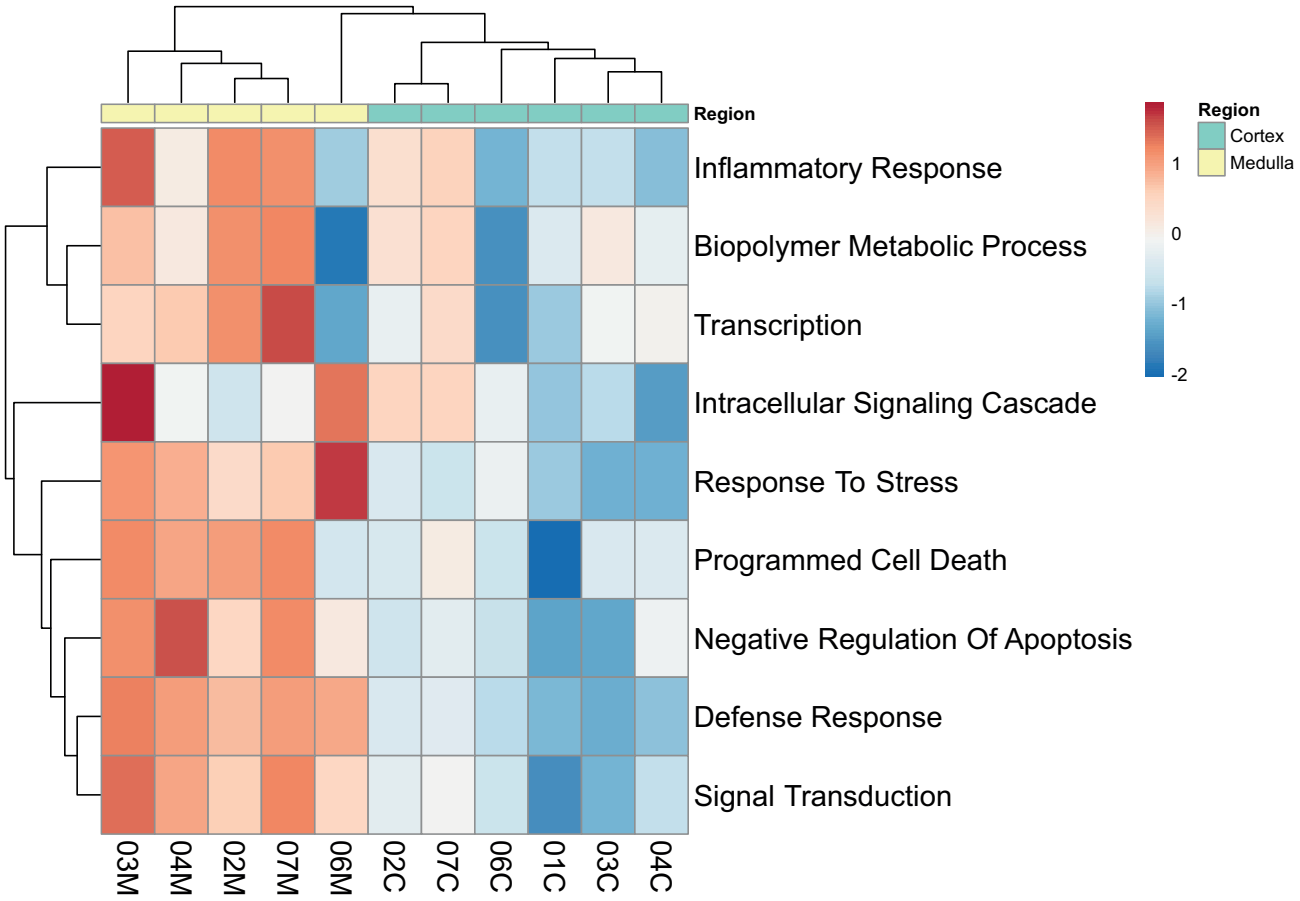

Fig. 6.10 **Pathway scores of human renal cortex and medulla following normothermic machine perfusion.**
To review the effect of transplant reperfusion upon inflammatory pathways in different kidney regions, inflammatory gene expression data, from paired cortical and medullary samples (n=5) after normothermic machine reperfusion, were fit to selected pathway scores using Nanostring advanced analysis software. Pathway scores were fitted using a linear combination of pathway gene expression, weighted to capture the greatest variability in the data using principle component analysis. Increasing scores correspond to a positive weight for at least half of a pathway's genes.

Chapter 7

Overall conclusions and future directions

The overall aims of this project were to use the normothermic machine perfusion of porcine and human kidneys to address gaps in our knowledge surrounding optimal perfusion conditions during NMP, and to examine patterns of regional oxygenation, perfusion and inflammation during transplant reperfusion.

7.1 Optimising perfusion conditions for kidney NMP

Through the perfusion of porcine kidneys with sequentially lowered perfusate oxygen, it was demonstrated that porcine kidneys could tolerate normoxic and even hypoxic normothermic perfusion without suffering increased injury or detriment to renal function. However, addition of carbon dioxide gas to perfusate was essential for pH maintenance.

7.2 Exploring regional variations in kidney perfusion, oxygenation and inflammation during NMP

An initial aim of this line of investigation was to ascertain baseline values for regional perfusion and oxygenation in the pre-ischaemic porcine kidney, as little data existed on the porcine renal medulla in particular, despite this being the large-animal model of choice in transplantation research. We were able to measure microvascular perfusion and tissue oxygenation in the cortex and medulla of the anaesthetised pig, and offer the first description of widespread and divergent changes to regional perfusion and oxygenation during subsequent clinically-relevant model of NMP.

We subsequently investigated the effects of NMP upon regional perfusion and oxygenation in a series of human kidneys in greater detail, and demonstrated profound and prolonged regional changes to microcirculation associated with greater medullary fibrin deposition. Of clinical importance, these regional changes, which may have significant impact on early and late graft function, were not readily identifiable by examining currently-used markers of renal function and haemodynamics during NMP.

Given the disparate effects of NMP upon kidney microvasculature, we finally questioned whether normothermic perfusion of human kidneys would prompt differential regional inflammation by examining human kidney cortical and medullary expression of an inflammatory gene panel. We were able to study and sample the renal medulla with relative ease during NMP, underlining the great value of this technique to the study of human renal physiology. We found that NMP provoked a marked inflammatory response in both renal cortex and medulla, but that there was particular medullary over-expression of cytokines associated with poor initial and later graft function.

Together, these findings strongly suggest that the human renal medulla experiences a unique, under-recognised and more hostile environment during NMP and early transplant reperfusion; one that may critically influence transplantation outcome.

7.3 Future directions

Our findings regarding perfusate oxygenation align with a field-wide move towards NMP conditions that more closely mimic normal physiology. Two major lines of current investigation regarding renal NMP optimisation include prolonged periods of perfusion, and the use of urine re-circulation in place of replacement crystalloid fluid (for example [168]). Given its non-inferiority to current hyperoxic protocols and possible reduction of oxidative damage, trialling a normoxic perfusate during such prolonged NMP protocols would appear logical.

Normothermic machine perfusion will continue to be an ideal platform for further investigation of both the pathophysiology and potential amelioration of the challenging medullary environment for which we have provided initial evidence. Recent developments in our group, regarding the successful use of plasminogen and tissue plasminogen activator to reduce cortical fibrin deposition and associated vascular plugging [42], raise the exciting possibility that a similar medullary predicament is amenable to therapeutics.

Investigation of the effect of plasminogen/tPA administration upon medullary fibrin deposition therefore represents a clear research priority; alongside the use of more granular sequencing techniques and measurement of compartmental oxygen kinetics and perfusion. Such a protocol would not only explore a therapeutic avenue with the potential for rapid clinical deployment, but also help better understand the relative importance of early vascular disturbance to ongoing graft health and function.

7.4 Final Conclusions

In summary, we have described novel porcine and human renal medullary physiology and inflammation during transplant reperfusion that highlight the need for medulla-specific strategies to ameliorate IRI. We have further determined changes to renal physiology and injury in response to perfusate oxygenation in a novel preservation technology that may guide clinical implementation.

Overall we hope that, through guiding the optimisation of transplant perfusion and stimulating further interest in medullary pathophysiology, this work will contribute to improving patient outcomes in transplantation and acute kidney injury.

References

[1] (2017). SARS abstracts. *BJS (British Journal of Surgery)*, 104(S3):7–57. _eprint: https://bjssjournals.onlinelibrary.wiley.com/doi/pdf/10.1002/bjs.10531.

[2] (2018a). Abstracts of the International Meeting on Ischemia Reperfusion Injury in Transplantation, Poitiers, France 19-20 April. *Transplant International: Official Journal of the European Society for Organ Transplantation*, 31 Suppl 2:5–15.

[3] (2018b). SARS abstracts. *BJS (British Journal of Surgery)*, 105(S1):7–46. _eprint: https://bjssjournals.onlinelibrary.wiley.com/doi/pdf/10.1002/bjs.10847.

[4] (2019a). Full Oral. *Transplant International*, 32(S2):7–126. _eprint: https://onlinelibrary.wiley.com/doi/pdf/10.1111/tri.13507.

[5] (2019b). Oral presentations. *BJS (British Journal of Surgery)*, 106(S3):6–27. _eprint: https://bjssjournals.onlinelibrary.wiley.com/doi/pdf/10.1002/bjs.11156.

[6] (2020). NHSBT Organ Donation and Transplantation Activity Report 2019/20.

[7] Abdel-Rahman, U., Risteski, P., Tizi, K., Kerscher, S., Bejati, S., Zwicker, K., Scholz, M., Brandt, U., and Moritz, A. (2009). Hypoxic reoxygenation during initial reperfusion attenuates cardiac dysfunction and limits ischemia–reperfusion injury after cardioplegic arrest in a porcine model. *The Journal of Thoracic and Cardiovascular Surgery*, 137(4):978 – 982.

[8] Abdelkader, A., Ho, J., Connie P.C. Ow, Eppel, G. A., Rajapakse, N. W., Schlaich, M. P., and Evans, R. G. (2014). Renal oxygenation in acute renal ischemia-reperfusion injury. *American Journal of Physiology - Renal Physiology*, 306(9):F1026–F1038.

[9] Adams, T. D., Hosgood, S. A., and Nicholson, M. L. (2019). Physiological effects of altering oxygenation during kidney normothermic machine perfusion. *American Journal of Physiology. Renal Physiology*, 316(5):F823–F829.

[10] Adams, T. D., Patel, M., Hosgood, S. A., and Nicholson, M. L. (2017). Lowering Perfusate Temperature From 37°C to 32°C Diminishes Function in a Porcine Model of Ex Vivo Kidney Perfusion. *Transplantation Direct*, 3(3):e140.

[11] Alejandro, V., Scandling, J. D., Sibley, R. K., Dafoe, D., Alfrey, E., Deen, W., and Myers, B. D. (1995). Mechanisms of filtration failure during postischemic injury of the human kidney. A study of the reperfused renal allograft. *Journal of Clinical Investigation*, 95(2):820–831.

[12] Althen, T. G., Ono, K., and Topel, D. G. (1977). Effect of Stress Susceptibility or Stunning Method on Catecholamine Levels in Swine. *Journal of Animal Science*, 44(6):985–989.

[13] Angelescu, M., Kraus, T., Wiesel, M., Hergesell, O., Haberkorn, U., and Klar, E. (2003). Assessment of renal graft function by perioperative monitoring of cortical microcirculation in kidney transplantation. *Transplantation*, 75(8):1190–1196.

[14] Aubert, O., Kamar, N., Vernerey, D., Viglietti, D., Martinez, F., Duong-Van-Huyen, J.-P., Eladari, D., Empana, J.-P., Rabant, M., Verine, J., Rostaing, L., Congy, N., Guilbeau-Frugier, C., Mourad, G., Garrigue, V., Morelon, E., Giral, M., Kessler, M., Ladrière, M., Delahousse, M., Glotz, D., Legendre, C., Jouven, X., Lefaucheur, C., and Loupy, A. (2015). Long term outcomes of transplantation using kidneys from expanded criteria donors: prospective, population based cohort study. *BMJ*, 351:h3557.

[15] Bagul, A., Hosgood, S. A., Kaushik, M., Kay, M. D., Waller, H. L., and Nicholson, M. L. (2007). Experimental renal preservation by normothermic resuscitation perfusion with autologous blood. *British Journal of Surgery*, 95(1):111–118.

[16] Bailey, P., Edwards, A., and Courtney, A. E. (2016). Living kidney donation. *BMJ*, 354:i4746.

[17] Balsinde, J., Winstead, M. V., and Dennis, E. A. (2002). Phospholipase a2 regulation of arachidonic acid mobilization. *FEBS Letters*, 531(1):2 – 6. Lipid Signalling: Cellular Events and their Biophysical Mechanisms.

[18] Bankir, L. and Yang, B. (2012). New insights into urea and glucose handling by the kidney, and the urine concentrating mechanism. *Kidney International*, 81(12):1179–1198.

[19] Basile, D. P. (2007). The endothelial cell in ischemic acute kidney injury: implications for acute and chronic function. *Kidney International*, 72(2):151–156.

[20] Basile, D. P., Donohoe, D., Roethe, K., and Osborn, J. L. (2001). Renal ischemic injury results in permanent damage to peritubular capillaries and influences long-term function. *American Journal of Physiology - Renal Physiology*, 281(5):F887–F899.

[21] Basile, D. P. and Yoder, M. C. (2014). Renal endothelial dysfunction in acute kidney ischemia reperfusion injury. *Cardiovascular & Hematological Disorders Drug Targets*, 14(1):3–14.

[22] Belzer, F. O., Ashby, B. S., and Dunphy, J. E. (1967). 24-hour and 72-hour preservation of canine kidneys. *Lancet)*, 2(7515):536–538.

[23] Belzer, F. O. and Southard, J. H. (1988). Principles of solid-organ preservation by cold storage. *Transplantation*, 45(4):673–676.

[24] Berry, M. R., Mathews, R. J., Ferdinand, J. R., Jing, C., Loudon, K. W., Wlodek, E., Dennison, T. W., Kuper, C., Neuhofer, W., and Clatworthy, M. R. (2017). Renal Sodium Gradient Orchestrates a Dynamic Antibacterial Defense Zone. *Cell*, 170(5):860–874.e19.

[25] Bert, P. (1878). *La Pression Barométrique*. Recherches de Physiologie Expérimentale. Masson, Paris.

[26] Bonventre, J. V. and Yang, L. (2011). Cellular pathophysiology of ischemic acute kidney injury. *Journal of Clinical Investigation*, 121(11):4210–4221.

[27] Brasile, L., Buelow, R., Stubenitsky, B. M., and Kootstra, G. (2003a). Induction of heme oxygenase-1 in kidneys during ex vivo warm perfusion:. *Transplantation*, 76(8):1145–1149.

[28] Brasile, L., Stubenitsky, B., Haisch, C. E., Kon, M., and Kootstra, G. (2005). Potential of repairing ischemically damaged kidneys ex vivo. *Transplantation Proceedings*, 37(1):375–376.

[29] Brasile, L., Stubenitsky, B. M., Booster, M. H., Haisch, C., and Kootstra, G. (2003b). NOS: the underlying mechanism preserving vascular integrity and during ex vivo warm kidney perfusion. *American Journal of Transplantation*, 3(6):674–679.

[30] Brezis, M., Heyman, S. N., and Epstein, F. H. (1994). Determinants of intrarenal oxygenation. II. Hemodynamic effects. *The American Journal of Physiology*, 267(6 Pt 2):F1063–8.

[31] Brezis, M. and Rosen, S. (1995). Hypoxia of the renal medulla–its implications for disease. *New England Journal of Medicine*, 332(10):647–655.

[32] Calzavacca, P., Evans, R. G., Bailey, M., Bellomo, R., and May, C. N. (2015). Variable responses of regional renal oxygenation and perfusion to vasoactive agents in awake sheep. *American Journal of Physiology. Regulatory, Integrative and Comparative Physiology*, 309(10):R1226–33.

[33] Carlström, M., Wilcox, C. S., and Arendshorst, W. J. (2015). Renal autoregulation in health and disease. *Physiological Reviews*, 95(2):405–511.

[34] Carrel, A. (1912). On the permanent life of tissues outside of the organism. *The Journal of Experimental Medicine*, 15(5):516–528.

[35] Carrel, A. and Lindbergh, C. A. (1938). Carrel: The Culture of Organs. New York: Hoeber.

[36] Chatauret, N., Coudroy, R., Delpech, P. O., Vandebrouck, C., Hosni, S., Scepi, M., and Hauet, T. (2014). Mechanistic analysis of nonoxygenated hypothermic machine perfusion's protection on warm ischemic kidney uncovers greater eNOS phosphorylation and vasodilation. *American Journal of Transplantation*, 14(11):2500–2514.

[37] Chiari, P. C., Bienengraeber, M. W., Pagel, P. S., Krolikowski, J. G., Kersten, J. R., and Warltier, D. C. (2005). Isoflurane Protects against Myocardial Infarction during Early Reperfusion by Activation of Phosphatidylinositol-3-Kinase Signal Transduction: Evidence for Anesthetic-induced Postconditioning in Rabbits. *Anesthesiology*, 102(1):102–109.

[38] Chouchani, E. T., Pell, V. R., Gaude, E., Aksentijević, D., Sundier, S. Y., Robb, E. L., Logan, A., Nadtochiy, S. M., Ord, E. N. J., Smith, A. C., Eyassu, F., Shirley, R., Hu, C.-H., Dare, A. J., James, A. M., Rogatti, S., Hartley, R. C., Eaton, S., Costa, A. S. H., Brookes, P. S., Davidson, S. M., Duchen, M. R., Saeb-Parsy, K., Shattock, M. J., Robinson, A. J.,

Work, L. M., Frezza, C., Krieg, T., and Murphy, M. P. (2014). Ischaemic accumulation of succinate controls reperfusion injury through mitochondrial ROS. *Nature*, 515(7527):431–435.

[39] Chung, A. C. K. and Lan, H. Y. (2011). Chemokines in renal injury. *Journal of the American Society of Nephrology : JASN*, 22(5):802–809.

[40] Cippa, P. E., Sun, B., Liu, J., Chen, L., Naesens, M., and McMahon, A. P. (2018). Transcriptional trajectories of human kidney disease progression. *bioRxiv*, page 342972.

[41] Cooper, D. K. C. (2012). A brief history of cross-species organ transplantation. *Proceedings (Baylor University. Medical Center)*, 25(1):49–57.

[42] DiRito, J. R., Hosgood, S. A., Reschke, M., Albert, C., Bracaglia, L. G., Ferdinand, J. R., Stewart, B. J., Edwards, C. M., Vaish, A. G., Thiru, S., Mulligan, D. C., Haakinson, D. J., Clatworthy, M. R., Saltzman, W. M., Pober, J. S., Nicholson, M. L., and Tietjen, G. T. (2020). Lysis of cold-storage-induced microvascular obstructions for ex vivo revitalization of marginal human kidneys. *American Journal of Transplantation*, n/a(n/a):1–13.

[43] Downey, P., Sapirstein, A., Oleary, E., Sun, T.-X., Brown, D., and Bonventre, J. V. (2001). Renal concentrating defect in mice lacking group iv cytosolic phospholipase a2. *American Journal of Physiology-Renal Physiology*, 280(4).

[44] Dyson, A., Bezemer, R., Legrand, M., Balestra, G., Singer, M., and Ince, C. (2011). Microvascular and interstitial oxygen tension in the renal cortex and medulla studied in a 4-h rat model of LPS-induced endotoxemia. *Shock (Augusta, Ga.)*, 36(1):83–89.

[45] Eneström, S., Druid, H., and Rammer, L. (1988). Fibrin deposition in the kidney in post-ischaemic renal damage. *British Journal of Experimental Pathology*, 69(3):387–394.

[46] Ergin, B., Bezemer, R., Kandil, A., Demirci-Tansel, C., and Ince, C. (2015). TEMPOL has limited protective effects on renal oxygenation and hemodynamics but reduces kidney damage and inflammation in a rat model of renal ischemia/reperfusion by aortic clamping. *Journal of Clinical and Translational Research*, 1(2):1–13.

[47] Eriksson, S., Nilsson, J., and Sturesson, C. (2014). Non-invasive imaging of microcirculation: a technology review. *Medical Devices (Auckland, N.Z.)*, 7:445–452.

[48] Evans, R. G., Eppel, G. A., Michaels, S., Burke, S. L., Nematbakhsh, M., Head, G. A., Carroll, J. F., and O'Connor, P. M. (2010). Multiple mechanisms act to maintain kidney oxygenation during renal ischemia in anesthetized rabbits. *American Journal of Physiology - Renal Physiology*, 298(5):F1235–F1243.

[49] Evans, R. G., Gardiner, B. S., Smith, D. W., and O'Connor, P. M. (2008). Intrarenal oxygenation: unique challenges and the biophysical basis of homeostasis. *American Journal of Physiology - Renal Physiology*, 295(5):F1259–70.

[50] Evans, R. G., Goddard, D., Eppel, G. A., and O'Connor, P. M. Stability of tissue PO2 in the face of altered perfusion: a phenomenon specific to the renal cortex and independent of resting renal oxygen consumption. *Clinical and Experimental Pharmacology & Physiology*.

[51] Evans, R. G., Goddard, D., Eppel, G. A., and O'Connor, P. M. (2011). Factors that render the kidney susceptible to tissue hypoxia in hypoxemia. *American Journal of Physiology. Regulatory, Integrative and Comparative Physiology*, 300(4):R931–R940.

[52] Evans, R. G., Ince, C., Joles, J. A., Smith, D. W., May, C. N., O'Connor, P. M., and Gardiner, B. S. Haemodynamic influences on kidney oxygenation: clinical implications of integrative physiology. *Clinical and Experimental Pharmacology & Physiology*.

[53] Evans, R. G., Leong, C.-L., Anderson, W. P., and O'Connor, P. M. (2007). Don't be so BOLD: potential limitations in the use of BOLD MRI for studies of renal oxygenation. *Kidney International*, 71(12):1327–8– author reply 1328.

[54] Evans, R. G., Smith, J. A., Wright, C., Gardiner, B. S., Smith, D. W., and Cochrane, A. D. (2014). Urinary oxygen tension: a clinical window on the health of the renal medulla? *American Journal of Physiology. Regulatory, Integrative and Comparative Physiology*, 306(1):R45–50.

[55] Ferdinand, J. R., Hosgood, S. A., Moore, T., Ward, C. J., Castro-Dopico, T., Nicholson, M. L., and Clatworthy, M. R. (2019). Investigation of the transcriptional profile of human kidneys during machine perfusion reveals potential benefits of haemoadsorption. *bioRxiv*.

[56] Frank, R. D., Schabbauer, G., Holscher, T., Sato, Y., Tencati, M., Pawlinski, R., and Mackman, N. (2005). The synthetic pentasaccharide fondaparinux reduces coagulation, inflammation and neutrophil accumulation in kidney ischemia-reperfusion injury. *Journal of Thrombosis and Haemostasis*, 3(3):531–540.

[57] Froněk, J. and MacPhee, I. (2012). History of Transplantation. In *Handbook of Renal and Pancreatic Transplantation*, pages 1–7. John Wiley & Sons, Ltd, Chichester, UK.

[58] Fung, A., Zhao, H., Yang, B., Lian, Q., and Ma, D. (2016). Ischaemic and inflammatory injury in renal graft from brain death donation: an update review. *Journal of Anesthesia*, pages 1–10.

[59] Fuquay, R., Renner, B., Kulik, L., McCullough, J. W., Amura, C., Strassheim, D., Pelanda, R., Torres, R., and Thurman, J. M. (2013). Renal ischemia-reperfusion injury amplifies the humoral immune response. *Journal of the American Society of Nephrology: JASN*, 24(7):1063–1072.

[60] Giraud, S., Favreau, F., Chatauret, N., Thuillier, R., Maiga, S., and Hauet, T. (2011). Contribution of large pig for renal ischemia-reperfusion and transplantation studies: the preclinical model. *Journal of Biomedicine and Biotechnology*, 2011.

[61] Grams, M. E., Garg, A. X., and Lentine, K. L. (2016). Kidney-Failure Risk Projection for the Living Kidney-Donor Candidate. *The New England Journal of Medicine*, 374(21):2094–2095.

[62] Gstraunthaler, G., Pfaller, W., and Kotanko, P. (1985). Interrelation between oxygen consumption and Na-K-ATPase activity in rat renal proximal tubule suspension. *Renal Physiology*, 8(1):38–44.

[63] GTEx Consortium (2013). The Genotype-Tissue Expression (GTEx) project. *Nature Genetics*, 45(6):580–585.

[64] Guven, G., Hilty, M. P., and Ince, C. (2020). Microcirculation: physiology, pathophysiology, and clinical application. *Blood Purification*, 49(1-2):143–150.

[65] Habuka, M, Fagerberg, L, Hallstrom, B M, Kampf, C, Edlund, K, Sivertsson, A, Yamamoto, T, Ponten, F, Uhlen, M, and Odeberg, J (2014). The kidney transcriptome and proteome defined by transcriptomics and antibody-based profiling. *PLoS ONE*, 9(12):e116125.

[66] Haddock, B. T., Francis, S. T., Larsson, H. B. W., and Andersen, U. B. (2018). Assessment of perfusion and oxygenation of the human renal cortex and medulla by quantitative MRI during handgrip exercise. *Journal of the American Society of Nephrology: JASN*, 29(10):2510–2517.

[67] Hameed, A. M., Lu, D. B., Patrick, E., Xu, B., Hu, M., Chew, Y. V., Keung, K., P'Ng, C. H., Gaspi, R., Zhang, C., and et al. (2019). Brief normothermic machine perfusion rejuvenates discarded human kidneys. *Transplantation Direct*, 5(11).

[68] Hameed, A. M., Pleass, H. C., Wong, G., and Hawthorne, W. J. (2016). Maximizing kidneys for transplantation using machine perfusion: from the past to the future: A comprehensive systematic review and meta-analysis. *Medicine*, 95(40):e5083.

[Hansell et al.] Hansell, P., Welch, W. J., Blantz, R. C., and Palm, F. Determinants of kidney oxygen consumption and their relationship to tissue oxygen tension in diabetes and hypertension. *Clinical and Experimental Pharmacology & Physiology*.

[70] Hausenloy, D. J. and Yellon, D. M. (2003). The mitochondrial permeability transition pore: its fundamental role in mediating cell death during ischaemia and reperfusion. *Journal of Molecular and Cellular Cardiology*, 35(4):339–341.

[71] Hausenloy, D. J. and Yellon, D. M. (2016). Ischaemic conditioning and reperfusion injury. *Nature Reviews Cardiology*, 13(4):193–209.

[72] Hellberg, P. O. A., Källskog, Ö., and Wolgast, M. (1991). Red cell trapping and postischemic renal blood flow. Differences between the cortex, outer and inner medulla. *Kidney International*, 40(4):625–631.

[73] Hirt-Minkowski, P., Rush, D. N., Gao, A., Hopfer, H., Wiebe, C., Nickerson, P. W., Schaub, S., and Ho, J. (2016). Six-month urinary CCL2 and CXCL10 levels predict long-term renal allograft outcome. *Transplantation*, 100(9):1988–1996.

[74] Hosgood, S., Harper, S., Kay, M., Bagul, A., Waller, H., and Nicholson, M. L. (2006). Effects of arterial pressure in an experimental isolated haemoperfused porcine kidney preservation system. *British Journal of Surgery*, 93(7):879–884.

[75] Hosgood, S. A., Bagul, A., Yang, B., and Nicholson, M. L. (2008). The relative effects of warm and cold ischemic injury in an experimental model of nonheartbeating donor kidneys. *Transplantation*, 85(1):88–92.

[76] Hosgood, S. A., Barlow, A. D., Hunter, J. P., and Nicholson, M. L. (2015a). Ex vivo normothermic perfusion for quality assessment of marginal donor kidney transplants. *British Journal of Surgery*, 102(11):1433–1440.

[77] Hosgood, S. A. and Nicholson, M. L. (2011). Normothermic kidney preservation. *Current Opinion in Organ Transplantation*, 16(2):169–173.

[78] Hosgood, S. A. and Nicholson, M. L. (2016). An assessment of urinary biomarkers in a series of declined human kidneys measured during ex-vivo normothermic kidney perfusion. *Transplantation*, page 1.

[79] Hosgood, S. A. and Nicholson, M. L. (2017). An Assessment of Urinary Biomarkers in a Series of Declined Human Kidneys Measured During Ex Vivo Normothermic Kidney Perfusion. *Transplantation*, 101(9):2120–2125.

[80] Hosgood, S. A., Patel, M., and Nicholson, M. L. (2013). The conditioning effect of ex vivo normothermic perfusion in an experimental kidney model. *The Journal of surgical research*, 182(1):153–160.

[81] Hosgood, S. A., Shah, K., Patel, M., and Nicholson, M. L. (2015b). The effect of prolonged of warm ischaemic injury on renal function in an experimental ex vivo normothermic perfusion system. *Journal of Translational Medicine*, 13.

[82] Inslee, M. (2017). Advanced Analysis 2.0 Quick Start Guide. pages 1–4.

[83] Iyer, A., Chew, H. C., Gao, L., Villanueva, J., Hicks, M., Doyle, A., Kumarasinghe, G., Jabbour, A., Jansz, P. C., Feneley, M. P., Harvey, R. P., Graham, R. M., Dhital, K. K., and Macdonald, P. S. (2016). Pathophysiological trends during withdrawal of life support: implications for organ donation after circulatory death. *Transplantation*, 100(12):2621–2629.

[84] Jang, H. R. and Rabb, H. (2015). Immune cells in experimental acute kidney injury. *Nature reviews. Nephrology*, 11(2):88–101.

[85] Jochmans, I., Akhtar, M. Z., Nasralla, D., Kocabayoglu, P., Boffa, C., Kaisar, M., Brat, A., O'Callaghan, J., Pengel, L. H. M., Knight, S., and Ploeg, R. J. (2016). Past, present, and future of dynamic kidney and liver preservation and resuscitation. *American Journal of Transplantation*, 16(9):2545–2555.

[86] Jochmans, I., Moers, C., Smits, J. M., Leuvenink, H. G. D., Treckmann, J., Paul, A., Rahmel, A., Squifflet, J.-P., van Heurn, E., Monbaliu, D., Ploeg, R. J., and Pirenne, J. (2010). Machine perfusion versus cold storage for the preservation of kidneys donated after cardiac death: a multicenter, randomized, controlled trial. *Annals of Surgery*, 252(5):756–764.

[87] Jochmans, I., Nicholson, M. L., and Hosgood, S. A. (2017). Kidney perfusion: some like it hot others prefer to keep it cool. *Current Opinion in Organ Transplantation*, 22(3):260–266.

[88] Johnson, R. J., Bradbury, L. L., Martin, K., Neuberger, J., and UK Transplant Registry (2014). Organ donation and transplantation in the UK-the last decade: a report from the UK national transplant registry. *Transplantation*, 97 Suppl 1:S1–S27.

[89] Kainuma, M., Yamada, M., and Miyake, T. (1996). Continuous urine oxygen tension monitoring in patients undergoing cardiac surgery. *Journal of cardiothoracic and vascular anesthesia*, 10(5):603–608.

[90] Kaths, J. M., Cen, J. Y., Chun, Y. M., Echeverri, J., Linares, I., Ganesh, S., Yip, P., John, R., Bagli, D., Mucsi, I., Ghanekar, A., Grant, D. R., Robinson, L. A., and Selzner, M. (2016). Continuous Normothermic Ex Vivo Kidney Perfusion Is Superior to Brief Normothermic Perfusion Following Static Cold Storage in Donation After Circulatory Death Pig Kidney Transplantation. *American Journal of Transplantation*, pages n/a–n/a.

[91] Kaths, J. M., Echeverri, J., Chun, Y. M., Cen, J. Y., Goldaracena, N., Linares, I., Dingwell, L. S., Yip, P. M., John, R., Bagli, D., Mucsi, I., Ghanekar, A., Grant, D. R., Robinson, L. A., and Selzner, M. (2017a). Continuous normothermic ex vivo kidney perfusion improves graft function in donation after circulatory death pig kidney transplantation. *Transplantation*, 101(4):754.

[92] Kaths, J. M., Echeverri, J., Linares, I., Cen, J. Y., Ganesh, S., Hamar, M., Urbanellis, P., Yip, P., John, R., Bagli, D., Mucsi, I., Ghanekar, A., Grant, D., Robinson, L. A., and Selzner, M. (2017b). Normothermic Ex Vivo Kidney Perfusion Following Static Cold Storage-Brief, Intermediate, or Prolonged Perfusion for Optimal Renal Graft Reconditioning? *American Journal of Transplantation*, 341(108):1725.

[93] Keeley, T. P. and Mann, G. E. (2019). Defining physiological normoxia for improved translation of cell physiology to animal models and humans. *Physiological Reviews*, 99(1):161–234.

[94] Kellum, J. A. (2011). Impaired renal blood flow and the 'spicy food' hypothesis of acute kidney injury. *Critical Care Medicine*, 39(4):901–903.

[95] Kielar, M. L., John, R., Bennett, M., Richardson, J. A., Shelton, J. M., Chen, L., Jeyarajah, D. R., Zhou, X. J., Zhou, H., Chiquett, B., Nagami, G. T., and Lu, C. Y. (2005). Maladaptive role of il-6 in ischemic acute renal failure. *Journal of the American Society of Nephrology*, 16(11):3315–3325.

[96] Kootstra, G., Daemen, J. H., and Oomen, A. P. (1995). Categories of non-heart-beating donors. *Transplantation Proceedings*, 27(5):2893–2894.

[97] Kriz, W. and Kaissling, B. (2007a). Chapter 20: Structural Organization of the Mammalian Kidney.

[98] Kriz, W. and Kaissling, B. (2007b). Chapter 20: Structural Organization of the Mammalian Kidney.

[99] Kuziel, W. A., Morgan, S. J., Dawson, T. C., Griffin, S., Smithies, O., Ley, K., and Maeda, N. (1997). Severe reduction in leukocyte adhesion and monocyte extravasation in mice deficient in cc chemokine receptor 2. *Proceedings of the National Academy of Sciences*, 94(22):12053–12058.

[100] Lankadeva, Y. R., Kosaka, J., Evans, R. G., Bailey, S. R., Bellomo, R., and May, C. N. (2016). Intrarenal and urinary oxygenation during norepinephrine resuscitation in ovine septic acute kidney injury. *Kidney International*, 90(1):100–108.

[101] Lankadeva, Y. R., Kosaka, J., Evans, R. G., Bellomo, R., and May, C. N. (2018). Urinary oxygenation as a surrogate measure of medullary oxygenation during angiotensin II therapy in septic acute kidney injury. *Critical Care Medicine*, 46(1):e41–e48.

[102] Le Dorze, M., Legrand, M., Payen, D., and Ince, C. (2009). The role of the microcirculation in acute kidney injury. *Current Opinion in Critical Care*, 15(6):503–508.

[103] Lee, J. W., Chou, C.-L., and Knepper, M. A. (2015). Deep sequencing in microdissected renal tubules identifies nephron segment–specific transcriptomes. *Journal of the American Society of Nephrology*.

[104] Leek, J. T., Scharpf, R. B., Bravo, H. C., Simcha, D., Langmead, B., Johnson, W. E., Geman, D., Baggerly, K., and Irizarry, R. A. (2010). Tackling the widespread and critical impact of batch effects in high-throughput data. *Nature Reviews Genetics*, 11(10):733–739.

[105] Legrand, M., Mik, E. G., Johannes, T., Payen, D., and Ince, C. (2008). Renal hypoxia and dysoxia after reperfusion of the ischemic kidney. *MOLECULAR . . .* , 14(7-8):502–516.

[106] Leong, C.-L., O'Connor, P. M., Eppel, G. A., Anderson, W. P., and Evans, R. G. (2008). Measurement of renal tissue oxygen tension: systematic differences between fluorescence optode and microelectrode recordings in anaesthetized rabbits. *Nephron. Physiology*, 108(2):p11–7.

[107] Leonhardt, K. O. (1965). Urinary oxygen pressure in renal parenchymal and vascular disease. *JAMA*, 194(4):345.

[108] Lima, A., van Rooij, T., Ergin, B., Sorelli, M., Ince, Y., Specht, P. A. C., Mik, E. G., Bocchi, L., Kooiman, K., de Jong, N., and Ince, C. (2018). Dynamic contrast-enhanced ultrasound identifies microcirculatory alterations in sepsis-induced acute kidney injury. *Critical Care Medicine*, 46(8):1284–1292.

[109] Lübbers, D. W. and Baumgärtl, H. (1997). Heterogeneities and profiles of oxygen pressure in brain and kidney as examples of the pO2 distribution in the living tissue. *Kidney international*, 51(2):372–380.

[110] Luyendyk, J. P., Schoenecker, J. G., and Flick, M. J. (2019). The multifaceted role of fibrinogen in tissue injury and inflammation. *Blood*, 133(6):511–520.

[111] Maïga, S., Allain, G., Hauet, T., Roumy, J., Baulier, E., Scepi, M., Dierick, M., Van Hoorebeke, L., Hannaert, P., Guy, F., and Favreau, F. (2017). Renal autotransplantation promotes cortical microvascular network remodeling in a preclinical porcine model. *PloS one*, 12(7):e0181067.

[112] Manara, A. R., Murphy, P. G., and O'Callaghan, G. (2012). Donation after circulatory death. *British Journal of Anaesthesia*, 108 Suppl 1(suppl 1):i108–21.

[113] Martin, D. S. and Grocott, M. P. W. (2013). Oxygen therapy in critical illness: precise control of arterial oxygenation and permissive hypoxemia. *Critical Care Medicine*, 41(2):423–432.

[114] McKeown, D. W., Bonser, R. S., and Kellum, J. A. (2012). Management of the heartbeating brain-dead organ donor. *BJA: British Journal of Anaesthesia*, 108(suppl$_1$) : $i96 - -i107$.

[115] Metcalfe, M. S., Waller, J. R., Hosgood, S. A., Shaw, M., Hassanein, W., and Nicholson, M. L. (2002). A paired study comparing the efficacy of renal preservation by normothermic autologous blood perfusion and hypothermic pulsatile perfusion. *Transplantation Proceedings*, 34(5):1473–1474.

[116] Metsalu, T. and Vilo, J. (2015). ClustVis: a web tool for visualizing clustering of multivariate data using Principal Component Analysis and heatmap. *Nucleic acids research*, 43(W1):W566–70.

[117] Metzger, R. A., Delmonico, F. L., Feng, S., Port, F. K., Wynn, J. J., and Merion, R. M. (2003). Expanded criteria donors for kidney transplantation. *American Journal of Transplantation*, 3(s4):114–125.

[118] Mik, E. G., Johannes, T., Payen, D., and Ince, C. (2008). Renal hypoxia and dysoxia after reperfusion of the ischemic kidney. *Molecular Medicine*.

[119] Moeckli, B., Sun, P., Lazeyras, F., Morel, P., Moll, S., Pascual, M., and Bühler, L. H. (2019). Evaluation of donor kidneys prior to transplantation: an update of current and emerging methods. *Transplant International*, 50(1):235.

[120] Murphy, M. P. (2009). How mitochondria produce reactive oxygen species. *Biochemical Journal*, 417(Pt 1):1–13.

[121] Murphy, P. G. (2012). Donor management: care of the heartbeating brain-dead multiorgan Donor. In *Handbook of Renal and Pancreatic Transplantation*, pages 77–90. John Wiley & Sons, Ltd, Chichester, UK.

[122] Nawata, C. M. and Pannabecker, T. L. (2018). Mammalian urine concentration: a review of renal medullary architecture and membrane transporters. *Journal of Comparative Physiology. B, Biochemical, systemic, and environmental Physiology*, 188(6):899–918.

[123] Ngo, J. P., Connie P.C. Ow, Gardiner, B. S., Kar, S., Pearson, J. T., Smith, D. W., and Evans, R. G. (2016). Diffusive shunting of gases and other molecules in the renal vasculature: physiological and evolutionary significance. *American Journal of Physiology. Regulatory, Integrative and Comparative Physiology*, 311(5):R797–R810.

[124] Nicholson, M. L. and Hosgood, S. A. (2013). Renal transplantation after ex vivo normothermic perfusion: the first clinical study. *American Journal of Transplantation*, 13(5):1246–1252.

[125] O'Callaghan, J. M., Knight, S. R., Morgan, R. D., and Morris, P. J. (2012). Preservation solutions for static cold storage of kidney allografts: a systematic review and meta-analysis. *American Journal of Transplantation*, 12(4):896–906.

[126] O'Connor, P. M., Anderson, W. P., Kett, M. M., and Evans, R. G. (2006). Renal preglomerular arterial-venous O2 shunting is a structural anti-oxidant defence mechanism of the renal cortex. *Clinical and Experimental Pharmacology & Physiology*, 33(7):637–641.

[127] O'Connor, P. M. and Evans, R. G. (2010). Structural antioxidant defense mechanisms in the mammalian and nonmammalian kidney: different solutions to the same problem? *American Journal of Physiology. Regulatory, Integrative and Comparative Physiology*, 299(3):R723–7.

[128] Ojo, A. (2014). Addressing the global burden of chronic kidney disease through clinical and translational research. *Transactions of the American Clinical and Climatological Association*, 125:229–43– discussion 243–6.

[129] Oram, J. and Murphy, P. (2011). Diagnosis of death. *Continuing Education in Anaesthesia Critical Care and Pain*, 11(3):77–81.

[130] Pallone, T. L., Edwards, A., and Mattson, D. L. (2011). *Renal Medullary Circulation*, volume 2. American Cancer Society, Hoboken, NJ, USA, 4 edition.

[131] Pallone, T. L., Zhang, Z., and Rhinehart, K. (2003). Physiology of the renal medullary microcirculation. *American Journal of Physiology - Renal Physiology*, 284(2):F253–66.

[132] Parekh, S., Ziegenhain, C., Vieth, B., Enard, W., and Hellmann, I. (2016). The impact of amplification on differential expression analyses by RNA-seq. *Scientific Reports*, 6:25533.

[133] Parikh, C. R., Hall, I. E., Bhangoo, R. S., Ficek, J., Abt, P. L., Thiessen-Philbrook, H., Lin, H., Bimali, M., Murray, P. T., Rao, V., Schröppel, B., Doshi, M. D., Weng, F. L., and Reese, P. P. (2016). Associations of perfusate biomarkers and pump parameters with delayed graft function and deceased donor kidney allograft function. *American Journal of Transplantation*, 16(5):1526–1539.

[134] Park, J., Shrestha, R., Qiu, C., Kondo, A., Huang, S., Werth, M., Li, M., Barasch, J., and Suszták, K. (2018). Single-cell transcriptomics of the mouse kidney reveals potential cellular targets of kidney disease. *Science*, 360(6390):758–763.

[135] Peperhove, M., Vo Chieu, V. D., Jang, M.-S., Gutberlet, M., Hartung, D., Tewes, S., Warnecke, G., Fegbeutel, C., Haverich, A., Gwinner, W., Lehner, F., Bräsen, J. H., Haller, H., Wacker, F., Gueler, F., and Hueper, K. (2018). Assessment of acute kidney injury with T1 mapping MRI following solid organ transplantation. *European Radiology*, 28(1):44–50.

[136] Ponticelli, C. E. (2015). The impact of cold ischemia time on renal transplant outcome. *Kidney International*, 87(2):272–275.

[137] Post, E. H., Su, F., Righy Shinotsuka, C., Taccone, F. S., Creteur, J., De Backer, D., and Vincent, J.-L. (2018). Renal autoregulation in experimental septic shock and its response to vasopressin and norepinephrine administration. *Journal of Applied Physiology (Bethesda, Md. : 1985)*, 125(6):1661–1669.

[138] Ramaswamy, D., Corrigan, G., Polhemus, C., Boothroyd, D., Scandling, J., Sommer, F. G., Alfrey, E., Higgins, J., Deen, W. M., Olshen, R., and Myers, B. D. (2002a). Maintenance and recovery stages of postischemic acute renal failure in humans. *American Journal of Physiology - Renal Physiology*, 282(2):F271–80.

[139] Ramaswamy, D., Corrigan, G., Polhemus, C., Boothroyd, D., Scandling, J., Sommer, F. G., Alfrey, E., Higgins, J., Deen, W. M., Olshen, R., and Myers, B. D. (2002b). Maintenance and recovery stages of postischemic acute renal failure in humans. *American Journal of Physiology - Renal Physiology*, 282(2):F271–80.

[140] Ravikumar, R., Jassem, W., Mergental, H., Heaton, N., Mirza, D., Perera, M. T. P. R., Quaglia, A., Holroyd, D., Vogel, T., Coussios, C. C., and Friend, P. J. (2016). Liver transplantation after ex vivo normothermic machine preservation: a phase 1 (first-in-man) clinical trial. *American Journal of Transplantation*, 16(6):1779–1787.

[141] Reese, P. P., Boudville, N., and Garg, A. X. (2015). Living kidney donation: outcomes, ethics, and uncertainty. *Lancet)*, 385(9981):2003–2013.

[142] Regner, K. R. and Roman, R. J. (2012a). Role of medullary blood flow in the pathogenesis of renal ischemia-reperfusion injury. *Current Opinion in Nephrology and Hypertension*, 21(1):33–38.

[143] Regner, K. R. and Roman, R. J. (2012b). Role of medullary blood flow in the pathogenesis of renal ischemia–reperfusion injury. *Current Opinion in Nephrology and Hypertension*, 21(1):33–38.

[144] Regner, K. R., Zuk, A., Van Why, S. K., Shames, B. D., Ryan, R. P., Falck, J. R., Manthati, V. L., McMullen, M. E., Ledbetter, S. R., and Roman, R. J. (2009). Protective effect of 20-HETE analogues in experimental renal ischemia reperfusion injury. *Kidney International*, 75(5):511–517.

[145] Salvadori, M., Rosso, G., and Bertoni, E. (2015). Update on ischemia-reperfusion injury in kidney transplantation: Pathogenesis and treatment. *World Journal of Transplantation*, 5(2):52–67.

[146] Sawant, K. V., Poluri, K. M., Dutta, A. K., Sepuru, K. M., Troshkina, A., Garofalo, R. P., and Rajarathnam, K. (2016). Chemokine cxcl1 mediated neutrophil recruitment: Role of glycosaminoglycan interactions. *Scientific Reports*, 6(1).

[147] Schmitz, V., Schaser, K.-D., Olschewski, P., Neuhaus, P., and Puhl, G. (2008). In vivo visualization of early microcirculatory changes following ischemia/reperfusion injury in human kidney transplantation. *European surgical research. Europaische chirurgische Forschung. Recherches chirurgicales europeennes*, 40(1):19–25.

[148] Scian, M. J., Maluf, D. G., Archer, K. J., Turner, S. D., Suh, J. L., David, K. G., King, A. L., Posner, M. P., Brayman, K. L., and Mas, V. R. (2012). Identification of biomarkers to assess organ quality and predict posttransplantation outcomes. *Transplantation*, 94(8):851–858.

[149] Segar, W. E. (1958). Effect of Hypothermia on Tubular Transport Mechanisms. *The American Journal of Physiology*, 195(1):91–96.

[150] Serianni, R., Barash, J., Bentley, T., Sharma, P., Fontana, J. L., Via, D., Duhm, J., Bunger, R., and Mongan, P. D. (2003). Porcine-specific hemoglobin saturation measurements. *Journal of Applied Physiology*, 94(2):561–566.

[151] Sgouralis, I., Evans, R. G., and Layton, A. T. (2016). Renal medullary and urinary oxygen tension during cardiopulmonary bypass in the rat. *Mathematical Medicine and Biology*.

[152] Sharkey, R. A., Mulloy, E. M., and O'Neill, S. J. (1998). Acute effects of hypoxaemia, hyperoxaemia and hypercapnia on renal blood flow in normal and renal transplant subjects. *The European Respiratory Journal*, 12(3):653–657.

[153] Siegemund, M., van Bommel, J., Stegenga, M. E., Studer, W., van Iterson, M., Annaheim, S., Mebazaa, A., and Ince, C. (2010). Aortic cross-clamping and reperfusion in pigs reduces microvascular oxygenation by altered systemic and regional blood flow distribution. *Anesthesia and Analgesia*, 111(2):345–353.

[154] Song, D., Zhou, W., Sheerin, S. H., and Sacks, S. H. (1998). Compartmental localization of complement component transcripts in the normal human kidney. *Nephron*, 78(1):15–22.

[155] Spagnolli, E. and Zapol, W. M. (2011). *The Role of Reactive Oxygen and Nitrogen Species in Ischemia/Reperfusion Injury*. John Wiley & Sons, Ltd.

[156] Stein, J. H. and Fadem, S. Z. (1978). The renal circulation. *JAMA*, 239(13):1308–1312.

[157] Stubenitsky, B. m., Booster, M. h., Brasile, L., Araneda, D., Haisch, C. E., and Kootstra, G. (2000). Exsanguinous metabolic support perfusion–a new strategy to improve graft function after kidney transplantation. *Transplantation*, 70(8):1254–1258.

[158] Stubenitsky, B. m., Booster, M. h., Kootstra, G., Brasile, L., and Haisch, C. (2001). Deletrious effect of prolonged cold ischemia on renal function. *Transplant International*, 14(4):256–260.

[159] Su, H., Lei, C.-T., and Zhang, C. (2017). Interleukin-6 Signaling Pathway and Its Role in Kidney Disease: An Update. *Frontiers in Immunology*, 8:405.

[160] Summers, D. M., Johnson, R. J., Allen, J., Fuggle, S. V., Collett, D., Watson, C. J., and Bradley, J. A. (2010). Analysis of factors that affect outcome after transplantation of kidneys donated after cardiac death in the UK: a cohort study. *Lancet*, 376(9749):1303–1311.

[161] Sörensen-Zender, I., Rong, S., Susnik, N., Lange, J., Gueler, F., Degen, J. L., Melk, A., Haller, H., and Schmitt, R. (2013). Role of fibrinogen in acute ischemic kidney injury. *American Journal of Physiology-Renal Physiology*, 305(5):F777–F785. PMID: 23804451.

[162] Tasoulis, M.-K. and Douzinas, E. E. (2016). Hypoxemic reperfusion of ischemic states: an alternative approach for the attenuation of oxidative stress mediated reperfusion injury. *Journal of Biomedical Science*, 23:7.

[163] Vandesompele, J., De Preter, K., Pattyn, F., Poppe, B., Van Roy, N., De Paepe, A., and Speleman, F. (2002). Accurate normalization of real-time quantitative RT-PCR data by geometric averaging of multiple internal control genes. *Genome Biology*, 3(7):research0034.1.

[164] Waiser, J., Budde, K., Katalinic, A., Kuerzdorfer, M., Riess, R., and Neumayer, H. H. (1997). Interleukin-6 expression after renal transplantation. *Nephrology Dialysis Transplantation*, 12(4):753–759.

[165] Waller, H. L., Harper, S. J. F., Hosgood, S. A., Bagul, A., Kay, M. D., Kaushik, M., Yang, B., Bicknell, G. R., and Nicholson, M. L. (2007). Differential expression of cytoprotective and apoptotic genes in an ischaemia-reperfusion isolated organ perfusion model of the transplanted kidney. *Transplant International*, 20(7):625–631.

[166] Watson, C. J. E., Kosmoliaptsis, V., Randle, L. V., Russell, N. K., Griffiths, W. J. H., Davies, S., Mergental, H., and Butler, A. J. (2016). Preimplant normothermic liver perfusion of a suboptimal liver donated after circulatory death. *American Journal of Transplantation*, 16(1):353–357.

[167] Watson, C. J. E., Wells, A. C., Roberts, R. J., Akoh, J. A., Friend, P. J., Akyol, M., Calder, F. R., Allen, J. E., Jones, M. N., Collett, D., and Bradley, J. A. (2010). Cold machine perfusion versus static cold storage of kidneys donated after cardiac death: a UK multicenter randomized controlled trial. *American Journal of Transplantation*, 10(9):1991–1999.

[168] Weissenbacher, A., Lo Faro, L., Boubriak, O., Soares, M. F., Roberts, I. S., Hunter, J. P., Voyce, D., Mikov, N., Cook, A., Ploeg, R. J., Coussios, C. C., and Friend, P. J. (2019). Twenty-four–hour normothermic perfusion of discarded human kidneys with urine recirculation. *American Journal of Transplantation*, 19(1):178–192.

[169] Welch, W. J., Baumgärtl, H., Lübbers, D., and Wilcox, C. S. (2001). Nephron pO2 and renal oxygen usage in the hypertensive rat kidney. *Kidney International*, 59(1):230–237.

[170] Whitehouse, T., Stotz, M., Taylor, V., Stidwill, R., and Singer, M. (2006). Tissue oxygen and hemodynamics in renal medulla, cortex, and corticomedullary junction during hemorrhage-reperfusion. *American Journal of Physiology - Renal Physiology*, 291(3):F647–53.

[171] Yagil, Y., Miyamoto, M., and Jamison, R. L. (1989). Inner medullary blood flow in postischemic acute renal failure in the rat. *The American Journal of Physiology*, 256(3 Pt 2):F456–61.

[172] Zhang, H., Bosch-Marce, M., Shimoda, L. A., Tan, Y. S., Baek, J. H., Wesley, J. B., Gonzalez, F. J., and Semenza, G. L. (2008). Mitochondrial autophagy is an HIF-1-dependent adaptive metabolic response to hypoxia. *The Journal of Biological Chemistry*, 283(16):10892–10903.

[173] Zhang, J. L., Morrell, G., Rusinek, H., Warner, L., Vivier, P.-H., Cheung, A. K., Lerman, L. O., and Lee, V. S. (2014). Measurement of renal tissue oxygenation with blood oxygen level-dependent MRI and oxygen transit modeling. *American Journal of Physiology - Renal Physiology*, 306(6):F579–87.

[174] Zhao, Y., Ding, C., Xue, W., Ding, X., Zheng, J., Gao, Y., Xia, X., Li, S., Liu, J., Han, F., Zhu, F., and Tian, P. (2017). Genome-wide DNA methylation analysis in renal ischemia reperfusion injury. *Gene*, 610:32–43.

[175] Zhou, T., Chuang, C.-C., Zuo, L., Zhou, T., Chuang, C.-C., and Zuo, L. (2015). Molecular characterization of reactive oxygen species in myocardial ischemia-reperfusion injury, molecular characterization of reactive oxygen species in myocardial ischemia-reperfusion injury. *BioMed Research International*, 2015, 2015:e864946.

[176] Zuk, A. and Bonventre, J. V. (2019). Recent advances in acute kidney injury and its consequences and impact on chronic kidney disease. *Current Opinion in Nephrology and Hypertension*, 28(4):397–405.

Appendix A

Publications, Abstracts and Awards

A.1 Publications

The following publication describes work outlined in chapter 3:

1. **Adams, T. D.**, Hosgood, S. A., and Nicholson, M. L. (2019). Physiological effects of altering oxygenation during kidney normothermic machine perfusion. American Journal of Physiology. Renal Physiology, 316(5):F823–F829

The following publications contain collaborative work that did not contribute towards this thesis:

1. Smith, S. F., **Adams, T.**, Hosgood, S. A., Nicholson, M. L. (2017). The administration of argon during ex vivo normothermic perfusion in an experimental model of kidney ischemia–reperfusion injury. Journal of Surgical Research, 218, 202–208.

2. Hosgood, S. A., Moore T., Kleverlan T., **Adams, T. D.**, Nicholson M. L. (2017). Haemoadsorption reduces the inflammatory response and improves blood flow during ex vivo renal perfusion in an experimental model. Journal of Translantional Medicine, 15(1), 216.

3. **Adams, T. D.**, Patel, M., Hosgood, S. A., Nicholson, M. L. (2017). Lowering perfusate temperature from 37°C to 32° diminishesfFunction in a porcine model of ex vivo kidney perfusion. Transplantation Direct, 3(3), e140.

A.2 Published Abstracts

A.2.1 Presentations

1. European Society of Organ Transplantation (ESOT) Annual Conference. Copenhagen, Denmark. 16th Sept. 2019. "Renal medullary physiology during transplant reperfusion." [4]

2. Society of Academic and Research Surgeons Annual Meeting. 8-9th Jan. 2019. Regional microvascular perfusion and oxygenation during human kidney reperfusion."[5]

3. International Meeting on Ischaemia-Reperfusion injury in Transplantation (IMIRT). Poitiers, France. 20-21st Apr. 2018. "Kidney oxygenation during normothermic machine perfusion." [2]

4. Society of Academic and Research Surgeons (SARS) Annual Meeting. London, UK. 10-11th Jan. 2018 "Hydrogen gas and renal ischaemia-reperfusion injury in a pre-clinical model" [3]

5. Society of Academic and Research Surgeons Annual Meeting. Dublin, Ireland. 18-19th Jan. 2017. "The assessment of different oxygen tensions during ex-vivo normothermic kidney perfusion." and "The effect of perfusate temperature on renal function during ex-vivo kidney perfusion." [1]

A.2.2 Posters

1. British Transplantation Society Annual Meeting. Harrogate, UK. 2017 "Kidney Oxygenation during Ex-Vivo Normothermic Perfusion."

A.3 Awards

1. **Rosetrees Trust PhD Fellowship** 2017-19 (London, UK)
   Personal grant of £50,000, towards the continuation of current research to form a PhD.

2. **Geoffrey Fisk Scholarship** 2017-18 and 2018-19 (Darwin College, Cambridge, UK)
   Inaugural and second recipient of scholarship and £12,000 for graduate work in the medical sciences.

3. **Marmaduke Shield Fund** 2017 (University of Cambridge, UK)
   Grant of £13,000 awarded by the School of Biological Sciences, for the procurement of oxygen and flow probes.

4. **Public Engagement Video Competition** 2017 (NIHR Blood and Transplant Research Unit in Organ Donation and Transplantation) Winning entry in local competition.

Appendix B

MATLAB code

B.1 Creating brightfield image colour map

```
%load images and select pos/neg regions

close all
clear all

images = [dir('*02.tif'); dir('*03.tif')];
%loads images but does not read them yet

for ii = 1:length(images)
    img_name = images(ii).name;
    info = imfinfo(img_name);

    img.ui8 = imread(img_name);
    img.height = size(img.ui8,1);
```

```
img.width = size(img.ui8,2);


temp.ui8_r = uint8(img.ui8(:,:,1));
temp.ui8_g = uint8(img.ui8(:,:,2));
temp.ui8_b = uint8(img.ui8(:,:,3));


f1 = figure(1);
f1.Units = 'normalized';
f1.OuterPosition = [0 0.2 0.9 0.8];
imshow(img.ui8)


% select first positive region
h = msgbox('Select positive region 1');
uiwait(h);
findposreg1 = roipoly();
img.findposreg1 = findposreg1;


% select second positive region
h = msgbox('Select positive region 2');
uiwait(h);
%display('Select positive region 2')
findposreg2 = roipoly();
img.findposreg2 = findposreg2;


% make array where 1 is in selected positive regions and 0 is not
img.index_pos = img.findposreg1 + img.findposreg2;
```

```
% make index of the linear index of selected positive pixels
idx_pos = sort(unique(cat(1,find(img.findposreg1),find(img.findposreg2))));

% select first negative region
h = msgbox('Select negative region 1');
uiwait(h);
findnegreg1 = roipoly();
img.findnegreg1 = findnegreg1;

% select second negative region
h = msgbox('Select negative region 2');
uiwait(h);
findnegreg2 = roipoly();
img.findnegreg2 = findnegreg2;

% make array where 1 is in selected negative regions and 0 is not
img.index_neg = img.findnegreg1 + img.findnegreg2;

% make index of the linear index of selected negative pixels
idx_neg = sort(unique(cat(1,find(img.findnegreg1),find(img.findnegreg2))));

% convert to an indexed image with a colormap, display image
if ii == 1
    display('generating color map')
    [X,map] = rgb2ind(img.ui8,65536);
```

```
        %second input in this function is the number of colors
        %will run faster with fewer colors but you will get more false negative pixel
    else
        display('using previous color map')
        X = dither(img.ui8,map,8,7);
    end

    storeX = X;
    % find all colors from colormap in both positive and negative selected regions
    poscolors = sort(unique(X(idx_pos)));
    negcolors = sort(unique(X(idx_neg)));

    % make a list of all colors that
    nooverlap = poscolors(find(-1*(ismember(poscolors,negcolors) - 1)));

    for ll = 1:(size(X,1)*size(X,2))
        if ismember(X(ll),nooverlap) == 0
            X(ll) = 0;
        else
        continue
    end
end

    storedPosColors(1:length(nooverlap),ii) = nooverlap;

end
```

```
PosColorList = unique(nonzeros(reshape(storedPosColors,[],1)));
save('PosColors.mat','PosColorList');
save('RefColorMap.mat','map');

f2 = figure(2);
f2.Units = 'normalized';
f2.OuterPosition = [0 0.2 0.9 0.8];
imagesc(X)
colormap(map)
axis image
colorbar
```

B.2 Quantifying brightfield image positive areas

```
close all
clear all

images = dir('*.tif'); %loads images but does not read them yet

%select what you want to do, 1=true, 0=false
save_images = 0;

load('PosColors.mat');
```

```
load('RefColorMap.mat');


for ii = 1:length(images)
    imageNumber_outOf = [ii length(images)];
    imageNumber_outOf
    img_name = images(ii).name;
    info = imfinfo(img_name);


    img.ui8 = imread(img_name);
    img.height = size(img.ui8,1);
    img.width = size(img.ui8,2);
    img_area = img.height*img.width;


    indimage = dither(img.ui8,map,8,7);
    for ll = 1:(size(indimage,1)*size(indimage,2))
        if ismember(indimage(ll),PosColorList) == 0
            indimage(ll) = 0;
            else
        continue
        end
    end


    % convert indexed image to mask (zeros and ones)
    mask_idx = find(indimage);
    maskzeros = zeros(img.height,img.width);
    maskzeros(mask_idx) = 1;
```

```
% dilate, erode ,fill holes in mask
SE = strel('disk',5,4);
dilated = imdilate(maskzeros,SE);
eroded = imerode(dilated,SE);
filledBWmask = imfill(eroded,'holes');

conncomp = bwconncomp(filledBWmask);
numPixels = cellfun(@numel,conncomp.PixelIdxList);
img.stain = zeros(img.height, img.width);
    for kk = 1:conncomp.NumObjects
        if numPixels(kk) > 50
        img.stain(conncomp.PixelIdxList{kk}) = 1;
    end
end

% calculate the positive pixel number
pos_area = nnz(img.stain);

% make mask green
filledgreenmask = uint8(cat(3,zeros
(img.height,img.width),img.stain,zeros(img.height,img.width))*2^8);

fig = figure(3);
fig.Units = 'normalized';
fig.OuterPosition = [0 0.2 0.8 0.8];
```

```
    subplot(4,2,[1,4]), imshow(filledgreenmask+img.ui8);
    subplot(4,2,[5,8]), imshowpair(filledgreenmask,img.ui8,'montage');

    % save images
    if save_images == 1
    picturename = sprintf([img_name(1:end-4) '_detected_stain']);
    saveas(gcf, picturename,'tif');
    end

    % store image name, positive pixels, total pixels in Results table
    Results(ii,1) = {img_name};
    Results(ii,2) = {pos_area};
    Results(ii,3) = {img_area};
    Results(ii,4) = {pos_area/img_area};

end
save('Results.mat','Results');
```

Appendix C

Supplementary Figures

C.1 Chapter 4 supplementary figures

C.2 Chapter 5 supplementary figures

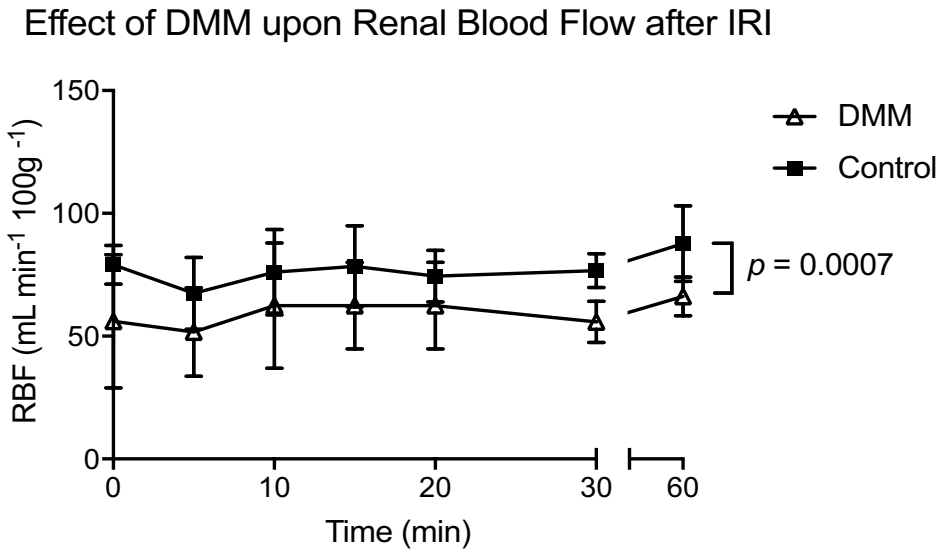

Fig. C.1 **The effect of dimethyl-malonate (DMM) upon renal blood flow during porcine kidney machine perfusion.**
As part of another unrelated experiment, the novel mitochondrial antioxidant compound dimethyl-malonate (DMM) was delivered in the cold flush to one kidney in each pair of those used in Chapter 4. To determine whether kidneys receiving this compound should be excluded from experiments investigating regional blood flow and oxygenation, the renal blood flow (RBF) over the normothermic machine perfusion period was compared in control (n=3) and DMM (n=3) kidneys were analysed alone. *P*-value is for Mann-Whitney U-value.

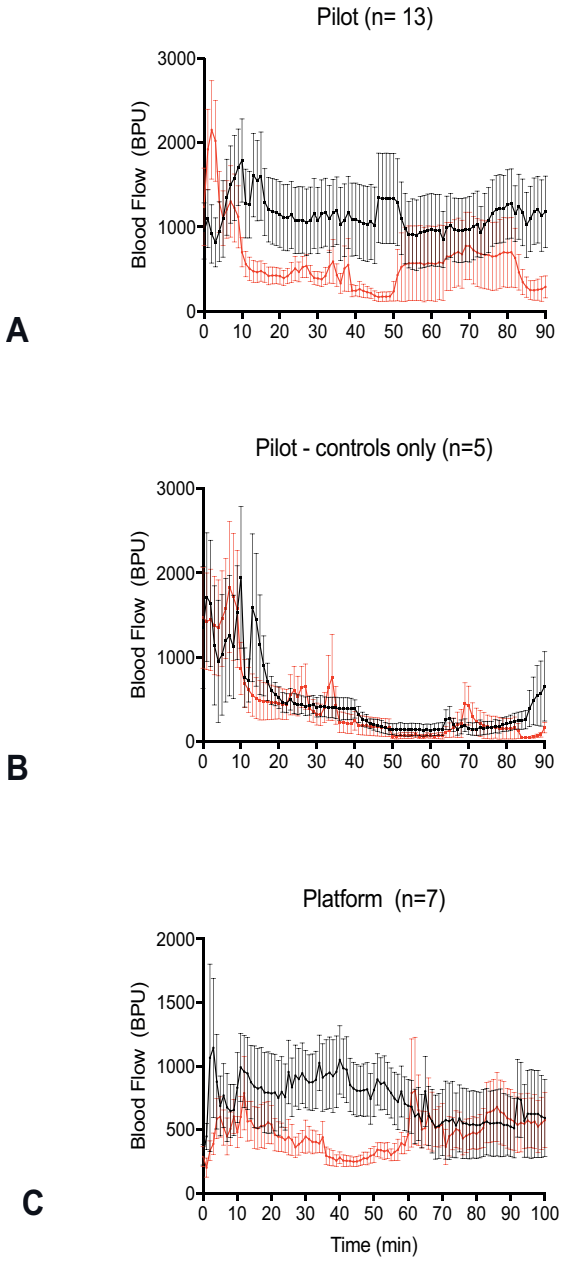

Fig. C.2 **Pilot and platform group regional microvascular perfusion during human kidney machine reperfusion.**
To investigate regional variations in kidney perfusion during transplant reperfusion, two series of human kidneys declined for transplantation (Pilot, n=13 and Platform, n=7)) underwent normothermic machine reperfusion for 90 minutes. Microvascular perfusion (MVP) was measured simultaneously in the cortex and medulla; a subgroup of controls from the Pilot series (n=5) was also analysed separately. A, Pilot series, $*P<0.0001$; B, Pilot control kidneys, $**P=0.025$; C, Platform series, $\#P<0.0001$. ; all two-tailed Mann-Whitney test. Mean and SEM.

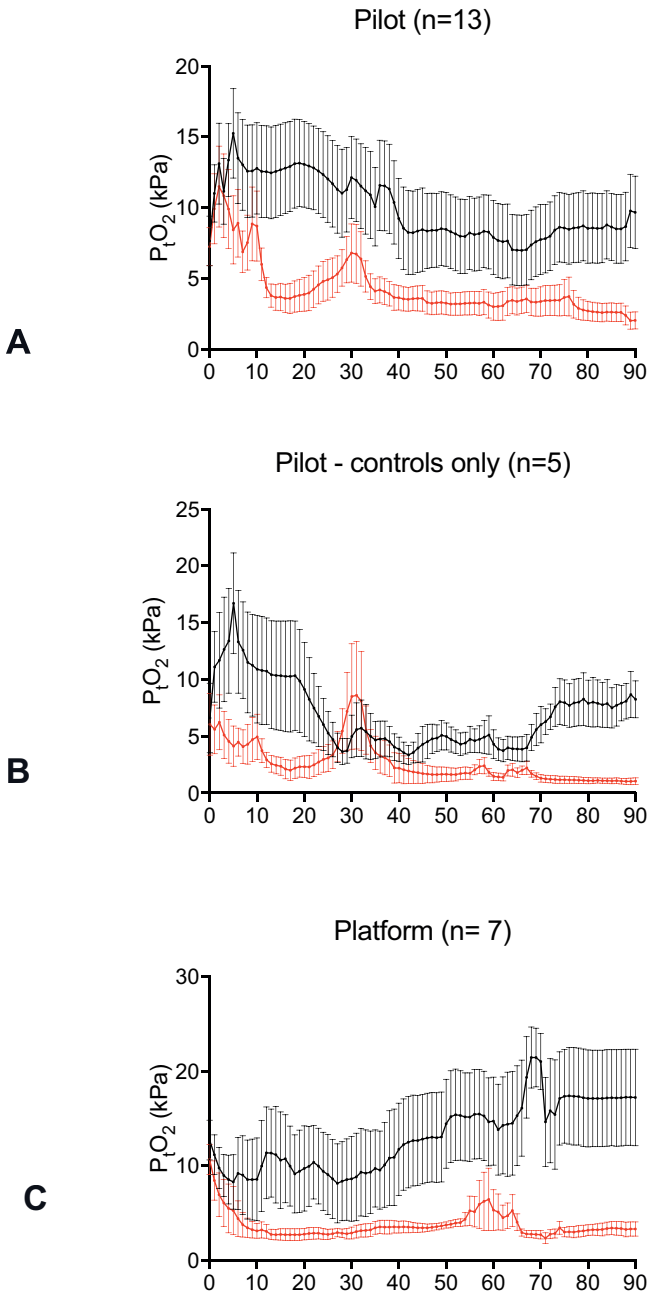

Fig. C.3 **Pilot and platform group regional tissue oxygenation during human kidney machine reperfusion.**
To investigate regional variations in kidney oxygenation during transplant reperfusion, two series of human kidneys declined for transplantation (Pilot, n=13 and Platform, n=7)) underwent normothermic machine reperfusion for 90 minutes. Tissue oxygenation (P_tO_2) was measured simultaneously in the cortex and medulla; a subgroup of controls from the Pilot series (n=5) was also analysed separately. A, Pilot series, $*P<0.0001$; B, Pilot control kidneys, $**P<0.0001$; C, Platform series, $\#P<0.0001$; all two-tailed Mann-Whitney test. Mean and SEM.

Appendix D

Nanostring Geneset Data

D.1 Nanostring nCounter human inflammation panel gene list

Name	Accession	Official Name
AGER	NM_001136.3	advanced glycosylation end product-specific receptor
ALOX12	NM_000697.1	arachidonate 12-lipoxygenase
ALOX15	NM_001140.3	arachidonate 15-lipoxygenase
ALOX5	NM_000698.2	arachidonate 5-lipoxygenase
AREG	NM_001657.2	amphiregulin
ARG1	NM_000045.2	arginase, liver
ATF2	NM_001880.2	activating transcription factor 2
BCL2L1	NM_138578.1	BCL2-like 1
BCL6	NM_001706.2	B-cell CLL/lymphoma 6
BIRC2	NM_001166.3	baculoviral IAP repeat containing 2
C1QA	NM_015991.2	complement component 1, q subcomponent, A chain
C1QB	NM_000491.3	complement component 1, q subcomponent, B chain
C1R	NM_001733.4	complement component 1, r subcomponent
C1S	NM_001734.2	complement component 1, s subcomponent
C2	NM_000063.3	complement component 2
C3	NM_000064.2	complement component 3

Name	Accession	Official Name
C3AR1	NM_004054.2	complement component 3a receptor 1
C4A	NM_007293.2	complement component 4A (Rodgers blood group)
C5	NM_001735.2	complement component 5
C6	NM_000065.2	complement component 6
C7	NM_000587.2	complement component 7
C8A	NM_000562.2	complement component 8, alpha polypeptide
C8B	NM_000066.2	complement component 8, beta polypeptide
C9	NM_001737.3	complement component 9
CCL11	NM_002986.2	chemokine (C-C motif) ligand 11
CCL13	NM_005408.2	chemokine (C-C motif) ligand 13
CCL16	NM_004590.2	chemokine (C-C motif) ligand 16
CCL17	NM_002987.2	chemokine (C-C motif) ligand 17
CCL19	NM_006274.2	chemokine (C-C motif) ligand 19
CCL2	NM_002982.3	chemokine (C-C motif) ligand 2
CCL20	NM_004591.1	chemokine (C-C motif) ligand 20
CCL21	NM_002989.2	chemokine (C-C motif) ligand 21
CCL22	NM_002990.3	chemokine (C-C motif) ligand 22

Name	Accession	Official Name
CCL23	NM_145898.1	chemokine (C-C motif) ligand 23
CCL24	NM_002991.2	chemokine (C-C motif) ligand 24
CCL3	NM_002983.2	chemokine (C-C motif) ligand 3
CCL4	NM_002984.2	chemokine (C-C motif) ligand 4
CCL5	NM_002985.2	chemokine (C-C motif) ligand 5
CCL7	NM_006273.2	chemokine (C-C motif) ligand 7
CCL8	NM_005623.2	chemokine (C-C motif) ligand 8
CCR1	NM_001295.2	chemokine (C-C motif) receptor 1
CCR2	NM_001123041.2	chemokine (C-C motif) receptor 2
CCR3	NM_001837.2	chemokine (C-C motif) receptor 3
CCR4	NM_005508.4	chemokine (C-C motif) receptor 4
CCR7	NM_001838.2	chemokine (C-C motif) receptor 7
CD163	NM_004244.4	CD163 molecule
CD4	NM_000616.3	CD4 molecule
CD40	NM_001250.4	CD40 molecule, TNF receptor superfamily member 5
CD40LG	NM_000074.2	CD40 ligand
CD55	NM_000574.3	CD55 molecule, decay accelerating factor for complement (Cromer blood group)

Name	Accession	Official Name
CD86	NM_175862.3	CD86 molecule
CDC42	NM_001039802.1	cell division cycle 42 (GTP binding protein, 25kDa)
CEBPB	NM_005194.2	CCAAT/enhancer binding protein (C/EBP), beta
CFB	NM_001710.5	complement factor B
CFD	NM_001928.2	complement factor D (adipsin)
CFL1	NM_005507.2	cofilin 1 (non-muscle)
CREB1	NM_134442.2	cAMP responsive element binding protein 1
CRP	NM_000567.2	C-reactive protein, pentraxin-related
CSF1	NM_000757.4	colony stimulating factor 1 (macrophage)
CSF2	NM_000758.2	colony stimulating factor 2 (granulocyte-macrophage)
CSF3	NM_000759.2	colony stimulating factor 3 (granulocyte)
CXCL1	NM_001511.1	chemokine (C-X-C motif) ligand 1 (melanoma growth stimulating activity, alpha)
CXCL10	NM_001565.1	chemokine (C-X-C motif) ligand 10
CXCL2	NM_002089.3	chemokine (C-X-C motif) ligand 2
CXCL3	NM_002090.2	chemokine (C-X-C motif) ligand 3
CXCL5	NM_002994.3	chemokine (C-X-C motif) ligand 5
CXCL6	NM_002993.3	chemokine (C-X-C motif) ligand 6 (granulocyte chemotactic protein 2)

Name	Accession	Official Name
CXCL9	NM_002416.1	chemokine (C-X-C motif) ligand 9
CXCR1	NM_000634.2	chemokine (C-X-C motif) receptor 1
CXCR2	NM_001557.2	chemokine (C-X-C motif) receptor 2
CXCR4	NM_003467.2	chemokine (C-X-C motif) receptor 4
CYSLTR1	NM_006639.2	cysteinyl leukotriene receptor 1
CYSLTR2	NM_020377.2	cysteinyl leukotriene receptor 2
DAXX	NM_001350.3	death-domain associated protein
DDIT3	NM_004083.4	DNA-damage-inducible transcript 3
DEFA1	NM_004084.2	defensin, alpha 1
ELK1	NM_005229.3	ELK1, member of ETS oncogene family
FASLG	NM_000639.1	Fas ligand (TNF superfamily, member 6)
FLT1	NM_002019.4	fms-related tyrosine kinase 1 (vascular endothelial growth factor)
FOS	NM_005252.2	FBJ murine osteosarcoma viral oncogene homolog
FXYD2	NM_021603.3	FXYD domain containing ion transport regulator 2
GNAQ	NM_002072.2	guanine nucleotide binding protein (G protein), q polypeptide
GNAS	NM_080425.1	GNAS complex locus
GNB1	NM_002074.3	guanine nucleotide binding protein (G protein), beta polypeptide 1

Name	Accession	Official Name
GNGT1	NM_021955.3	guanine nucleotide binding protein (G protein), gamma transducing activity polypeptide 1
GRB2	NM_203506.2	growth factor receptor-bound protein 2
HDAC4	NM_006037.3	histone deacetylase 4
HIF1A	NM_001530.2	hypoxia inducible factor 1, alpha subunit (basic helix-loop-helix transcription factor)
HLA-DRA	NM_019111.3	major histocompatibility complex, class II, DR alpha
HLA-DRB1	NM_002124.1	major histocompatibility complex, class II, DR beta 1
HMGB1	NM_002128.4	high mobility group box 1
HMGB2	NM_001130688.1	high mobility group box 2
HMGN1	NM_004965.6	high mobility group nucleosome binding domain 1
HRAS	NM_005343.2	v-Ha-ras Harvey rat sarcoma viral oncogene homolog
HSH2D	NM_032855.2	hematopoietic SH2 domain containing
HSPB1	NM_001540.3	heat shock 27kDa protein 1
HSPB2	NM_001541.3	heat shock 27kDa protein 2
IFI44	NM_006417.4	interferon-induced protein 44
IFIT1	NM_001548.3	interferon-induced protein with tetratricopeptide repeats 1
IFIT2	NM_001547.4	interferon-induced protein with tetratricopeptide repeats 2
IFIT3	NM_001031683.2	interferon-induced protein with tetratricopeptide repeats 3

Name	Accession	Official Name
IFNA1	NM_024013.1	interferon, alpha 1
IFNB1	NM_002176.2	interferon, beta 1, fibroblast
IFNG	NM_000619.2	interferon, gamma
IL10	NM_000572.2	interleukin 10
IL10RB	NM_000628.3	interleukin 10 receptor, beta
IL11	NM_000641.2	interleukin 11
IL12A	NM_000882.2	interleukin 12A (natural killer cell stimulatory factor 1)
IL12B	NM_002187.2	interleukin 12B (natural killer cell stimulatory factor 2)
IL13	NM_002188.2	interleukin 13
IL15	NM_000585.3	interleukin 15
IL17A	NM_002190.2	interleukin 17A
IL18	NM_001562.2	interleukin 18 (interferon-gamma-inducing factor)
IL18RAP	NM_003853.2	interleukin 18 receptor accessory protein
IL1A	NM_000575.3	interleukin 1, alpha
IL1B	NM_000576.2	interleukin 1, beta
IL1R1	NM_000877.2	interleukin 1 receptor, type I
IL1RAP	NM_002182.2	interleukin 1 receptor accessory protein

Name	Accession	Official Name
IL1RN	NM_173842.1	interleukin 1 receptor antagonist
IL2	NM_000586.2	interleukin 2
IL21	NM_021803.2	interleukin 21
IL22	NM_020525.4	interleukin 22
IL22RA2	NM_181309.1	interleukin 22 receptor, alpha 2
IL23A	NM_016584.2	interleukin 23, alpha subunit p19
IL23R	NM_144701.2	interleukin 23 receptor
IL3	NM_000588.3	interleukin 3 (colony-stimulating factor, multiple)
IL4	NM_000589.2	interleukin 4
IL5	NM_000879.2	interleukin 5 (colony-stimulating factor, eosinophil)
IL6	NM_000600.1	interleukin 6 (interferon, beta 2)
IL6R	NM_000565.2	interleukin 6 receptor
IL7	NM_000880.2	interleukin 7
IL8	NM_000584.2	interleukin 8
IL9	NM_000590.1	interleukin 9
IRF1	NM_002198.1	interferon regulatory factor 1
IRF3	NM_001571.5	interferon regulatory factor 3

Name	Accession	Official Name
IRF5	NM_002200.3	interferon regulatory factor 5
IRF7	NM_001572.3	interferon regulatory factor 7
ITGB2	NM_000211.2	integrin, beta 2 (complement component 3 receptor 3 and 4 subunit)
JUN	NM_002228.3	jun proto-oncogene
KEAP1	NM_012289.3	kelch-like ECH-associated protein 1
KNG1	NM_000893.2	kininogen 1
LIMK1	NM_002314.3	LIM domain kinase 1
LTA	NM_000595.2	lymphotoxin alpha (TNF superfamily, member 1)
LTB	NM_002341.1	lymphotoxin beta (TNF superfamily, member 3)
LTB4R	NM_181657.3	leukotriene B4 receptor
LTB4R2	NM_019839.4	leukotriene B4 receptor 2
LY96	NM_015364.2	lymphocyte antigen 96
MAFF	NM_001161572.1	v-maf musculoaponeurotic fibrosarcoma oncogene homolog F (avian)
MAFG	NM_002359.2	v-maf musculoaponeurotic fibrosarcoma oncogene homolog G (avian)
MAFK	NM_002360.3	v-maf musculoaponeurotic fibrosarcoma oncogene homolog K (avian)
MAP2K1	NM_002755.2	mitogen-activated protein kinase kinase 1
MAP2K4	NM_003010.2	mitogen-activated protein kinase kinase 4

Name	Accession	Official Name
MAP2K6	NM_002758.3	mitogen-activated protein kinase kinase 6
MAP3K1	NM_005921.1	mitogen-activated protein kinase kinase kinase 1, E3 ubiquitin protein ligase
MAP3K5	NM_005923.3	mitogen-activated protein kinase kinase kinase 5
MAP3K7	NM_145333.1	mitogen-activated protein kinase kinase kinase 7
MAP3K9	NM_033141.2	mitogen-activated protein kinase kinase kinase 9
MAPK1	NM_138957.2	mitogen-activated protein kinase 1
MAPK14	NM_001315.1	mitogen-activated protein kinase 14
MAPK3	NM_001040056.1	mitogen-activated protein kinase 3
MAPK8	NM_002750.2	mitogen-activated protein kinase 8
MAPKAPK2	NM_004759.3	mitogen-activated protein kinase-activated protein kinase 2
MAPKAPK5	NM_003668.2	mitogen-activated protein kinase-activated protein kinase 5
MASP1	NM_139125.3	mannan-binding lectin serine peptidase 1
MASP2	NM_139208.1	mannan-binding lectin serine peptidase 2
MAX	NM_002382.3	MYC associated factor X
MBL2	NM_000242.2	mannose-binding lectin (protein C) 2, soluble
MEF2A	NM_005587.2	myocyte enhancer factor 2A
MEF2BNB-MEF2B	NM_005919.2	MEF2BNB-MEF2B readthrough

Name	Accession	Official Name
MEF2C	NM_002397.3	myocyte enhancer factor 2C
MEF2D	NM_005920.2	myocyte enhancer factor 2D
MKNK1	NM_003684.3	MAP kinase interacting serine/threonine kinase 1
MMP3	NM_002422.3	matrix metallopeptidase 3 (stromelysin 1, progelatinase)
MMP9	NM_004994.2	matrix metallopeptidase 9 (gelatinase B, 92kDa gelatinase, 92kDa type IV collagenase)
MRC1	NM_002438.2	mannose receptor, C type 1
MX1	NM_002462.2	myxovirus (influenza virus) resistance 1, interferon-inducible protein p78 (mouse)
MX2	NM_002463.1	myxovirus (influenza virus) resistance 2 (mouse)
MYC	NM_002467.3	v-myc myelocytomatosis viral oncogene homolog (avian)
MYD88	NM_002468.3	myeloid differentiation primary response gene (88)
MYL2	NM_000432.3	myosin, light chain 2, regulatory, cardiac, slow
NFATC3	NM_004555.2	nuclear factor of activated T-cells, cytoplasmic, calcineurin-dependent 3
NFE2L2	NM_006164.3	nuclear factor (erythroid-derived 2)-like 2
NFKB1	NM_003998.2	nuclear factor of kappa light polypeptide gene enhancer in B-cells 1
NLRP3	NM_001079821.2	NLR family, pyrin domain containing 3
NOD1	NM_006092.1	nucleotide-binding oligomerization domain containing 1
NOD2	NM_022162.1	nucleotide-binding oligomerization domain containing 2

Name	Accession	Official Name
NOS2	NM_000625.4	nitric oxide synthase 2, inducible
NOX1	NM_007052.4	NADPH oxidase 1
NR3C1	NM_001018074.1	nuclear receptor subfamily 3, group C, member 1 (glucocorticoid receptor)
OAS2	NM_016817.2	2'-5'-oligoadenylate synthetase 2, 69/71kDa
OASL	NM_198213.1	2'-5'-oligoadenylate synthetase-like
OXER1	NM_148962.3	oxoeicosanoid (OXE) receptor 1
PDGFA	NM_002607.5	platelet-derived growth factor alpha polypeptide
PIK3C2G	NM_004570.4	phosphatidylinositol-4-phosphate 3-kinase, catalytic subunit type 2 gamma
PLA2G4A	NM_024420.2	phospholipase A2, group IVA (cytosolic, calcium-dependent)
PLCB1	NM_182734.1	phospholipase C, beta 1 (phosphoinositide-specific)
PPP1R12B	NM_002481.3	protein phosphatase 1, regulatory subunit 12B
PRKCA	NM_002737.2	protein kinase C, alpha
PRKCB	NM_212535.1	protein kinase C, beta
PTGDR2	NM_004778.1	prostaglandin D2 receptor 2
PTGER1	NM_000955.2	prostaglandin E receptor 1 (subtype EP1), 42kDa
PTGER2	NM_000956.2	prostaglandin E receptor 2 (subtype EP2), 53kDa
PTGER3	NM_000957.2	prostaglandin E receptor 3 (subtype EP3)

Name	Accession	Official Name
PTGER4	NM_000958.2	prostaglandin E receptor 4 (subtype EP4)
PTGFR	NM_000959.3	prostaglandin F receptor (FP)
PTGIR	NM_000960.3	prostaglandin I2 (prostacyclin) receptor (IP)
PTGS1	NM_000962.2	prostaglandin-endoperoxide synthase 1 (prostaglandin G/H synthase & cyclooxygenase)
PTGS2	NM_000963.1	prostaglandin-endoperoxide synthase 2 (prostaglandin G/H synthase & cyclooxygenase)
PTK2	NM_005607.3	PTK2 protein tyrosine kinase 2
RAC1	NM_198829.1	ras-related C3 botulinum toxin substrate 1 (rho family, small GTP binding protein Rac1)
RAF1	NM_002880.2	v-raf-1 murine leukemia viral oncogene homolog 1
RAPGEF2	NM_014247.2	Rap guanine nucleotide exchange factor (GEF) 2
RELA	NM_021975.2	v-rel reticuloendotheliosis viral oncogene homolog A (avian)
RELB	NM_006509.2	v-rel reticuloendotheliosis viral oncogene homolog B
RHOA	NM_001664.2	ras homolog family member A
RIPK1	NM_003804.3	receptor (TNFRSF)-interacting serine-threonine kinase 1
RIPK2	NM_003821.5	receptor-interacting serine-threonine kinase 2
ROCK2	NM_004850.3	Rho-associated, coiled-coil containing protein kinase 2
RPS6KA5	NM_004755.2	ribosomal protein S6 kinase, 90kDa, polypeptide 5
SHC1	NM_001130040.1	SHC (Src homology 2 domain containing) transforming protein 1

Name	Accession	Official Name
SMAD7	NM_005904.2	SMAD family member 7
STAT1	NM_007315.2	signal transducer and activator of transcription 1, 91kDa
STAT2	NM_005419.2	signal transducer and activator of transcription 2, 113kDa
STAT3	NM_139276.2	signal transducer and activator of transcription 3 (acute-phase response factor)
TBXA2R	NM_001060.3	thromboxane A2 receptor
TCF4	NM_003199.1	transcription factor 4
TGFB1	NM_000660.3	transforming growth factor, beta 1
TGFB2	NM_003238.2	transforming growth factor, beta 2
TGFB3	NM_003239.2	transforming growth factor, beta 3
TGFBR1	NM_004612.2	transforming growth factor, beta receptor 1
TLR1	NM_003263.3	toll-like receptor 1
TLR2	NM_003264.3	toll-like receptor 2
TLR3	NM_003265.2	toll-like receptor 3
TLR4	NM_138554.2	toll-like receptor 4
TLR5	NM_003268.3	toll-like receptor 5
TLR6	NM_006068.2	toll-like receptor 6
TLR7	NM_016562.3	toll-like receptor 7

Name	Accession	Official Name
TLR8	NM_016610.2	toll-like receptor 8
TLR9	NM_017442.2	toll-like receptor 9
TNF	NM_000594.2	tumor necrosis factor
TNFAIP3	NM_006290.2	tumor necrosis factor, alpha-induced protein 3
TNFSF14	NM_003807.2	tumor necrosis factor (ligand) superfamily, member 14
TOLLIP	NM_019009.2	toll interacting protein
TRADD	NM_003789.2	TNFRSF1A-associated via death domain
TRAF2	NM_021138.3	TNF receptor-associated factor 2
TREM2	NM_018965.3	triggering receptor expressed on myeloid cells 2
TSLP	NM_033035.4	thymic stromal lymphopoietin
TWIST2	NM_057179.2	twist homolog 2 (Drosophila)
TYROBP	NM_003332.3	TYRO protein tyrosine kinase binding protein
Internal reference genes		
CLTC	NM_004859.2	clathrin, heavy chain (Hc)
GAPDH	NM_002046.3	glyceraldehyde-3-phosphate dehydrogenase
GUSB	NM_000181.1	glucuronidase, beta
HPRT1	NM_000194.1	hypoxanthine phosphoribosyltransferase 1

Name	Accession	Official Name
PGK1	NM_000291.2	phosphoglycerate kinase 1
TUBB	NM_178014.2	tubulin, beta class I

D.2 Cortical tissue normalized mRNA counts

	NMP						CSS					
mRNA	Cortex 1	Cortex 2	Cortex 3	Cortex 4	Cortex 6	Cortex 7	Cortex 5	Cortex 8	Cortex 9	Cortex 10	Cortex 11	
AGER	14.6959402	7.04337958	2.76409065	8.18458805	5.4064734	11.5743592	15.596043	11.5320893	13.0753234	10.9293825	9.85808292	
ALOX12	1.13045694	4.02478833	1.38204533	3.27383522	1.08129468	4.62974369	3.11920859	9.36982255	1.153705	5.1003785	1.47871244	
ALOX15	9.04365552	2.01239417	4.14613598	8.18458805	6.48776807	6.94461553	3.11920859	15.8566228	3.84568335	4.371753	2.46452073	
ALOX5	21.4786819	10.0619708	13.8204533	14.7322585	33.5201351	23.1487184	40.5497117	44.686846	48.0710418	61.204542	58.6555934	
AREG	12.4350263	11.0681679	13.8204533	11.4584233	18.3820095	31.2507699	3.11920859	11.5320893	3.84568335	34.2453985	9.85808292	
ARG1	6.78274164	3.01859125	6.91022664	3.27383522	4.32517872	5.78717961	3.11920859	24.5056897	1.153705	22.5873905	4.43613731	
ATF2	65.5665025	100.619708	69.1022664	49.1075283	82.1783956	106.484105	31.1920859	82.1661362	103.064314	96.9071915	83.3008007	
BCL2L1	227.221845	180.109278	153.407031	158.781008	132.999246	173.615388	271.371148	208.298363	254.968806	205.472391	226.735907	
BCL6	120.958893	74.4585841	52.5177224	104.762727	130.836656	109.956413	90.4570492	80.724625	117.293342	153.73998	147.871244	
BIRC2	167.307627	122.756044	131.294306	158.781008	162.194202	151.624106	102.933884	164.332272	119.600752	130.423964	124.704749	
C1QA	22.6091388	25.1549271	31.7870425	18.0060937	9.73165211	17.3615388	9.35762578	44.686846	32.6883084	45.9034065	29.0813446	
C1QB	67.8274164	99.6135112	95.3611276	83.4827981	75.6906275	111.113849	18.7152516	130.45676	78.8365086	85.977809	63.5846348	
C1R	413.74724	237.462512	187.958165	564.736575	825.02784	268.525134	471.000498	426.687304	623.000702	362.126873	325.809641	
C1S	148.089859	98.6073141	116.091808	175.150184	263.835902	92.5948738	155.96043	143.430361	199.975534	179.241873	121.25442	
C2	133.393919	38.2354892	85.6868103	152.233338	91.9100477	94.9097456	134.12597	121.086938	166.902657	29.8736455	15.7729327	
C3	114.176151	22.1363358	96.7431729	78.5720453	231.397061	107.641541	87.3378406	23.7849342	77.2982353	39.345777	28.5884405	
C3AR1	12.4350263	14.0867592	22.1127252	16.3691761	16.2194202	17.3615388	6.23841719	30.2717344	22.6895317	32.059522	14.2942202	
C4A	972.192968	344.119402	543.143814	721.880666	549.297697	643.534373	1927.67091	952.838877	1141.78339	753.398767	838.429953	
C5	15.8263972	15.0929562	16.5845439	11.4584233	8.65035743	12.7317951	15.596043	24.5056897	16.9210067	29.14502	9.36517878	
C6	191.047223	7.04337958	9.67431729	9.82150566	77.8532169	60.186668	56.1457547	25.2264453	39.2259701	67.033546	19.2232617	
C7	638.708171	517.185301	421.523825	815.18497	631.476093	375.009239	570.815173	1154.65044	1390.5991	946.484524	1200.2216	
C8A	4.52182776	4.02478833	4.14613598	6.54767044	4.32517872	3.47230777	3.11920859	8.64906697	0.38456833	18.2156375	1.97161658	
C8B	4.52182776	3.01859125	1.38204533	3.27383522	1.08129468	3.47230777	3.11920859	13.694356	0.38456833	14.57251	1.47871244	
C9	37.305079	14.0867592	12.4384079	21.2799289	43.2517872	28.9358981	21.8344602	23.7849342	38.4568335	35.7026495	8.37937048	
CCL11	5.6522847	22.1363358	6.91022664	11.4584233	5.4064734	12.7317951	3.11920859	17.2981339	4.61482002	35.7026495	0.98580829	
CCL13	2.26091388	5.03098541	4.14613598	4.91075283	5.4064734	8.10205146	3.11920859	16.5773784	1.153705	7.286255	0.98580829	
CCL16	3.39137082	4.02478833	1.38204533	4.91075283	2.16258936	3.47230777	9.35762578	24.5056897	6.15309335	4.371753	1.47871244	
CCL17	7.91319858	6.0371825	9.67431729	1.63691761	10.8129468	10.4169233	3.11920859	0.72075558	0.76913667	3.6431275	2.46452073	
CCL19	3.39137082	5.03098541	4.14613598	4.91075283	10.8129468	15.046667	3.11920859	13.694356	12.3061867	9.4721315	5.42194561	
CCL2	270.179209	274.691804	145.114759	337.205028	192.470453	318.294879	6.23841719	28.8302232	64.6074802	73.5911755	60.1343058	
CCL20	23.7395957	26.1611242	20.7306799	21.2799289	94.0726371	35.8805136	3.11920859	20.9019118	9.9987767	56.1041635	48.3046063	
CCL21	6.78274164	22.1363358	20.7306799	24.5537641	44.3330818	11.5743592	21.8344602	48.2906239	30.7654668	52.461036	30.5600571	
CCL22	2.26091388	3.01859125	6.91022664	3.27383522	2.16258936	3.47230777	3.11920859	20.1811563	2.69197834	3.6431275	1.47871244	
CCL23	2.26091388	6.0371825	4.14613598	6.54767044	1.08129468	4.62974369	34.3112945	9.36982255	7.69136669	5.1003785	2.95742488	

	NMP						CSS				
mRNA	Cortex 1	Cortex 2	Cortex 3	Cortex 4	Cortex 6	Cortex 7	Cortex 5	Cortex 8	Cortex 9	Cortex 10	Cortex 11
CCL24	7.91319858	9.05577375	4.14613598	8.18458805	4.32517872	11.5743592	3.11920859	9.36982255	1.92284167	2.1858765	1.47871244
CCL3	5.6522847	18.1115475	16.5845439	26.1906818	43.2517872	41.6676932	3.11920859	30.99249	8.07593503	36.431275	6.90065805
CCL4	5.6522847	33.2045037	24.8768159	29.464517	55.1460286	60.186668	3.11920859	20.9019118	5.38395668	37.888526	4.43613731
CCL5	3.39137082	14.0867592	9.67431729	9.82150566	2.16258936	9.25948738	3.11920859	23.7849342	9.22964003	15.3011355	12.8155078
CCL7	10.1741125	5.03098541	5.52818131	9.82150566	2.16258936	9.25948738	3.11920859	2.16226674	1.153705	0.7286255	0.98580829
CCL8	4.52182776	9.05577375	5.52818131	8.18458805	1.08129468	8.10205146	3.11920859	14.4151116	1.53827334	19.6728885	0.98580829
CCR1	2.26091388	6.0371825	5.52818131	4.91075283	7.56906275	17.3615388	3.11920859	18.7396451	4.23025168	5.1003785	2.46452073
CCR2	5.6522847	3.01859125	4.14613598	11.4584233	7.56906275	6.94461553	3.11920859	23.0641786	5.76852502	23.316016	2.95742488
CCR3	5.6522847	6.0371825	4.14613598	8.18458805	4.32517872	8.10205146	6.23841719	18.7396451	1.53827334	10.200757	3.45032902
CCR4	4.52182776	2.01239417	4.14613598	6.54767044	6.48776807	8.10205146	6.23841719	22.343423	3.84568335	16.7583865	2.46452073
CCR7	1.13045694	6.0371825	2.76409065	4.91075283	8.65035743	8.10205146	3.11920859	6.48680022	1.53827334	5.1003785	0.49290415
CD163	39.5659929	23.1425329	16.5845439	22.9168465	52.9834393	50.9271806	49.9073375	41.0830681	33.8420134	81.606056	42.8826607
CD4	6.78274164	12.074365	6.91022664	9.82150566	7.56906275	16.2041029	3.11920859	24.5056897	9.9987767	12.3866335	13.3084119
CD40	24.8700527	54.3346425	41.4613598	40.9229402	34.6014297	74.075899	37.4305031	49.7321351	37.3031285	40.803028	28.5884405
CD40LG	1.13045694	1.00619708	6.91022664	1.63691761	3.24388404	2.31487184	3.11920859	3.6037779	1.92284167	5.829004	0.49290415
CD55	15.8263972	15.0929562	15.2024986	6.54767044	8.65035743	15.046667	3.11920859	17.2981339	14.9981651	16.029761	17.2516451
CD86	5.6522847	2.01239417	5.52818131	3.27383522	3.24388404	1.15743592	3.11920859	14.4151116	4.61482002	26.9591435	5.42194561
CDC42	885.147784	709.368944	838.901514	908.489273	973.165211	795.158479	692.464308	624.174333	496.093152	596.015659	506.212558
CEBPB	275.831493	270.667015	218.363162	217.710042	487.6639	292.831288	93.5762578	77.8416027	51.5321568	136.981594	107.946008
CFB	191.047223	74.4585841	88.450901	220.983877	329.794877	195.606671	124.768344	100.185026	193.822441	83.063307	56.6839768
CFD	4.52182776	3.01859125	8.29227196	4.91075283	4.32517872	9.25948738	6.23841719	11.5320893	4.23025168	5.829004	6.4077539
CFL1	867.060473	735.530068	753.214703	883.935509	942.88896	767.380016	692.464308	631.381889	701.837211	583.629025	619.580512
CREB1	37.305079	45.2788687	31.7870425	39.2860226	50.8208499	52.0846165	65.5033805	51.1736462	53.8395668	63.3904185	47.8117022
CRP	4.52182776	4.02478833	2.76409065	4.91075283	2.16258936	3.47230777	3.11920859	9.36982255	0.38456833	19.6728885	0.49290415
CSF1	14.6959402	34.2107008	23.4947706	14.7322585	16.2194202	42.8251291	9.35762578	30.2717344	23.0741001	34.974024	42.8826607
CSF2	3.39137082	3.01859125	4.14613598	1.63691761	3.24388404	2.31487184	3.11920859	4.32453348	0.76913667	2.1858765	0.49290415
CSF3	6.78274164	25.1549271	12.4384079	13.0953409	29.1949563	23.1487184	3.11920859	3.6037779	0.38456833	2.914502	1.97161658
CXCL1	134.524376	130.805621	71.866357	139.137997	229.234472	123.845644	34.3112945	40.3623125	16.5364384	87.43506	62.1059224
CXCL10	6.78274164	13.0805621	23.4947706	16.3691761	10.8129468	24.3061544	3.11920859	20.1811563	4.99938835	34.974024	8.37937048
CXCL2	354.963479	488.005585	210.07089	329.02044	440.086934	546.309755	28.0728773	34.5962679	55.7624085	60.4759165	52.7407436
CXCL3	29.3918804	75.4647812	30.4049972	60.5659516	90.828753	85.6502582	3.11920859	15.8566228	4.61482002	22.5873905	14.2942202
CXCL5	3.39137082	3.01859125	1.38204533	3.27383522	4.32517872	3.47230777	3.11920859	7.20755581	0.76913667	10.9293825	0.49290415
CXCL6	16.9568541	20.1239417	8.29227196	21.2799289	41.0891978	13.8892311	18.7152516	17.2981339	16.1518701	67.033546	37.4607151
CXCL9	6.78274164	5.03098541	6.91022664	3.27383522	9.73165211	6.94461553	24.9536687	19.4604007	4.99938835	29.14502	13.8013161

	NMP						CSS				
mRNA	Cortex 1	Cortex 2	Cortex 3	Cortex 4	Cortex 6	Cortex 7	Cortex 5	Cortex 8	Cortex 9	Cortex 10	Cortex 11
CXCR1	3.39137082	2.01239417	1.38204533	1.63691761	2.16258936	1.15743592	3.11920859	16.5773784	1.153705	18.2156375	0.49290415
CXCR2	5.6522847	4.02478833	4.14613598	1.63691761	3.24388404	2.31487184	3.11920859	17.2981339	1.92284167	3.6431275	2.46452073
CXCR4	29.3918804	68.4214016	73.2484024	13.0953409	45.4143765	94.9097456	24.9536687	30.99249	34.6111501	115.851454	53.2336478
CYSLTR1	3.39137082	6.0371825	9.67431729	4.91075283	4.32517872	11.5743592	9.35762578	10.0905781	3.46111501	20.401514	4.43613731
CYSLTR2	6.78274164	4.02478833	5.52818131	4.91075283	4.32517872	5.78717961	3.11920859	15.8566228	2.30741001	36.431275	3.45032902
DAXX	59.9142178	81.5019637	70.4843117	57.2921163	62.7150914	50.9271806	37.4305031	67.7510246	74.9908253	51.7324105	65.0633473
DDIT3	366.268048	428.639957	385.590646	471.432272	132.999246	509.271806	280.728773	156.403961	144.213125	243.360917	307.079283
DEFA1	2.26091388	4.02478833	4.14613598	1.63691761	1.08129468	4.62974369	3.11920859	86.4906697	5.38395668	48.089283	5.42194561
ELK1	22.6091388	19.1177446	19.3486346	19.6430113	15.1381255	26.6210262	6.23841719	15.8566228	14.9981651	15.3011355	16.2658368
FASLG	2.26091388	2.01239417	6.91022664	3.27383522	5.4064734	4.62974369	3.11920859	11.5320893	1.153705	9.4721315	0.98580829
FLT1	148.089859	130.805621	215.599071	261.906818	240.047419	247.691287	471.000498	356.053257	163.056974	630.261057	737.877507
FOS	1246.894	2203.57161	1156.77194	540.182811	218.421525	3641.29341	68.622589	139.826583	63.8383435	394.915021	437.698882
FXYD2	7812.58791	4095.22213	6574.38962	4758.51949	4507.91752	5122.81139	4934.58799	5754.51255	8160.15549	5820.26049	7592.69547
GNAQ	54.2619331	55.3408396	53.8997678	54.0182811	57.308618	68.2887194	68.622589	95.8604922	92.2964003	104.193446	87.736938
GNAS	359.485307	298.840534	331.690879	238.989971	246.535187	387.7441034	361.828197	377.675924	490.324627	527.524862	657.041227
GNB1	390.007644	315.945884	317.870425	376.49105	410.891978	336.8138353	508.431001	330.106056	297.655891	306.751335	299.192817
GNGT1	1.13045694	1.00619708	6.91022664	3.27383522	3.24388404	8.10205146	3.11920859	6.48680022	1.53827334	16.029761	0.98580829
GRB2	18.087311	10.0619708	12.4384079	22.9168465	8.65035743	6.94461553	6.23841719	6.48680022	7.69136669	9.4721315	4.43613731
HDAC4	37.305079	24.14873	23.4947706	27.8275994	27.032367	40.5102573	43.6689203	35.3170234	29.9963301	33.516773	21.6877824
HIF1A	1639.16256	726.474294	697.93289	1569.80399	925.588245	989.607713	427.331577	870.672741	1152.93587	673.249962	695.48775
HLA-DRA	874.973671	606.736841	801.58629	1100.00863	1109.40834	1087.98977	542.742295	533.35913	700.683506	661.591954	465.794418
HLA-DRB1	438.617293	68.4214016	341.365196	194.793196	509.289794	621.54309	486.596541	842.563274	1089.09752	459.76269	392.3517
HMGB1	182.003567	184.134066	124.384079	137.501079	171.925854	178.245132	109.172301	299.834321	155.750176	424.788666	201.597796
HMGB2	14.6959402	12.074365	20.7306799	14.7322585	8.65035743	31.2507699	15.596043	47.5698683	26.9197834	50.2751595	45.3471814
HMGN1	241.917785	277.710395	222.509298	183.334772	259.510723	284.729237	449.166037	351.728723	297.271323	358.483746	361.791643
HRAS	18.087311	27.1673212	17.9665893	26.1906818	38.9266084	18.5189748	31.1920859	24.5056897	16.5364384	18.2156375	13.8013161
HSH2D	7.91319858	5.03098541	1.38204533	8.18458805	10.8129468	4.62974369	6.23841719	10.0905781	4.23025168	8.743506	6.90065805
HSPB1	188.786309	838.16217	420.14178	527.08747	386.0222	768.5374452	286.967191	423.804281	655.304442	696.565978	819.699595
HSPB2	41.8269068	37.2292921	26.2588612	50.7444459	45.4143765	18.5189748	65.5033805	25.9472009	44.9944952	40.0744025	35.4890985
IFI44	5.6522847	16.0991533	12.4384079	1.63691761	5.4064734	21.9912825	6.23841719	21.6226674	18.4592801	26.230518	22.6735907
IFIT1	31.6527943	102.632102	87.0688556	88.3935509	29.1949563	60.186668	34.3112945	58.381202	45.7636318	51.003785	44.8542773
IFIT2	24.8700527	31.1921096	27.6409065	19.6430113	20.5445989	49.7697447	9.35762578	26.6679565	18.0747117	40.803028	15.7729327
IFIT3	19.217768	20.1239417	29.0229519	45.8336931	15.1381255	25.4635903	3.11920859	24.5056897	19.9975534	23.316016	13.3084119
IFNA1	5.6522847	3.01859125	1.38204533	3.27383522	3.24388404	2.31487184	3.11920859	25.2264453	0.38456833	42.260279	3.45032902

	NMP						CSS				
mRNA	Cortex 1	Cortex 2	Cortex 3	Cortex 4	Cortex 6	Cortex 7	Cortex 5	Cortex 8	Cortex 9	Cortex 10	Cortex 11
IFNB1	4.52182776	2.01239417	1.38204533	1.63691761	2.16258936	6.94461553	3.11920859	15.8566228	0.76913667	21.858765	0.49290415
IFNG	1.13045694	3.01859125	2.76409065	1.63691761	2.16258936	5.78717961	3.11920859	18.0188895	0.76913667	29.14502	0.98580829
IL10	2.26091388	12.074365	6.91022664	1.63691761	6.48776807	11.5743592	3.11920859	5.76604464	1.153705	2.914502	1.97161658
IL10RB	59.9142178	56.3470366	46.9895411	47.4706107	54.064734	53.2420524	71.7417976	80.724625	63.8383435	66.3049205	63.5846348
IL11	1.13045694	6.0371825	2.76409065	8.18458805	1.08129468	11.5743592	3.11920859	2.16226674	10.383345	1.457251	4.43613731
IL12A	1.13045694	9.05577375	6.91022664	6.54767044	3.24388404	5.78717961	3.11920859	1.44151116	1.153705	0.7286255	0.98580829
IL12B	7.91319858	6.0371825	5.52818131	11.4584233	1.08129468	4.62974369	6.23841719	20.1811563	2.69197834	22.5873905	3.45032902
IL13	1.13045694	2.01239417	1.38204533	4.91075283	1.08129468	2.31487184	3.11920859	5.04528906	0.76913667	1.457251	0.98580829
IL15	5.6522847	5.03098541	8.29227196	1.63691761	4.32517872	5.78717961	3.11920859	7.92831139	13.4598917	5.1003785	10.8438912
IL17A	7.91319858	7.04337958	6.91022664	13.0953409	5.4064734	9.25948738	9.35762578	7.92831139	3.46111501	3.6431275	2.95742488
IL18	32.7832513	40.2478833	35.9331785	34.3752698	54.064734	92.5948738	34.3112945	70.6340469	87.6815803	95.4499405	53.2336478
IL18RAP	3.39137082	1.00619708	2.76409065	4.91075283	10.8129468	10.4169233	3.11920859	17.2981339	1.92284167	21.1301395	3.45032902
IL1A	2.26091388	2.01239417	8.29227196	8.18458805	4.32517872	8.10205146	3.11920859	15.8566228	1.53827334	26.9591435	3.94323317
IL1B	10.1741125	32.1983067	20.7306799	11.4584233	45.4143765	48.6123087	3.11920859	19.4604007	3.07654668	45.9034065	8.37937048
IL1R1	52.0010192	34.2107008	29.0229519	37.649105	156.787728	55.5569243	81.0994234	57.6604464	39.9951068	45.9034065	39.4323317
IL1RAP	22.6091388	26.1611242	24.8768159	24.5537641	31.3575457	27.7784621	15.596043	27.3887121	20.3821217	39.345777	31.0529612
IL1RN	1.13045694	6.0371825	4.14613598	4.91075283	5.4064734	8.10205146	3.11920859	2.88302232	1.53827334	3.6431275	0.98580829
IL2	4.52182776	6.0371825	5.52818131	8.18458805	4.32517872	5.78717961	6.23841719	16.5773784	2.30741001	24.773267	1.97161658
IL21	2.26091388	2.01239417	1.38204533	1.63691761	1.08129468	3.47230777	3.11920859	11.5320893	0.76913667	16.7583865	1.47871244
IL22	5.6522847	1.00619708	1.38204533	4.91075283	1.08129468	6.94461553	3.11920859	7.20755581	0.38456833	9.4721315	0.49290415
IL22RA2	3.39137082	2.01239417	1.38204533	3.27383522	2.16258936	2.31487184	3.11920859	0.72075558	0.38456833	4.371753	0.49290415
IL23A	2.26091388	2.01239417	5.52818131	11.4584233	5.4064734	6.94461553	6.23841719	20.1811563	4.61482002	2.1858765	0.98580829
IL23R	4.52182776	7.04337958	6.91022664	1.63691761	4.32517872	2.31487184	3.11920859	17.2981339	0.76913667	28.4163945	2.46452073
IL3	5.6522847	2.01239417	1.38204533	1.63691761	1.08129468	2.31487184	3.11920859	6.48680022	0.38456833	2.1858765	0.49290415
IL4	13.5654833	3.01859125	9.67431729	4.91075283	5.4064734	3.47230777	6.23841719	20.1811563	1.153705	4.371753	4.92904146
IL5	3.39137082	1.00619708	4.14613598	1.63691761	2.16258936	3.47230777	3.11920859	15.8566228	1.53827334	34.2453985	1.47871244
IL6	21.4786819	42.2602775	20.7306799	117.858068	67.0402701	62.5015398	3.11920859	1.44151116	1.92284167	5.1003785	2.46452073
IL6R	44.0878206	52.3222483	41.4613598	62.2028692	102.722995	43.982565	59.2649633	61.2642243	57.3006819	42.9889045	62.1059224
IL7	5.6522847	4.02478833	1.38204533	3.27383522	5.4064734	1.15743592	6.23841719	14.4151116	2.30741001	16.029761	0.98580829
IL8	35.0441651	464.863052	183.812029	505.807541	776.36958	587.977448	12.4768344	22.343423	5.76852502	83.063307	77.3859509
IL9	4.52182776	6.0371825	8.29227196	1.63691761	7.56906275	6.94461553	3.11920859	1.44151116	0.76913667	8.0148805	0.49290415
IRF1	156.003058	94.5825258	88.450901	116.22115	58.3899127	151.624106	21.8344602	26.6679565	34.9957185	44.4461555	52.7407436
IRF3	12.4350263	17.1053504	9.67431729	9.82150566	10.8129468	9.25948738	18.7152516	23.0641786	28.0734884	21.858765	26.1239197
IRF5	27.1309666	23.1425329	20.7306799	21.2799289	17.3007149	16.2041029	21.8344602	26.6679565	31.9191718	26.9591435	24.6452073

	NMP						CSS				
mRNA	Cortex 1	Cortex 2	Cortex 3	Cortex 4	Cortex 6	Cortex 7	Cortex 5	Cortex 8	Cortex 9	Cortex 10	Cortex 11
IRF7	18.087311	17.1053504	12.4384079	19.6430113	16.2194202	26.6210262	31.1920859	30.2717344	26.9197834	21.858765	20.7019741
ITGB2	7.91319858	12.074365	19.3486346	4.91075283	33.5201351	28.9358981	12.4768344	32.4340011	46.5327685	31.3308965	31.0529612
JUN	855.755903	1109.83538	518.266998	366.669545	306.006394	1488.4626	37.4305031	64.8680022	38.4568335	135.524343	155.264806
KEAP1	33.9137082	20.1239417	26.2588612	18.0060937	36.7640191	17.3615388	18.7152516	21.6226674	58.0698185	24.0446415	31.0529612
KNG1	418.269068	592.650082	400.793145	266.81757	198.958221	388.89847	739.252437	818.057584	258.045353	371.599005	625.002457
LIMK1	23.7395957	18.1115475	13.8204533	26.1906818	17.3007149	17.3615388	9.35762578	27.3887121	35.3802868	32.7881475	38.9394275
LTA	6.78274164	7.04337958	4.14613598	4.91075283	2.16258936	9.25948738	3.11920859	19.4604007	3.07654668	2.1858765	2.46452073
LTB	1.13045694	7.04337958	9.67431729	3.27383522	4.32517872	3.47230777	3.11920859	15.1358672	25.3815101	16.029761	5.91484975
LTB4R	9.04365552	3.01859125	4.14613598	9.82150566	4.32517872	3.47230777	3.11920859	12.9736004	9.9987767	8.0148805	4.92904146
LTB4R2	26.0005096	14.0867592	9.67431729	3.27383522	25.9510723	15.046667	9.35762578	27.3887121	22.3049634	15.3011355	12.3226037
LY96	12.4350263	8.04957666	12.4384079	18.0060937	6.48776807	19.6764107	18.7152516	10.8113337	17.3055751	5.829004	12.3226037
MAFF	40.6964498	141.873789	140.968623	144.04875	60.552502	208.338466	15.596043	25.9472009	28.8426251	102.00757	145.406723
MAFG	45.2182776	36.223095	33.1690879	36.0121874	42.1704925	55.5569243	81.0994234	48.2906239	44.9944952	45.9034065	49.7833188
MAFK	104.002038	119.737453	80.158629	101.488892	103.804289	155.096414	87.3378406	57.6604464	107.294565	123.866335	172.023547
MAP2K1	102.871582	116.718862	127.14817	93.3043037	94.0726371	118.058464	71.7417976	91.5359587	69.6068686	82.3346815	67.0349639
MAP2K4	73.4797011	51.3160512	51.1356771	45.8336931	60.552502	57.8717961	34.3112945	49.7321351	24.2278051	56.832789	25.1381115
MAP2K6	31.6527943	34.2107008	24.8768159	21.2799289	16.2194202	28.9358981	59.2649633	49.0113795	28.4580568	42.260279	38.9394275
MAP3K1	124.350263	102.632102	80.158629	93.3043037	99.4791105	90.2800019	90.4570492	71.3548025	94.9883787	100.550319	84.286609
MAP3K5	38.4355359	32.1983067	20.7306799	26.1906818	31.3575457	35.8805136	34.3112945	33.8755123	41.1488118	34.2453985	38.4465234
MAP3K7	92.6974691	80.4957666	48.3715865	65.4767044	87.584869	99.5394893	96.6954664	120.366182	115.755069	119.494582	111.889241
MAP3K9	20.3482249	14.0867592	5.52818131	6.54767044	6.48776807	9.25948738	9.35762578	25.9472009	7.69136669	17.487012	11.3367954
MAPK1	191.047223	180.109278	161.699303	178.424019	185.982685	180.560004	199.62935	193.162496	169.210067	182.156375	175.96678
MAPK14	126.611177	106.656891	103.6534	119.494985	128.674067	120.373336	215.225393	173.702095	222.280497	163.212112	167.094506
MAPK3	79.1319858	91.5639346	107.799536	103.125809	103.804289	92.5948738	106.053092	98.7435145	125.753845	96.9071915	94.6375961
MAPK8	113.045694	74.4585841	69.1022664	86.7566333	125.430183	96.0671815	46.7881289	55.4981797	55.7624085	52.461036	55.2052644
MAPKAPK2	148.089859	161.99773	158.935213	171.876349	134.08054	171.300516	196.510141	114.600137	130.753234	114.394203	134.562832
MAPKAPK5	64.4360456	56.3470366	45.6074958	32.7383522	60.552502	39.3528214	81.0994234	95.8604922	93.4501053	83.7919325	83.3008007
MASP1	12.4350263	22.1363358	20.7306799	9.82150566	11.8942415	15.046667	3.11920859	30.2717344	4.99938835	26.9591435	5.91484975
MASP2	6.78274164	6.0371825	4.14613598	14.7322585	8.65035743	6.94461553	3.11920859	6.48680022	4.99938835	2.1858765	3.94323317
MAX	124.350263	143.886183	118.855898	144.04875	169.763265	138.892311	109.172301	113.879382	116.908774	153.73998	129.63379
MBL2	2.26091388	3.01859125	1.38204533	4.91075283	1.08129468	5.78717961	3.11920859	2.88302232	1.153705	2.914502	1.47871244
MEF2A	120.958893	110.681679	91.2149916	101.488892	97.3165211	167.828209	262.013522	197.487029	209.205174	289.992949	280.955363
MEF2B	11.3045694	11.0681679	4.14613598	24.5537641	14.0568308	6.94461553	18.7152516	24.5056897	13.4598917	7.286255	12.3226037
MEF2C	28.2614235	37.2292921	35.9331785	21.2799289	10.8129468	45.140001	21.8344602	36.7585346	39.2259701	48.089283	40.41814

	NMP						CSS				
mRNA	Cortex 1	Cortex 2	Cortex 3	Cortex 4	Cortex 6	Cortex 7	Cortex 5	Cortex 8	Cortex 9	Cortex 10	Cortex 11
MEF2D	31.6527943	58.3594308	30.4049972	37.649105	44.3330818	43.982565	71.7417976	49.0113795	49.2247468	48.089283	61.6130183
MKNK1	66.6969594	57.3532337	53.8997678	49.1075283	54.064734	85.6502582	81.0994234	85.7699141	89.2198536	87.43506	106.467296
MMP3	1.13045694	2.01239417	1.38204533	1.63691761	2.16258936	1.15743592	3.11920859	14.4151116	0.38456833	28.4163945	0.49290415
MMP9	1.13045694	4.02478833	5.52818131	1.63691761	4.32517872	3.47230777	3.11920859	2.88302232	5.38395668	2.1858765	3.94323317
MRC1	39.5659929	46.2850658	38.6972692	21.2799289	49.7395552	63.6589757	28.0728773	33.8755123	28.0734884	52.461036	34.0103861
MX1	57.6533039	56.3470366	98.1252183	121.131903	75.6906275	129.632823	62.3841719	133.339782	84.2204653	92.5354385	86.7511297
MX2	14.6959402	7.04337958	8.29227196	8.18458805	12.9755361	11.5743592	6.23841719	18.0188895	4.23025168	18.944263	15.7729327
MYC	107.393409	128.793227	116.091808	98.2150566	310.331573	195.606671	37.4305031	30.99249	27.6889201	56.1041635	37.4607151
MYD88	48.6096484	45.2788687	42.8434052	50.7444459	40.0079031	35.8805136	31.1920859	54.7774241	48.0710418	47.3606575	32.5316736
MYL2	5.6522847	6.0371825	4.14613598	13.0953409	6.48776807	4.62974369	3.11920859	8.64906697	1.153705	3.6431275	0.49290415
NFATC3	78.0015288	78.4833725	53.8997678	39.2860226	77.8532169	57.8717961	24.9536687	67.7510246	56.5315452	67.033546	60.62721
NFE2L2	275.831493	215.326176	212.83498	247.174559	269.242375	266.210262	171.556473	155.683205	181.900822	260.119303	245.959169
NFKB1	36.1746221	27.1673212	17.9665893	55.6551987	70.2841541	59.029232	6.23841719	19.4604007	16.5364384	29.8736455	20.20907
NLRP3	13.5654833	12.074365	22.1127252	3.27383522	7.56906275	19.6764107	3.11920859	12.2528449	4.23025168	8.0148805	4.43613731
NOD1	7.91319858	2.01239417	1.38204533	3.27383522	4.32517872	10.4169233	6.23841719	38.2000458	16.9210067	32.059522	13.3084119
NOD2	3.39137082	7.04337958	4.14613598	3.27383522	6.48776807	9.25948738	6.23841719	18.7396451	1.92284167	13.8438845	5.91484975
NOS2	15.8263972	5.03098541	2.76409065	8.18458805	9.73165211	5.78717961	3.11920859	19.4604007	8.8450717	5.829004	4.43613731
NOX1	11.3045694	14.0867592	17.9665893	24.5537641	21.6258936	12.7317951	3.11920859	20.9019118	8.07593503	22.5873905	9.36517878
NR3C1	108.523866	132.818015	111.945672	85.1197157	125.430183	130.790259	137.245178	172.260584	202.667512	193.085757	178.924205
OAS2	12.4350263	14.0867592	29.0229519	11.4584233	5.4064734	23.1487184	9.35762578	33.1547567	16.1518701	45.174781	14.7871244
OASL	6.78274164	9.05577375	11.0563626	11.4584233	10.8129468	10.4169233	3.11920859	16.5773784	4.99938835	1.457251	2.95742488
OXER1	14.6959402	11.0681679	13.8204533	19.6430113	6.48776807	13.8892311	21.8344602	26.6679565	17.3055751	13.8438845	19.2232617
PDGFA	5.6522847	8.04957666	8.29227196	16.3691761	10.8129468	17.3615388	9.35762578	23.0641786	24.2278051	39.345777	50.769127
PIK3C2G	35.0441651	18.1115475	30.4049972	11.4584233	9.73165211	39.3528214	43.6689203	57.6604464	63.8383435	99.0930679	98.0879251
PLA2G4A	15.8263972	5.03098541	11.0563626	8.18458805	10.8129468	10.4169233	12.4768344	21.6226674	8.46050336	26.230518	10.3509871
PLCB1	9.04365552	15.0929562	1.38204533	3.27383522	5.4064734	19.6764107	34.3112945	33.1547567	23.8432367	32.7881475	48.7975105
PPP1R12B	21.4786819	27.1673212	15.2024986	19.6430113	17.3007149	39.3528214	31.1920859	54.7774241	46.1482002	71.405299	64.5704431
PRKCA	48.6096484	62.3842191	40.0793145	26.1906818	47.5769659	52.0846165	99.814675	85.7699141	72.2988469	85.977809	79.3575675
PRKCB	5.6522847	6.0371825	11.0563626	6.54767044	6.48776807	1.15743592	3.11920859	10.8113337	7.69136669	10.200757	11.3367954
PTGDR2	10.1741125	5.03098541	9.67431729	14.7322585	9.73165211	4.62974369	3.11920859	11.5320893	4.23025168	5.1003785	3.94323317
PTGER1	3.39137082	4.02478833	1.38204533	4.91075283	2.16258936	1.15743592	3.11920859	1.44151116	2.30741001	1.457251	3.45032902
PTGER2	9.04365552	15.0929562	2.76409065	14.7322585	14.0568308	9.25948738	6.23841719	18.0188895	18.0747117	24.773267	16.758741
PTGER3	314.267029	134.830409	77.3945383	137.501079	117.86112	287.044109	458.523663	330.106056	399.181931	275.420439	346.018711
PTGER4	22.6091388	26.1611242	12.4384079	22.9168465	12.9755361	20.8338466	31.1920859	29.5509788	26.1506468	46.632032	33.0245778

	NMP						CSS				
mRNA	Cortex 1	Cortex 2	Cortex 3	Cortex 4	Cortex 6	Cortex 7	Cortex 5	Cortex 8	Cortex 9	Cortex 10	Cortex 11
PTGFR	20.3482249	11.0681679	12.4384079	18.0060937	5.4064734	25.4635903	15.596043	20.1811563	16.9210067	33.516773	16.758741
PTGIR	7.91319858	6.0371825	9.67431729	13.0953409	4.32517872	9.25948738	9.35762578	10.0905781	16.5364384	20.401514	14.7871244
PTGS1	7.91319858	14.0867592	4.14613598	4.91075283	9.73165211	15.046667	3.11920859	23.0641786	2.69197834	21.858765	6.4077539
PTGS2	4.52182776	9.05577375	9.67431729	14.7322585	6.48776807	12.7317951	15.596043	12.9736004	4.99938835	29.14502	9.36517878
PTK2	209.134534	224.38195	160.317258	147.322585	170.844559	267.367698	252.655896	308.483388	363.801645	335.896355	358.341314
RAC1	344.789367	260.605044	270.880884	286.460582	337.36394	250.006159	187.152516	204.694585	162.287837	198.186136	192.232617
RAF1	194.438594	190.171249	185.194074	129.316491	150.29996	181.71744	127.887552	135.502049	99.6031987	110.751076	89.7085546
RAPGEF2	52.0010192	54.3346425	46.9895411	39.2860226	50.8208499	71.7610272	49.9073375	75.679336	69.6068686	78.691554	67.0349639
RELA	37.305079	26.1611242	23.4947706	45.8336931	28.1136617	42.8251291	24.9536687	28.8302232	24.2278051	34.974024	27.109728
RELB	39.5659929	34.2107008	27.6409065	67.113622	38.9266084	49.7697447	6.23841719	8.64906697	23.0741001	24.773267	20.20907
RHOA	180.87311	125.774635	116.091808	137.501079	149.218666	112.271284	34.3112945	88.6529364	115.3705	127.509462	125.197653
RIPK1	143.568031	110.681679	55.2818131	85.1197157	147.056076	133.105131	124.768344	108.113337	111.140249	120.223207	101.538254
RIPK2	55.39239	85.5267521	74.6304477	62.2028692	64.8776807	83.3353864	12.4768344	34.5962679	26.5352151	47.3606575	27.6026322
ROCK2	159.394428	126.780832	76.012493	104.762727	121.105004	126.160516	190.271724	211.181385	241.124346	205.472391	259.267581
RPS6KA5	20.3482249	18.1115475	16.5845439	14.7322585	27.032367	37.0379495	31.1920859	12.2528449	19.6129851	8.0148805	13.8013161
SHC1	75.740615	106.656891	64.9561304	94.9412213	108.129468	129.632823	127.887552	139.826583	174.978592	139.896096	146.392531
SMAD7	146.959402	107.663088	113.327717	76.9351276	52.9834393	98.3820534	118.529927	92.9774699	87.297012	120.951833	139.984777
STAT1	125.48072	86.5329491	69.1022664	153.870255	190.307864	103.011797	12.4768344	67.7510246	111.140249	98.3644425	100.552446
STAT2	78.0015288	89.5515404	77.3945383	76.9351276	77.8532169	126.160516	202.748559	206.136096	258.814489	199.643387	217.863633
STAT3	748.362494	448.763899	411.849508	525.450553	825.02784	685.202066	577.05359	590.29882	925.655981	792.744544	919.266232
TBXA2R	2.26091388	10.0619708	4.14613598	6.54767044	7.56906275	8.10205146	3.11920859	7.20755581	10.383345	9.4721315	11.8296995
TCF4	20.3482249	19.1177446	17.9665893	16.3691761	24.8697776	38.1953854	43.6689203	51.1736462	79.2210769	73.5911755	68.0207722
TGFB1	39.5659929	37.2292921	33.1690879	18.0060937	50.8208499	31.2507699	24.9536687	97.3020034	136.521759	117.308705	117.311187
TGFB2	19.217768	26.1611242	15.2024986	11.4584233	24.8697776	25.4635903	6.23841719	7.92831139	8.8450717	13.115259	9.85808292
TGFB3	23.7395957	17.1053504	8.29227196	29.464517	19.4633042	13.8892311	24.9536687	28.8302232	16.9210067	62.661793	57.6697851
TGFBR1	40.6964498	39.2416862	30.4049972	36.0121874	29.1949563	53.2420524	96.6954664	77.1208471	57.3006819	97.635817	84.286609
TLR1	15.8263972	24.14873	16.5845439	14.7322585	8.65035743	17.3615388	15.596043	38.9208013	25.3815101	48.089283	12.8155078
TLR2	22.6091388	32.1983067	23.4947706	34.3752698	55.1460286	30.093334	9.35762578	29.5509788	23.0741001	40.803028	18.2374534
TLR3	29.3918804	41.2540804	29.0229519	44.1967755	22.7071883	39.3528214	46.7881289	43.2453348	22.3049634	47.3606575	29.5742488
TLR4	48.6096484	38.2354892	20.7306799	40.9229402	46.4956712	68.2887194	84.218632	61.9849799	59.2235235	76.5056775	48.3046063
TLR5	13.5654833	12.074365	6.91022664	6.54767044	8.65035743	10.4169233	15.596043	29.5509788	13.4598917	32.7881475	13.3084119
TLR6	10.1741125	8.04957666	11.0563626	16.3691761	9.73165211	6.94461553	18.7152516	21.6226674	10.7679134	32.059522	6.4077539
TLR7	9.04365552	3.01859125	4.14613598	16.3691761	8.65035743	12.7317951	12.4768344	17.2981339	7.30679836	13.115259	1.97161658
TLR8	6.78274164	7.04337958	5.52818131	9.82150566	7.56906275	12.7317951	3.11920859	12.2528449	6.15309335	21.1301395	5.42194561

	NMP						CSS				
mRNA	Cortex 1	Cortex 2	Cortex 3	Cortex 4	Cortex 6	Cortex 7	Cortex 5	Cortex 8	Cortex 9	Cortex 10	Cortex 11
TLR9	9.04365552	6.0371825	8.29227196	6.54767044	6.48776807	13.8892311	3.11920859	3.6037779	1.92284167	0.7286255	3.94323317
TNF	10.1741125	35.2168979	17.9665893	6.54767044	36.7640191	28.9358981	3.11920859	7.92831139	5.76852502	8.743506	8.37937048
TNFAIP3	144.698488	283.747577	161.699303	145.685667	222.746704	293.988724	18.7152516	41.8038237	37.3031285	99.8216934	86.2582256
TNFSF14	2.26091388	4.02478833	4.14613598	3.27383522	7.56906275	11.5743592	12.4768344	13.694356	8.46050336	5.1003785	2.95742488
TOLLIP	178.612196	182.121672	200.396572	168.602514	156.787728	145.836926	193.390933	183.792673	145.751399	103.464821	128.647982
TRADD	7.91319858	18.1115475	6.91022664	19.6430113	7.56906275	11.5743592	18.7152516	25.2264453	32.6883084	29.14502	21.1948783
TRAF2	27.1309666	32.1983067	22.1127252	13.0953409	22.7071883	24.3061544	12.4768344	27.3887121	21.9203951	31.3308965	19.7161658
TREM2	5.6522847	2.01239417	8.29227196	3.27383522	5.4064734	3.47230777	3.11920859	13.694356	4.99938835	2.914502	1.97161658
TSLP	3.39137082	7.04337958	11.0563626	14.7322585	4.32517872	9.25948738	3.11920859	22.343423	8.46050336	22.5873905	4.43613731
TWIST2	9.04365552	9.05577375	8.29227196	11.4584233	8.65035743	8.10205146	6.23841719	10.0905781	6.15309335	14.57251	4.43613731
TYROBP	56.522847	84.520555	70.4843117	47.4706107	60.552502	72.9184631	34.3112945	61.2642243	45.7636318	53.918287	37.4607151

D.3 Medullary tissue normalized mRNA counts

	NMP						Control				
mRNA	Medulla 1	Medulla 2	Medulla 3	Medulla 4	Medulla 6	Medulla 7	Medulla 5	Medulla 8	Medulla 9	Medulla 10	Medulla 11
AGER	9.71872627	1.2368975	4.8874785	8.19145032	14.069654	15.8001081	35.2256307	14.5984856	6.76688217	12.1250647	10.9392077
ALOX12	1.38838947	2.473795	1.22186963	4.09572516	1.4069654	5.92504056	28.1805046	12.435747	6.28353345	0.44907647	1.36740097
ALOX15	8.33033681	6.1844875	6.10934813	4.09572516	12.6626886	7.90005407	35.2256307	12.9764317	1.93339491	2.69445882	2.27900161
ALOX5	12.4955052	23.5010525	12.2186963	16.3829006	36.5811003	35.5502433	154.992775	72.4517435	29.0009236	32.3335059	41.9336296
AREG	20.825842	40.8176175	73.3121776	73.7230529	40.8019965	75.0505137	32.8772553	14.5984856	10.1503233	16.1667529	18.6878132
ARG1	5.55355787	6.1844875	2.44373925	13.6524172	1.4069654	11.8500811	68.102886	17.3019089	9.18362581	4.04168824	5.46960386
ATF2	61.0891366	107.610082	118.521354	95.5669204	99.8945432	136.275933	103.328517	127.601578	103.436628	84.4263765	93.8948663
BCL2L1	297.115346	144.717007	138.071268	107.854096	119.592059	130.350892	197.263532	162.746081	142.104526	123.945106	223.342158
BCL6	188.820968	132.348032	164.9524	128.332722	168.835848	238.976636	187.87003	295.213821	172.072147	104.634818	132.182093
BIRC2	199.928083	132.348032	245.595795	163.829006	227.928394	152.076041	178.476529	194.646475	155.154941	129.7831	157.706911
C1QA	23.602621	12.368975	23.2155229	12.2871755	33.7671695	9.87506759	100.980141	43.2547723	19.8172978	24.6992059	28.2596199
C1QB	76.3614207	68.0293625	69.6465687	55.9749105	111.150266	118.500811	166.734652	169.234296	79.2691912	74.0976177	71.1048502
C1R	441.507851	258.511577	516.850852	608.897807	689.413045	479.928285	1296.30321	816.433826	800.90884	538.442688	374.667864
C1S	144.392505	107.610082	244.373925	206.1515	267.323426	156.026068	584.74547	402.810067	264.875102	203.880718	158.618512
C2	145.780894	3.7106925	23.2155229	5.46096688	7.03482699	11.8500811	79.8447629	17.3019089	13.0504156	5.38891765	13.2182093
C3	124.955052	14.84277	36.6560888	15.0176589	63.3134429	7.90005407	126.812271	11.3543777	29.4842723	11.6759882	13.6740097
C3AR1	19.4374525	16.0796675	20.7717836	15.0176589	22.5114464	15.8001081	68.102886	38.929295	28.5175749	12.1250647	11.8508084
C4A	1452.25538	32.159335	131.96192	135.15893	83.0109585	57.275392	1016.84654	92.9977604	143.554572	68.7087	438.024109
C5	16.6606736	12.368975	9.77495701	13.6524172	15.4766194	15.8001081	54.0126338	36.2258718	25.1341338	13.4722941	9.57180676
C6	217.977146	3.7106925	3.66560888	5.46096688	16.8835848	15.8001081	56.3610091	19.4646475	33.3510621	9.87968235	20.5110145
C7	470.66403	372.306147	1155.88867	999.356939	776.6449	513.503515	2268.53062	1193.83171	1305.04156	1129.42732	1233.85147
C8A	4.1651684	4.94759	7.33121776	4.09572516	4.22089619	1.97501352	35.2256307	6.48821584	8.21692835	0.89815294	1.82320129
C8B	1.38838947	4.94759	1.22186963	2.73048344	2.8139308	3.95002704	32.8772553	9.73232376	8.21692835	1.34722941	0.91160064
C9	37.4865156	11.1320775	6.10934813	6.8262086	11.2557232	9.87506759	51.6642584	23.2494401	17.8839029	9.87968235	12.3066087
CCL11	5.55355787	17.316565	21.9936533	28.6700761	7.03482699	21.7251487	16.4386277	15.6798549	14.5004618	19.7593647	15.0414106
CCL13	2.77677894	3.7106925	9.77495701	5.46096688	8.44179239	7.90005407	46.9675076	27.5749173	13.0504156	3.14353529	4.55800322
CCL16	2.77677894	3.7106925	3.66560888	1.36524172	1.4069654	7.90005407	37.5740061	25.4121787	8.70027708	0.44907647	4.1022029
CCL17	6.94194734	3.7106925	6.10934813	8.19145032	7.03482699	13.8250946	37.5740061	18.9239629	0.48334873	2.69445882	3.19060225
CCL19	6.94194734	2.473795	13.4405659	5.46096688	8.44179239	3.95002704	49.315883	13.5171163	18.8506003	13.0232176	11.395008
CCL2	344.320588	876.960327	1610.42417	2573.48064	471.333408	1842.68761	39.9223815	80.5620133	119.387135	171.996288	111.671079
CCL20	44.428463	16.0796675	59.8716117	27.3048344	32.3602041	57.275392	32.8772553	14.5984856	6.76688217	1.79630588	28.2596199
CCL21	12.4955052	2.473795	21.9936533	21.8438675	18.2905502	5.92504056	112.722018	30.2783406	53.6517087	15.2686	19.1436135
CCL22	4.1651684	8.6582825	6.10934813	5.46096688	4.22089619	11.8500811	16.4386277	20.5460168	8.21692835	2.24538235	0.45580032
CCL23	8.33033681	1.2368975	7.33121776	2.73048344	9.84875778	3.95002704	49.315883	12.435747	9.18362581	2.24538235	2.27900161

	NMP						Control				
mRNA	Medulla 1	Medulla 2	Medulla 3	Medulla 4	Medulla 6	Medulla 7	Medulla 5	Medulla 8	Medulla 9	Medulla 10	Medulla 11
CCL24	12.4955052	8.6582825	7.33121776	9.55669204	9.84875778	11.8500811	21.1353784	7.56958515	0.48334873	1.34722941	1.36740097
CCL3	18.0490631	40.8176175	53.7622635	12.2871755	18.2905502	43.4502974	98.631766	30.8190252	14.0171131	3.14353529	5.01380354
CCL4	12.4955052	34.63313	51.3185243	28.6700761	12.6626886	41.4752839	112.722018	24.3308094	13.5337643	3.59261177	5.01380354
CCL5	6.94194734	8.6582825	20.7717836	10.9219338	18.2905502	7.90005407	32.8772553	11.3543777	8.70027708	4.93984118	5.46960386
CCL7	9.71872627	12.368975	10.9968266	19.1133841	7.03482699	9.87506759	2.34837538	2.70342327	1.45004618	1.79630588	1.82320129
CCL8	4.1651684	39.58072	37.8779584	69.6273277	8.44179239	53.325365	37.5740061	9.19163911	7.2502309	5.83799412	6.3812045
CCR1	4.1651684	3.7106925	4.8874785	8.19145032	12.6626886	9.87506759	32.8772553	14.5984856	10.633672	3.59261177	2.27900161
CCR2	8.33033681	4.94759	13.4405659	5.46096688	14.069654	11.8500811	56.3610091	15.1391703	17.8839029	5.83799412	2.73480193
CCR3	5.55355787	2.473795	6.10934813	12.2871755	8.44179239	11.8500811	58.7093845	17.3019089	7.73357963	2.69445882	4.1022029
CCR4	6.94194734	4.94759	6.10934813	9.55669204	7.03482699	5.92504056	35.2256307	23.2494401	12.5670669	2.24538235	3.64640257
CCR7	1.38838947	6.1844875	4.8874785	13.6524172	2.8139308	3.95002704	21.1353784	11.8950624	0.96669745	0.44907647	1.36740097
CD163	58.3123576	14.84277	18.3280444	13.6524172	99.8945432	29.6252028	218.39891	60.0159965	38.6678981	46.703953	40.1104283
CD4	15.2722841	4.94759	6.10934813	8.19145032	7.03482699	11.8500811	56.3610091	20.0053322	14.5004618	5.38891765	12.3066087
CD40	51.3704103	65.5555675	107.524527	72.3578111	80.1970277	69.1254731	82.1931383	81.102698	40.601293	38.6205765	30.9944219
CD40LG	1.38838947	2.473795	2.44373925	1.36524172	5.62786159	1.97501352	28.1805046	5.40684653	7.73357963	0.44907647	0.45580032
CD55	12.4955052	24.73795	25.6592621	12.2871755	11.2557232	13.8250946	46.9675076	32.4410792	13.0504156	10.7778353	17.3204122
CD86	2.77677894	1.2368975	4.8874785	9.55669204	8.44179239	7.90005407	39.9223815	15.6798549	12.0837182	7.6343	5.46960386
CDC42	1087.10895	801.50958	937.174003	806.857856	1059.44494	920.3563	774.963876	1024.59742	820.726138	749.50863	744.321925
CEBPB	365.14643	280.775732	601.159856	384.998165	543.088644	369.327528	194.915157	189.239629	62.3519857	107.778353	115.317481
CFB	256.852052	66.792465	69.6465687	129.697963	125.21992	130.350892	162.037901	121.113362	144.521269	79.0374588	78.3976553
CFD	6.94194734	14.84277	26.8811318	25.9395927	12.6626886	23.7001622	63.4061353	34.6038178	28.5175749	21.1065941	16.4088116
CFL1	1080.16701	855.93307	825.983867	916.077194	823.074758	1021.08199	617.622725	619.624613	651.554084	749.50863	818.617378
CREB1	65.254305	44.52831	89.1964827	38.2267681	84.4179239	65.1754461	110.373643	98.4046069	84.5860272	60.1762471	70.6490499
CRP	4.1651684	2.473795	3.66560888	2.73048344	4.22089619	7.90005407	42.2707568	16.2205396	9.18362581	0.44907647	0.45580032
CSF1	22.2142315	51.949695	74.5340472	68.262086	30.9532387	39.5002704	61.0577599	56.7718886	33.8344109	45.8058	43.3010306
CSF2	2.77677894	4.94759	7.33121776	5.46096688	4.22089619	3.95002704	16.4386277	8.65095445	1.45004618	2.24538235	0.91160064
CSF3	13.8838947	19.79036	61.0934813	75.0882946	85.8248893	37.5252568	39.9223815	23.2494401	1.45004618	0.89815294	0.91160064
CXCL1	363.758041	247.3795	760.002907	522.887579	851.214066	633.979339	84.5415137	31.9003945	8.21692835	22.0047471	54.6960386
CXCL10	6.94194734	14.84277	47.6529154	6.8262086	9.84875778	27.6501893	44.6191322	17.8425936	9.18362581	3.59261177	22.3342158
CXCL2	270.735946	1024.15113	2217.69337	1044.40992	1119.94446	1216.60833	72.7996368	35.6851871	36.7345032	45.8058	58.3424412
CXCL3	29.1561788	94.00421	221.158402	99.6626455	150.545298	124.425852	42.2707568	13.5171163	7.2502309	12.1250647	24.1574171
CXCL5	4.1651684	6.1844875	1.22186963	2.73048344	5.62786159	11.8500811	32.8772553	9.19163911	4.35013854	0.89815294	0.91160064
CXCL6	29.1561788	11.1320775	14.6624355	9.55669204	15.4766194	17.7751217	58.7093845	21.0867015	11.1170207	8.08337647	15.9530113
CXCL9	15.2722841	6.1844875	9.77495701	12.2871755	8.44179239	3.95002704	46.9675076	17.3019089	12.5670669	1.34722941	9.11600643

	NMP						Control				
mRNA	Medulla 1	Medulla 2	Medulla 3	Medulla 4	Medulla 6	Medulla 7	Medulla 5	Medulla 8	Medulla 9	Medulla 10	Medulla 11
CXCR1	6.94194734	3.7106925	4.8874785	4.09572516	5.62786159	7.90005407	39.9223815	12.9764317	9.66697453	1.79630588	0.91160064
CXCR2	2.77677894	3.7106925	3.66560888	4.09572516	4.22089619	5.92504056	23.4837538	18.3832782	9.66697453	0.89815294	3.19060225
CXCR4	41.651684	48.2390025	129.51818	30.0353178	47.8368235	49.375338	129.160646	27.0342327	28.0342261	54.7873294	57.4308405
CYSLTR1	2.77677894	4.94759	6.10934813	5.46096688	2.8139308	11.8500811	46.9675076	12.435747	14.0171131	4.04168824	10.4834074
CYSLTR2	5.55355787	3.7106925	8.55308738	17.7481424	16.8835848	15.8001081	49.315883	38.929295	7.73357963	5.38891765	10.9392077
DAXX	77.7498102	79.16144	76.9777864	50.5139436	88.6388201	73.0755002	108.025268	100.567346	82.6526323	52.9910235	67.0026473
DDIT3	431.789124	348.805095	516.850852	243.013026	61.9064775	325.877231	201.960283	181.129359	71.5356115	134.273865	389.253475
DEFA1	4.1651684	1.2368975	6.10934813	6.8262086	2.8139308	5.92504056	86.8898891	54.60915	24.6507851	2.69445882	3.64640257
ELK1	24.9910104	25.9748475	21.9936533	32.7658013	22.5114464	21.7251487	18.787003	21.6273861	24.6507851	10.3287588	12.762409
FASLG	4.1651684	7.421385	3.66560888	5.46096688	5.62786159	9.87506759	21.1353784	7.02890049	8.21692835	0.44907647	2.27900161
FLT1	212.423589	97.7149025	213.827185	177.481424	464.298581	152.076041	436.797821	243.848779	158.055034	170.649059	362.817056
FOS	538.695114	6739.85447	3715.70553	1029.39226	191.347294	5934.91562	225.444037	123.276101	47.8515239	177.834282	574.308405
FXYD2	9345.24951	7141.84616	4896.03159	6943.61939	3842.4225	6120.56689	3966.40602	3436.05097	7207.69621	5934.99464	8845.26104
GNAQ	88.8569259	47.002105	42.7654369	49.1487019	77.3830969	53.325365	126.812271	89.7536524	86.0360733	63.3197824	99.3644701
GNAS	458.168524	646.897392	576.722463	617.089257	416.461758	527.328609	453.236448	547.713554	670.404684	625.563524	765.744541
GNB1	503.985377	447.756895	430.098108	423.224933	493.844855	440.428015	439.146196	504.999466	453.864454	458.058	422.071098
GNGT1	1.38838947	3.7106925	3.66560888	1.36524172	7.03482699	5.92504056	25.8321292	3.78479257	5.31683599	0.44907647	3.19060225
GRB2	11.1071157	13.6058725	13.4405659	20.4786258	15.4766194	15.8001081	14.0902523	7.02890049	8.21692835	6.28707059	5.01380354
HDAC4	31.9329578	22.264155	18.3280444	31.4005595	52.0577197	27.6501893	91.5866398	47.0395648	44.9514316	19.7593647	26.892219
HIF1A	2778.16733	1252.97717	1655.63334	2375.52059	1723.53261	2212.01514	523.68771	1401.99531	1284.74092	789.925512	931.655858
HLA-DRA	1045.45727	470.02105	827.205737	682.62086	787.900623	521.403569	690.422362	435.251146	909.662304	736.036335	606.670228
HLA-DRB1	427.623956	54.42349	311.576755	124.236996	391.136381	325.877231	657.545107	497.970566	522.499973	360.159329	407.485488
HMGB1	204.093252	180.587035	194.277271	202.055774	254.660737	244.901676	502.552331	495.807827	370.728473	305.372	273.935993
HMGB2	13.8838947	43.2914125	25.6592621	24.574351	16.8835848	39.5002704	42.2707568	64.8821584	26.1008312	48.5002588	56.9750402
HMGN1	304.057293	260.985372	322.573581	214.34295	333.450799	333.777285	629.364602	410.920336	400.696094	334.561971	403.839085
HRAS	27.7677894	29.68554	17.1061748	24.574351	36.5811003	37.5252568	23.4837538	22.7087554	25.1341338	22.0047471	21.4226151
HSH2D	5.55355787	6.1844875	7.33121776	10.9219338	9.84875778	7.90005407	44.6191322	28.6562866	5.31683599	8.98152941	5.01380354
HSPB1	549.802229	1725.47201	1264.63506	1514.05307	433.345342	1518.7854	354.604682	569.34094	280.342261	359.261177	644.501655
HSPB2	48.5936314	66.792465	37.8779584	27.3048344	26.7323426	41.4752839	84.5415137	54.0684653	54.1350574	44.9076471	39.654628
IFI44	11.1071157	13.6058725	21.9936533	19.1133841	15.4766194	27.6501893	44.6191322	57.3125732	24.6507851	30.9862765	25.524818
IFIT1	61.0891366	136.058725	78.1996561	88.7407118	32.3602041	122.450838	58.7093845	88.6722831	60.9019396	83.9773	104.834074
IFIT2	61.0891366	61.844875	29.324871	23.2091092	49.2437889	177.751217	75.1480122	38.929295	34.8011083	26.9445882	34.1850241
IFIT3	40.2632946	40.8176175	28.1030014	87.3754701	50.6507543	235.026609	23.4837538	42.173403	20.7839952	13.0232176	22.3342158
IFNA1	2.77677894	6.1844875	1.22186963	4.09572516	2.8139308	3.95002704	46.9675076	17.8425936	21.7506927	1.34722941	2.73480193

	NMP						Control				
mRNA	Medulla 1	Medulla 2	Medulla 3	Medulla 4	Medulla 6	Medulla 7	Medulla 5	Medulla 8	Medulla 9	Medulla 10	Medulla 11
IFNB1	1.38838947	2.473795	2.44373925	5.46096688	5.62786159	1.97501352	46.9675076	14.5984856	7.73357963	0.89815294	1.36740097
IFNG	4.1651684	2.473795	3.66560888	5.46096688	5.62786159	1.97501352	58.7093845	15.6798549	9.18362581	2.24538235	10.0276071
IL10	8.33033681	18.5534625	25.6592621	20.4786258	12.6626886	47.4003244	21.1353784	8.65095445	4.83348727	3.14353529	4.55800322
IL10RB	76.3614207	127.400442	114.855745	99.6626455	84.4179239	138.250946	105.676892	165.449504	91.3529093	83.9773	82.0440579
IL11	1.38838947	6.1844875	40.3216977	47.7834602	32.3602041	21.7251487	25.8321292	17.3019089	1.45004618	0.89815294	3.19060225
IL12A	6.94194734	13.6058725	4.8874785	10.9219338	11.2557232	17.7751217	2.34837538	1.62205396	0.48334873	0.89815294	1.36740097
IL12B	6.94194734	9.89518	4.8874785	4.09572516	7.03482699	1.97501352	63.4061353	18.9239629	15.4671593	2.69445882	3.64640257
IL13	2.77677894	2.473795	1.22186963	1.36524172	2.8139308	3.95002704	61.0577599	24.3308094	0.96669745	0.44907647	2.27900161
IL15	6.94194734	6.1844875	12.2186963	10.9219338	11.2557232	13.8250946	30.5288799	7.02890049	18.3672516	12.1250647	10.9392077
IL17A	9.71872627	1.2368975	4.8874785	12.2871755	12.6626886	21.7251487	7.04512614	5.40684653	2.41674363	2.69445882	5.01380354
IL18	55.5355787	16.0796675	47.6529154	42.3224933	101.301509	49.375338	91.5866398	88.6722831	81.2025861	43.1113412	56.0634396
IL18RAP	6.94194734	4.94759	6.10934813	6.8262086	9.84875778	7.90005407	30.5288799	10.2730084	10.1503233	0.89815294	2.27900161
IL1A	8.33033681	9.89518	6.10934813	5.46096688	5.62786159	15.8001081	49.315883	15.6798549	8.21692835	1.34722941	5.01380354
IL1B	12.4955052	60.6079775	84.3090042	28.6700761	42.2089619	51.3503515	56.3610091	28.6562866	12.5670669	13.9213706	13.2182093
IL1R1	88.8569259	58.1341825	129.51818	120.141271	178.684606	67.1504596	86.8898891	59.4753119	72.9856577	59.2780941	71.1048502
IL1RAP	56.9239682	11.1320775	28.1030014	21.8438675	30.9532387	15.8001081	46.9675076	21.0867015	18.3672516	10.7778353	16.8646119
IL1RN	4.1651684	16.0796675	21.9936533	39.5920099	14.069654	31.6002163	2.34837538	23.7901247	1.93339491	3.59261177	9.57180676
IL2	9.71872627	8.6582825	2.44373925	8.19145032	5.62786159	13.8250946	23.4837538	11.3543777	11.6003694	4.04168824	15.4972109
IL21	2.77677894	1.2368975	4.8874785	2.73048344	2.8139308	1.97501352	39.9223815	14.5984856	7.2502309	0.89815294	3.64640257
IL22	5.55355787	4.94759	4.8874785	2.73048344	7.03482699	5.92504056	23.4837538	10.8136931	9.66697453	1.34722941	2.27900161
IL22RA2	4.1651684	2.473795	1.22186963	4.09572516	4.22089619	1.97501352	2.34837538	3.24410792	0.96669745	0.44907647	0.91160064
IL23A	5.55355787	8.6582825	8.55308738	9.55669204	5.62786159	3.95002704	32.8772553	29.1969713	7.73357963	0.89815294	4.1022029
IL23R	9.71872627	3.7106925	4.8874785	6.8262086	11.2557232	7.90005407	25.8321292	12.9764317	9.18362581	1.79630588	3.64640257
IL3	1.38838947	1.2368975	3.66560888	4.09572516	1.4069654	7.90005407	25.8321292	12.9764317	2.41674363	0.44907647	1.36740097
IL4	6.94194734	4.94759	3.66560888	2.73048344	7.03482699	13.8250946	37.5740061	11.3543777	4.83348727	1.34722941	4.1022029
IL5	2.77677894	1.2368975	3.66560888	5.46096688	2.8139308	3.95002704	28.1805046	18.9239629	11.6003694	2.69445882	5.01380354
IL6	22.2142315	153.37529	525.403939	621.184982	191.347294	341.677339	2.34837538	3.78479257	0.96669745	4.04168824	4.1022029
IL6R	124.955052	11.1320775	21.9936533	31.4005595	59.0925467	29.6252028	44.6191322	18.9239629	15.4671593	12.1250647	30.0828212
IL7	9.71872627	2.473795	6.10934813	4.09572516	5.62786159	7.90005407	37.5740061	11.8950624	8.70027708	3.59261177	5.46960386
IL8	209.64681	452.704485	1684.95821	1316.09302	1449.17436	902.581178	46.9675076	27.0342327	13.0504156	32.3335059	64.2678454
IL9	1.38838947	8.6582825	4.8874785	6.8262086	4.22089619	5.92504056	7.04512614	4.32547723	1.93339491	0.89815294	2.27900161
IRF1	148.557673	169.454957	206.495967	122.871755	59.0925467	355.502433	44.6191322	36.2258718	24.1674363	39.0696529	55.1518389
IRF3	18.0490631	13.6058725	14.6624355	5.46096688	11.2557232	21.7251487	21.1353784	28.6562866	22.2340414	16.1667529	21.8784154
IRF5	41.651684	21.0272575	21.9936533	21.8438675	32.3602041	43.4502974	39.9223815	60.0159965	18.8506003	33.6807353	38.7430273

	NMP						Control				
mRNA	Medulla 1	Medulla 2	Medulla 3	Medulla 4	Medulla 6	Medulla 7	Medulla 5	Medulla 8	Medulla 9	Medulla 10	Medulla 11
IRF7	16.6606736	37.106925	42.7654369	39.5920099	15.4766194	90.8506218	61.0577599	45.4175109	13.5337643	23.3519765	24.6132174
ITGB2	6.94194734	7.421385	20.7717836	4.09572516	35.1741349	15.8001081	103.328517	46.4988802	26.58418	18.4121353	21.8784154
JUN	563.686124	1689.60198	1251.1945	466.912668	164.614952	1975.01352	82.1931383	168.152927	77.3357963	153.584153	226.07696
KEAP1	31.9329578	18.5534625	30.5467406	8.19145032	15.4766194	23.7001622	46.9675076	38.3886104	29.4842723	17.9630588	30.5386216
KNG1	573.40485	905.40897	1033.7017	614.358774	718.959318	460.17815	636.409728	298.998613	1045.4833	644.424735	881.517822
LIMK1	18.0490631	35.8700275	25.6592621	24.574351	42.2089619	29.6252028	32.8772553	63.8007891	32.3843647	30.9862765	41.4778293
LTA	6.94194734	3.7106925	3.66560888	5.46096688	8.44179239	7.90005407	39.9223815	27.0342327	2.41674363	0.44907647	2.27900161
LTB	11.1071157	18.5534625	4.8874785	5.46096688	11.2557232	15.8001081	35.2256307	22.7087554	12.0837182	2.24538235	2.73480193
LTB4R	11.1071157	3.7106925	7.33121776	6.8262086	8.44179239	3.95002704	39.9223815	17.3019089	14.5004618	5.38891765	6.3812045
LTB4R2	19.4374525	8.6582825	8.55308738	6.8262086	26.7323426	13.8250946	35.2256307	40.551349	17.4005542	11.2269118	15.9530113
LY96	6.94194734	17.316565	23.2155229	9.55669204	21.104481	19.7501352	35.2256307	37.8479257	20.7839952	8.98152941	16.4088116
MAFF	98.5756522	421.782047	288.361232	393.189615	108.336336	456.228123	37.5740061	24.8714941	14.5004618	29.1899706	102.099272
MAFG	58.3123576	27.211745	36.6560888	28.6700761	60.4995121	37.5252568	54.0126338	27.5749173	19.3339491	13.4722941	38.287227
MAFK	149.946063	132.348032	257.814491	202.055774	244.811979	254.776744	77.4963876	127.060894	124.220623	112.718194	164.999716
MAP2K1	133.285389	138.53252	114.855745	128.332722	135.068678	152.076041	133.857397	158.961288	133.404249	106.431124	95.7180676
MAP2K4	76.3614207	55.6603875	84.3090042	70.9925694	99.8945432	57.275392	68.102886	75.1551668	60.4185908	38.6205765	44.2126312
MAP2K6	30.5445683	19.79036	18.3280444	31.4005595	19.6975156	27.6501893	68.102886	31.9003945	35.284457	18.4121353	45.5800322
MAP3K1	141.615726	142.243212	150.289964	94.2016786	167.428882	142.200973	136.205772	191.943052	206.389906	139.213706	119.875485
MAP3K5	52.7587998	28.4486425	35.4342192	32.7658013	30.9532387	23.7001622	68.102886	45.9581955	36.7345032	25.1482824	25.0690177
MAP3K7	81.9149786	85.3459275	164.9524	124.236996	143.510471	102.700703	154.992775	174.100458	133.887597	109.125582	123.066087
MAP3K9	15.2722841	17.316565	13.4405659	8.19145032	19.6975156	11.8500811	30.5288799	23.7901247	17.4005542	10.7778353	7.29280515
MAPK1	237.414599	284.486425	284.695623	233.456334	271.544322	254.776744	258.321292	284.940812	269.708589	290.552477	235.648766
MAPK14	187.432578	115.031467	171.061748	96.9321621	95.673647	161.951109	187.87003	164.368135	159.50508	120.352494	154.972109
MAPK3	88.8569259	131.111135	117.299484	122.871755	101.301509	183.676257	133.857397	188.698944	172.555495	154.033229	131.270493
MAPK8	111.071157	76.687645	96.5277005	95.5669204	92.8597162	79.0005407	75.1480122	69.2076356	79.7525399	70.5050059	68.3700483
MAPKAPK2	183.26741	153.37529	168.618008	192.499082	191.347294	148.126014	112.722018	85.9688599	94.7363504	95.2042118	137.195897
MAPKAPK5	49.9820208	54.42349	62.3153509	55.9749105	71.7552353	47.4003244	126.812271	83.2654366	87.4861195	70.9540824	103.922473
MASP1	4.1651684	6.1844875	14.6624355	4.09572516	2.8139308	13.8250946	30.5288799	12.435747	13.0504156	3.14353529	5.01380354
MASP2	6.94194734	7.421385	8.55308738	9.55669204	7.03482699	9.87506759	35.2256307	22.1680708	2.90009236	4.04168824	2.73480193
MAX	133.285389	112.557672	160.064921	120.141271	194.161225	116.525798	154.992775	143.822118	128.087413	122.597876	144.944502
MBL2	1.38838947	1.2368975	1.22186963	2.73048344	4.22089619	5.92504056	11.7418769	3.24410792	3.38344109	0.44907647	2.27900161
MEF2A	162.441568	160.796675	205.274097	177.481424	191.347294	181.701244	335.817679	270.883011	223.79046	279.774641	327.720431
MEF2B	8.33033681	8.6582825	14.6624355	12.2871755	18.2905502	31.6002163	84.5415137	32.9817639	6.28353345	5.83799412	13.2182093
MEF2C	27.7677894	34.63313	39.099828	40.9572516	30.9532387	31.6002163	82.1931383	56.7718886	49.7849188	48.9493353	48.7706344

	NMP						Control				
mRNA	Medulla 1	Medulla 2	Medulla 3	Medulla 4	Medulla 6	Medulla 7	Medulla 5	Medulla 8	Medulla 9	Medulla 10	Medulla 11
MEF2D	36.0981262	38.3438225	50.0966547	38.2267681	54.8716505	41.4752839	96.2833906	55.6905193	62.3519857	46.2548765	58.3424412
MKNK1	77.7498102	70.5031575	70.8684383	55.9749105	125.21992	110.600757	154.992775	124.898155	99.086489	83.9773	97.5412689
MMP3	1.38838947	1.2368975	3.66560888	5.46096688	9.84875778	1.97501352	39.9223815	15.6798549	6.76688217	2.24538235	2.27900161
MMP9	4.1651684	1.2368975	3.66560888	4.09572516	7.03482699	1.97501352	23.4837538	11.8950624	1.45004618	0.44907647	2.73480193
MRC1	38.8749051	22.264155	35.4342192	24.574351	94.2666816	37.5252568	110.373643	58.3939426	38.6678981	33.6807353	35.5524251
MX1	68.0310839	123.68975	180.836705	211.612467	104.115439	187.626284	136.205772	188.698944	80.2358886	109.125582	108.024676
MX2	6.94194734	18.5534625	7.33121776	16.3829006	19.6975156	5.92504056	56.3610091	25.9528634	17.4005542	8.08337647	12.3066087
MYC	192.986136	239.958115	480.194763	204.786258	243.405014	428.577933	89.2382645	31.9003945	14.0171131	61.5234765	55.1518389
MYD88	48.5936314	30.9224375	54.9841332	51.8791853	53.4646851	49.375338	86.8898891	67.044897	46.8848265	41.7641118	36.9198261
MYL2	6.94194734	3.7106925	2.44373925	5.46096688	18.2905502	17.7751217	25.8321292	9.73232376	7.2502309	0.89815294	1.82320129
NFATC3	76.3614207	69.26626	96.5277005	53.2444271	47.8368235	75.0505137	84.5415137	111.381039	79.2691912	63.7688588	61.9888438
NFE2L2	372.088377	205.324985	266.367578	309.90987	333.450799	248.851703	164.386277	241.68604	180.772424	206.1261	233.825565
NFKB1	43.0400735	29.68554	57.4278724	81.9145032	118.185093	71.1004867	28.1805046	34.0631332	32.3843647	25.5973588	22.7900161
NLRP3	8.33033681	7.421385	28.1030014	6.8262086	18.2905502	21.7251487	23.4837538	11.3543777	5.80018472	5.83799412	6.3812045
NOD1	4.1651684	6.1844875	4.8874785	4.09572516	5.62786159	9.87506759	28.1805046	27.5749173	25.1341338	22.0047471	21.8784154
NOD2	6.94194734	6.1844875	9.77495701	2.73048344	9.84875778	1.97501352	21.1353784	17.3019089	13.0504156	4.49076471	5.01380354
NOS2	8.33033681	4.94759	9.77495701	9.55669204	14.069654	11.8500811	46.9675076	17.8425936	4.35013854	3.14353529	3.19060225
NOX1	26.3793999	13.6058725	7.33121776	31.4005595	22.5114464	29.6252028	58.7093845	22.1680708	17.4005542	4.93984118	5.46960386
NR3C1	134.673778	129.874237	175.949226	113.315063	140.69654	146.151	288.850172	222.762077	197.20628	165.709218	216.960953
OAS2	12.4955052	17.316565	30.5467406	21.8438675	11.2557232	15.8001081	63.4061353	45.9581955	25.1341338	15.2686	18.2320129
OASL	8.33033681	17.316565	8.55308738	10.9219338	12.6626886	25.6751757	37.5740061	15.1391703	5.80018472	5.38891765	5.46960386
OXER1	9.71872627	8.6582825	6.10934813	6.8262086	15.4766194	11.8500811	46.9675076	27.0342327	9.66697453	1.79630588	12.3066087
PDGFA	11.1071157	29.68554	45.2091762	25.9395927	21.104481	39.5002704	51.6642584	62.7194198	24.1674363	66.0142412	61.0772431
PIK3C2G	33.3213472	34.63313	23.2155229	17.7481424	60.4995121	31.6002163	63.4061353	83.2654366	79.2691912	82.6300706	81.1324573
PLA2G4A	9.71872627	24.73795	45.2091762	16.3829006	12.6626886	45.4253109	49.315883	92.4570757	46.4014778	40.8659588	47.4032335
PLCB1	4.1651684	44.52831	61.0934813	32.7658013	26.7323426	59.2504056	46.9675076	72.4517435	80.2358886	107.329276	97.5412689
PPP1R12B	49.9820208	18.5534625	56.2060028	23.2091092	63.3134429	43.4502974	138.554147	78.3992747	116.970392	118.107112	82.0440579
PRKCA	54.1471892	42.054515	30.5467406	31.4005595	68.9413045	25.6751757	126.812271	105.433507	68.6355192	61.972553	75.2070531
PRKCB	4.1651684	14.84277	17.1061748	13.6524172	14.069654	15.8001081	21.1353784	39.4699797	12.5670669	13.4722941	10.9392077
PTGDR2	12.4955052	11.1320775	4.8874785	13.6524172	11.2557232	17.7751217	37.5740061	31.3597099	3.86678981	3.59261177	9.11600643
PTGER1	5.55355787	1.2368975	1.22186963	1.36524172	5.62786159	9.87506759	2.34837538	3.24410792	2.41674363	3.14353529	1.36740097
PTGER2	11.1071157	18.5534625	40.3216977	25.9395927	32.3602041	21.7251487	39.9223815	30.2783406	18.3672516	27.3936647	25.524818
PTGER3	329.048304	248.616397	217.492793	204.786258	240.591083	298.227041	328.772553	128.682947	339.310806	291.001553	431.642905
PTGER4	26.3793999	25.9748475	32.9904799	13.6524172	22.5114464	25.6751757	65.7545107	25.4121787	16.9172054	14.8195235	23.7016167

	NMP						Control				
mRNA	Medulla 1	Medulla 2	Medulla 3	Medulla 4	Medulla 6	Medulla 7	Medulla 5	Medulla 8	Medulla 9	Medulla 10	Medulla 11
PTGFR	11.1071157	14.84277	10.9968266	21.8438675	28.139308	15.8001081	23.4837538	25.9528634	13.0504156	13.9213706	23.7016167
PTGIR	8.33033681	2.473795	17.1061748	16.3829006	15.4766194	23.7001622	28.1805046	18.3832782	6.76688217	13.4722941	19.1436135
PTGS1	9.71872627	34.63313	20.7717836	31.4005595	36.5811003	29.6252028	54.0126338	92.9977604	29.0009236	15.2686	20.5110145
PTGS2	2.77677894	59.37108	65.9809598	176.116182	8.44179239	43.4502974	35.2256307	35.1445025	11.1170207	17.9630588	30.0828212
PTK2	262.405609	300.566092	349.454713	214.34295	337.671695	339.702325	265.366418	536.899861	442.264085	435.604177	413.410892
RAC1	391.52583	327.777837	332.348538	384.998165	400.985138	389.077663	319.379052	368.206249	337.86076	348.932418	262.085185
RAF1	223.530704	206.561882	206.495967	191.133841	208.230879	165.901136	147.947649	197.349898	212.67344	154.482306	159.074312
RAPGEF2	73.5846418	34.63313	70.8684383	43.687735	80.1970277	43.4502974	39.9223815	71.3703742	74.9190526	52.0928706	59.7098421
RELA	51.3704103	45.7652075	79.4215257	77.818778	63.3134429	53.325365	30.5288799	48.6616188	35.7678058	29.6390471	23.7016167
RELB	65.254305	29.68554	48.874785	87.3754701	84.4179239	84.9255813	14.0902523	11.8950624	11.6003694	12.1250647	17.3204122
RHOA	188.820968	163.27047	178.392965	131.063205	182.905502	165.901136	117.418769	171.397035	141.621177	189.061194	146.311903
RIPK1	151.334452	66.792465	101.415179	98.2974038	177.27764	116.525798	164.386277	137.333902	148.871408	85.3245294	105.289874
RIPK2	76.3614207	77.9245425	122.186963	141.985139	135.068678	154.051054	56.3610091	53.5277807	38.6678981	35.9261177	37.8314267
ROCK2	192.986136	160.796675	237.042707	167.924732	337.671695	163.926122	267.714793	275.208489	256.174825	229.478077	280.317198
RPS6KA5	20.825842	32.159335	53.7622635	28.6700761	29.5462734	25.6751757	32.8772553	29.7376559	33.8344109	19.3102882	18.6878132
SHC1	101.352431	85.3459275	136.849398	114.680304	167.428882	104.675716	230.140787	125.979524	139.204433	138.315553	142.665501
SMAD7	69.4194734	150.901495	139.293137	64.1663608	83.0109585	158.001081	199.611907	120.031993	110.20351	142.357241	165.455517
STAT1	149.946063	115.031467	217.492793	177.481424	184.312467	179.72623	65.7545107	96.7825529	99.5698377	110.472812	107.568876
STAT2	93.0220943	118.74216	144.180616	88.7407118	156.173159	161.951109	328.772553	192.483737	238.774271	172.445365	210.123948
STAT3	981.591354	541.761105	922.511568	776.822538	1062.25888	886.78107	678.680485	680.721978	838.126692	798.457965	906.58684
TBXA2R	4.1651684	2.473795	1.22186963	1.36524172	7.03482699	5.92504056	11.7418769	11.3543777	2.90009236	3.14353529	6.83700483
TCF4	31.9329578	55.6603875	70.8684383	46.4182185	39.3950311	73.0755002	108.025268	122.735416	89.4195144	79.4865353	71.1048502
TGFB1	37.4865156	47.002105	42.7654369	50.5139436	70.3482699	65.1754461	98.631766	161.124027	87.9694682	105.532971	123.066087
TGFB2	23.602621	37.106925	36.6560888	50.5139436	43.6159273	51.3503515	21.1353784	29.7376559	26.58418	27.3936647	11.395008
TGFB3	36.0981262	16.0796675	42.7654369	53.2444271	50.6507543	21.7251487	70.4512614	37.3072411	26.1008312	75.4448471	72.4722512
TGFBR1	43.0400735	39.58072	69.6465687	24.574351	57.6855813	59.2504056	129.160646	84.8874906	63.8020319	66.4633177	97.0854685
TLR1	12.4955052	25.9748475	20.7717836	16.3829006	21.104481	21.7251487	96.2833906	40.551349	36.7345032	29.1899706	30.5386216
TLR2	38.8749051	33.3962325	29.324871	45.0529767	53.4646851	33.5752298	72.7996368	37.3072411	27.5508774	26.9445882	26.4364187
TLR3	34.7097367	59.37108	50.0966547	54.6096688	36.5811003	51.3503515	86.8898891	117.869254	83.6193297	70.5050059	55.1518389
TLR4	43.0400735	50.7127975	57.4278724	49.1487019	61.9064775	61.2254191	110.373643	74.0737975	36.7345032	36.8242706	54.6960386
TLR5	6.94194734	32.159335	45.2091762	20.4786258	21.104481	23.7001622	56.3610091	67.5855817	47.3681752	28.7408941	27.8038196
TLR6	22.2142315	12.368975	10.9968266	10.9219338	8.44179239	27.6501893	68.102886	26.493548	16.4338567	7.6343	13.6740097
TLR7	5.55355787	2.473795	8.55308738	5.46096688	1.4069654	5.92504056	30.5288799	16.2205396	10.633672	2.24538235	3.64640257
TLR8	9.71872627	4.94759	7.33121776	5.46096688	7.03482699	17.7751217	61.0577599	17.3019089	13.0504156	2.69445882	5.46960386

	NMP						Control				
mRNA	Medulla 1	Medulla 2	Medulla 3	Medulla 4	Medulla 6	Medulla 7	Medulla 5	Medulla 8	Medulla 9	Medulla 10	Medulla 11
TLR9	8.33033681	7.421385	6.10934813	17.7481424	14.069654	15.8001081	37.5740061	20.0053322	1.93339491	3.14353529	2.73480193
TNF	4.1651684	76.687645	56.2060028	24.574351	39.3950311	47.4003244	39.9223815	15.6798549	12.0837182	1.34722941	4.55800322
TNFAIP3	154.111231	295.618502	640.259684	339.945188	467.112512	359.45246	105.676892	29.7376559	27.0675287	57.4817882	101.187671
TNFSF14	19.4374525	9.89518	7.33121776	9.55669204	11.2557232	11.8500811	70.4512614	21.6273861	4.83348727	1.79630588	3.19060225
TOLLIP	280.454673	160.796675	168.618008	90.1059535	101.301509	144.175987	209.005409	135.711848	144.521269	117.658035	152.693108
TRADD	18.0490631	8.6582825	12.2186963	15.0176589	4.22089619	15.8001081	16.4386277	14.5984856	10.1503233	8.53245294	16.4088116
TRAF2	33.3213472	33.3962325	34.2123495	34.131043	26.7323426	13.8250946	96.2833906	36.2258718	22.7173902	18.8612118	25.0690177
TREM2	4.1651684	1.2368975	1.22186963	1.36524172	1.4069654	5.92504056	25.8321292	12.9764317	5.80018472	5.38891765	2.73480193
TSLP	19.4374525	13.6058725	9.77495701	16.3829006	12.6626886	29.6252028	35.2256307	25.4121787	20.7839952	7.18522353	10.4834074
TWIST2	11.1071157	4.94759	7.33121776	5.46096688	11.2557232	17.7751217	30.5288799	26.493548	7.73357963	3.14353529	10.0276071
TYROBP	54.1471892	53.1865925	100.193309	53.2444271	95.673647	59.2504056	157.34115	102.730084	74.9190526	59.7271706	47.8590338